UNIVERSIDADE FEDERAL DA BAHIA
INSTITUTO DE GEOCIÊNCIAS
PROGRAMA DE PESQUISA E PÓS-GRADUAÇÃO EM GEOLOGIA
ÁREA DE CONCENTRAÇÃO:
PETROLOGIA, METALOGÊNESE E EXPLORAÇÃO MINERAL

TESE DE DOUTORADO

GEOLOGIA, PETROLOGIA E GEOCRONOLOGIA DO *GREENSTONE BELT* MUNDO NOVO E DO DEPÓSITO DE Zn E Pb DA FAZENDA COQUEIRO, CRÁTON DO SÃO FRANCISCO, NE DO BRASIL

RICARDO RAMOS SPREAFICO

SALVADOR

2019

GEOLOGIA, PETROLOGIA E GEOCRONOLOGIA DO *GREENSTONE BELT* MUNDO NOVO E DO DEPÓSITO DE Zn E Pb DA FAZENDA COQUEIRO, CRÁTON DO SÃO FRANCISCO, NE DO BRASIL

Ricardo Ramos Spreafico

Orientador: Prof. Dr. Johildo Salomão Figueiredo Barbosa

<div align="right">

Tese de Doutorado apresentada ao Programa de Pós-Graduação em Geologia do Instituto de Geociências da Universidade Federal da Bahia como requisito parcial à obtenção do Título de Doutor em Geologia, Área de Concentração: Petrologia, Metalogênese e Exploração Mineral.

</div>

SALVADOR
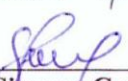
2019
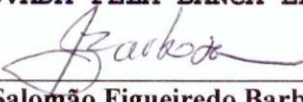
RICARDO RAMOS SPREAFICO

GEOLOGIA, PETROLOGIA E GEOCRONOLOGIA DO *GREENSTONE*

***BELT* MUNDO NOVO E DO DEPÓSITO DE Zn E Pb DA FAZENDA**

COQUEIRO, CRÁTON DO SÃO FRANCISCO,

NE DO BRASIL

Tese apresentada ao Programa de Pós-Graduação em Geologia da Universidade Federal da Bahia, como requisito para a obtenção do Grau de Doutor em Geologia na área de concentração em Petrologia, Metalogênese e Exploração Mineral em 13/09/2019.
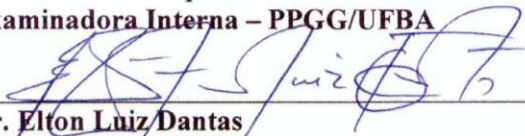
TESE APROVADA PELA BANCA EXAMINADORA:
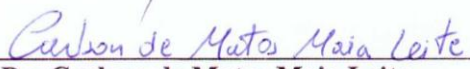
Dr. Johildo Salomão Figueiredo Barbosa
Orientador – PPGG/UFBA
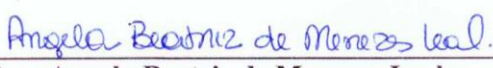
Dra. Simone Cerqueira Pereira Cruz
Examinadora Interna – PPGG/UFBA

Dr. Elton Luiz Dantas
Examinador Externo – PPGG/UnB

Dr. Carlson de Matos Maia Leite
Examinador Externo – PETROBRAS

Dra. Angela Beatriz de Menezes Leal
Examinadora Interna – PPGG/UFBA

Salvador - BA
2019

Aos meus pais, Sebastião e Maraíza, aos familiares e professores que de alguma forma contribuíram para a realização desta Tese.

AGRADECIMENTOS

RESUMO

Dados de campo, petrográficos, litogeoquímicos, geocronológicos U-Pb em zircão por LA-ICP-MS e isotópicos de Nd e Sr foram usados para determinar a evolução geológica, a idade do vulcanismo e o ambiente tectônico do *greenstone belt* Mundo Novo (GBMN) e das unidades geológicas adjacentes como o embasamento e rochas graníticas mais jovens da porção leste do Cráton do São Francisco (NE do Brasil). Dados geocronológicos Pb-Pb por TIMS permitiram determinar a idade e a gênese do depósito de Zn-Pb do tipo *volcanogenic massive sulfide* da Fazenda Coqueiro (FC), hospedado no GBMN. O embasamento do *greenstone belt* (Bloco Gavião) é composto por tonalito-trondhjemito-granodiorito ortognaisses e migmatitos, além de metariolitos e metagranitos subordinados. O GBMN está dividido em três sequências litológicas: (i) unidade superior (metakomatiitos); (ii) unidade média (metabasaltos, metadacitos e metassedimentares químicas); e (iii) unidade superior (metassedimentares siliciclásticas). Adicionalmente, dois plútons graníticos Riacianos-Orosirianos ocorrem na área, metagranitos Areia Branca e Jequitibá. O metabasalto hospeda duas zonas de alteração hidrotermal na FC: uma carbonática, que hospeda sulfetos maciços compostos por esfalerita e galena; e outra argílica-clorítica, que hospeda calcopirita disseminada. Dados U-Pb em zircão dos metagranitos Miguel Calmon e Fazenda Coqueiro (Bloco Gavião) geraram idades de cristalização de 3355 ± 16 Ma e 3227 ± 23 Ma, respectivamente, ambos derivados da crosta continental inferior, com base nos baixos valores da razão $^{87}Sr/^{86}Sr_i$ (0,699 e 0,705, respectivamente), e valores negativos de $\epsilon_{Nd(t)}$ (-3,7 e -3,6, respectivamente). A idade U-Pb em zircão de cristalização de 2595 ± 21 Ma de metadacitos permitiu determinar a idade do vulcanismo de fundo oceânico da sequência média do GBMN. As idades de cristalização U-Pb em zircão de 2106 ± 71 Ma e 1975 ± 36 Ma dos metagranitos Areia Branca and Jequitibá, respectivamente, ambos interpretados como derivados de protólitos crustais com base nos altos valores da razão $^{87}Sr/^{86}Sr_i$ (0,744 e 0,730, respectivamente) e nos valores negativos de $\epsilon_{Nd(t)}$ (-7,7 e -6,5, respectivamente), marcam um evento tectonotermal Riaciano-Orosiriano que afetou o GBMN e proximidades. Dados Pb-Pb em sulfetos das zonas maciça e disseminada da FC, originados da crosta superior, geraram idade modelo aproximada de 2794 Ma. Uma idade isocrônica Pb-Pb de cristalização de 2747 ± 16 Ma foi obtida de amostras de esfalerita e calcopirita das zonas maciça e disseminada. Portanto, cinco estágios são propostos para a evolução tectônica da região estudada: estágios (i) e (ii), caracterizados pelo estabelecimento do embasamento TTG em 3,35 Ga e a consolidação do granito Miguel Calmon, seguido por rifteamento que formou riolitos e posteriormente granitos em 3,22 Ga (granito Fazenda Coqueiro), seguido pela interrupção do rifteamento e por um evento de fechamento. O vulcanismo durante o estágio (iii), entre 2,74 Ga e 2,59 Ga no GBMN, ocorreu em uma crosta oceânica entre blocos cratônicos Arqueanos, relacionado à gênese do depósito da FC, e os estágios (iv) e (v), entre 2,10 Ga e 1,97 Ga (formação de granitos), que representam dois estágios de um evento colisional progressivo no qual a crosta oceânica foi amalgamada entre blocos tectônicos da porção leste do Cráton do São Francisco.

Palavras-chave: Neoarqueano. Geocronologia. *Greenstone belt*. *Volcanogenic Massive Sulfide*. Crosta oceânica.

ABSTRACT

Field, petrographic, lithogeochemical, LA-ICP-MS U-Pb zircon geochronology, and Nd and Sr isotopic data were used to determine the geologic evolution, timing of volcanism and tectonic setting of the Mundo Novo greenstone belt (MNGB) including nearby units, such as the basement and younger granitic rocks in the eastern São Francisco Craton (NE Brazil). TIMS Pb-Pb geochronologic data allow determination of the timing and genesis of the Fazenda Coqueiro volcanogenic massive sulfide Zn-Pb deposit (FC) hosted in the MNGB. The basement of the greenstone belt (Gavião Block) comprises tonalite-trondhjemite-granodiorite orthogneisses, migmatites and subordinate metarhyolites and metagranites. The MNGB is divided into three lithological sequences: (i) the lowermost unit (metakomatiites); (ii) the middle unit (metabasalts, metadacites and metasedimentary chemical rocks); and (iii) the uppermost unit (metasedimentary siliciclastic rocks). Additionally, two Rhyacian-Orosirian granitic plutons occur in the area, the Areia Branca and Jequitibá metagranites. The metabasalt hosts two hydrothermal alteration zones in the FC: one carbonate, hosting massive sulfides composed mainly of sphalerite and galena; and the other argillic/chloritic, hosting mainly disseminated chalcopyrite. U-Pb zircon data from the Miguel Calmon and Fazenda Coqueiro metagranites in the Gavião Block yield crystallization ages of 3355 ± 16 Ma and 3227 ± 23 Ma, respectively, and both metagranites were derived from the lower continental crust based on low $^{87}Sr/^{86}Sr_i$ values (0.699 and 0.705, respectively) and negative values of $\varepsilon_{Nd(t)}$ (-3.7 and -3.6, respectively). The 2595 ± 21 Ma U-Pb zircon crystallization age of the metadacites allowed the determination of the timing of ocean floor volcanism in the middle sequence of the MNGB. The 2106 ± 71 Ma and 1975 ± 36 Ma U-Pb zircon crystallization ages for the Areia Branca and Jequitibá metagranites, respectively, which are both interpreted as derived from crustal protoliths based on high $^{87}Sr/^{86}Sr_i$ values (0.744 and 0.730, respectively) and negative values of $\varepsilon_{Nd(t)}$ (-7.7 and -6.5, respectively), record a Rhyacian-Orosirian tectonothermal event that affected the MNGB and the adjoining region. Pb-Pb sulfide data from the massive and disseminated zones in the FC yield a model age of approximately 2794 Ma sourced from the upper crust. The Pb-Pb crystallization age of 2747 ± 16 Ma was obtained from sphalerite and chalcopyrite samples from the massive and disseminated zones. Therefore, the following five stages are proposed for the tectonic evolution of the study region: stages (i) and (ii) were characterized by the establishment of the TTG basement by 3.35 Ga, when the Miguel Calmon granite was consolidated, followed by a rifting that formed the rhyolites, and subsequent granite formations occurred at 3.22 Ga (Fazenda Coqueiro granite formation), followed by the abort of the rift and a closure event. The volcanism during stage (iii) between 2.74 Ga and 2.59 Ga in the MNGB occurred in the oceanic crust between Archean cratonic blocks and related to FC genesis, and stages (iv) and (v) between 2.10 Ga and 1.97 Ga (granite formations) represent two stages of a progressive collision event in which the oceanic crust was compressed between the tectonic blocks from the eastern São Francisco Craton.

Keywords: Neoarchean. Geochronology. Greenstone belt. Volcanogenic Massive Sulfide. Oceanic crust.

SUMÁRIO

CAPÍTULO 1
INTRODUÇÃO GERAL

Greenstone belts são entidades geológicas, em geral Arqueanas, muito variadas. Estes cinturões contêm grande diversidade de rochas que passaram por múltiplos estágios de deformação, metamorfismo e alteração metassomática/hidrotermal devido à longa história geológica, constituindo ambientes tectônicos posteriormente intrudidos por rochas máficas e ultramáficas, além de granitoides (Anhaeusser, 2014). Além disso, o predomínio de basaltos e komatiitos depositados subaquaticamente nos *greenstone belts* resulta na definição de uma grande variedade de ambientes tectônicos, como por exemplo, arcos de ilha, platôs submarinos relacionados a plumas, cadeias meso-oceânicas (incluindo ofiolitos) e bacias de *back-arc* (De Wit et al., 1987; Storey et al., 1991; Parman et al., 2001; Chavagnac, 2004; Furnes et al., 2013). Os terrenos granito-gnáissicos adjacentes aos *greenstone belts* são interpretados como o resultado de processos de exumação de complexos da crosta média à superior, que levam à formação do embasamento dos *greenstone belts* (Dziggel et al., 2002). O tectonismo pode ter contribuído também para o cavalgamento dos *greenstones* sobre os terrenos granito-gnáissicos durante processos de amalgamação. Dessa forma, o entendimento do ambiente geológico dos *greenstone belts* e suas relações com as unidades granito-gnáissicas adjacentes, são importantes para a caracterização da gênese e da evolução tectônica destes tipos de terrenos.

Os terrenos do tipo *greenstone belt* da porção leste do Cráton do São Francisco, no estado da Bahia, têm sido intensivamente estudados desde a década de 1970, quando o primeiro mapa geológico da região de Mundo Novo foi elaborado (Couto et al., 1978; Loureiro, 1991) e o depósito de Zn e Pb da Fazenda Coqueiro foi descoberto. Porém, a definição da sequência metavulcanossedimentar de Mundo Novo, como um terreno do tipo *greenstone belt*, ocorreu apenas na década de 1990 por Mascarenhas e Silva (1994). Além desta definição, a ocorrência do depósito da Fazenda Coqueiro aumentou o interesse na área, pois sua existência abriu possibilidades para a pesquisa e a descoberta de novos depósitos minerais (Souza et al., 2002; Monteiro et al., 2009). A localização da área de estudo está indicada nos três artigos que compõem esta Tese.

As rochas metavulcânicas félsicas que ocorrem próximas ao depósito da Fazenda Coqueiro, com idade de cristalização de 3305 ± 9 Ma (Peucat et al., 2002; Zincone et al., 2016), são atualmente interpretadas como parte do embasamento do *greenstone belt* Mundo

Novo (GBMN), tendo sido originadas a partir de um sistema plutônico-vulcânico do tipo intraplaca (Zincone et al., 2016). Esta interpretação deixou em aberto questões sobre a idade do vulcanismo de fundo oceânico no GBMN e, consequentemente, sua evolução tectônica e sua relação com as unidades geológicas adjacentes. Entretanto, a história geológica da área de estudo se estende desde a formação do embasamento durante o Paleoarqueano (Mougeot, 1996) até o último evento tectonotermal registrado na região, por meio da granitogênese Riaciana-Orosiriana (Leite, 2002). Esta granitogênese, no entanto, foi contemporânea à formação das bacias Paleoproterozoicas da unidade superior do GBMN e do Complexo Saúde (Barbuena et al., 2016; Zincone et al., 2017).

Nesta Tese, idades U-Pb em zircão obtidas por *laser ablation inductively coupled plasma mass spectrometry* (LA-ICP-MS) e dados isotópicos de Nd e Sr analisados por *thermal ionization mass spectrometry* (TIMS) foram compatibilizados aos dados petrográficos, de química mineral e de geoquímica de rocha total do GBMN e de unidades adjacentes. Dois metagranitos do embasamento, um metadacito relacionado às rochas metamáficas e metaultramáficas do GBMN e dois metagranitos mais novos foram analisados com o objetivo de propor um modelo para a evolução tectônica do *greenstone belt* em foco. Assim, o presente estudo aborda a formação do embasamento cratônico durante o Paleoarqueano, a idade e o ambiente tectônico onde o vulcanismo do GBMN ocorreu, a amalgamação do *greenstone* entre blocos cratônicos durante a orogenia Paleoproterozoica, além da subsequente estabilidade tectônica e eventos sedimentares tardios, contribuindo assim, para o conhecimento geológico da porção leste do Cráton do São Francisco na Bahia.

Depósitos minerais do tipo *volcanogenic massive sulfide* (VMS) são acumulações *stratabound* de sulfetos formadas sobre ou próximas ao assoalho oceânico, espacialmente, temporalmente e geneticamente associadas a vulcanismos contemporâneos (Franklin et al., 2005). Dessa forma, o depósito de Zn e Pb do tipo VMS da Fazenda Coqueiro, hospedado na porção central do GBMN, é uma importante evidência de atividade hidrotermal de fundo oceânico com precipitação de sulfeto durante a formação do GBMN. Porém, a deformação durante eventos tectônicos colisionais posteriores, a grande profundidade do depósito e as ocorrências de sulfetos identificadas somente em testemunhos de sondagem, tornaram difícil definir claramente a tipologia e o modelo metalogenético do depósito, assim como observado por Souza et al. (2002) e Monteiro et al. (2009).

O depósito da Fazenda Coqueiro está hospedado no metabasalto da sequência média do GBMN, que possui intercalações de dois tipos de zonas de alteração hidrotermal: uma carbonática e outra argílica-clorítica. A zona de alteração hidrotermal carbonática hospeda as

ocorrências maciças de esfalerita e galena, e a zona de alteração hidrotermal argílica-clorítica, que é periférica, hospeda calcopirita de forma disseminada (Spreafico, 2017). O evento tectônico Riaciano-Orosiriano deformou o depósito da Fazenda Coqueiro e obliterou suas feições iniciais, tornando difícil interpretar seu modelo metalogenético e levando à interpretação da possibilidade de que processos hidrotermais tardios tenham afetado a mineralização. Entretanto, os novos dados geocronológicos de metadacitos do GBMN, apresentados nesta Tese, indicaram idades Neoarqueanas para o GBMN (Spreafico et al., 2019), sugerindo que o depósito da Fazenda Coqueiro tenha se formado contemporaneamente a estas rochas.

Dessa forma, estudos geológicos e geocronológicos Pb-Pb obtidos por TIMS em sulfetos do depósito da Fazenda Coqueiro foram conduzidos para se chegar a uma melhor compreensão sobre a idade e a gênese do depósito. Uma analogia com os componentes do *pipe* inicial, a descrição de estilos, controles e possíveis fontes da mineralização, levaram à interpretação sobre os processos de deformação do depósito e sua relação com o Lineamento Contendas-Jacobina (Sabaté et al., 1990), além da possibilidade de que processos tardios de remobilização dos sulfetos tenha ocorrido.

A presente Tese constitui-se de três artigos científicos elaborados durante o desenvolvimento do doutorado. O primeiro artigo, intitulado "Geology and petrology of metavolcanic rocks in the Neoarchean Mundo Novo greenstone belt, eastern São Francisco Craton, NE Brazil: Tectonic setting considerations", foi submetido para a revista "Brazilian Journal of Geology", está em fase de revisão e corresponde ao Capítulo 2 desta Tese. O segundo artigo, intitulado "Tectonic evolution of the Neoarchean Mundo Novo greenstone belt, eastern São Francisco Craton, NE Brazil: Petrology, U-Pb geochronology, and Nd and Sr isotopic constraints", foi devidamente aprovado e aceito para publicação na revista "Journal of South American Earth Sciences", e corresponde ao Capítulo 3. Por fim, o terceiro artigo, intitulado "TIMS Pb-Pb geochronology of sulfides in the Fazenda Coqueiro VMS deposit, São Francisco Craton, NE Brazil: Timing and genesis constraints on the mineralization", foi submetido para a revista "Geologia USP – Série Científica", está em fase de revisão e corresponde ao Capítulo 4 do presente trabalho.

Referências

Anhaeusser, C.R., 2014. Archaean greenstone belts and associated granitic rocks - A review. Journal of African Earth Sciences 100, 684-732.

Barbuena, D., Oliveira, E.P., Zincone, S.A., 2016. Estudos de proveniência dos quartzitos do Greenstone Belt Mundo Novo (BA) e implicações tectono-estratigráficas. In: 48° Congresso Brasileiro de Geologia. Porto Alegre, Anais, p. 818.

Chavagnac, V., 2004. A geochemical and Nd isotopic study of Barberton komatiites (South Africa): implication for the Archean mantle. Lithos 75, 253-281.

Couto, P.A., Sampaio, A.R., Gil, C.A.A., Loureiro, H.C., Arcanjo, J.B., Fernandes Filho, J., Guimarães, J.T., Campelo, R., Mascarenhas, J.F., Bruni, D.C., Toledo, L.A.A., 1978. Projeto Serra de Jacobina: Geologia e Prospecção Geoquímica. Convênio DNPM-CPRM, Relatório Final. Salvador, 1, 415 p.

De Wit, M.J., Hart, R.A., Hart, R.J., 1987. The Jamestown ophiolite complex, Barberton mountain belt: a section through 3.5 Ga oceanic crust. Journal of African Earth Sciences 5, 681-730.

Dziggel, A., Stevens, G., Poujol, M., Anhaeusser, C.R., Armstrong, R.A., 2002. Metamorphism of the granite-greenstone terrane south of the Barberton greenstone belt, South Africa: an insight into the tectono-thermal evolution of the 'lower' portions of the Onverwacht Group. Precambrian Research 114, 221-247.

Franklyn, J.M., Gibson, H.L., Jonasson, I.R., Galley, A.G., 2005. Volcanogenic Massive Sulfide Deposits. Economic Geology 100th anniversary volume, 523-560.

Furnes, H., de Wit, M., Robins, B., 2013. A review of new interpretations of the tectonostratigraphy, geochemistry and evolution of the Onverwacht Suite, Barberton Greenstone Belt, South Africa. Gondwana Research 23 (2), 403-428.

Leite, C.M.M., 2002. A Evolução Geodinâmica da Orogênese Paleoproterozóica nas Regiões de Capim Grosso, Jacobina e Pintadas - Mundo Novo (Bahia-Brasil): Metamorfismo, Anatexia Crustal e Tectônica. Ph. D. Thesis, Universidade Federal da Bahia, Salvador, 408 p.

Loureiro, H.S.C., 1991. Programa Levantamentos Geológicos Básicos do Brasil. Mundo Novo. Folha SC24-Y-D-IV. Estado da Bahia. Salvador, DNPM/CPRM, 177 p.

Mascarenhas, J.F., Silva, E.F.A., 1994. Greenstone Belt de Mundo Novo: caracterização e implicações metalogenéticas e geotectônicas no Cráton do São Francisco. Série Arquivos Abertos, n. 5, 32 p.

Monteiro, M.D., Silva, R.W.S., Cunha, J.C., 2009. Projeto Fazenda Coqueiro. Salvador: CBPM, 57 p.

Mougeot, R., 1996. Étude de la limite Archéen-Protérozoïque et des minéralisations Au ± U associées. Exemples de la région de Jacobina (Etat de Bahia, Brésil) et de Carajas (Etat de Para, Brésil). 1996. 306 f. Thèse de l'Université de Montpellier II, Montpellier.

Parman, S.W., Grove, T.L., Dann, J.C., 2001. The production of Barberton komatiites in an Archean subduction zone. Geophysical Research Letters 28 (13), 2513-2516.

Peucat, J.J., Mascarenhas, J.F., Barbosa, J.S.F., Souza, S.L., Marinho, M.M., Fanning, C.M., Leite, C.M.M., 2002. 3.3 Ga SHRIMP U-Pb zircon age of a felsic metavolcanic rock from the Mundo Novo Greenstone Belt in the São Francisco Craton, Bahia (NE Brazil). Journal of South American Earth Sciences 15 (3), 363-373.

Sabaté, P., Marinho, M.M., Vidal, P., Caen Vachette, M., 1990. The 2-Ga peraluminous magmatism of the Jacobina–Contendas Mirante belts (Bahia, Brazil): geologic and isotopic constraints on the sources. Chemical Geology 83 (3-4), 325-338.

Souza, S.L., Garrido, I.A.A., Oliveira, N.S., Fróes, R.J., 2002. Projeto Greenstone Belt de Mundo Novo: estudos geológicos regionais. Salvador: CBPM, 1, 62 p.

Spreafico, R.R., 2017. Projeto Mundo Novo: texto e mapas. Salvador: CBPM, 2017. 84 p.

Spreafico, R.R., Barbosa, J.S.F., Barbosa, N.S., Moraes, A.M.V., 2019. Tectonic evolution of the Neoarchean Mundo Novo greenstone belt, eastern São Francisco Craton, NE Brazil: petrology, U-Pb geochronology, and Nd and Sr isotopic constraints. Journal of South American Earth Sciences 95.

Storey, M., Mahoney, J.J., Kroenke, L.W., Saunders, A.D., 1991. Are oceanic plateaus sites of komatiite formation? Geology 19, 376-379.

Zincone, S.A., Barbuena, D., Oliveira, E.P., Baldim, M.R., 2017. Detrital zircon U-Pb ages as evidence for deposition of the Saúde Complex in a Paleoproterozoic foreland basin, northern São Francisco Craton, Brazil. Journal of South American Earth Sciences 79, 537-548.

Zincone, S.A., Oliveira, E.P., Laurent, O., Zhang, H., Zhai, M., 2016. 3.3 Ga High-Silica Intraplate Volcanic-Plutonic System of the Gavião Block, São Francisco Craton, Brazil: Implications of an intracontinental rift following the creation of insulating continental crust. Lithos 266-267, 414-434.

CAPÍTULO 2

ARTIGO 1 - GEOLOGY AND PETROLOGY OF METAVOLCANIC ROCKS IN THE NEOARCHEAN MUNDO NOVO GREENSTONE BELT, EASTERN SÃO FRANCISCO CRATON, NE BRAZIL: TECTONIC SETTING CONSIDERATIONS

Abstract

Field and petrological data of metakomatiite, eastern and western metabasalts and metadacite were used to propose an intraoceanic or intracontinental provenance for the Neoarchean Mundo Novo greenstone belt (MNGB), eastern São Francisco Craton. Despite deformation, the metakomatiite preserves the spinifex texture and the eastern metabasalt's pillow lava structure. The metavolcanics are recovered by an ocean floor lithological association composed of chemical metasedimentary rocks and the western metabasalt hosts ocean floor hydrothermal alteration zones. The eastern metabasalt plots in the IAT and MORB fields and western metabasalt is mainly in the MORB field in the Zr vs. Zr/Y diagram, suggesting nearby oceanic settings. Heterogeneous crustal assimilation and metamorphism during the Rhyacian-Orosirian explain the mineralogical differences between the two metabasalts. The metakomatiite and metabasalts feature a vector from the MORB-OIB array to the volcanic arc array in the Nb/Yb vs. Th/Yb diagram, similar to the intraoceanic arc-basin system of the Archean greenstone belts. The average $(La/Yb)_N$ ratio of 8.87 for the metadacite indicates a crustal contamination in subducting oceanic crust. An intraoceanic provenance in arc-basin settings and oceanic crust assimilations are proposed for the Neoarchean MNGB, which was posteriorly compressed between cratonic blocks during the Rhyacian-Orosirian, and lies in the Contendas-Jacobina Lineament.

Keywords: Mundo Novo greenstone belt; metavolcanic rocks; intraoceanic setting; petrology; São Francisco Craton

1. Introduction

The Neoarchean Mundo Novo greenstone belt (MNGB), in the eastern boundary of the Gavião Block (Barbosa & Sabaté 2002, 2003, 2004) and eastern portion of the São Francisco Craton, and lying within the Contendas-Jacobina Lineament (Sabaté *et al*. 1990), NE Brazil, hosts the Zn-Pb Fazenda Coqueiro deposit and has been a subject of study since the 1970s (Mascarenhas *et al*. 1975, Mascarenhas 1976, Couto *et al*. 1978, Loureiro 1991, Mascarenhas & Silva 1994, Mascarenhas *et al*. 1998, Zincone *et al*. 2016, Reis *et al*. 2017; Figs. 1A, 1B and 1C). However, the MNGB lacks detailed discussions on its tectonic setting of volcanism, mainly concerning its intraoceanic or intracontinental provenance.

Greenstone belts are highly varied Archean geological entities that contain a vast diversity of rocks. Generally, their rocks experienced multiple stages of deformation, metamorphism and metasomatic alteration due their great age and diversity of geotectonic settings, which was intruded by mafic, ultramafic and granitoid rocks (Anhaeusser 2014). Moreover, the intraoceanic or intracontinental provenance of volcanic rocks in Archean greenstone belts has been a recurring discussion topic and whole-rock chemical tools have been constantly applied for such research purposes (Polat & Kerrich 2001, Polat *et al*. 2002, Pearce 2008, 2014).

The predominance of subaqueously deposited basalt and komatiite has been interpreted in a wide variety of geological settings proposed for greenstone belt terrains in intraoceanic crust, ranging from primitive island arcs to plume-related submarine plateaus, mid-ocean ridges (including ophiolites) and back-arc basins (De Wit *et al*. 1987, Storey *et al*. 1988, Parman *et al*. 2001, Chavagnac 2004, Furnes *et al*. 2013). Furthermore, the intraoceanic Archean greenstone belts present a set of evidence as follows: basalt and komatiite occurrence, the absence of zircon xenocrysts, mid-ocean ridge basalt (MORB) and island arc tholeiitic (IAT) geochemical patterns, and Th enrichment due to crustal contamination processes (Pearce 2008). The crustal contamination, however, would have been produced by subduction components, metamorphism, intraoceanic contamination, crustal recycling, high Th-Nb proxy and delamination (Pearce 2008, 2014).

The metabasalt of the Nova Lima Group in the Archean Rio das Velhas greenstone belt of the southern São Francisco Craton (Fig. 1B), for example, has been considered as derived from an ocean-floor setting based on a pillow lava structure and an association with chemical sediments and volcanic rocks (Zucchetti *et al*. 2000b). Moreover, the geochemical pattern of this metabasalt suggests a submarine plateau setting and crustal contamination rocks; the felsic volcanic rocks would indicate the presence of an island arc or back-arc type setting (Zucchetti *et al*. 2000a). In the Neoarchean Contendas-Mirante volcano-sedimentary sequence, south of the Contendas-Jacobina Lineament (Fig. 1B), which contains geochemical and age equivalences with the MNGB, intraoceanic basalt occurrences have been interpreted as being related to banded iron formation (BIF; Rios 2017). The South Abitibi (Kerrich & Xie 2002, Xie & Kerrich 1994), Barberton (Jochum *et al*. 1991, Parman *et al*. 1997, Chavagnac 2004) and Isua (Polat & Hofmann 2003, Polat *et al*. 2002) are other examples of intraoceanic interpretations for Archean greenstone belts, which Pearce (2008) discusses in his examination of the ocean floor's origin with crustal contamination along their geological evolution based on a Th-Nb proxy. Despite the contamination issues of analyzing Archean rocks, the geochemical pattern of the modern Mariana Arc, which indicates an arc-basin system in oceanic crust, was properly used to compare to older intraoceanic settings in the Nb/Yb vs. Th/Yb diagram (Pearce 2005, 2008).

The intracontinental provenance of volcanic rocks in Archean greenstone belts, on the other hand, has been related to oceanic-continent subduction processes or with the genesis on ensialic settings (Pearce 2008). Greenstones of the Wawa belt in the Superior Province, for

example, were formed in an arc-related association (Polat & Kerrich 2001); the Umburanas greenstone belt in the eastern São Francisco Craton (Fig. 1B) was formed over a continental crust (Leal *et al*. 2003). Bickle *et al*. (1994) concluded that the continental provenance for Archean greenstone belts could not easily identify complete ophiolitic sequences, which would thus explain a possible oceanic origin; the presence zircon xenocrysts, geochemical and isotopic evidence for crustal contamination, intrusive relationships with older basement rocks and their internal stratigraphy would also indicate continental provenance.
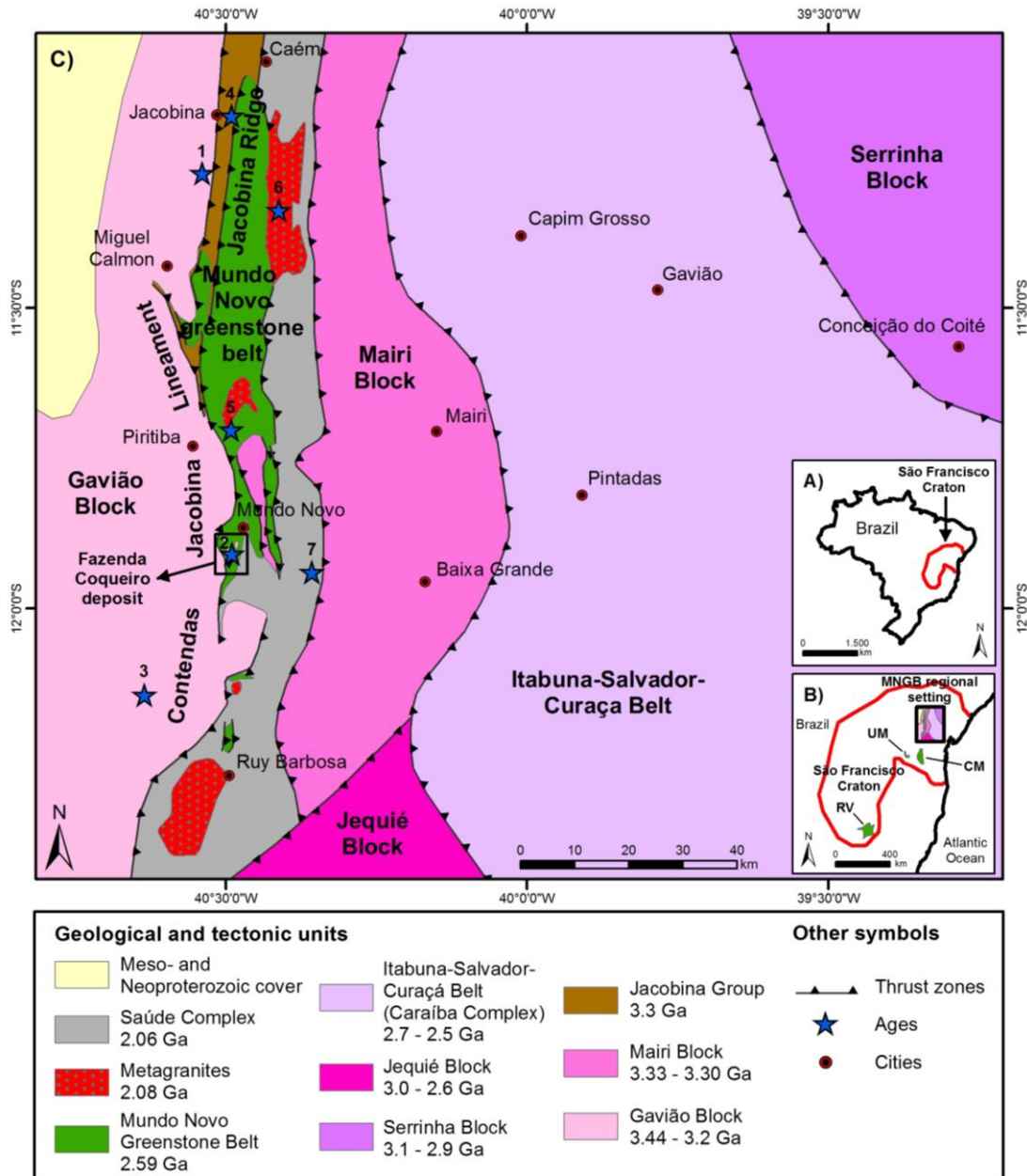
Figure 1. A) Location of the São Francisco Craton in NE Brazil. B) Study area in the eastern portion of the São Francisco Craton and other greenstone belts and volcano-sedimentary sequences: **CM**- Contendas-Mirante; **RV**-Rio das Velhas; **UM**- Umburanas. C) Regional tectonic setting where the MNGB is inserted (modified from Barbosa & Sabaté 2002, 2003, 2004). Ages in the points highlighted on the map: **1-** 3442 ± 2 Ma (U-Pb zircon, TTG; Mougeot 1996); **2-** 3303 ± 11 Ma (U-Pb zircon, metarhyolite from the Gavião Block obtained by Zincone *et al*. 2016); **3-** 3292 ± 3 Ma (U-Pb zircon, metagranite from the Gavião Block obtained by Zincone *et al*. 2016); **4-** 3500 - 3220 Ma (U-Pb zircon, quartzite from the Jacobina Group obtained by Teles *et al*. 2015); **5-** 2595 ± 21 Ma (U-Pb zircon, metadacite from the MNGB obtained by Spreafico *et al*. 2018); **6-** 2080 ± 18 Ma (U-Pb monazite, Cachoeira Grande granite obtained by Leite 2002); **7-** 2068 ± 12 Ma (U-Pb zircon, biotite schist from the Saúde Complex obtained by Zincone *et al*. 2017).

Therefore, field, petrographic and whole-rock chemical data from the metakomatiite, eastern and western metabasalts and metadacite in the MNGB, completed by the mineral chemistry of the two metabasalts, were used to characterize the metavolcanic rocks and study the tectonic setting of the MNGB. The intraoceanic provenance of the volcanic rocks rather than the intracontinental provenance and a comparison with other Archean greenstone belts were also considered. The insertion of the Neoarchean MNGB within the regional geologic context in the eastern portion of the São Francisco Craton and the subsequent tectonic events were also contemplated.

2. Geological setting

The eastern portion of the São Francisco Craton, where the MNGB is situated (state of Bahia), was formed through the amalgamation of four Archean blocks during the Paleoproterozoic continent-continent collision (Barbosa & Sabaté 2002, 2003, 2004): the Gavião, Serrinha and Jequié blocks and the Itabuna-Salvador-Curaçá Belt (Fig. 1C). The Paleoproterozoic event captured the MNGB and surrounding crust between the cratonic blocks, and the uplift caused by this event possibly resulted in the erosion and the formation of Paleoproterozoic sedimentary basins, such as the uppermost sequence of the MNGB and the Saúde Complex.

Briefly, the MNGB is in contact to the west with 3.4 Ga (Mougeot 1996) tonalite-trondhjemite-granodiorite (TTG) basement rocks and subordinate metagranites in the Gavião Block and to the east and south with paragneiss in the Saúde Complex with a maximum age between 2.20 and 2.06 Ga (Zincone *et al*. 2017; Fig. 2). To the north and northwest, the MNGB is in contact with quartzites in the Jacobina Group, which were deposited between 3.55 and 3.22 Ga (Teles *et al*. 2015), and Paleoproterozoic granitic intrusives.

Additionally, the geological setting includes granulites (3.0 Ga) and multiple charnockite intrusions (2.7 and 2.6 Ga) in the Jequié Block (Wilson 1987, Silva *et al*. 2002), the Itabuna-Salvador-Curaçá Belt (2574 ± 6 Ma and 2695 ± 12 Ma obtained by Oliveira *et al*. 2010, Silva *et al*. 1997; respectively), and the Serrinha Block (3152 ± 5 Ma obtained by Oliveira *et al*. 2002a, 2002b; 2989 ± 11 Ma, 3072 ± 2 Ma and 3162 ± 26 Ma obtained by Rios *et al*. 2009); although the Itabuna-Salvador-Curaçá Belt and Serrinha Block are far from the MNGB, they are important for understanding the collisional Paleoproterozoic tectonic context of the study area (Fig. 1C). Table 1 shows regional geochronological data from the MNGB and surrounding units.

The eastern margin of the Gavião Block is in tectonic contact with the lithologies of the MNGB (Fig. 1C) and is composed of TTG gneiss and migmatites that host mafic rock enclaves (Barbosa *et al*. 2012a), metagranites and metarhyolites (Zincone *et al*. 2016). This block corresponds to the basement of the MNGB. Three groups of TTG gneiss are described in the Gavião Block: two groups are trondhjemitic with U-Pb zircon ages (SHRIMP) of 3403 ± 5 Ma and 3158 ± 5 Ma (Barbosa 1997, Leal 1998), and the other group, with granodioritic compositions, includes the 3225 ± 10 Ma Aracatu granitoid (Barbosa *et al*. 2012a). The Gavião Block age, near the MNGB, is 3.4 Ga (Mougeot 1996), but metarhyolites with ages of 3303 ± 11 Ma (Peucat *et al*. 2002, Zincone *et al*. 2016) and metagranites, such as Boa Sorte at 3291 ± 2.5 Ma, occur as well (Zincone *et al*. 2016).

The Mairi Block, composed of gneiss, migmatites, and granitic and tonalitic orthogneiss, with some occurrences of basic and ultrabasic bodies (Peucat *et al*. 2002) to the east and southeast of the MNGB, is in tectonic contact with thrust zones with a west vergence. The LA-ICP-MS U-Pb zircon ages of 3.33 Ga and 3.30 Ga (Sousa *et al*. 2018) for the orthogneiss in the Mairi Block indicate that this complex is coeval with the Gavião Block and, therefore, the two may have been joined at the time of their formation.

The Jacobina Group is in tectonic contact with the MNGB along thrust zones, with all zones striking north-south and verging to the west (Fig. 1C) with the Gavião Block in the footwall. The Jacobina Group comprises metaconglomerates that host an important gold deposit, quartzites, metarenites, phyllites, chlorite schists and quartz-sericite schists (Mascarenhas *et al.* 1998) deposited in a passive margin setting (Reis *et al.* 2018). This group has a depositional age, based on detrital zircons, between 3500 Ma and 3220 Ma (Teles 2013, Teles *et al.* 2015, Barbuena *et al.* 2016), with a large portion of the zircon populations situated between 3.3 Ga and 3.4 Ga (Magee *et al.* 2001, Teles *et al.* 2015). Jacobina Ridge represents an Archean supracrustal sequence with a maximum age of 3.28 Ga, and its sources are likely rocks from both the plutonic-volcanic system and the TTG suite in the Gavião Block (Zincone *et al.* 2016).

The MNGB, which Zincone *et al.* (2016) referred to as the Mundo Novo supracrustal belt, is inserted into the Contendas-Jacobina Lineament and is divided into three stratigraphic sequences - a lower sequence (ultramafic rocks), a middle sequence (mafic and felsic igneous rocks and clastic and chemical metasedimentary rocks) and an upper sequence (siliciclastic metasedimentary rocks; Spreafico *et al.* 2018). Carbonate and argilic-chloritic hydrothermal alteration zones in the ocean floor setting have been identified and described in the Fazenda Coqueiro deposit related to Zn-Pb mineralization hosted in the western metabasalt of the middle sequence (Spreafico 2017). Two ductile and compressional and progressive Paleoproterozoic deformational phases in the MNGB, D_1 and D_2, are described in the area in a previous study (Spreafico 2017). The D_1 deformational phase is characterized by isoclinal and recumbent folds vergent to the west that generated greenschist metamorphic facies rocks. The D_2 deformational phase is characterized by a refolding that generated vertical and subvertical axial planes that eventually resulted in the formation of a coaxial interference pattern (Ramsay & Huber 1987) or compressive and transpressive shear zones, which bound the MNGB lithologies and generated greenschist rocks to amphibolite metamorphic facies. The most prominent brittle structures are east-trending faults and fractures. The age of the MNGB has been previously studied, and geochronological studies have defined the Neoarchean age of the volcanism (Spreafico *et al.* 2018), such as the Paleoproterozoic sedimentation on the top of the sequence (Barbuena *et al.* 2016), which is coeval with the Rhyacian-Orosirian tectonothermal event (Leite 2002, Spreafico 2017). These rocks lie upon the 3.4 - 3.2 Ga basement rocks of the northern part of the Gavião Block comprised of TTG gneiss, metagranites and metarhyolites (Mougeot 1996, Barbosa 1997, Leal 1998, Peucat *et al.* 2002, Barbosa *et al.* 2012a, Zincone *et al.* 2016).

The Saúde Complex occurs to the east of the MNGB (Fig. 1C), where the two units are in tectonic contact along west-vergent thrust zones. This complex comprises aluminous paragneiss, biotite gneiss and subordinate quartzites that are widely distributed in a north-south trend with significant occurrences in the Mundo Novo region and in the eastern portion of the Jacobina Ridge (Couto *et al.* 1978, Mascarenhas *et al.* 1998, Leite *et al.* 2007, Reis *et al.* 2017; Fig. 1C). The maximal depositional age of 2.06 Ga (Zincone *et al.* 2017) for the Saúde Complex again indicates the presence of a basin near the MNGB in the Paleoproterozoic; however, the rocks in the Saúde Complex were subjected to a higher metamorphic grade than the sedimentary rocks at the top of the MNGB along the tectonic contact.

Finally, Rhyacian-Orosirian granites are present along the Contendas-Jacobina Lineament (Leite 2002, Spreafico 2017; Fig. 1C). In general, these granites are undeformed leucogranites, comprising quartz, feldspar, biotite and muscovite with some occurrences of garnet and sillimanite (Barbosa *et al.* 2012b). The Cachoeira Grande granite, for example, is a peraluminous leucogranite situated to the northeast of the MNGB, which has an average age

of 2080 ± 18 Ma (Leite 2002), and is coeval with the Rhyacian-Orosirian granitic intrusions in the MNGB (Spreafico 2017, Spreafico *et al*. 2018).

Table 1. Compilation of regional geochronological data of the MNGB and surrounding units

Geological/tectonic unit	Lithotype	Age	Method	Mineral dated	Author
Saúde Complex	Biotite schist	2068 ± 12 Ma	U-Pb (LA-MC-ICP-MS)	Detrital zircon	Zincone *et al*. (2017)
Cachoeira Grande granite	Leucogranite	2080 ± 18 Ma	U-Pb (Electron microprobe)	Monazite (crystallization age)	Leite (2002)
Upper sequence (MNGB)	Quartzite	2133 ± 14 Ma	U-Pb (LA-ICP-MS)	Detrital zircon	Barbuena *et al*. (2016)
Mundo Novo greenstone belt	Metadacite	2595 ± 21 Ma	U-Pb (LA-ICP-MS)	Zircon (crystallization age)	Spreafico *et al*. (2018)
Itabuna-Salvador-Curaçá Belt	Tonalitic granulite	2574 ± 6 Ma	U-Pb (SHRIMP)	Zircon (crystallization age)	Oliveira *et al*. (2010)
	Enderbite	2695 ± 12 Ma	U-Pb (SHRIMP)	Zircon (crystallization age)	Silva *et al*. (1997)
Jequié Block	Granulites	2715 ± 29 Ma	U-Pb (SHRIMP)	Zircon (crystallization age)	Silva *et al*. (2002)
	Charnockite	2900 ± 24 Ma	Rb-Sr	Whole-rock (crystallization age)	Wilson (1987)
Serrinha Block	Granitoid	2989 ± 11 Ma 3072 ± 2 Ma 3162 ± 26 Ma	U-Pb (SHRIMP)	Zircon (crystallization age)	Rios *et al*. (2009)
	Gneiss, migmatite	3152 ± 5 Ma	U-Pb (SHRIMP)	Zircon (crystallization age)	Oliveira *et al*. (2002a, 2002b)
Jacobina Group	Quartzite	3500 - 3220 Ma	U-Pb (LA-MC-ICP-MS)	Detrital zircon	Magee *et al*. (2001); Teles (2013); Teles *et al*. (2015); Barbuena *et al*. (2016)
Mairi Block	Orthogneiss	3.33 - 3.30 Ga	U-Pb (LA-SF-ICP-MS)	Zircon (crystallization age)	Sousa *et al*. (2018)
Gavião Block	Metagranite	3291 ± 2.5 Ma	U-Pb (LA-ICP-MS)	Zircon (crystallization age)	Zincone *et al*. (2016)
	Metarhyolite	3303 ± 11 Ma	U-Pb (LA-ICP-MS and SHRIMP)	Zircon (crystallization age)	Peucat *et al*. (2002); Zincone *et al*. (2016)
	TTG	3442 ± 2 Ma	U-Pb (ID-TIMS)	Zircon (crystallization age)	Mougeot (1996)

3. Analytical methods

The study of the metavolcanic rocks of the MNGB and considerations of the tectonic setting involved petrography, mineral chemistry and whole-rock chemical analyses.

For petrography, we analyzed 127 thin sections of metakomatiite, eastern and western metabasalts and metadacite to determine the mineralogical composition, textures and microstructures of the rocks using the ZEISS Axio Scope.A1 microscope provided by Companhia Baiana de Pesquisa Mineral (CBPM). The mineral abbreviations used on photomicrographs mainly follow those of Kretz (1983) and Siivola & Schmid (2007) and are completed with abbreviations of Whitney & Evans (2010).

Six of the thin sections were used for mineral chemistry analysis to detail the mineral differences between the two metabasalt types complementing the petrographic studies. Thus, a CAMECA SX50 electron microprobe was used with four wavelength-dispersive spectroscopes (WDS) and one Kevex energy dispersive spectroscope (EDS) of the University of Brasília. The standards used are naturals and synthetics with defined compositions, such as albite (for the element Na_2O), andradite (for the elements CaO and FeO), forsterite (for the element MgO), microcline (for the elements Al_2O_3, SiO_2 and K_2O), $MnTiO_3$ (for the element TiO_2) and $MnTiO_3$ (for the element MnO). The analyzed spots were selected on polished

sections in plagioclase (6 spots in 5 samples), amphibole (6 spots in 5 samples), pyroxene (4 spots in 2 samples), ilmenite (2 spots in 2 samples), titanite (2 spots in 2 samples) and biotite (1 spot in 1 sample) grains (Table 2). The chemical contents are expressed by SiO_2, TiO_2, Al_2O_3, FeO, MnO, MgO, CaO, Na_2O and K_2O. The data were processed using the Gabbrosoft spreadsheets (http://www.gabbrosoft.org) and the plagioclase results were plotted in the ternary diagram of feldspar; the amphiboles were plotted in the calcic amphibole diagrams (Leake *et al*. 1997) and the pyroxene in the classification diagram of pyroxenes (Morimoto 1988) using the Minpet program. The EDS data were used to show evidence of manganiferous ilmenite, and in this case, a backscattered electron image was obtained.

The whole-rock chemical analysis of 49 samples was conducted in the SGS-Geosol laboratory. The samples were dried and crushed so 75 % of the sample was smaller than 3 mm. A 300 g sample was quartered and pulverized (until 95 % was smaller than 105 microns) to form a powder for subsequent processes. The powders were melted at a high temperature with lithium metaborate, and the major, minor, trace, and rare earth elements (REE) were determined using ICP-MS and inductively coupled plasma optical emission spectrometry (ICP-OES) analysis. The international standard samples used are TILL-3 (a description and values are in Lynch 1996) and GRE-05 (reference material from Geostats PTY Ltd.). The error for all analyzed elements in each sample was calculated based on analytical accuracy according to the content of the analyte in the sample, the statistical detection limit and the repeatability limit, and represented in terms of standard deviation (1σ) (Thompson, 1988). The coefficient of variation of the analytical results for each element by sample analyzed, calculated from the standard deviation (1σ), was predominantly lower than 15%, which corresponds to well-represented results around the arithmetic mean. Only the samples with a loss on ignition (LOI) values of ≤ 5 % were considered. The geochemical data were plotted and interpreted using the GCDKit software (Janousek *et al*. 2006). The data in the REE diagram and the $(La/Yb)_N$, $Eu/Eu*$ and $(Gd/Yb)_N$ ratios were normalized by chondrite values (Boynton 1984), and the data in the multielement diagram were normalized by N (normal)-MORB values (Hofmann 1988).

4. Geological, petrographic and mineral chemistry characterization

The geologic characterization of the Neoarchean MNGB, which was carried out to support interpretations of the tectonic setting, consisted of field and petrographic observations performed in metavolcanic rocks, including metakomatiite, eastern and western metabasalts and metadacite (Fig. 2). The mineral chemistry was used to detail petrographic analyses in the eastern and western metabasalts.

4.1. Mundo Novo greenstone belt

Many Paleo- to Neoarchean greenstone belts have been characterized as volcano-sedimentary sequences deformed and metamorphosed over time at low to medium grades; they show, from the base to the top, a progressive variation from volcanic (ultramafic, mafic and felsic rocks) to sedimentary rocks (chemical and clastic rocks); they are commonly associated with orthogneisses and are intruded by syn- to posttectonic granites (Anhaeusser 2014).

Based on these concepts, the MNGB is interpreted as part of a typical greenstone belt terrain and is divided into three stratigraphic sequences: the **lower sequence**, composed of metakomatiite; the **middle sequence**, composed of eastern and western metabasalts and, subordinately, tremolitite, calc-silicate rock (carbonate hydrothermal alteration zone), aluminous schist (argilic-chloritic hydrothermal alteration zone), BIF, ferruginous metachert,

metadacite and metarhyolite; and the **upper sequence**, composed of siliciclastic metasedimentary rocks, such as metarenite, quartzite, metagraywacke, metasiltite, phyllite, rhythmite, quartz-sericite schist and garnet-tremolite-quartz schist (Fig. 2). This study focused on metavolcanic rocks of the lower and middle sequences.
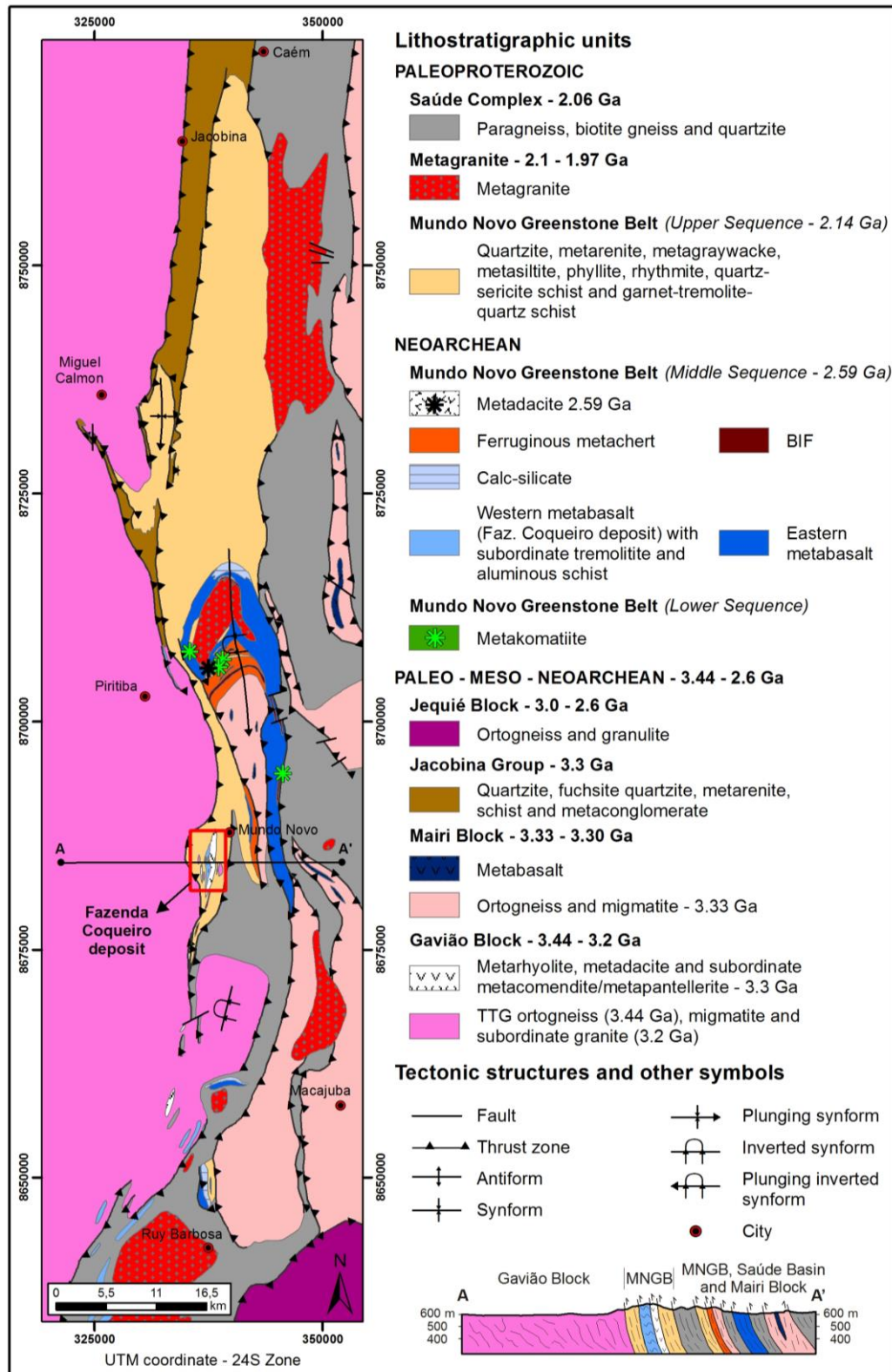
Figure 2. Geologic map of the MNGB and adjoining units. Modified and updated from Loureiro (1991), Mascarenhas & Silva (1994) and Souza *et al*. (2002).

Lower Sequence

The lower sequence is composed of metakomatiite located at the base of the MNGB and comprises the ultramafic volcanic component of the MNGB. The metakomatiite has field relationships with the mafic volcanic rock of the middle sequence; however, these rocks are separated into different sequences due to the mineral content and the textural particularities. There are four restricted occurrences of metakomatiite in the central portion of the MNGB (Fig. 2), which are northeast of Mundo Novo city and northeast of Piritiba city.

Generally, the metakomatiite of the MNGB has a relict spinifex texture composed of skeletal grains with planar growths that intersect each other (Figs. 3A and 4A) and do not intercept former structures for igneous relicts' texture in komatiites as Arndt (1994) described. The fine-grained spinifex texture is identified only in hand samples or by using a hand lens or microscope.

The metakomatiite of the MNGB has a light green color and a silky aspect and is not magnetic (Fig. 3A). The olivine and pyroxene crystals are entirely replaced by acicular and prismatic pseudomorphic grains of anthophyllite and tremolite (80 % of the rock) with a grain size of 0.5 mm (Fig. 4A). The fine-grained groundmass is composed of talc and clinochlore (20 % of the rock) without a preferred orientation. Traces of pyrite and pyrrhotite are dispersed in the sample.
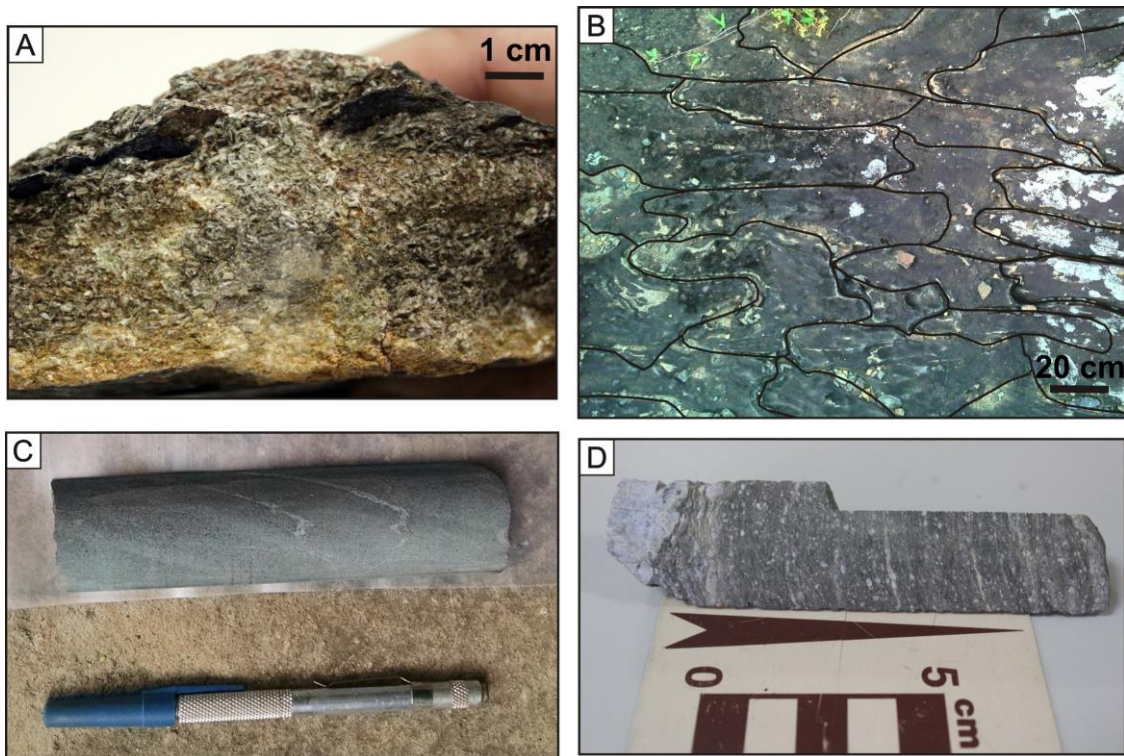
Figure 3. A) Typical spinifex texture of the MNGB metakomatiite. B) Highlighted pillow lava structure of the eastern metabasalt from south of the MNGB. C) Drill hole sample of the western metabasalt in the MNGB. D) Drill hole sample of the porphyroclastic metadacite in the MNGB.
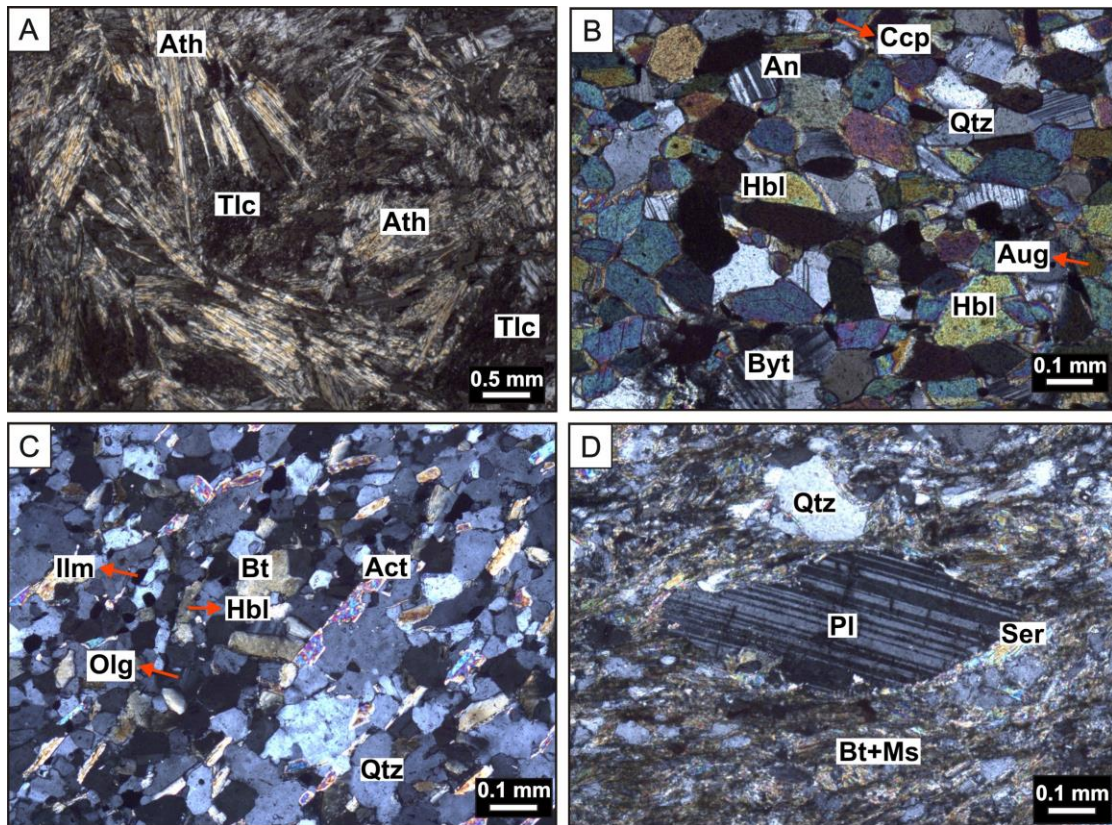
Figure 4. Petrographic images of the MNGB: A) Spinifex texture of metakomatiite composed of pseudomorphic anthophyllite lath in a fine-grained groundmass of talc (XP, 2,5×; sample FD-058A). B) Granonematoblastic texture of the eastern metabasalt (XP, 10×; sample RR-018A). C) Typical very fine-grained texture of the western metabasalt (XP, 10×; sample RR-F6-001). D) Porphyroclast of plagioclase with a sericitized border in a fine-grained groundmass of quartz, biotite and muscovite in the metadacite in the middle sequence of the MNGB (XP, 10×; sample FD-052). Mineral abbreviations: Act: actinolite, An: anorthite, Ath: anthophyllite, Aug: augite, Bt: biotite, Byt: Bytownite, Ccp: chalcopyrite, Hbl: hornblende, Ilm: ilmenite, Ms: muscovite, Olg: oligoclase, Pl: plagioclase, Qtz: quartz, Ser: sericite, and Tlc: talc. XP: crossed polarizers.

Middle Sequence

The middle sequence is composed of metabasalt and, subordinately, tremolitite, calc-silicate rock, aluminous schist, BIF, ferruginous metachert, metadacite and subordinate metarhyolite; metabasalt and metadacite are the main topics of this study.

Metabasalt and metadacite are the terms used in this paper to define the mafic and felsic volcanic components, respectively, of the middle sequence of the MNGB. This terminology was adopted based on the protolith because of its usefulness in determining the original nature of the rock, even though in many cases, a protolith name does not reflect the principal minerals and structural features of the rocks under observation (Schmid *et al*. 2007). Moreover, some occurrences of metavolcanic mafic rocks in the MNGB preserve primary structures such as pillow lava. Therefore, the term metabasalt is used in this manuscript rather than amphibolite, which is also correctly used if the texture and mineral content are considered as proposed by Fettes & Desmons (2007).

The metabasalts are distributed along a north-south trend (Fig. 2) and are divided into two coeval groups based on petrography, supported by mineral chemistry analysis, and whole-rock chemical data. The first group, defined as the eastern metabasalt, occurs along the eastern portion of the MNGB and corresponds to the main outcrops of the sequence near Piritiba city and extending to Ruy Barbosa city (Fig. 2). The second group, defined as the western metabasalt, occurs along the western portion of the MNGB, mainly within the

Fazenda Coqueiro deposit (Mundo Novo city), and in a restricted area with a north-south trend near Piritiba city (Fig. 2).

4.1.1. Eastern metabasalt

The eastern metabasalt preserves the pillow lava structures that occur in a large area to the south of the MNGB (Fig. 3B). It is composed of anorthite (15 %), bytownite (15 %), magnesiohornblende and ferrohornblende (40 %), small amounts of oligoclase (5 %) and low percentages (20 % combined) of augite, edenite and quartz, as well as ilmenite and titanite as accessory minerals, and traces of pyrrhotite, chalcopyrite and igneous relicts of hypersthene micrograins identified only in microprobe analysis (5 %; Table 2; Figs. 5A, 5B, 5C and 5D). The minerals show polyhedral contacts with nematoblastic and granonematoblastic textures (Fig. 4B).

4.1.2. Western metabasalt

The western metabasalt hosts the Zn and Pb sulfides of the Fazenda Coqueiro deposit, particularly in carbonate hydrothermal alteration zones, and is easily observed from drill hole samples (Fig. 3C). Based on petrography and mineral chemistry results, this rock is very fine grained and is mainly composed of oligoclase and andesine (50 %), actinolite, magnesiohornblende and ferrotschermakite (30 %) with a low percentage of quartz, biotite and igneous relicts of hypersthene micrograins (15 %), as well as ilmenite and titanite as accessory minerals (5 %; Table 2; Figs. 5A, 5B, 5C and 5D). Traces of manganiferous ilmenite (Figs. 6A and 6B), pyrrhotite, pyrite, chalcopyrite, galena, sphalerite and arsenopyrite are also observed. The grains of biotite and actinolite are oriented and define highly developed planes of foliation (Fig. 4C).

Table 2. Electron microprobe data of minerals in the eastern and western metabasalts (wt. %)

Geologic unit	Sample ID	Mineral	SiO$_2$	TiO$_2$	Al$_2$O$_3$	FeO	MnO	MgO	CaO	Na$_2$O	K$_2$O	Sum
Eastern metabasalt	RR-072	Anorthite	46.60	0.08	35.37	0.29	0	0.01	18.41	1.17	0.03	101.96
Eastern metabasalt	RR-072	Anorthite	46.15	0	35.53	0.38	0	0.01	18.34	1.09	0.02	101.52
Eastern metabasalt	RR-018A	Bytownite	49.26	0.08	32.93	0.16	0.11	0.02	15.80	2.56	0.10	101.02
Eastern metabasalt	RR-011C	Oligoclase	62.40	0	22.79	0.09	0	0	3.50	9.20	0.08	98.06
Eastern metabasalt	RR-072	Fe-Hornblende	44.13	0.3	14.20	17.28	0.19	8.92	11.76	1.08	0.24	98.1
Eastern metabasalt	RR-011C	Mg-Hornblende	48.25	0.12	7.27	12.51	0.24	14.27	11.07	1.53	0.14	95.40
Eastern metabasalt	RR-018A	Edenite	51.46	0.18	0.62	14.97	0.41	9.19	22.71	0.16	0.01	99.71
Eastern metabasalt	RR-072	Hypersthene	53.07	0.19	0.55	25.94	0.60	15.04	0.93	0.06	0	96.38
Eastern metabasalt	RR-072	Hypersthene	52.59	0.04	1.00	26.40	0.56	15.07	1.40	0.08	0	97.14
Eastern metabasalt	RR-072	Hypersthene	52.77	0.18	0.40	26.53	0.74	15.14	0.86	0.07	0	96.69
Eastern metabasalt	RR-072	Ilmenite	0.10	50.58	0.03	45.84	0.79	0.07	0.02	0.03	0.01	97.47
Eastern metabasalt	RR-072	Titanite	16.79	42.49	1.06	25.39	0.66	0.70	14.00	0.03	0	101.12
Western metabasalt	RR-F6-001	Oligoclase	59.95	0.23	23.20	0.04	0	0	5.09	8.71	0.04	97.26
Western metabasalt	RR-F6-010	Andesine	56.79	0.03	26.89	0.14	0	0	9.04	6.45	0.05	99.39
Western metabasalt	RR-F1-001	Mg-Hornblende	46.43	0.67	8.44	18.06	0.42	10.09	11.7	0.90	0.38	97.09
Western metabasalt	RR-F1-001	Fe-Tschermakite	40.86	0.88	11.69	27.16	0.33	3.85	11.67	0.92	1.13	98.49
Western metabasalt	RR-F6-010	Fe-Tschermakite	41.31	0.89	11.28	26.92	0.37	3.91	11.58	1.03	1.06	98.35
Western metabasalt	RR-F6-001	Hypersthene	51.63	0.07	0.86	27.03	0.66	15.62	0.73	0.13	0	96.73
Western metabasalt	RR-F1-001	Biotite	33.06	2.45	15.68	28.96	0.33	4.86	0.04	0.16	9.46	95.00
Western metabasalt	RR-F6-001	Ilmenite	0	54.86	0	46.66	2.32	0.06	0.07	0	0.01	103.98
Western metabasalt	RR-F1-001	Titanite	29.95	36.06	2.29	1.99	0.09	0.24	26.69	0.02	0.41	97.74
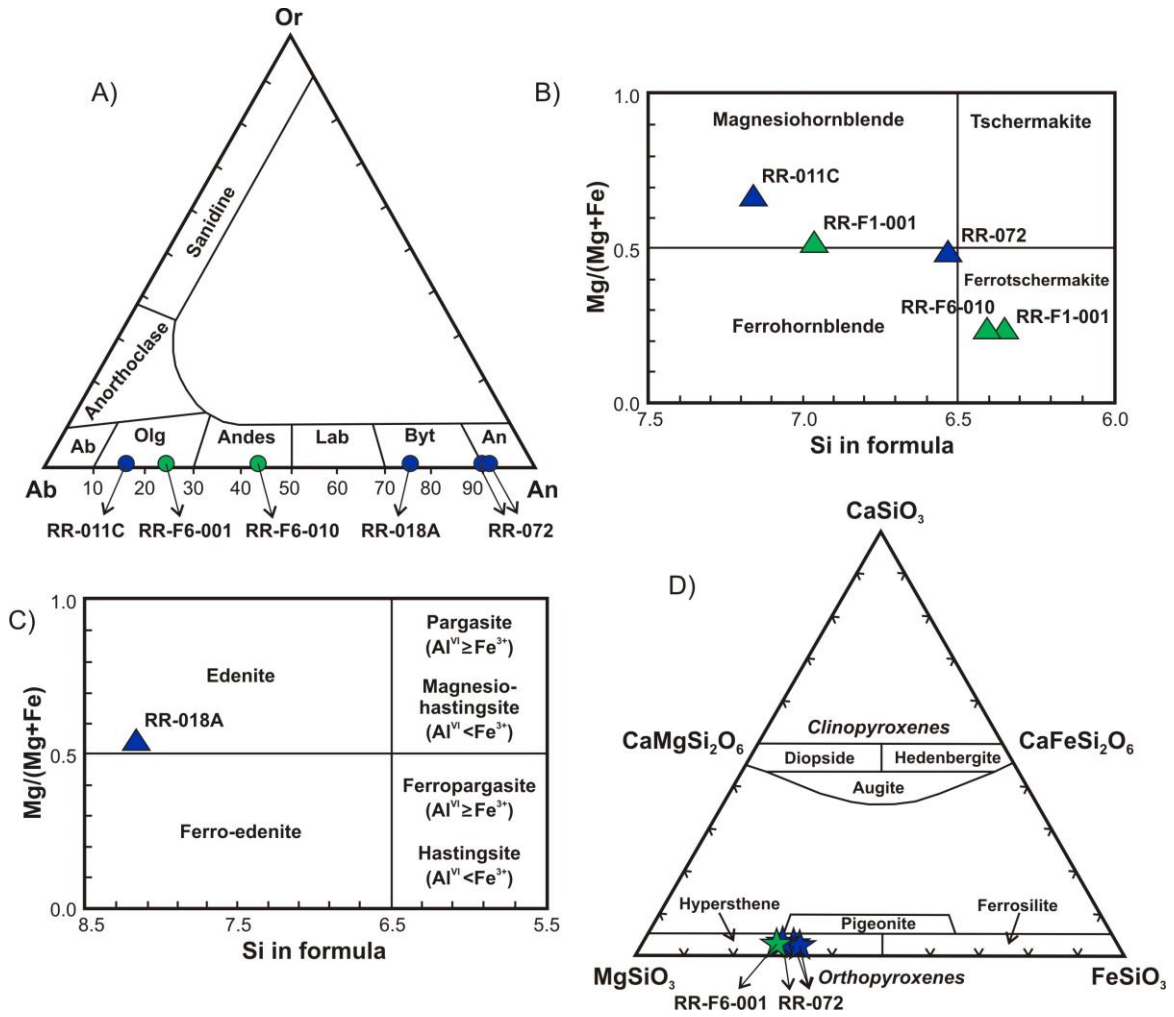
Figure 5. Classification diagrams of minerals in the eastern (blue symbols) and western (green symbols) metabasalts in the MNGB. A) Ternary diagram of feldspar: Ab: albite, Andes: andesine, An: anorthite, Byt: bytownite, Lab: labradorite, Olg: oligoclase, Or: orthoclase. B-C) Classification diagrams of the calcic amphiboles (Leake *et al*. 1997). D) Classification diagram of pyroxenes (Morimoto 1988).
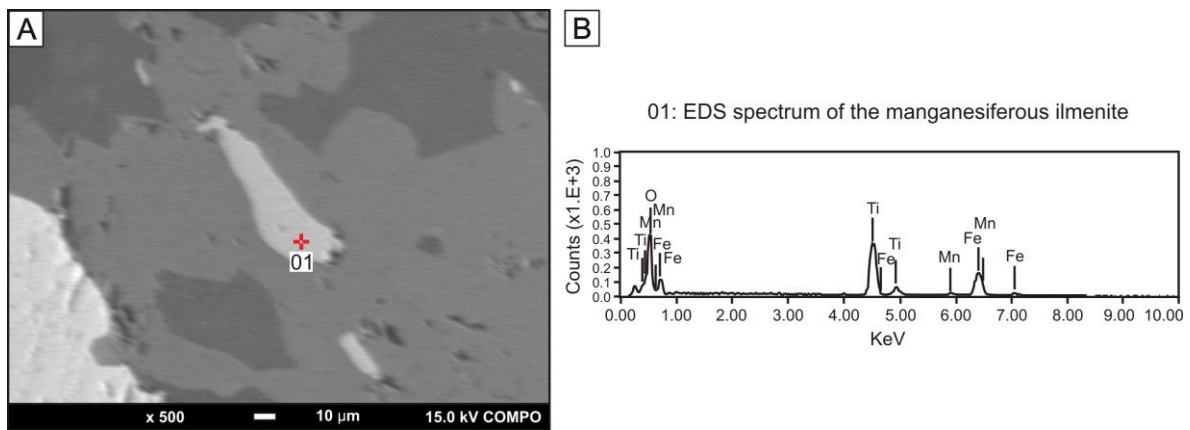
Figure 6. A) Backscattered electron image with the analysis spot and B) the EDS spectrum of the manganiferous ilmenite present in the western metabasalt of the MNGB, as evidence of an ocean floor setting (sample RR-F16-027).

4.1.3. Metadacite

Metadacite and subordinate metarhyolite have restricted occurrences and correspond to the top of the MNGB middle sequence based on field relationships and a felsic mineral content typical of the later stages of volcanism. These units occur to the northeast of Piritiba city and were identified in a drill hole sample obtained by CBPM and in outcrops. These rocks are distributed along a northeast-southwest trend and are in contact with eastern metabasalt and ferruginous metachert (Fig. 2).

The metadacite has a gray color, is strongly foliated and is not magnetic. This rock contains submillimetric porphyroclasts of plagioclase with sericitized borders and quartz (40 % of the rock), which are dispersed in a fine-grained groundmass composed of quartz, plagioclase, biotite, muscovite and sericite (60 % of the rock; Figs. 3D and 4D).

The subordinate metarhyolite has a gray color and is fine grained and foliated. It is composed of quartz (25 %), K-feldspar (40 %), plagioclase (20 %), biotite (10 %) and sericite (5 %). This rock contains granolepidoblastic grains that are submillimetric and highly oriented, tabular crystals of plagioclase (usually sericitized) and grains of quartz, fine biotite and opaque minerals.

5. Whole-rock chemical characterization

The lithochemistry characterization of the metavolcanic rocks in the Neoarchean MNGB was used to refine the classification of rocks previously classified on the basis of petrography and mineral chemistry and to evaluate the related petrological processes and tectonic settings. Therefore, this analysis also included samples of metakomatiite, eastern metabasalt, western metabasalt and metadacite in the MNGB. The whole-rock chemical data of those rocks are listed in Tables 3, 4 and 5.

Table 3. Whole-rock major and minor oxide chemical data (wt. %)

| Unit and classification	Sample ID	W. Long.	S. Lat.	SiO_2	TiO_2	Al_2O_3	Fe_2O_3t	MnO	MgO	CaO	Na_2O	K_2O	P_2O_5	LOI	Sum
Mundo Novo greenstone belt															
Metakomatiite	RR-011B	40°25'02.20"	11°48'39.22"	47.01	0.25	7.33	10.18	0.22	24.46	2.99	0.08	0.03	0.005	5.49	98.05
Metakomatiite	FD-37-017	40°30'22.03"	11°41'07.33"	54.39	0.23	7.12	6.68	0.65	17.57	10.15	0.65	0.3	0.19	3.73	101.66
Metakomatiite	FD-058A	40°28'45.53"	11°41'43.47"	57.22	0.07	2.19	6.12	0.11	24.38	2.42	0.05	0.03	0.005	4.52	97.12
Metakomatiite	FD-070	40°28'36.03"	11°41'39.19"	55.02	0.07	2.81	9.38	0.23	18.91	7.4	0.11	0.03	0.005	4.03	98.00
Eastern metabasalt	RR-006	40°25'40.85"	11°53'04.26"	49.78	0.83	14.05	11.97	0.21	8.1	12.53	0.96	0.25	0.04	0.55	99.27
Eastern metabasalt	RR-011C	40°25'02.20"	11°48'39.22"	49.08	1.19	13.39	14.03	0.24	6.98	10.67	0.8	0.32	0.05	0.8	97.55
Eastern metabasalt	RR-014B	40°30'21.91"	11°41'40.20"	50.49	1	13.71	13.42	0.22	6.33	10.69	2.2	0.26	0.06	1.22	99.60
Eastern metabasalt	RR-018A	40°30'07.88"	12°13'43.29"	48.93	1.04	14.18	14.11	0.23	7.16	11.39	2.1	0.26	0.07	0.52	99.99
Eastern metabasalt	RR-018B	40°30'07.94"	12°13'43.35"	51.33	1.07	13.74	14.04	0.24	7.26	10.41	2.55	0.26	0.08	0.53	101.51
Eastern metabasalt	RR-018C	40°30'08.01"	12°13'43.42"	52.48	1.1	14.19	13.39	0.21	5.68	11.57	1.95	0.18	0.1	0.43	101.28
Eastern metabasalt	RR-018D	40°30'08.08"	12°13'43.48"	51.83	1.06	14.16	13.4	0.21	5.47	13.27	1.39	0.15	0.09	0.48	101.51
Eastern metabasalt	RR-071	40°28'39.28"	11°36'42.51"	54.77	1.46	13.32	15.76	0.26	6.36	10.05	0.65	0.23	0.03	0.85	103.74
Eastern metabasalt	RR-072	40°29'25.44"	11°37'14.46"	54.68	1.52	13.45	15.19	0.22	6.72	9.73	0.41	0.13	0.05	0.67	102.77
Eastern metabasalt	RR-078	40°28'06.14"	11°39'32.83"	52.46	1.15	13.76	13.35	0.21	6.49	10.56	1.68	0.19	0.04	0.63	100.52
Eastern metabasalt	RR-080	40°26'38.53"	11°40'09.08"	51.14	0.97	15.65	13.38	0.2	6.47	10.27	2.88	0.31	0.09	0.6	101.96
Eastern metabasalt	FD-37-001	40°30'22.03"	11°41'07.33"	50.14	0.97	14.33	12.6	0.22	6.47	10.84	1.98	0.09	0.08	0.9	98.62
Eastern metabasalt	FD-37-002	40°30'22.03"	11°41'07.33"	52.47	0.98	14.47	12.95	0.21	6.63	10.72	2.14	0.12	0.07	0.57	101.33
Eastern metabasalt	FD-37-004	40°30'22.03"	11°41'07.33"	51.5	1.11	14.03	14.35	0.23	5.49	9.95	2.08	0.16	0.09	0.36	99.35
Eastern metabasalt	FD-37-005	40°30'22.03"	11°41'07.33"	50.92	1.21	13.21	15.04	0.23	4.97	9.92	2.13	0.15	0.1	0.68	98.56
Eastern metabasalt	FD-37-006	40°30'22.03"	11°41'07.33"	50.81	0.71	15.59	11.17	0.18	7.74	11.18	2.22	0.15	0.06	0.89	100.70
Eastern metabasalt	FD-37-007	40°30'22.03"	11°41'07.33"	51.08	0.99	14.56	13.92	0.21	6.58	9.96	2.57	0.25	0.09	0.92	101.13
Eastern metabasalt	FD-37-009	40°30'22.03"	11°41'07.33"	52.74	0.93	14.95	13.57	0.21	7.53	10.68	2.38	0.18	0.08	0.61	103.86
Eastern metabasalt	FD-37-011	40°30'22.03"	11°41'07.33"	52.94	1.02	13.62	13.86	0.21	6.88	10.32	2.06	0.24	0.04	0.89	102.08

Eastern metabasalt	FD-37-012	40°30'22.03"	11°41'07.33"	53.63	1.23	14.07	15.43	0.25	5.07	10.01	2.36	0.16	0.12	0.88	103.21
Eastern metabasalt	FD-37-013	40°30'22.03"	11°41'07.33"	52.66	0.99	14.75	13.09	0.22	6.23	10.62	2.16	0.18	0.09	0.82	101.81
Eastern metabasalt	FD-37-015	40°30'22.03"	11°41'07.33"	48.91	1.12	15.58	14.27	0.24	6.58	11.58	2.33	0.21	0.1	0.93	101.85
Eastern metabasalt	FD-37-016	40°30'22.03"	11°41'07.33"	48.7	1.28	17.47	13.65	0.18	7.7	9.23	2.04	0.93	0.17	2.46	103.81
Eastern metabasalt	FD-37-019	40°30'22.03"	11°41'07.33"	53.15	0.99	14.19	13.06	0.22	6.16	10.68	2.39	0.13	0.1	0.77	101.84
Eastern metabasalt	FD-016	40°29'24.00"	11°42'01.07"	53.15	1.02	12.62	12.62	0.26	5.85	8.6	2.1	0.34	0.06	0.94	97.56
Eastern metabasalt	FD-028	40°26'43.09"	11°48'24.59"	52.18	1.27	13.24	12.86	0.21	5.74	12.44	1.58	0.24	0.07	0.78	100.61
Western metabasalt	RR-022	40°36'07.38"	12°18'51.47"	49.47	0.95	14.28	12.39	0.23	5.88	10.75	2.3	0.61	0.07	0.76	97.69
Western metabasalt	RR-F1-001	40°29'40.00"	11°53'22.35"	55.52	0.99	14.69	12.23	0.23	7.17	9.34	1.89	0.53	0.1	1.28	103.97
Western metabasalt	RR-F4-006	40°29'31.17"	11°54'14.89"	49.75	1.26	15.1	12.96	0.2	4.74	8.19	3.72	0.31	0.17	0.24	96.64
Western metabasalt	RR-F4-007	40°29'31.17"	11°54'14.89"	49.8	1.35	15.05	12.58	0.19	4.74	7.63	2.33	1.57	0.19	0.32	95.75
Western metabasalt	RR-F6-001	40°29'35.54"	11°53'35.26"	57.06	1.34	16.4	7.24	0.11	2.37	5.92	4.71	1.18	0.2	0.8	97.33
Western metabasalt	RR-F6-002	40°29'35.54"	11°53'35.26"	48.04	1.56	17.37	11.27	0.19	4.64	7.21	4.03	0.99	0.17	0.64	96.11
Western metabasalt	RR-F6-003	40°29'35.54"	11°53'35.26"	46.4	1.45	15.54	12.8	0.24	5.95	8.21	2.93	0.98	0.17	0.68	95.35
Western metabasalt	RR-F6-004	40°29'35.54"	11°53'35.26"	48.72	1.3	14.51	11.68	0.2	5.15	9.4	2.04	0.83	0.19	1.04	95.06
Western metabasalt	RR-F6-005	40°29'35.54"	11°53'35.26"	50.26	1.28	15.5	13.09	0.2	4.94	8.52	3.14	0.96	0.17	0.35	98.41
Western metabasalt	RR-F6-006	40°29'35.54"	11°53'35.26"	50.5	1.34	15.71	12.96	0.2	4.44	8.48	3.53	0.83	0.19	0.26	98.44
Western metabasalt	RR-F6-007	40°29'35.54"	11°53'35.26"	52.73	1.4	15.78	10.57	0.17	4.16	8.13	3.74	0.18	0.2	0.25	97.31
Western metabasalt	RR-F6-008	40°29'35.54"	11°53'35.26"	48.98	1.29	15.2	12.44	0.2	5.18	8.36	3.3	0.91	0.16	0.35	96.37
Western metabasalt	RR-F6-009	40°29'35.54"	11°53'35.26"	48.1	1.33	15.23	13.02	0.22	6.3	8.15	2.59	0.22	0.16	0.14	95.46
Western metabasalt	RR-F6-010	40°29'35.54"	11°53'35.26"	50.64	1.4	15.08	12.75	0.22	5.37	7.19	2.54	0.63	0.18	0.05	96.05
Western metabasalt	RR-F6-016	40°29'35.54"	11°53'35.26"	54.48	0.71	16.43	11.03	0.23	6.07	3.52	4.04	1.19	0.07	2.47	100.24
Western metabasalt	RR-F6-018	40°29'35.54"	11°53'35.26"	53.79	0.63	15.71	9.44	0.2	6.19	9.82	2.35	0.24	0.09	0.77	99.23
Western metabasalt	RR-F16-027	40°29'27.40"	11°53'33.16"	57.24	0.73	14.2	10.32	0.16	5.01	8.5	2.57	0.74	0.05	1.36	100.88
Metadacite	FD-052	40°29'26.72"	11°42'09.52"	70.98	0.34	14.22	5.08	0.07	2.09	1.24	2.02	2.46	0.04	1.55	100.09
Metarhyolite	RR-FST-002	40°29'33.55"	11°42'52.06"	73.2	0.41	11.49	6.58	0.08	1.63	1.81	1.41	2.69	0.08	0.74	100.12

Table 4. Whole-rock REE chemical data (ppm)

Unit and classification	Sample ID	La	Ce	Pr	Nd	Sm	Eu	Gd	Tb	Dy	Ho	Er	Tm	Yb	Lu
Mundo Novo greenstone belt															
Metakomatiite	RR-011B	9.5	13.2	1.18	3.8	0.6	0.2	0.68	0.12	0.74	0.16	0.49	0.07	0.5	0.07
Metakomatiite	FD-37-017	7.2	12.6	1.62	6.7	1.4	0.43	1.56	0.21	1.49	0.3	0.94	0.13	0.9	0.13
Metakomatiite	FD-058A	7.1	6.5	1.3	5.3	1.2	0.42	1.6	0.26	1.6	0.32	1	0.14	0.8	0.025
Metakomatiite	FD-070	4.9	3.7	1.17	4.7	1.3	0.51	1.74	0.29	1.81	0.41	1.11	0.19	1.1	0.11
Eastern metabasalt	RR-006	5	10.2	1.46	7	2.1	0.76	2.71	0.46	3.01	0.63	1.88	0.26	1.7	0.26
Eastern metabasalt	RR-011C	10.7	24.1	3.15	14.4	3.7	1.04	4.02	0.64	3.92	0.79	2.25	0.3	1.8	0.27
Eastern metabasalt	RR-014B	6.4	11.9	1.95	9.3	2.9	1	3.8	0.69	4.83	1.03	3.09	0.45	2.9	0.44
Eastern metabasalt	RR-018A	7	16.3	2.22	10.3	2.9	1	3.73	0.66	4.31	0.93	2.72	0.41	2.6	0.39
Eastern metabasalt	RR-018B	7.3	13.4	1.87	9.1	2.8	0.9	3.54	0.61	4.17	0.89	2.69	0.38	2.5	0.38
Eastern metabasalt	RR-018C	9.3	20.9	2.66	12.1	3.2	1.04	3.9	0.68	4.42	0.96	2.88	0.41	2.7	0.41
Eastern metabasalt	RR-018D	8	18	2.31	10.7	2.8	0.98	3.58	0.63	4.16	0.91	2.67	0.38	2.5	0.39
Eastern metabasalt	RR-071	11.6	19.1	2.9	13.1	3.4	1.06	4.63	0.69	4.52	0.87	2.54	0.33	2.1	0.32
Eastern metabasalt	RR-072	11	24.6	2.93	13.9	3.8	1.28	4.67	0.77	4.6	0.94	2.6	0.37	2.2	0.37
Eastern metabasalt	RR-078	10	12.8	2.19	10.3	3.1	1.17	4.41	0.75	5.28	1.09	3.39	0.5	3.3	0.51
Eastern metabasalt	RR-080	10.1	14.1	1.96	8.9	2.7	0.99	3.95	0.71	4.69	0.99	3.09	0.43	2.8	0.46
Eastern metabasalt	FD-37-001	6.1	12.6	1.83	8.9	2.5	0.99	3.62	0.64	4.28	0.88	2.76	0.38	2.6	0.4
Eastern metabasalt	FD-37-002	5	11.3	1.7	8.4	2.5	0.96	3.44	0.63	4.21	0.9	2.63	0.37	2.5	0.39
Eastern metabasalt	FD-37-004	5.7	13.7	2.08	9.9	3.4	1.22	4.39	0.79	5.28	1.15	3.22	0.5	3.3	0.49
Eastern metabasalt	FD-37-005	6.5	14.9	2.26	10.5	3.2	1.12	4.55	0.78	5.16	1.13	3.4	0.49	3.1	0.49
Eastern metabasalt	FD-37-006	4.9	8.4	1.2	6.2	1.9	0.7	2.73	0.49	3.09	0.68	1.96	0.3	1.9	0.28
Eastern metabasalt	FD-37-007	6.2	12	1.77	8.3	2.6	0.94	3.41	0.6	4.31	0.88	2.45	0.4	2.6	0.38
Eastern metabasalt	FD-37-009	5.7	11.7	1.61	7.9	2.4	0.86	3.31	0.59	4.05	0.83	2.54	0.38	2.4	0.37
Eastern metabasalt	FD-37-011	6.1	12.7	1.82	8.4	2.5	0.96	3.46	0.6	3.96	0.87	2.63	0.37	2.5	0.41
Eastern metabasalt	FD-37-012	6.3	14.1	2.02	10	3.3	1.16	4.49	0.77	5.42	1.11	3.33	0.49	3.3	0.48
Eastern metabasalt	FD-37-013	4.6	11.2	1.7	8.9	2.7	0.97	4	0.71	4.35	0.96	2.86	0.47	2.7	0.43
Eastern metabasalt	FD-37-015	6.9	12.9	1.91	9.2	3	1.07	4.21	0.73	4.82	1.06	3.12	0.46	3	0.5
Eastern metabasalt	FD-37-016	6.9	14.8	2.32	11.1	3.7	1.27	4.86	0.87	5.5	1.22	3.64	0.52	3.4	0.54
Eastern metabasalt	FD-37-019	7.1	14.1	1.95	9.3	2.8	1	3.62	0.67	4.45	0.96	2.81	0.42	2.8	0.46
Eastern metabasalt	FD-016	7.4	12	1.94	9	2.6	0.94	3.78	0.65	4.42	0.92	2.93	0.39	2.6	0.4
Eastern metabasalt	FD-028	5.7	13.1	1.99	10.2	3.2	1.12	4.34	0.72	4.82	1	2.92	0.44	2.9	0.42
Western metabasalt	RR-022	18.6	27.6	4.74	19.2	4.8	1.42	4.98	0.84	5.49	1.14	3.28	0.48	3.1	0.44

Western metabasalt	RR-F1-001	21.1	39.1	5.18	20	4.7	1.41	5.23	0.84	5.07	0.98	2.72	0.38	2.6	0.41
Western metabasalt	RR-F4-006	23	44.3	5.6	23.4	5.5	1.54	6.15	1	6.56	1.33	4	0.57	3.8	0.56
Western metabasalt	RR-F4-007	25	45.8	5.79	23.4	5.6	1.59	6.4	1.04	6.79	1.31	3.94	0.56	3.7	0.58
Western metabasalt	RR-F6-001	25.8	48.7	6.24	24.9	5.7	1.45	6.51	1.06	6.74	1.32	3.79	0.59	3.7	0.55
Western metabasalt	RR-F6-002	26.5	55.2	7.1	28.2	6.8	1.67	7.62	1.22	7.71	1.56	4.58	0.66	4.4	0.64
Western metabasalt	RR-F6-003	27.7	47.5	5.96	24.3	5.8	1.63	6.67	1.1	6.86	1.42	4.26	0.67	4	0.66
Western metabasalt	RR-F6-004	23.9	45.4	5.88	23.6	5.9	1.4	6.56	1.08	6.87	1.41	3.99	0.6	3.8	0.54
Western metabasalt	RR-F6-005	23.4	45.9	5.91	24.2	5.8	1.72	6.58	1.06	6.59	1.38	4.26	0.58	3.9	0.6
Western metabasalt	RR-F6-006	21.7	45.1	5.82	23	5.7	2.06	6.48	1	6.67	1.37	4.12	0.56	3.8	0.58
Western metabasalt	RR-F6-007	22.2	45.8	6.05	24.2	5.8	2.01	6.86	1.09	6.9	1.39	4.13	0.59	3.9	0.6
Western metabasalt	RR-F6-008	23.9	48	6.04	24.8	6	1.93	6.65	1.05	6.62	1.32	3.99	0.6	3.8	0.58
Western metabasalt	RR-F6-009	21.3	44.8	5.84	23.9	5.9	1.82	6.59	1.02	6.79	1.36	4.15	0.57	3.8	0.57
Western metabasalt	RR-F6-010	23	44.3	5.79	23.6	5.4	1.56	6.8	1.04	6.61	1.36	4	0.66	3.8	0.61
Western metabasalt	RR-F6-016	10.9	19.2	2.35	9.5	2	0.53	2.59	0.43	3.01	0.72	2.09	0.33	2.2	0.34
Western metabasalt	RR-F6-018	16.2	31.8	3.92	15.7	3.4	0.98	3.88	0.61	3.66	0.77	2.34	0.34	2.1	0.35
Western metabasalt	RR-F16-027	24.1	30.9	3.65	14.2	3.1	0.83	3.61	0.56	3.64	0.75	2.17	0.35	2.1	0.33
Metadacite	FD-052	16.3	29.8	2.97	12.4	2.8	0.69	2.62	0.43	2.81	0.52	1.54	0.18	1.3	0.16
Metarhyolite	RR-FST-002	35.5	64.4	6.27	23.9	4.4	0.94	4.09	0.6	3.66	0.73	2.25	0.27	2.2	0.26

Table 5. Whole-rock trace and minor element chemical data (ppm)

Unit and classification	Sample ID	Cs	Ba	Th	U	Ta	Nb	Zr	Hf	Ti	Y	Sr	Rb	Ni	V
Mundo Novo greenstone belt															
Metakomatiite	RR-011B	0.37	5	1.2	0.35	0.025	2.45	13	0.53	1500	4.47	12	1.2	945	2.5
Metakomatiite	FD-37-017	0.51	176	2.8	1.38	0.3	1.69	43	1.31	1380	8.83	49	10.3	644	42
Metakomatiite	FD-058A	0.06	42	2.6	0.72	0.36	1.27	20	0.63	420	10.47	5	1.6	587	2.5
Metakomatiite	FD-070	0.11	50	0.8	0.39	0.025	0.58	15	0.2	420	12.02	5	1	493	2.5
Eastern metabasalt	RR-006	0.76	104	0.5	0.16	0.025	3.3	40	1.27	4980	18.07	90	8.1	115	207
Eastern metabasalt	RR-011C	1.52	134	2.3	0.66	0.17	7.32	93	2.48	7140	21.67	100	8.1	110	232
Eastern metabasalt	RR-014B	0.13	122	0.8	0.13	0.025	2.66	69	1.96	6000	28.43	108	6.1	112	283
Eastern metabasalt	RR-018A	0.3	110	1.8	0.31	0.025	5.3	77	2.15	6240	26.24	109	4	112	295
Eastern metabasalt	RR-018B	0.21	80	1	0.27	0.025	3.59	67	1.87	6420	24.46	120	5.8	110	306
Eastern metabasalt	RR-018C	0.17	132	1.8	0.42	0.025	9.69	75	1.99	6600	27.2	128	2.1	112	306
Eastern metabasalt	RR-018D	0.16	119	2.7	0.42	0.34	7.56	72	2.07	6360	25.88	162	1.8	109	292
Eastern metabasalt	RR-071	0.77	73	2.3	0.31	0.025	5.52	84	2.52	8760	22.27	66	5.2	92	306
Eastern metabasalt	RR-072	0.36	30	1.1	0.29	0.025	4.77	88	2.71	9120	22.77	185	4	97	315
Eastern metabasalt	RR-078	0.25	242	0.8	0.29	0.025	3.08	69	2.23	6900	28.29	94	7.6	125	315
Eastern metabasalt	RR-080	0.27	102	0.9	0.39	0.025	2.91	83	2	5820	24.88	133	11.7	124	386
Eastern metabasalt	FD-37-001	0.2	108	0.4	0.35	0.025	2.26	78	1.97	5820	22.32	109	2.6	90	366
Eastern metabasalt	FD-37-002	0.17	46	0.1	0.22	0.025	1.93	69	1.99	5880	22.86	110	2.8	108	371
Eastern metabasalt	FD-37-004	0.09	40	0.4	0.23	0.025	2.46	85	2.28	6660	27.81	107	2.3	72	423
Eastern metabasalt	FD-37-005	0.07	34	0.4	0.26	0.025	2.75	91	2.36	7260	29.87	127	1.6	62	425
Eastern metabasalt	FD-37-006	0.41	53	0.05	0.18	0.025	1	48	1.37	4260	16.4	107	4.9	152	298
Eastern metabasalt	FD-37-007	0.42	232	0.3	0.24	0.025	1.99	79	1.91	5940	23.31	122	6.6	142	362
Eastern metabasalt	FD-37-009	0.24	185	0.2	0.24	0.025	1.84	73	1.87	5580	22.88	117	3.3	164	374
Eastern metabasalt	FD-37-011	0.29	127	0.5	0.27	0.025	4.03	56	1.69	6120	22.3	111	4.7	148	299
Eastern metabasalt	FD-37-012	0.12	40	0.4	0.27	0.025	3.5	96	2.41	7380	28.27	109	2	49	490
Eastern metabasalt	FD-37-013	0.41	54	0.05	0.21	0.025	2.23	73	1.93	5940	22.35	113	4.6	106	379
Eastern metabasalt	FD-37-015	0.51	116	0.2	0.27	0.025	2.62	87	2.15	6720	26.05	120	5.5	116	415
Eastern metabasalt	FD-37-016	1.29	768	5	0.47	1.61	4.5	96	3.96	7680	28.83	107	32.9	110	451
Eastern metabasalt	FD-37-019	0.09	35	0.7	0.27	0.025	2.52	77	2.16	5940	23.28	112	1.5	77	409
Eastern metabasalt	FD-016	0.32	161	1.5	0.36	0.14	2.64	78	2.09	6120	24.9	111	8.2	104	323
Eastern metabasalt	FD-028	0.92	56	0.7	0.21	0.17	2.92	75	1.91	7620	25.05	132	8.9	111	322
Western metabasalt	RR-022	0.31	78	1.9	0.46	0.32	5.25	87	2.36	5700	28.44	574	13.7	83	192
Western metabasalt	RR-F1-001	1.2	141	4.2	0.95	0.025	6.22	138	3.44	5940	25.4	127	16.3	148	257
Western metabasalt	RR-F4-006	0.12	72	3.4	1.06	0.15	7.06	169	4.5	7560	32.18	187	4.5	88	331
Western metabasalt	RR-F4-007	0.63	480	3.3	1.08	0.08	7.8	171	4.31	8100	35.3	180	46.2	89	338
Western metabasalt	RR-F6-001	1.6	216	4.4	1.39	0.26	9.05	177	4.94	8040	32.77	131	43.7	106	358
Western metabasalt	RR-F6-002	1.9	188	4.3	1.3	0.24	8.7	192	5.27	9360	40.14	108	29.5	91	312
Western metabasalt	RR-F6-003	1.11	244	3.6	1.16	0.025	8.05	183	4.73	8700	36.53	127	19.8	97	366
Western metabasalt	RR-F6-004	1.31	184	3.3	1.09	0.025	7.05	161	4.52	7800	33.53	80	20.9	93	310
Western metabasalt	RR-F6-005	2.57	278	3.3	1.09	0.025	7.1	171	4.45	7680	34.07	205	19.2	92	316

Western metabasalt	RR-F6-006	0.46	228	3.3	1.11	0.025	7.49	167	4.41	8040	36.03	214	16.5	91	322
Western metabasalt	RR-F6-007	0.12	98	3.4	1.11	0.025	7.34	172	4.32	8400	35.58	148	2.7	86	322
Western metabasalt	RR-F6-008	1.01	157	3.2	1.01	0.025	6.82	163	4.46	7740	34.29	152	16.5	88	326
Western metabasalt	RR-F6-009	0.19	55	3.2	1.03	0.025	7.48	162	4.4	7980	37.08	204	3.3	93	319
Western metabasalt	RR-F6-010	0.55	184	3.1	1.08	0.025	7.51	170	4.36	8400	34.44	171	12.2	89	328
Western metabasalt	RR-F6-016	2	130	2.8	0.96	0.025	4.54	130	3.07	4260	17.1	54	27.2	51	241
Western metabasalt	RR-F6-018	0.33	59	2.7	0.93	0.025	4.04	118	2.86	3780	20.71	220	4.3	82	221
Western metabasalt	RR-F16-027	0.55	136	3.1	1.08	0.31	2.85	121	2.82	4380	20.78	112	21.5	80	313
Metadacite	FD-052	3.29	553	7	5.24	1.01	9.57	83	2.72	2040	14.94	109	92.3	99	76
Metarhyolite	RR-FST-002	5.83	631	17.1	5.37	0.26	8.37	152	4.88	2460	19.91	144	95.3	49	67

5.1. Mundo Novo greenstone belt

The bivariate diagrams of TiO_2 and Al_2O_3 (the least mobile major elements), FeO_t and MgO (mobile major elements), Ni (conservative trace element), Y (immobile trace element), and La and Ce (light REE) against Zr were drawn for the metakomatiite from the lower sequence and the eastern and western metabasalts and metadacite from the middle sequence of the MNGB; the diagrams are shown in Figure 7, and show important correlations. Zr was used as a crystal fractionation index because of its immobility during alteration and metamorphism and its large range of concentration in igneous suites, resulting from varying degrees of partial melting and fractional crystallization (Furnes *et al*. 2013). The Zr concentrations are 13-43 ppm in the metakomatiite, 40-192 ppm in the eastern and western metabasalts and 83-152 ppm in the metadacite.

TiO_2 defines a positive pattern versus Zr, and the eastern and western metabasalts form separate groups with the same slope. The Al_2O_3 diagram features a positive asymptotic pattern in which the metakomatiite samples plot near the origin, the metabasalt samples form a trend where the western metabasalt exhibits relatively high values of Al_2O_3, and the metadacite is approximately aligned in the trend. Four distinct and dispersed groups are formed in the FeO_t plot, possibly because of the mobility of Fe during the alteration. The negative asymptotic patterns in the MgO and Ni diagrams form highly defined trends that can be explained by the fractional crystallization of olivine and pyroxene in the metakomatiite and eastern and western metabasalts. Y, La and Ce, which are considered immobile elements, show highly defined positive correlations versus Zr. Therefore, they were used to demonstrate that the metakomatiite, eastern and western metabasalts and metadacite from the MNGB may be related by fractional crystallization.

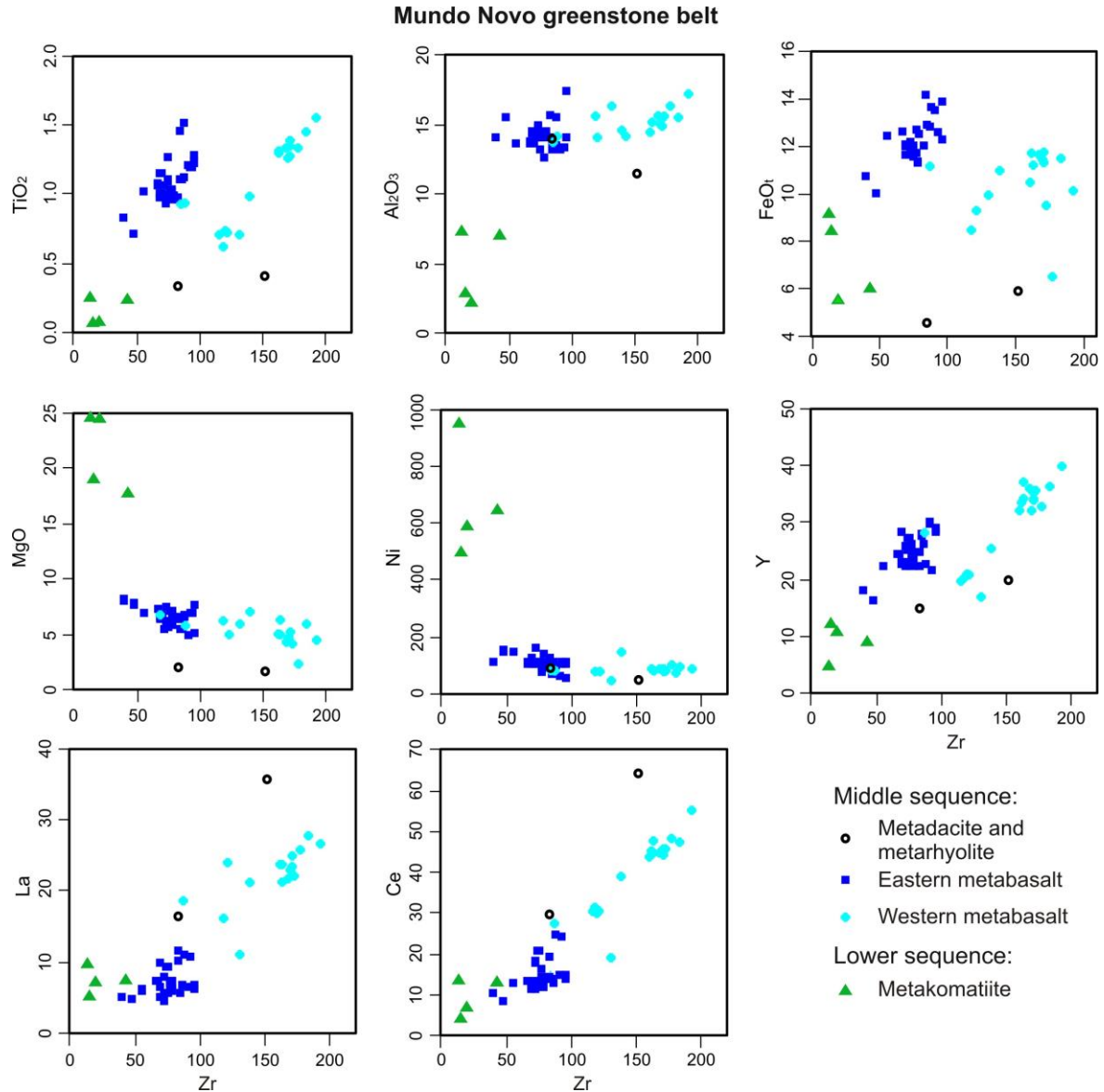**Mundo Novo greenstone belt**

Figure 7. Binary plots using Zr as a differentiation index for the metavolcanic rocks of the MNGB.

Lower Sequence

The metakomatiite of the MNGB is peridotitic, with MgO concentrations of 17-25 wt. % (Fig. 8A), and plots near the MgO vertex in the AFM diagram (Irvine & Baragar 1971; Fig. 8B). The chondrite-normalized REE geochemical pattern (Boynton 1984) indicates enrichment in light REE in the metakomatiite in the MNGB, similar to the komatiite pattern from the Onverwacht Suite of the Barberton greenstone belt, South Africa (Jahn *et al*. 1982; Fig. 8D). The $(La/Yb)_N$ ratios in the MNGB's metakomatiite show low values, with an average of approximately 5 and a minimum of 2.69.

The low values of Nb ($\leq$ 2.45 ppm), Ti ($\leq$ 0.150 ppm) and the Ti/Zr ratio ($\leq$ 0.012), in addition to the enrichment in U and Th can be observed in Fig. 9A. High CaO/Al_2O_3 ratios (Herzberg 1995) in the metakomatiite of the MNGB, between 1.1 and 2.6, allow this rock to be classified as Al-depleted. In addition, the high $(Gd/Yb)_N$ ratios (Herzberg 1995) between 1.09 and 1.60 indicate partial melting at high pressures and that the garnet remained in the residue during the melting process.

In the multielement diagram normalized to N-MORB (Hofmann 1988), the Cs, Ba, Th and U elements show high and anomalous concentrations in the metakomatiite (Fig. 9A), a flat pattern from Lu to Nd and a negative anomaly of Nb.

The tectonic setting discrimination diagram of immobile elements, the Nb/Yb vs. Th/Yb diagram, indicates that the metakomatiite plots form a trend with other mafic volcanic rocks of the MNGB which extends from N-MORB point to volcanic arc array (Fig. 9E). This displacement of the plots oblique to MORB-ocean island basalt (OIB) array is a result of the transportation of subduction-mobile Th content (Pearce *et al.* 2005, Pearce 2008).

Middle Sequence

5.1.1. Eastern and western metabasalts

The division of MNGB metabasalt into the two eastern and western groups, as previously discussed based on petrography, was further confirmed by the REE pattern. REE patterns are reliable because of the immobility of these elements during low-grade metamorphism, weathering and hydrothermal alteration, and therefore, a degree of confidence can be placed in the obtained patterns (Rollinson 1993).

The two groups have subtle differences. The eastern metabasalt has higher percentages of Fe and Ti than the western metabasalt (Fig. 8A), which suggests a small andesitic trend in some western metabasalt samples. In the AFM diagram, two distinct groups of samples are also present, both in the tholeiitic series field, with just two samples of western metabasalt plotting in the calc-alkalic series field (Fig. 8B).

In the chondrite-normalized REE diagram (Boynton 1984), the western metabasalt is more fractionated and enriched in light REE, with La normalized values near 100, than the eastern metabasalt, which shows a flat REE pattern and La normalized values between 10 and 40 (Figs. 8E and 8F). The fractionation difference is also observed in the average $(La/Yb)_N$ ratio: the western metabasalt has a value of 5.11 and the eastern metabasalt has a value of 1.91.

The geochemical patterns of the major and trace elements normalized to the fertile mantle MORB (FMM) values as a tectonic setting marker (Pearce & Parkinson 1993) are similar for both metabasalt types of the MNGB. The patterns in which normalized Nb (24.06) and Zr (11.48) > TiO_2 (6.47) and in which Y (6.98) and Yb (7.04) ≥ CaO (3.00), Al_2O_3 (3.91) and V (4.20) into the two metabasalts are similar to the patterns in ocean floor basalts in a back-arc basin setting, as demonstrated in the Barberton greenstone belt (Furnes *et al.* 2013).

In the multielement diagram of trace elements normalized to N-MORB (Hofmann 1988; Figs. 9B and 9C), both metabasalt groups show a flat pattern from Lu to Zr and a negative Ta anomaly. The difference between the two groups is subtle but consistent. The negative Ti anomaly is more accentuated in the western metabasalt than in the eastern metabasalt. The western metabasalt is more enriched in La, Ce and Nd than the eastern metabasalt, and the Th and Cs values of the western metabasalt (Th values greater than 10 and some values of Cs greater than 100) are greater than the values of the same elements in the eastern metabasalt (Th values smaller than 10 and Cs values between 20 and 30).

The Nb/Yb vs. Th/Yb discrimination diagram of immobile elements in the eastern and western metabasalts of the MNGB indicates a trend that extends from N-MORB in the MORB-OIB array to the volcanic arc array, with a principal axis of dispersion of the plots oblique to the MORB-OIB array (Fig. 9E). This pattern is similar to oceanic subduction-related basalts of the Mariana Arc and Isua, Barberton and South Abitibi Archean greenstone belts (Fig. 9E). The eastern metabasalt has an IAT-type pattern, with some samples

overlapping the MORB field, and the western metabasalt mainly features a MORB pattern with a few occurrences plotting in the within-plate basalt field (WPB; Fig. 9F).

5.1.2 Metadacite

The felsic metavolcanic rocks of the middle sequence of the MNGB are classified as metadacite and subordinate metarhyolite in the SiO_2 vs. $Na_2O + K_2O$ diagram (Middlemost 1994; Fig. 8C). The chondrite-normalized REE diagram (Boynton 1984) for these felsic metavolcanic rocks subtly slopes from Lu to Gd with a negative Eu anomaly (Fig. 8G), as indicated by the average Eu/Eu* ratio of 0.64. There is enrichment in light REE with strong fractionation from Sm to La, and the average of the $(La/Yb)_N$ ratio is 8.87.

In the N-MORB-normalized multielement diagram (Hofmann 1988; Fig. 9D), the metadacite is enriched in Nb and Ta; high Cs, Ba, Th and U values, a negative Ti anomaly and moderate values of Hf (2.72-4.88 ppm) and Zr (83-152 ppm) are shown. Moreover, the metadacite and subordinate metarhyolite plot in the volcanic arc field in the tectonic diagrams of Pearce *et al*. (1984; Figs. 9G and 9H) and do not match the anorogenic field of the A-type granitoid diagram (Whalen 1987; Fig. 9I) according to the observations of metakomatiite and eastern and western metabasalts in the MNGB.
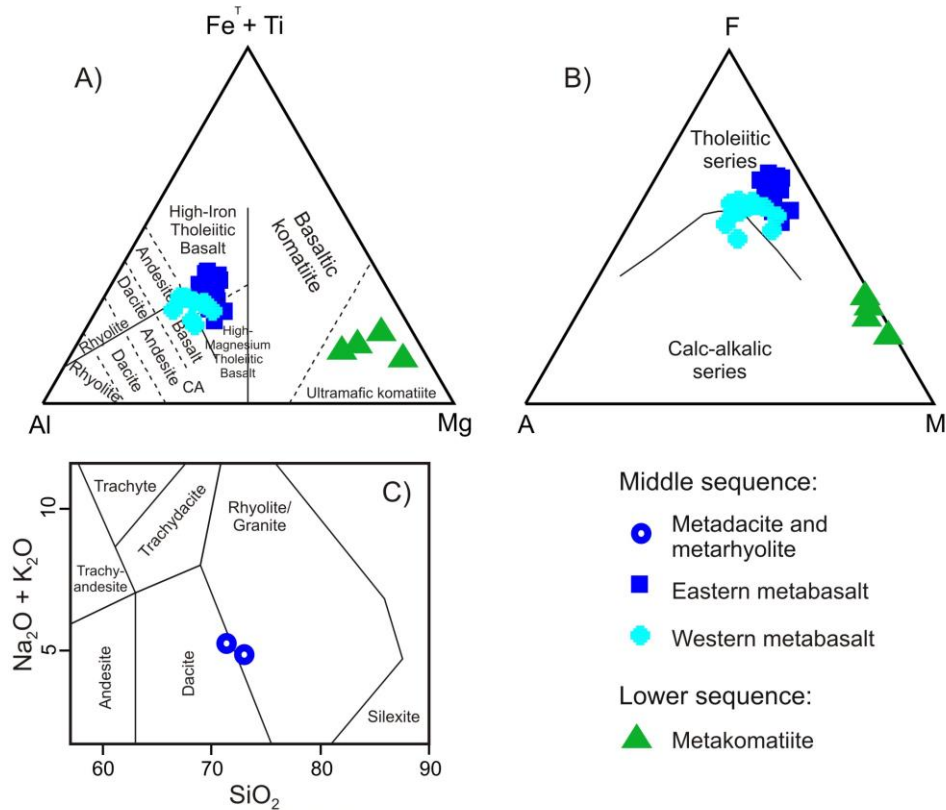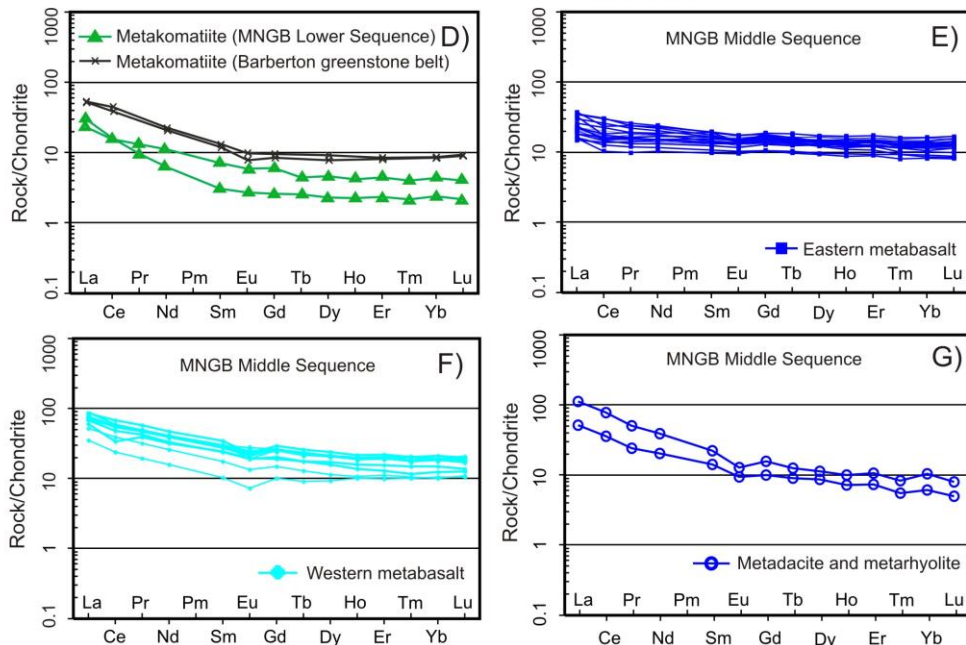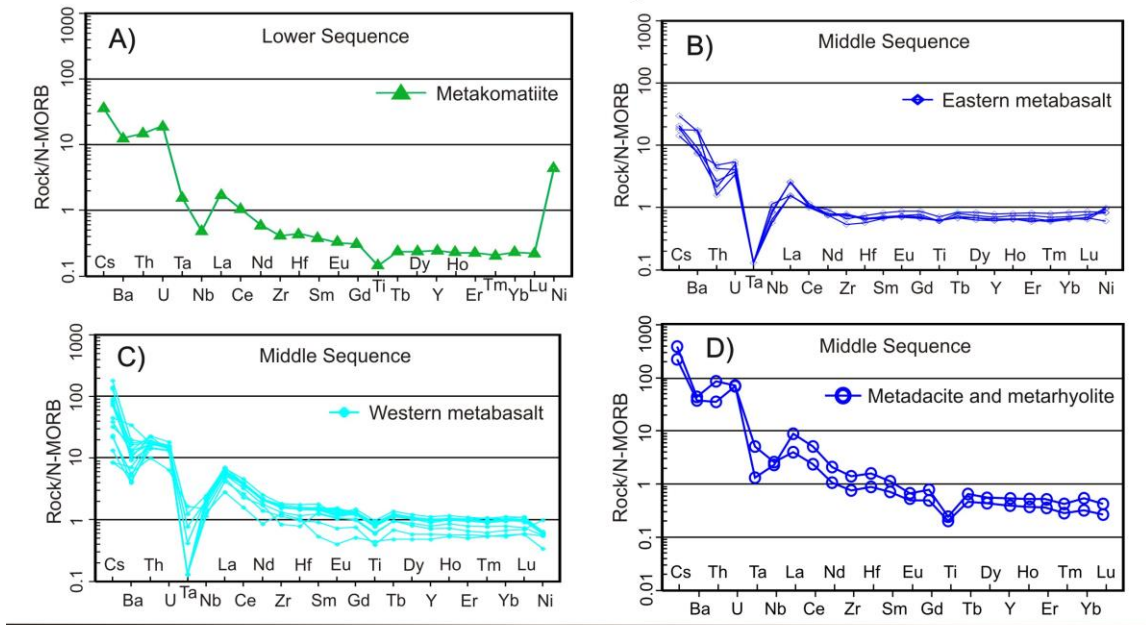
Figure 8. Lithochemical diagrams for MNGB rocks. A) Classification diagram of Jensen (1976): $Fe^T + Ti = FeO + Fe_2O_3 + TiO_2$; $Al = Al_2O_3$; $Mg = MgO$. B) AFM diagram, tholeiitic and calc-alkalic series (Irvine & Baragar 1971), $A = Na_2O + K_2O$; $F = FeO + 0.8998Fe_2O_3$; $M = MgO$. C) SiO_2 vs. $Na_2O + K_2O$ classification diagram (Middlemost 1994). Chondrite-normalized REE diagram (Boynton 1984): D) Metakomatiite in the MNGB lower sequence compared to the metakomatiite in the Barberton greenstone belt (Jahn *et al*. 1982); E) eastern metabasalt in the MNGB middle sequence; F) western metabasalt in the MNGB middle sequence; and G) metadacite and metarhyolite in the MNGB middle sequence.
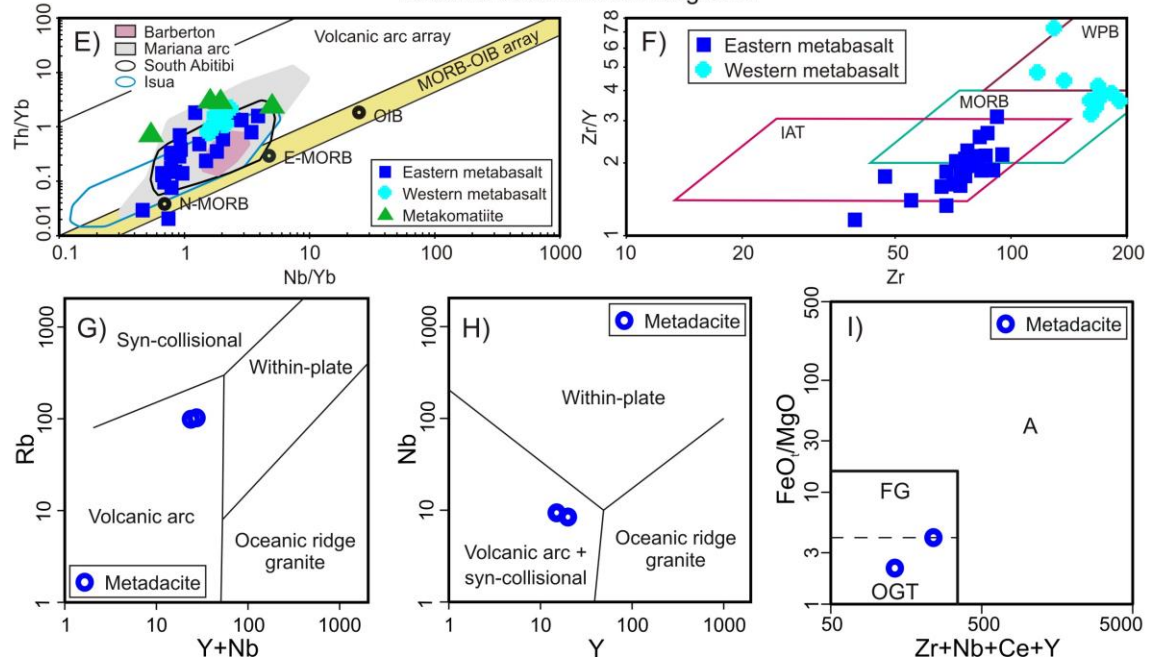
Figure 9. Lithochemical diagrams for MNGB rocks. Multielement diagram of trace elements normalized to N-MORB (Hofmann 1988): A) metakomatiite in the MNGB lower sequence; B) eastern metabasalt in the MNGB middle sequence; C) western metabasalt in the middle sequence and D) metadacite and metarhyolite in the MNGB middle sequence. Tectonic setting discrimination diagram: E) metakomatiite and eastern and western metabasalts in the MNGB lower and middle sequences plotted in the Nb/Yb vs. Th/Yb diagram (N-MORB: Normal – Middle ocean ridge basalts, E-MORB: Enriched – Middle ocean ridge basalts, OIB: Ocean island basalts; Pearce 2008) compared with basalts from South Abitibi (Kerrich & Xie 2002, Xie & Kerrich 1994), Barberton (Jochum *et al*. 1991, Parman *et al*. 1997, Chavagnac 2004) and Isua Archean greenstone belts (Polat & Hofmann 2003, Polat *et al*. 2002) and the Mariana Arc (Pearce *et al*. 2005); F) eastern and western metabasalts in the MNGB middle sequence plotted in the Zr vs. Zr/Y diagram (IAT: Island arc tholeiitic, MORB: Middle ocean ridge basalts, WPB: Within-plate basalts); G-H) metadacite in the MNGB middle sequence plotted in the Y + Nb vs. Rb and Y vs. Nb diagrams (Pearce *et al*. 1984); and I) in the Zr + Nb + Ce + Y vs. FeOt/MgO diagram (A: A-type granites, FG: fractionated felsic granites, OGT: M-, I- and S-type granites; Whalen 1987).

6. Discussion

The fine-grained texture of the metakomatiite in the MNGB is composed of skeletal grains with planar growths that intersect each other and do not intercept former structures, which indicates a relict spinifex texture preserved in chilled margins of the komatiite flows. This spinifex texture in the metakomatiite and the occurrence of pillow lava structure in the eastern metabasalt suggest rapid and subaquatic crystallization such as that widely observed and interpreted in other greenstone belt terrains (Anhaeusser 2014). The recovery of the volcanic rocks of the MNGB composed of metachert and BIF by lithological association, the absence of zircon xenocrysts, the manganiferous ilmenite occurrence in the western metabasalt and the carbonate and argilic-chloritic hydrothermal alteration zones developed on the western metabasalt indicate ocean floor settings (Zucchetti *et al*. 2000a, 2000b, Grachev *et al*. 2011, Spreafico 2017, Spreafico *et al*. 2018).

Enrichments of Cs, Ba, Th and light REE relative to Ta, Nb, Zr, Hf, Ti, Y and heavy REE and the flat pattern from Lu to Nd in the multielement diagram (Figs. 9A, 9B and 9C) show that the metakomatiite and the two metabasalts of the MNGB were generated from the metasomatized mantle above the subducting altered oceanic crust; Furnes *et al*. (2013) interpreted a similar enrichment in the Onverwacht Suite in the Barberton greenstone belt. However, the enrichment of light REE relative to heavy REE in the chondrite-normalized REE diagram (Boynton 1984; Figs. 8E and 8F) was more accentuated in the tholeiitic-calc-alkalic western metabasalt relative to the tholeiitic eastern metabasalt, indicating stronger assimilation processes in the western metabasalt that must have been accentuated by the metamorphic events during the Rhyacian-Orosirian period.

The effect of the heterogeneous crustal assimilation and metamorphism in the eastern and western metabasalts of the MNGB in the Paleoproterozoic may explain the differences in the mineral paragenesis. The eastern metabasalt, for example, is composed mainly of anorthite, bytownite, magnesiohornblende, ferrohornblende, augite, edenite and quartz; the western metabasalt comprises oligoclase, andesine, actinolite, ferrotschermakite, magnesiohornblende, biotite and quartz.

Both the eastern and western metabasalt samples of the MNGB plot in the IAT, MORB and WPB fields in the Zr vs. Zr/Y diagram (Fig. 9F); the eastern metabasalt plots in the IAT and MORB fields and the western metabasalt plots in the MORB and WPB field. The duplicity of fields by each metabasalt type appears initially uncertain; however, the proximity of settings during volcanism and the transition from one setting to other due to subsequent tectonic events with crustal enrichment must be considered. Therefore, the eastern and western metabasalts must be cogenetic and consistent with nearby intraoceanic settings in the MNGB, with different levels of crustal contamination during the formation in the oceanic crust by subduction components or intraoceanic contamination, and during metamorphism that probably occurred during the Rhyacian-Orosirian period. The stronger crustal assimilation in the western metabasalt displaces the plots to the WPB field, which is not observed in the eastern metabasalt plots.

The plots of the metakomatiite and eastern and western metabasalts of the MNGB in the Nb/Yb vs. Th/Yb diagram feature a steep vector oblique to the MORB-OIB array (Fig. 9E). Those MNGB plots extend from near the N-MORB point, in the MORB-OIB array, and enter the field of the volcanic arc array, avoiding the OIB point. This plot distribution is similar to the South Abitibi (Kerrich & Xie 2002, Xie & Kerrich 1994), Barberton (Jochum *et al*. 1991, Parman *et al*. 1997, Chavagnac 2004) and Isua (Polat & Hofmann 2003, Polat *et al*. 2002) Archean greenstone belts (Fig. 9E), which are interpreted as an intraoceanic provenance as discussed in Pearce (2008), and similar to the modern Mariana intraoceanic arc-basin system (Pearce *et al*. 2005). Moreover, the MNGB geochemical pattern observed in

the Nb/Yb vs. Th/Yb diagram shows that a subduction-related setting, in this case an intraoceanic arc, contributes to the increase in Th content in the rocks displacing the samples from the MORB-OIB array to the volcanic arc array. However, the eastern metabasalt samples remaining in the MORB-OIB array register the initial ocean crust and back-arc setting in the MNGB and, with increasing island arc proximity, the plots displace from the MORB-OIB array. The samples most affected by tectonothermal Rhyacian-Orosirian events would be those most displaced from the MORB-OIB array and with higher Th content, such as the western metabasalt samples.

The metadacite samples of the MNGB in which feldspars were removed from the melt via crystal fractionation plot in the volcanic arc field in the diagrams of Pearce *et al.* (1984; Figs. 9G and 9H) and do not match the anorogenic-type field in the diagram of Whalen (1987; Fig. 9I), thus excluding intracratonic possibilities. In addition, the average $(La/Yb)_N$ ratio of 8.87 in the metadacite may be interpreted as an oceanic crust setting with a slight crustal contamination subducting the oceanic crust according to Condie & Kronër (2013).

Rios (2017) interpreted an intraoceanic setting with a back-arc provenance for basalts in the Neoarchean Contendas-Mirante volcano-sedimentary sequence, which is also inserted in the Contendas-Jacobina Lineament (southern part); this volcano-sedimentary sequence is similar and coeval relative to the MNGB. In the Archean Rio das Velhas greenstone belt, southern São Francisco Craton, ocean floor metabasalts and the felsic volcanic rocks were interpreted as occurrences of island arc or back-arc basin settings (Zucchetti *et al.* 2000a, 2000b), which we also interpreted in the MNGB.

An intracontinental provenance has been described for the Umburanas greenstone belt, in the southern part of the Gavião Block in the eastern São Francisco Craton (Leal *et al.* 2003), with deposition over a continental crust. This provenance suggests a diversity of settings for the greenstone belts in the eastern part of the São Francisco Craton, more specifically in the Gavião Block; alternatively, the crustal contamination and tectonism may have intensively altered the mineralogical and geochemical pattern of the rocks, making identification of the former oceanic crust difficult.

Therefore, the intraoceanic arc-basin system appears suitable for defining the tectonic setting of the Neoarchean MNGB. The final amalgamation of the oceanic crust between the cratonic blocks (Gavião, Mairi and Serrinha blocks and Itabuna-Salvador-Curaçá Belt) of the northern and eastern São Francisco Craton in the Orosirian period (Leite 2002; Figs. 10A and 10B) contributed to changing mineralogical and geochemical patterns that hid the primary oceanic crust signatures in the MNGB rocks.
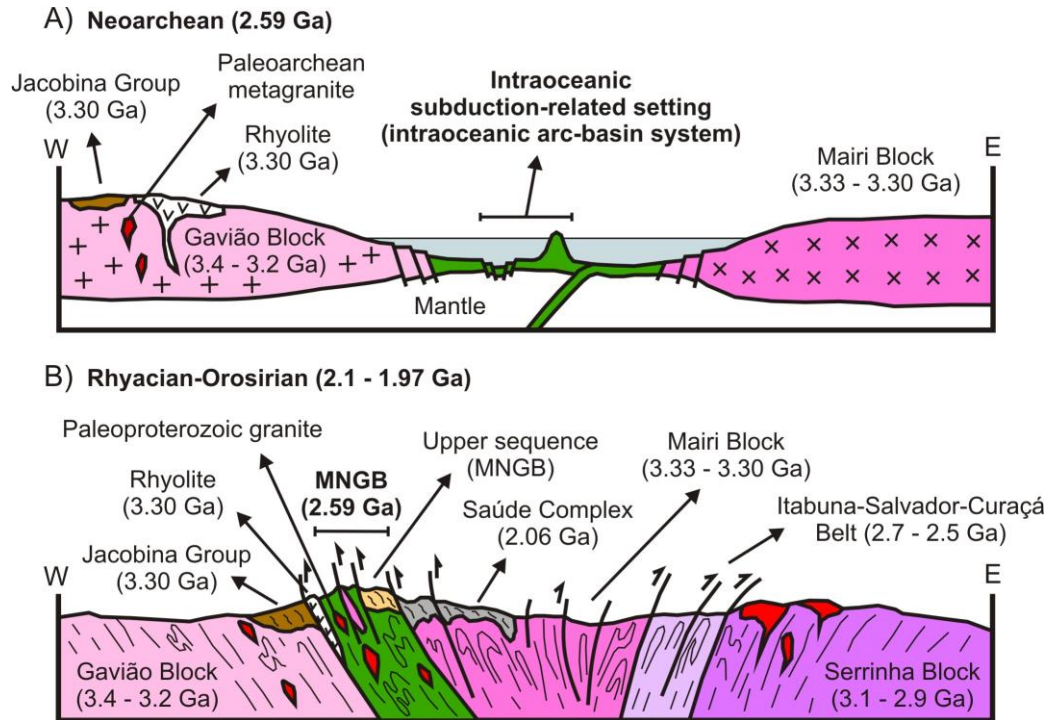
Figure 10. Intraoceanic setting proposed for the MNGB formation based on new data presented in this study and compiled ages for the Gavião Block, MNGB and Rhyacian-Orosirian granites (Mougeot 1996, Leite 2002, Peucat *et al*. 2002, Zincone *et al*. 2016, Spreafico 2017, Spreafico *et al*. 2018), Mairi Block (Sousa *et al*. 2018), Jacobina Group (Teles 2013, Teles *et al*. 2015, Barbuena *et al*. 2016), Serrinha Block (Oliveira *et al*. 2002a, 2002b, Rios *et al*. 2009), Itabuna-Salvador-Curaçá Belt (Silva *et al*. 1997, Oliveira *et al*. 2010) and Saúde Complex (Barbuena *et al*. 2016, Zincone *et al*. 2017). A) Oceanic crust between the Gavião and Mairi blocks and formation of the MNGB at 2595 Ma. B) Rhyacian-Orosirian tectonic event that compressed the MNGB between the cratonic blocks of the eastern São Francisco Craton.

7. Conclusions

1.   The intraoceanic and intracontinental provenance of Archean greenstone belts are described in the Gavião Block, eastern São Francisco Craton. However, those greenstones or volcano-sedimentary sequences inserted into regional tectonic lineaments show lithological and geochemical patterns of intraoceanic provenances, such as the MNGB and the Contendas-Mirante volcano-sedimentary sequence; both of which are placed in the Contendas-Jacobina Lineament. The MNGB has geological and tectonic similarities relative to other greenstones in other regions of the São Francisco Craton, such as the Rio das Velhas greenstone belt in the metallogenic province of the Quadrilátero Ferrífero.

2.   The volcanism in the MNGB was formed in an intraoceanic arc-basin system. The metakomatiite, eastern metabasalt and western metabasalt were formed in the near back-arc basin and island arc settings, mainly with MORB and IAT geochemical patterns. The tectonic processes in the oceanic arc systems enriched the Cs, Ba, Th and light REE content in the volcanic rocks. However, the compressional Rhyacian-Orosirian tectonothermal event contributed to accentuating the enrichment, mainly in the western metabasalt that was directly affected by Gavião Block rocks during compressional tectonism, forming tectonic slices emplaced in the basement to the west of the MNGB. The metakomatiite and eastern metabasalt were mainly affected by intraoceanic assimilations and the Rhyacian-Orosirian tectonism may have been heterogeneous in these rocks, which preserved primary textures such as spinifex in the metakomatiite and primary structures such as pillow lava in the eastern metabasalt.

3. The mineralogical particularities between eastern and western metabasalts are products of enrichment processes during the metamorphism in the Rhyacian-Orosirian. However, primary mineralogical differences can remain, since the volcanism is in nearby but different settings such as the back-arc basin and island arc.

4. The Neoarchean MNGB, formed in an intraoceanic arc-basin system, was compressed between cratonic blocks (Gavião, Mairi and Serrinha blocks and Itabuna-Salvador-Curaçá Belt) of the eastern São Francisco Craton during the Rhyacian-Orosirian period (Leite 2002; Figs. 10A and 10B), thus forming the Contendas-Jacobina Lineament within which the greenstone was accommodated. After the Rhyacian-Orosirian compressional tectonothermal event, the MNGB was juxtaposed to the Paleoarchean Gavião Block to the west and south, the Paleoarchean Jacobina Group to the northwest and the Paleoarchean Mairi Block to the east, beyond the Rhyacian-Orosirian intrusion of granites. The formation of the siliciclastic metasedimentary rocks of the upper sequence of the MNGB and the Saúde Complex are interpreted as coeval to the Rhyacian-Orosirian event.

5. For improving the geological and petrological interpretations present in this manuscript, we recommend geochronological and Nd and Sr isotope studies of the metavolcanic rocks for a more thorough understanding of the tectonic setting during the formation of the MNGB.

Acknowledgements

References

Anhaeusser C.R. 2014. Archaean greenstone belts and associated granitic rocks - A review. *Journal of African Earth Sciences*, **100**:684-732. https://doi.org/10.1016/j.jafrearsci.2014.07.019

Arndt N.T. 1994. Archean Komatiites. *Developments in Pre Cambrian Geology*, **1**:11-44. https://doi.org/10.1016/S0166-2635(08)70219-6

Barbosa J. S. F. 1997. Síntese do Conhecimento sobre a Evolução Geotectônica das Rochas Metamórficas Arqueanas e Paleoproterozóicas do Embasamento do Cráton do São Francisco na Bahia. *Revista Brasileira de Geociências*, **27**(3):241-256. DOI:10.25249/0375-7536.1997241256

Barbosa J.S.F., Cruz S.C.P., Souza J.S. 2012a. Terrenos metamórficos do embasamento. In: Barbosa, J.S.F. (Ed.). Geologia da Bahia: Pesquisa e Atualização. Salvador, CBPM, p. 101-201. http://www.cbpm.ba.gov.br/modules/conteudo/conteudo.php?conteudo=24

Barbosa J.S.F., Pinto M.S., Cruz S.C.P., Souza J.S. 2012b. Granitoides. In: Barbosa, J.S.F. (Ed.). Geologia da Bahia: Pesquisa e Atualização. Salvador, CBPM, p. 327-396. http://www.cbpm.ba.gov.br/modules/conteudo/conteudo.php?conteudo=24

Barbosa J.S.F. & Sabaté P. 2002. Geological features and the Paleoproterozoic collision of four Archean crustal segments of the São Francisco Craton, Bahia, Brazil. A synthesis. Rio de Janeiro, *Anais da Academia Brasileira de Ciências*, **74**(2):343-359. http://dx.doi.org/10.1590/S0001-37652002000200009

Barbosa J.S.F. & Sabaté P. 2003. Colagem paleoproterozoica de placas arqueanas do Cráton do São Francisco na Bahia. *Revista Brasileira de Geociências*, **33**(1-suplemento):7-14. DOI: 10.25249/0375-7536.200333S10714

Barbosa J.S.F. & Sabaté P. 2004. Archean and Paleoproterozoic crust of the São Francisco Craton, Bahia, Brazil: geodynamic features. *Precambrian Research*, **133**(1-2): 1-27. https://doi.org/10.1016/j.precamres.2004.03.001

Barbuena D., Oliveira E.P., Zincone S.A. 2016. Estudos de proveniência dos quartzitos do Greenstone Belt Mundo Novo (BA) e implicações tectono-estratigráficas. In: 48° Congresso Brasileiro de Geologia. Porto Alegre, *Anais*, p. 818. http://cbg2017anais.siteoficial.ws/anais48cbgcompleto.pdf

Bickle M.J., Nisbet E.G., Martin A. 1994. Archean greenstone belts are not oceanic crust. *The Journal of Geology*, **102**(2):121-137. https://doi.org/10.1086/629658

Boynton W.V. 1984. Geochemistry of the rare earth elements: meteorite studies. In: Henderson, P. (Ed.). Rare Earth Element Geochemistry. Amsterdan, Elsevier, p. 63-114. https://doi.org/10.1016/B978-0-444-42148-7.50008-3

Chavagnac V. 2004. A geochemical and Nd isotopic study of Barberton komatiites (South Africa): implication for the Archean mantle. *Lithos*, **75**(3-4):253-281. https://doi.org/10.1016/j.lithos.2004.03.001

Condie K.C. & Kronër A. 2013. The building blocks of continental crust: Evidence for a major change in the tectonic setting of continental growth at the end of the Archean. *Gondwana Research*, **23**:394-402. https://doi.org/10.1016/j.gr.2011.09.011

Couto P.A., Sampaio A.R., Gil C.A.A., Loureiro H.C., Arcanjo J.B., Fernandes Filho J., Guimarães J.T., Campelo R., Mascarenhas J.F., Bruni D.C., Toledo L.A.A. 1978. *Projeto Serra de Jacobina: Geologia e Prospecção Geoquímica*. Relatório Final. Salvador, DNPM/CPRM, 415 p. http://rigeo.cprm.gov.br/jspui/handle/doc/9602

De Wit M.J., Hart R.A., Hart R.J. 1987. The Jamestown ophiolite complex, Barberton Mountain Belt: a section through 3.5 Ga oceanic crust. *Journal of African Earth Sciences*, **6**(5):681-730. https://doi.org/10.1016/0899-5362(87)90007-8

Fettes D.J., Desmons J., Árkai P., Brodie K., Bryhni I. 2007. *Metamorphic rocks: a classification and glossary terms*. Cambridge, Cambridge University Press, 244 p. https://lib.ugent.be/catalog/rug01:001234988

Furnes H., de Wit M., Robins B. 2013. A review of new interpretations of the tectonostratigraphy, geochemistry and evolution of the Onverwacht Suite, Barberton Greenstone Belt, South Africa. *Gondwana Research*, **23**:403-428. https://doi.org/10.1016/j.gr.2012.05.007

Grachev A.F., Pechersky D.M., Tsel'movich V.A. 2011. Titanomagnetites and ilmenites from the Early Cenozoic Basalts and Limburgites of the Northern Tien Shan. *Physics of the Solid Earth* **47**(6):475-487. https://doi.org/10.1134/S106935131105003X

Herzberg C. 1995. Generation of plume magmas through time: an experimental perspective. *Chemical Geology*, **126**(1):1-16. https://doi.org/10.1016/0009-2541(95)00099-4

Hofmann A.W. 1988. Chemical differentiation of the Earth: the relationship between mantle, continental crust, and oceanic crust. *Earth and Planetary Science Letters*, **90**:297-314. https://doi.org/10.1016/0012-821X(88)90132-X

Irvine T.N. & Baragar W.R.A. 1971. A guide to the Chemical Classification of the Common Volcanic Rocks. *Canadian Journal of Earth Sciences*, **8**:523-548. https://doi.org/10.1139/e71-055

Jahn B.M., Gruau G., Glikson A.Y. 1982. Komatiites of the Onverwacht Group, S. Africa: REE Geochemistry, Sm/Nd Age and Mantle Evolution. *Contributions to Mineralogy and Petrology*, **80**:25-40. https://link.springer.com/article/10.1007/BF00376732

Janousek V., Farrow C.M., Erban V. 2006. Interpretation of whole-rock geochemical data in igneous geochemistry: introducing Geochemical Data Toolkit (GCDkit). *Journal of Petrology*, **47**(6):1255-1259. https://doi.org/10.1093/petrology/egl013

Jensen L.S. 1976. A new cation plot for classifying subalkalic volcanic rocks. Ontario, Ontario Division of Mines, Miscellaneous Paper 66, 22 p. http://www.geologyontario.mndmf.gov.on.ca/mndmfiles/pub/data/imaging/MP066/MP066.pdf

Jochum K.P., Arndt N.T., Hofmann A.W. 1991. Nb-Th-La in komatiites and basalts; constraints on komatiite petrogenesis and mantle evolution. *Earth Planetary Science Letters*, **107**:272-289. https://doi.org/10.1016/0012-821X(91)90076-T

Kerrich R. & Xie Q. 2002. Compositional recycling structure of an Archean super-plume: Nb-Th-U-LREE systematics of Archean komatiites and basalts revisited. *Contributions to Mineralogy and Petrology*, **142**(4):476–484. https://doi.org/10.1007/s004100100301

Kretz R. 1983. Symbols for rock-forming minerals. *American Mineralogist*, **68**:277-279. https://www.researchgate.net/publication/216831138_Symbols_for_rock-forming_minerals

Leake B.E., Woolley A.R., Arps C.E.S., Birch W.D., Gilbert M.C., Grice J.D., Hawthorne F.C., Kato A., Kisch H.J., Krivovichev V.G., Linthout K., Laird J., Mandarino J.A., Maresch W.V., Nickel E.H., Rock N.M.S., Schumacher J.C., Smith D.C., Stephenson N.C.N., Ungaretti L., Whittaker E.J.W., Youzhi G. 1997. Nomenclature of Amphiboles: Report of the Subcommittee on Amphiboles of the International Mineralogical Association Commission on New Minerals and Mineral Names. *The Canadian Mineralogist*, **35**(1):219-246.

Leal L.R.B. 1998. *Geocronologia U/Pb (SHRIMP), 207Pb/206Pb, Rb/Sr, Sm/Nd e K/Ar dos Terrenos Granito-Greenstone do Bloco do Gavião: Implicações para a Evolução Arqueana e Paleoproterozoica do Cráton do São Francisco, Brasil*. PhD Thesis, Universidade de São Paulo, São Paulo, 178 p. http://www.teses.usp.br/teses/disponiveis/44/44134/tde-08012016-145912/pt-br.php

Leal L.R.B., Cunha J.C., Cordani U.G., Teixeira W., Nutman A.P., Leal A.B.M., Macambira M.J.B. 2003. Shrimp U-Pb, [207]Pb/[206]Pb zircon dating, and Nd isotopic signature of the Umburanas greenstone belt, northern São Francisco craton, Brazil. *Journal of South American Earth Sciences*, **15**(7):775-785. https://doi.org/10.1016/S0895-9811(02)00129-3

Leite C.M.M. 2002. *A Evolução Geodinâmica da Orogênese Paleoproterozóica nas Regiões de Capim Grosso, Jacobina e Pintadas - Mundo Novo (Bahia-Brasil): Metamorfismo, Anatexia Crustal e Tectônica.* PhD Thesis, Universidade Federal da Bahia, Salvador, 408 p.

Leite C.M.M., Barbosa J.S.F., Nicollet C., Sabaté P. 2007. Evolução metamórfica/metassomática paleoproterozóica do Complexo Saúde, da Bacia Jacobina e de leucogranitos peraluminosos na parte norte do Cráton do São Francisco. *Revista Brasileira de Geociências*, **37**(4):777-797. DOI: 10.25249/0375-7536.2007374777797

Loureiro H.S.C. 1991. *Programa Levantamentos Geológicos Básicos do Brasil. Mundo Novo. Folha SC24-Y-D-IV. Estado da Bahia.* Salvador, DNPM/CPRM, 177 p. http://rigeo.cprm.gov.br/jspui/handle/doc/8498

Lynch L. 1996. Provisional elemental values for four new geochemical soil and till reference materials, TILL-1, TILL-2, TILL-3 and TILL-4. *Geostandards and Geoanalytical Research*, **20**(2):277-287. https://doi.org/10.1111/j.1751-908X.1996.tb00189.x

Magee C.W., Palin J.M., Taylor W.R. 2001. Laser ICP-MS U/Pb analyses of detrital zircons from Proterozoic sediments in Bahia state, Brazil; implications for the evolution of the São Francisco craton prior to 3,3 Ga. In: 11th V.M. Goldschmidt Conference, Hot Springs, abstract 3501. https://www.lpi.usra.edu/meetings/gold2001/pdf/3501.pdf

Mascarenhas J.F. 1976. Estruturas do tipo greenstone belt no leste da Bahia. In: Congresso Brasileiro de Geologia. Belo Horizonte, *Anais*, v. 4, p. 25-49.

Mascarenhas J.F., Guimarães J.T., Moraes L.C., Queiroz C.J.A., Marinho M.M., Neves J.P. 1975. *Projeto Bahia: Geologia da Folha de Senhor do Bonfim.* Relatório Final. Salvador, DNPM/CPRM, v. 5.

Mascarenhas J.F., Ledru P., Souza S.L., Filho V.M.C., Melo L.F.A., Lorenzo C.L., Milesi J.P. 1998. Geologia e recursos minerais do Grupo Jacobina e da parte sul do Greenstone Belt de Mundo Novo. *Série Arquivos Abertos*, n. 13, 58 p. http://www.cbpm.ba.gov.br/modules/conteudo/conteudo.php?conteudo=23

Mascarenhas J.F. & Silva E.F.A. 1994. Greenstone Belt de Mundo Novo: caracterização e implicações metalogenéticas no Cráton do São Francisco. *Série Arquivos Abertos*, n. 5, 32 p. http://www.cbpm.ba.gov.br/modules/conteudo/conteudo.php?conteudo=23

Middlemost E.A.K. 1994. Naming materials in the magma/igneous rock system. *Earth Science Reviews*, **37**(3-4):215-224. https://doi.org/10.1016/0012-8252(94)90029-9

Morimoto N. 1988. Nomenclature of pyroxenes. *Mineralogy and Petrology*, **39:**55-76. https://link.springer.com/article/10.1007/BF01226262

Mougeot R. 1996. *Étude de la limite Archéen-Protérozoïque et des minéralisations Au ± U associées. Exemples de la région de Jacobina (Etat de Bahia, Brésil) et de Carajas (Etat de Para, Brésil).* PhD Thesis, Université de Montpellier II, Montpellier, 306 p. http://www.theses.fr/1996MON20131

Oliveira E.P., Mcnaughton N.J., Armstrong R. 2010. Mesoarchaean to Paleoproterozoic growth of the northern segment of the Itabuna-Salvador-Curaçá orogeny, São Francisco Cráton, Brazil. In: Kusky, T.M., Zhai, M.G., Xiao, W. (Eds.), The evolving continents: understanding processes of continental growth. London, Geological Society Special Publication, **338**, p. 263-286. https://doi.org/10.1144/SP338.1

Oliveira E.P., Mello E.F., Mcnaughton N. 2002a. Reconnaissance U–Pb geochronology of Precambrian quartzites from the Caldeirão belt and their basement, NE São Francisco Craton, Bahia, Brazil: implications for the early evolution of the Paleoproterozoic Itabuna-Salvador-Curaçá orogeny. *Journal of South American Earth Sciences*, **15**(3):349-362. https://doi.org/10.1016/S0895-9811(02)00039-1

Oliveira E.P., Mello E.F., McNaughton N.J., Choudhuri A. 2002b. SHRIMP U-Pb age of the basement to the Rio Itapicuru Greenstone Belt, NE São Francisco craton. In: 41° Congresso Brasileiro de Geologia. João Pessoa, *Anais*, p. 522.

Parman S.W., Dunn J.C., Grove T.L., De Wit M.J. 1997. Emplacement conditions of komatiite magmas from the 3.49 Ga Komati Formation, Barberton greenstone Belt, South Africa. *Earth and Planetary Science Letters*, **150**(3-4):303-323.

Parman S.W., Grove T.L., Dann J.C. 2001. The production of Barberton komatiites in an Archean subduction zone. *Geophysical Research Letters*, **28**(13):2513-2516. https://doi.org/10.1029/2000GL012713

Pearce, J.A. 2005. Mantle preconditioning by melt extraction during flow: theory and petrogenetic implications. *Journal of Petrology*, **46**(5):973-997. https://doi.org/10.1093/petrology/egi007

Pearce J.A. 2008. Geochemical fingerprinting of oceanic basalts with applications to ophiolite classification and the search for Archean oceanic crust. *Lithos*, **100**:14-48. https://doi.org/10.1016/j.lithos.2007.06.016

Pearce J.A. 2014. Geochemical fingerprinting of the Earth's Oldest Rocks. *Geology*, **42**(2):175-176. https://doi.org/10.1130/focus022014.1

Pearce J.A., Harris N.B.W., Tindle A.G. 1984. Trace element discrimination diagrams for the tectonic interpretation of granitic rocks. *Journal of Petrology*, **25**(4):956-983. https://doi.org/10.1093/petrology/25.4.956

Pearce J.A. & Parkinson I.J. 1993. Trace element models for mantle melting: application to volcanic arc petrogenesis. In: Prichard, H.M., Alabaster, T., Harris, N.B.W., Neary, C.R. (Eds.). Magmatic Processes and Plate Tectonics. London, Geological Society of London Special Publication, **76**, p. 373-403.

Pearce J.A., Stern R.J., Bloomer S.H., Fryer P. 2005. Geochemical mapping of the Mariana Arc-Basin System: implications for the nature and distribution of subduction components. *Geochemistry, Geophysics, Geosystems*, **6**(7):1-27. https://doi.org/10.1029/2004GC000895

Peucat J.J., Mascarenhas J.F., Barbosa J.S.F., Souza S.L., Marinho M.M., Fanning C.M., Leite C.M.M. 2002. 3,3 Ga SHRIMP U-Pb zircon age of a felsic metavolcanic rock from the Mundo Novo Greenstone Belt in the São Francisco Craton, Bahia (NE Brazil). *Journal of South American Earth Sciences*, **15**:363-373. https://doi.org/10.1016/S0895-9811(02)00044-5

Polat A. & Hoffmann A.W. 2003. Alteration and geochemical patterns in the 3.7-3.8 Ga Isua greenstone belt, West Greenland. *Precambrian Research*, **126**(3):197-218. DOI: 10.1016/S0301-9268(03)00095-0

Polat A., Hoffmann A.W., Rosing M.T. 2002. Boninite-like volcanic rocks in the 3.7-3.8 Ga Isua greenstone belt, West Greenland: geochemical evidence for intra-oceanic subduction zone processes in the early Earth. *Chemical Geology*, **184**(3-4):231-254. https://doi.org/10.1016/S0009-2541(01)00363-1

Polat A. & Kerrich R. 2001. Magnesian andesites, Nb-enriched basalt-andesites, and adakites from late-Archean 2.7 Ga Wawa greenstone belts, Superior Province, Canada: implications for late Archean subduction zone petrogenetic processes. *Contributions to Mineralogy and Petrology*, **141**(1):36-52. DOI: 10.1007/s004100000223

Ramsay J.G. & Huber M.I. 1987. *The techniques of Modern Structural Geology. Vol. 2: Folds and Fractures*. Londres, Pergamon Press, 703 p.

Reis C., Menezes R.C.L., Miranda D.A., Santos F.P., Loureiro H.C., Neves J.P., Viera R. 2017. *Mapa geológico-geofísico: Projeto ARIM Serra de Jacobina*. Salvador: CPRM. http://rigeo.cprm.gov.br/jspui/handle/doc/18679

Reis C., Oliveira R.C.L., Miranda D.A., Santos F.P., Guimarães J.T., Teles G. 2018. Estratigrafia do grupo Jacobina. In: 49° Congresso Brasileiro de Geologia. Rio de Janeiro, *Anais*, p. 1232. http://cbg2018anais.siteoficial.ws/resumos/7641.pdf

Rios C.V. 2017. *Geologia isotópica das formações ferríferas bandadas do Cráton São Francisco na transição Arqueano Paleoproterozoico*. PhD Thesis, Instituto de Geociências, Universidade de Brasília, Brasília, 243 p.

Rios D.C., Davis D.W., Conceição H., Davis W.J., Rosa M.L.S., Dickin A.P. 2009. Geologic evolution of the Serrinha nucleus granite-greenstone terrane (NE Bahia, Brazil) constrained by U-Pb single zircon geochronology. *Precambrian Research*, **170**(3-4):175-201. https://doi.org/10.1016/j.precamres.2008.10.001

Rollinson H. R. 1993. *Using Geochemical Data: Evaluation, Presentation, Interpretation*. England, Longman Scientific and Technical, 352 p.

Sabaté P., Marinho M.M., Vidal P., Caen Vachette M. 1990. The 2-Ga peraluminous magmatism of the Jacobina–Contendas Mirante belts (Bahia, Brazil): geologic and isotopic constraints on the sources. *Chemical Geology*, **83**(3-4):325-338. https://doi.org/10.1016/0009-2541(90)90288-I

Schmid R., Fettes D., Harte B., Davis E., Desmons J. How to name a metamorphic rock. Recommendations by the IUGS Subcommission on the Systematics of Metamorphic Rocks. Web version 01.02.07. IUGS Commission on the Systematics in Petrology. Available in <www.bgs.ac.uk/scmr/home.html>. Access on: 22 sep. 2018.

Siivola J. & Schmid R. A systematic nomenclature for metamorphic rocks. 12. List of mineral abbreviations. Recommendations by the IUGS Subcommission on the Systematics of Metamorphic Rocks. Web version 01.02.07. IUGS Commission on the Systematics in Petrology. Available in: <https://www.bgs.ac.uk/downloads/start.cfm?id=3197>. Access in: 16 nov. 2017.

Silva L.C., Armstrong R., Delgado I.M., Pimentel M., Arcanjo J.B., Melo R.C., Teixeira L.R., Jost H., Cardoso Filho J.M., Pereira L.H.M. 2002. Reavaliação da evolução geológica em terrenos Pré-Cambrianos brasileiros com base em novos dados U-Pb SHRIMP, Parte I: Limite centro-oriental do Cráton São Francisco na Bahia. *Revista Brasileira de Geociências*, **32**(4):501-512. DOI: 10.25249/0375-7536.2002324501512

Silva L.C., McNaughton N.J., Melo R.C., Fletcher I.R. 1997. U-Pb SHRIMP ages in the Itabuna-Caraíba TTG high-grade complex: the first window beyond the Paleoproterozoic overprinting of the eastern Jequié Craton, NE Brazil. In: Isgam International Symposium on Granites and Associated Mineralization. Salvador, *abstracts*, v. 1, p. 282-283. https://www.researchgate.net/publication/284106273

Sousa D.F.M., Oliveira E.P., Amaral W.S. 2018. Geologia e geocronologia U-Pb em zircão de ortognaisses e K-granitoides relacionados ao Bloco Gavião (Complexo Mairi) e Cinturão Salvador-Curaçá – Região da Mina Caraíba – Bahia. In: 49° Congresso Brasileiro de Geologia. Rio de Janeiro, *Anais*, p. 980. http://cbg2018anais.siteoficial.ws/resumos/8534.pdf

Souza S.L., Garrido I.A.A., Oliveira N.S., Fróes R.J. 2002. *Projeto Greenstone Belt de Mundo Novo: estudos geológicos regionais*. Salvador, CBPM, v. 1, 62 p.

Spreafico R.R. 2017. *Projeto Mundo Novo: texto e mapas*. Salvador, CBPM, 84 p.

Spreafico R.R., Barbosa J.S.F., Barbosa N.S., Moraes A.M.V., Souza Júnior F.D. 2018. A idade Neoarqueana (2,59 Ga, U-Pb) do *greenstone belt* Mundo Novo, Bahia, Brasil. In: 49° Congresso Brasileiro de Geologia. Rio de Janeiro, *Anais*, p. 1930. http://cbg2018anais.siteoficial.ws/resumos/7518.pdf

Storey M., Saunders A.D., Tarney J., Leat P.T., Thirlwall M.F., Thompson R.N., Menzies M.A., Marriner G.F. 1988. Geochemical evidence for plume-mantle interactions beneath Kerguelen and Heard Islands, Indian Ocean. *Nature*, **336**:371–374. https://doi.org/10.1038/336371a0

Teles G.S. 2013. *Proveniência e idades de deposição dos sedimentos auríferos da Bacia de Jacobina: Implicações sobre a evolução da bacia durante o Paleo-Arqueano e a gênese da mineralização*. MS Dissertation, Instituto de Geociências, Universidade de Brasília, Brasília, 122 p. http://repositorio.unb.br/handle/10482/14972

Teles G.S., Chemale F., Oliveira C.G. 2015. Paleoarchean record of the detrital pyrite-bearing, Jacobina Au-U deposits, Bahia, Brazil. *Precambrian Research*, **256**:289-313. https://doi.org/10.1016/j.precamres.2014.11.004

Thompson M. 1988. Variation of precision with concentration in an analytical system. *Analyst*, **113**:1579-1587. DOI: 10.1039/AN9881301579

Whalen, J.B., Currie, K.L., Chappell, B.W. 1987. A-type granites: geochemical characteristics, discrimination and petrogenesis. *Contributions to Mineralogy and Petrology*, **95**(4):407-419. https://link.springer.com/article/10.1007/BF00402202

Whitney D.L. & Evans B.W. 2010. Abbreviations for names of rock-forming minerals. *American Mineralogist*, **95**(1):185-187. https://doi.org/10.2138/am.2010.3371

Wilson N. 1987. *Combined Sm-Nd, Pb-Pb and Rb-Sr geochronology and isotope geochemistry in polymetamorphic precambrian terrains: examples from Bahia, Brazil and Channel Island*. MS Dissertation, U.K. Master, Oxford University, England, 150 p.

Xie Q. & Kerrich R. 1994. Silicate–perovskite and majorite signature komatiites from the Archean Abitibi greenstone belt; implications for early mantle differentiation and stratification. *Journal of Geophysical Research*, **99**(B8):15799-15812. https://doi.org/10.1029/94JB00544

Zincone S.A., Barbuena D., Oliveira E.P., Baldim M.R. 2017. Detrital zircon U-Pb ages as evidence for deposition of the Saúde Complex in a Paleoproterozoic foreland basin, northern São Francisco Craton, Brazil. *Journal of South American Earth Sciences*, **79**:537-548. https://doi.org/10.1016/j.jsames.2017.09.009

Zincone S.A., Oliveira E.P., Laurent O., Zhang H., Zhai M. 2016. 3,3 Ga High-Silica Intraplate Volcanic-Plutonic System of the Gavião Block, São Francisco Craton, Brazil: Implications of an intracontinental rift following the creation of insulating continental crust. *Lithos*, **266**:414-434. https://doi.org/10.1016/j.lithos.2016.10.011

Zucchetti M., Lobato L.M., Baars F.J. 2000a. Genetically diverse basalt geochemical signatures developed in the Rio das Velhas greenstone belt, Quadrilátero Ferrífero, Minas Gerais, Brazil. *Revista Brasileira de Geociências*, **30**(3):397-402.

Zucchetti M., Lobato L.M., Baltazar O.F. 2000b.Volcanic and volcaniclastic features in Archean rocks and their tectonic environments, Rio das Velhas greenstone belt, Quadrilátero Ferrífero, MG - Brazil. *Revista Brasileira de Geociências*, **30**(3):388-392.

CAPÍTULO 3

ARTIGO 2 - TECTONIC EVOLUTION OF THE NEOARCHEAN MUNDO NOVO GREENSTONE BELT, EASTERN SÃO FRANCISCO CRATON, NE BRAZIL: PETROLOGY, U-Pb GEOCHRONOLOGY, AND Nd AND Sr ISOTOPIC CONSTRAINTS

Abstract

Field, petrographic, lithogeochemical, LA-ICP-MS in situ U-Pb zircon geochronology, and Nd and Sr isotopic data were used to determine the geologic evolution, timing of volcanism and tectonic setting of the Mundo Novo greenstone belt (MNGB) including nearby units, such as the basement and younger granitic rocks in the eastern São Francisco Craton (NE Brazil). The basement of the greenstone belt corresponds to the Gavião Block, which comprises tonalite-trondhjemite-granodiorite orthogneisses, migmatites and subordinate metarhyolites and metagranites. The MNGB is divided into three lithological sequences: (i) the lowermost unit is composed of metakomatiites; (ii) the middle unit is composed mainly of metabasalts, metadacites and metasedimentary chemical rocks; and (iii) the uppermost unit is composed of metasedimentary siliciclastic rocks. Additionally, two Rhyacian-Orosirian granitic plutons occur in the area, the Areia Branca and Jequitibá metagranites. U-Pb zircon data from the Miguel Calmon and Fazenda Coqueiro metagranites in the Gavião Block yield crystallization ages of 3355 ± 16 Ma and 3227 ± 23 Ma, respectively, and both metagranites were derived from the lower continental crust based on low $^{87}Sr/^{86}Sr_i$ values (0.699 and 0.705, respectively) and negative values of $\varepsilon_{Nd(t)}$ (-3.7 and -3.6, respectively). The 2595 ± 21 Ma U-Pb zircon crystallization age of the metadacites allowed the determination of the timing of volcanism in the middle sequence of the MNGB. The 2106 ± 71 Ma and 1975 ± 36 Ma U-Pb zircon crystallization ages for the Areia Branca and Jequitibá metagranites, respectively, which are both interpreted as derived from crustal protoliths based on high $^{87}Sr/^{86}Sr_i$ values (0.744 and 0.730, respectively) and negative values of $\varepsilon_{Nd(t)}$ (-7.7 and -6.5, respectively), record a Rhyacian-Orosirian tectonothermal event that affected the MNGB and the adjoining region. The whole-rock geochemical data in tectonic discrimination and multielement diagrams show that the volcanic rocks of the MNGB formed in island arc and back-arc basin settings related to the oceanic crust. Therefore, the following five stages are proposed for the tectonic evolution of the study region: stages (i) and (ii) were characterized by the establishment of the TTG basement by 3.35 Ga, when the Miguel Calmon granite was consolidated, followed by a rifting that formed the rhyolites, and subsequent granite formations occurred at 3.22 Ga (Fazenda Coqueiro granite formation), followed by the abort of the rift and a closure event. The volcanism during stage (iii) at 2.59 Ga in the MNGB occurred in island arc and back-arc basins in the oceanic crust between Archean cratonic blocks, and stages (iv) and (v) between 2.10 Ga and 1.97 Ga represent two stages of a progressive collision event in which the oceanic crust was compressed between the Gavião, Mairi, Jequié and Serrinha blocks and the Itabuna-Salvador-Curaçá Belt from the eastern part of the São Francisco Craton. The collisional event of stages (iv) and (v) was coeval with the Rhyacian-Orosirian formation of

granites and basins such as that where the uppermost siliciclastic sequence of the MNGB was deposited.

Keywords: Mundo Novo greenstone belt; Neoarchean; U-Pb geochronology; São Francisco Craton; Brazil

1. Introduction

Greenstone belts are extremely varied Archean geological entities. These belts contain highly diverse rocks that have generally experienced multiple stages of deformation, metamorphism, and metasomatic alteration because of their great age and geotectonic settings and that have been intruded by mafic, ultramafic and granitoid rocks (Anhaeusser, 2014). Moreover, the predominance of basalts and komatiites deposited subaqueously has resulted in a wide variety of geotectonic settings proposed for greenstone belts, ranging from island arcs to plume-related submarine plateaus, mid-ocean ridges (including ophiolites) and back-arc basins (De Wit et al., 1987; Storey et al., 1991; Parman et al., 2001; Chavagnac, 2004; Furnes et al., 2013). The adjoining granite-gneiss terranes in the adjacencies of greenstone belts possibly represent an exhumed mid- to lower-crustal complex that formed the basement of greenstone belts (Dziggel et al., 2002). Tectonism may also contribute to the thrusting of the greenstone terranes on the granite-gneiss terranes during the amalgamation process. The understanding of the geologic setting of greenstone belts and their relationships with the granite-gneiss adjoining units is important in characterizing the genesis and tectonic evolution of these terranes.

The greenstone belt terrain in the eastern portion of the São Francisco Craton, Bahia State, NE Brazil (Fig. 1A-B), has been intensively studied since 1970, when the first geological map of the Mundo Novo region was completed (Couto et al., 1978; Loureiro, 1991) and the base metal deposit of Fazenda Coqueiro was discovered (Fig. 1C). The metavolcano-sedimentary sequence of Mundo Novo, defined as a greenstone belt terrain by Mascarenhas and Silva (1994), has been the subject of a recent geological survey by Companhia Baiana de Pesquisa Mineral (CBPM), Brazil, and new geological, petrological and geochronological data, mainly from outcrops and drill hole samples available from CBPM, are presented in this paper. The new komatiite occurrences discovered in the central portion of the Mundo Novo greenstone belt (MNGB), for example, allow better understanding of the Archean granite-greenstone terrains of the São Francisco Craton. Moreover, the Fazenda Coqueiro base metal deposit (Fig. 1C-2) has long been studied and has enhanced the interest in the MNGB because its existence suggests that the MNGB may host other important mineral deposits (Souza et al., 2002; Monteiro et al., 2009).

The first consideration regarding the existence of a greenstone belt in the Mundo Novo and Piritiba regions (Mascarenhas and Silva, 1994) included a larger area than that defined today (Fig. 1C). Thus, the ultramafic rocks and tholeiitic basalts of the Jacobina Group (Leo et al., 1964; Mascarenhas et al., 1998), the volcano-sedimentary association to the east of the Jacobina Ridge (Couto et al., 1978; Loureiro, 1991) and the metarhyolites of the Fazenda Coqueiro deposit, for example, are no longer considered part of the MNGB (Zincone et al., 2016; Spreafico, 2017; Reis et al., 2017; Barbosa et al., 2018). In this manner, the area assumed to be the MNGB in this paper, based on the geological, petrological and geochronological data presented herein, is shown in Fig. 2.

The felsic metavolcanic rocks that occur near the Fazenda Coqueiro deposit, with a previously published age of 3305 ± 9 Ma (Peucat et al., 2002; Zincone et al., 2016), are actually interpreted as part of the basement of the MNGB (Zincone et al., 2016). This interpretation has left open questions regarding the timing of the ocean floor volcanism in the

MNGB and the tectonic evolution of the MNGB and surrounding rocks. The geologic history of the study area extends from the formation of the basement during the Paleoarchean (Mougeot, 1996) until the last tectonothermal event recorded in the region, which was marked by Rhyacian-Orosirian granitogenesis (Leite, 2002) and was coeval with the formation of Paleoproterozoic basins, such as the uppermost unit in the MNGB and the Saúde Basin (Barbuena et al., 2016; Zincone et al., 2017).

   Laser ablation inductively coupled plasma mass spectrometry (LA-ICP-MS) U-Pb zircon ages and thermal ionization mass spectrometry (TIMS) Nd and Sr isotopic data have been combined with petrographic, mineral chemistry and whole-rock geochemical data from the MNGB and adjoining rocks. Two metagranites in the basement, one felsic metavolcanic rock related to the metamorphosed mafic and ultramafic rocks in the MNGB and two late metagranites were analyzed. The objective was to propose a model for the tectonic evolution of the MNGB in the eastern portion of the São Francisco Craton. Therefore, this study analyzes the formation of the cratonic basement during the Paleoarchean, the timing and tectonic setting of the volcanism in the MNGB, the amalgamation of the MNGB between cratonic blocks during the Paleoproterozoic orogeny, and the subsequent tectonic stability and late sedimentary events.
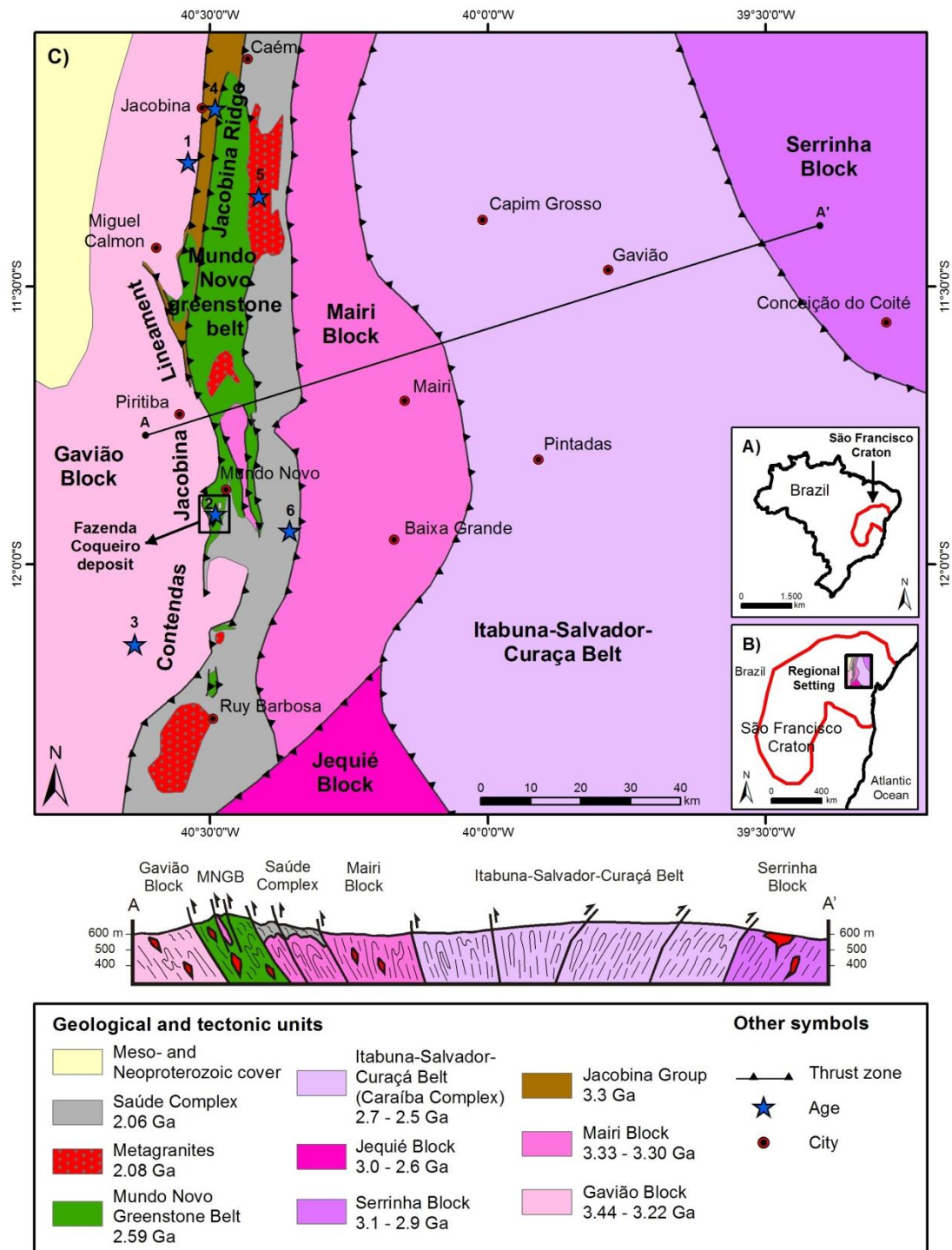
Fig. 1. A) Location of the São Francisco Craton in NE Brazil. B) Study area in the eastern portion of the São Francisco Craton. C) Regional tectonic setting of the MNGB (modified from Barbosa and Sabaté, 2002, 2003, 2004). Ages in the points highlighted on the map: 1- 3442 ± 2 Ma (ID-TIMS U-Pb zircon, TTG; Mougeot, 1996); 2- 3303 ± 11 Ma (LA-ICP-MS U-Pb zircon, metarhyolite from the Gavião Block; Zincone et al., 2016); 3- 3292 ± 3 Ma (LA-ICP-MS U-Pb zircon, metagranite from the Gavião Block; Zincone et al., 2016); 4- 3500 - 3220 Ma (LA-MC-ICP-MS U-Pb zircon, quartzite from the Jacobina Group; Teles et al., 2015); 5- 2080 ± 18 Ma (Electron Microprobe U-Pb monazite, Cachoeira Grande granite; Leite, 2002); 6- 2068 ± 12 Ma (LA-MC-ICP-MS U-Pb zircon, biotite schist from the Saúde Complex; Zincone et al., 2017).

2. Regional geologic setting of the MNGB and surrounding units

The MNGB is situated in the eastern portion of the São Francisco Craton, NE Brazil, more precisely, on the eastern boundary of the Gavião Block (Barbosa and Sabaté, 2002, 2003, 2004) and in the Contendas-Jacobina Lineament setting (Sabaté et al., 1990) (Fig. 1C).

The eastern portion of the São Francisco Craton, where the MNGB is situated (Bahia State), formed through the amalgamation of four Archean blocks during Paleoproterozoic continent-continent collisions (Barbosa and Sabaté, 2002, 2003, 2004), including the Gavião, Serrinha and Jequié blocks and the Itabuna-Salvador-Curaçá Belt (Fig. 1C). The Paleoproterozoic event captured oceanic crust between the cratonic blocks, and the uplift caused by this event possibly resulted in erosion and the formation of Paleoproterozoic sedimentary basins, such as the uppermost sequence of the MNGB and the Saúde Complex.

Briefly, the MNGB is in contact to the west with 3.4 Ga (Mougeot, 1996) tonalite-trondhjemite-granodiorite (TTG) basement rocks and subordinate metagranites in the Gavião Block and to the east and south with paragneisses in the Saúde Complex with a maximum age between 2.20 and 2.06 Ga (Zincone et al., 2017) (Fig. 2). To the north and northwest, the MNGB is in contact with quartzites of the Jacobina Group, which were deposited between 3.55 and 3.22 Ga (Teles et al., 2015), and Paleoproterozoic granitic intrusives.

Additionally, the geologic setting includes granulites (2.9 Ga) and multiple charnockite intrusions (2.7 and 2.6 Ga) in the Jequié Block (Wilson, 1987; Silva et al., 2002), the Itabuna-Salvador-Curaçá Belt, and the Mairi and Serrinha blocks. Although the Itabuna-Salvador-Curaçá Belt and Serrinha Block are far from the MNGB, they are important for understanding the tectonic evolution of the study area (Fig. 1C; Table 1).

The eastern margin of the Gavião Block is in tectonic contact with the MNGB along a north-south-trending thrust zone with a west vergence (Fig. 1C) and is composed of TTG gneisses and migmatites that host mafic rock enclaves (Barbosa et al., 2012a), metagranites and metarhyolites (Zincone et al., 2016). This block corresponds to the basement of the MNGB. Three groups of TTG gneisses are described in the Gavião Block: two groups are trondhjemitic with U-Pb zircon ages (SHRIMP) of 3403 ± 5 Ma and 3158 ± 5 Ma (Barbosa, 1997; Leal, 1998), and the other group, with a granodioritic composition, includes the 3225 ± 10 Ma Aracatu granitoid (Barbosa et al., 2012a). The age of the Gavião Block is 3.4 Ga (Mougeot, 1996), but metarhyolites with ages of 3303 ± 11 Ma and metagranites, such as Boa Sorte at 3291 ± 2.5 Ma, occur as well (Zincone et al., 2016).

The Mairi Block, composed of gneisses, migmatites, and granitic and tonalitic orthogneisses, with some occurrences of basic and ultrabasic bodies (Peucat et al., 2002) to the east and southeast of the MNGB and Saúde Complex, is in tectonic contact along north-south-trending thrust zones with a west vergence. The LA-ICP-MS U-Pb zircon ages of 3.33 Ga and 3.30 Ga (Sousa et al., 2018) for the orthogneisses in the Mairi Block indicate contemporaneity with the Gavião Block. Therefore, these blocks may have been joined at the time of their formation.

The Jacobina Group is in tectonic contact with the MNGB along thrust zones, all of which strike north-south and are vergent to the west (Fig. 1C), with the Gavião Block in the footwall. The Jacobina Group comprises metaconglomerates, quartzites, metarenites, phyllites, chlorite schists and quartz-sericite schists (Mascarenhas et al., 1998) deposited in a passive margin setting (Reis et al., 2018). This group has a depositional age, based on detrital zircons, of between 3500 Ma and 3220 Ma (Magee et al., 2001; Teles, 2013; Teles et al., 2015; Barbuena et al., 2016). Jacobina Ridge represents an Archean supracrustal sequence with a maximum depositional age of 3.22 Ga, and its sources are likely rocks from both the plutonic-volcanic system and the TTG suite in the Gavião Block (Zincone et al., 2016).

The Serrinha Block is in the northeast portion of the São Francisco Craton (Fig. 1C), and its oldest part is composed of Mesoarchean protolith (Barbosa et al., 2012a). The Serrinha Block mainly comprises gneisses, migmatites with ages of 3152 ± 5 Ma (Oliveira et al., 2002a; Oliveira et al., 2002b), and granitoids with ages of 3162 ± 26 Ma, 3072 ± 2 Ma and 2989 ± 11 Ma (Rios et al., 2009), as well as quartzite lenses, sillimanite-garnet-cordierite gneiss bands and subordinate amphibolites. An age of 2076 ± 10 Ma (Oliveira et al., 2002a) obtained from the rims of detrital zircons indicates the timing of regional metamorphism in the Serrinha Block.

The Jequié Block is approximately 10 km to the southeast of the MNGB, and reverse faults with northwest vergences mark its tectonic contact with the Mairi Block and Saúde Complex (Fig. 1C). The Jequié Block is composed of 3.0 Ga orthoderived granulites with subordinate mafic facies (Wilson, 1987) and a 2.7 and 2.6 Ga unit composed of enderbitic, charnoenderbitic and charnockitic granulites (Silva et al., 2002). Monazite ages of 2052 ± 2 Ma from S-type leucogranites are interpreted as the age of the regional deformation and granulitic metamorphism (Barbosa et al., 2004).

The Itabuna-Salvador-Curaçá Belt is situated between the Gavião and Serrinha blocks (Fig. 1C) and has a north-south extent of approximately 600 km (Oliveira et al., 2004). The Itabuna-Salvador-Curaçá Belt contains high-grade and ultrahigh-temperature granulitic rocks (Leite et al., 2009), with a limited area of amphibolite-facie rocks to the south (Barbosa et al., 2012a). The protolith age of the enderbite (orthopyroxene tonalite) is 2695 ± 12 Ma (Silva et al., 1997), and the tonalitic granulite has an age of 2574 ± 6 Ma (Oliveira et al., 2010). Metamorphic zircon ages of 2083 ± 1.9 Ma indicate the timing of metamorphism in the Itabuna-Salvador-Curaçá Belt (Peucat et al., 2011).

The MNGB is divided into three stratigraphic sequences (Spreafico, 2017) – a lower sequence (ultramafic rocks), a middle sequence (mafic and felsic igneous rocks and clastic and chemical metasedimentary rocks) and an upper sequence composed of siliciclastic metasedimentary rocks with an inherited age of 2133 ± 14 Ma (Barbuena et al., 2016). Two ductile and progressive Paleoproterozoic deformational phases are described in the MNGB (Spreafico, 2017). The D_1 deformational phase is characterized by isoclinal and recumbent folds vergent to the west that generated greenschist metamorphic-facie rocks. The D_2 deformational phase is characterized by a refolding that generated vertical and subvertical axial planes that eventually resulted in the formation of coaxial interference patterns or compressive and transpressive shear zones, which bound the MNGB lithologies and generated rocks of greenschist to amphibolite metamorphic facies. The most prominent brittle structures are east-trending faults and fractures. The age of the MNGB has been the subject of study, and the possibility of Neoarchean volcanism (Spreafico et al., 2018) with Paleoproterozoic sedimentation on the top of the sequence (Barbuena et al., 2016), coeval with the Paleoproterozoic tectonothermal event (Leite, 2002), has been considered, as will be explained later in this paper.

The Saúde Complex occurs to the east of the MNGB (Fig. 1C), where the two units are in tectonic contact along west-vergent thrust zones, and it is distributed along of the Contendas-Jacobina Lineament. The Saúde Complex comprises aluminous paragneisses, biotite gneisses and subordinate quartzites widely distributed in a north-south trend with significant occurrences in the Mundo Novo region and in the eastern portion of Jacobina Ridge (Couto et al., 1978; Mascarenhas et al., 1998; Leite et al., 2007; Reis et al., 2017) (Fig. 1C). The maximal depositional age of 2.06 Ga (Zincone et al., 2017) for the Saúde Complex again indicates the presence of a basin near the MNGB in the Paleoproterozoic; however, the rocks in the Saúde Complex were subjected to a higher metamorphic grade than were the sedimentary rocks at the top of the MNGB along the tectonic contact.

Finally, Paleoproterozoic granites are present along the Contendas-Jacobina Lineament (Fig. 1C) (Leite, 2002). In general, these granites are undeformed leucogranites, comprising quartz, feldspar, biotite and muscovite, with some occurrences of garnet and sillimanite (Barbosa et al., 2012b). The Cachoeira Grande granite, for example, is a peraluminous leucogranite situated to the northeast of the MNGB that has an average age of 2080 ± 18 Ma (Leite, 2002), coeval with the Rhyacian-Orosirian granitic intrusions in the MNGB.

Table 1. Compilation of regional geochronological data of the MNGB and adjoining units

Geologic/tectonic unit	Lithotype	Age*	Method	Mineral dated	Author
Saúde Complex	Biotite schist	2068 ± 12 Ma	U-Pb	Detrital zircon (inherited age)	Zincone et al. (2017)
Cachoeira Grande granite[1]	Leucogranite	2080 ± 18 Ma	U-Pb	Monazite (crystallization age)	Leite (2002)
Upper sequence (MNGB)[2]	Quartzite	2133 ± 14 Ma	U-Pb	Detrital zircon (inherited age)	Barbuena et al. (2016)
Itabuna-Salvador-Curaçá Belt	Tonalitic granulite	2574 ± 6 Ma	U-Pb	Zircon (crystallization age)	Oliveira et al. (2010)
	Enderbite	2695 ± 12 Ma	U-Pb	Zircon (crystallization age)	Silva et al. (1997)
Jequié Block	Granulite	2715 ± 29 Ma	U-Pb	Zircon (crystallization age)	Silva et al. (2002)
	Charnockite	2900 ± 24 Ma	Rb-Sr	Whole-rock (crystallization age)	Wilson (1987)
Serrinha Block	Granitoid	2989 ± 11 Ma 3072 ± 2 Ma 3162 ± 26 Ma	U-Pb	Zircon (crystallization age)	Rios et al. (2009)
	Gneiss, migmatite	3152 ± 5 Ma	U-Pb	Zircon (crystallization age)	Oliveira et al. (2002a); Oliveira et al. (2002b)
Jacobina Group	Quartzite	3500 - 3220 Ma	U-Pb	Detrital zircon (inherited age)	Magee et al. (2001); Teles (2013); Teles et al. (2015); Barbuena et al. (2016)
Mairi Block	Orthogneiss	3.33 - 3.30 Ga	U-Pb	Zircon (crystallization age)	Sousa et al. (2018)
Gavião Block[3]	Metagranite	3291 ± 2.5 Ma	U-Pb	Zircon (crystallization age)	Zincone et al. (2016)
	Metarhyolite	3303 ± 11 Ma	U-Pb	Zircon (crystallization age)	Peucat et al. (2002); Zincone et al. (2016)
	TTG	3442 ± 2 Ma	U-Pb	Zircon (crystallization age)	Mougeot (1996)

Note: 1. Paleoproterozoic granitic intrusive in the MNGB. 2. Sedimentary rock from the uppermost sequence of the MNGB. 3. Basement of the MNGB. *For U-Pb ages, the data correspond to the upper intercept in the concordia diagram.

3. Analytical methodology

The study of the basement rocks and volcanism of the MNGB and intrusive granites involved petrographic, mineral chemistry, lithogeochemistry, geochronologic and isotopic analyses.

For petrography, we analyzed thin sections to determine the mineralogical composition, textures and microstructures of the rocks using a ZEISS Axio Scope.A1 microscope provided by CBPM. One of the thin sections was used for mineral chemistry analysis using a CAMECA SX50 electron microprobe at the University of Brasília. In this analysis, energy dispersive spectroscopy (EDS) data were used to identify specific minerals, and a backscattered electron image was obtained.

The whole-rock chemical analysis was conducted in the SGS-Geosol laboratory. The samples were dried and crushed so that 75% of the sample was smaller than 3 mm. A 300 g sample was quartered and pulverized (until 95% was smaller than 105 microns) to form a

powder for subsequent processes. The powder was melted at a high temperature with lithium metaborate, and the major, minor, trace, and rare earth elements (REE) were determined using ICP-MS and inductively coupled plasma optical emission spectrometry (ICP-OES) analysis. The international standard samples used were TILL-3 (description and values in Lynch, 1996) and GRE-05 (reference material from Geostats PTY Ltd.). The error for all analyzed elements in each sample was calculated based on the analytical accuracy according to the content of the analyte in the sample, the statistical detection limit and the repeatability limit and is presented in terms of the standard deviation (1σ) (Thompson, 1988). The coefficient of variation of the analytical results for each element by sample was predominantly lower than 15%, which corresponds to well-represented results around the arithmetic mean. Only the samples with loss on ignition (LOI) values of $\leq 5\%$ were considered. The geochemical data were plotted and interpreted using the GCDKit software (Janousek et al., 2006). The REE were normalized with the chondrite values of Boynton (1984) and the multielement diagram against N-MORB (normal mid-ocean ridge basalt) values (Hofmann, 1988).

The U-Pb geochronologic analyses were conducted at the Center of Geochronology Research at the Institute of Geosciences, University of São Paulo. The zircon grains from each sample were separated using binocular microscopy and placed in a 2.5 cm epoxy support. Then, the zircons were polished with sandpaper, and photomicrographs were captured. The internal structures of the zircon grains were characterized using cathodoluminescence (CL) images obtained by an FEI Quanta 250 scanning electron microscope (SEM) and a XMAX CL detector (Oxford Instruments), and the analysis was acquired using in situ LA-ICP-MS. The analysis was performed with a Neptune (Thermo) multicollector instrument and an ArF-193 nm Photon laser system (frequency of 6 Hz) with a spot size diameter of 32 μm. The final results match the average obtained after the calculation of two standard deviations. Isotopic ratios are reported at the 1σ level. Finally, the discordant values for the zircon data greater than 10% were eliminated. Corrections for the laser-induced elemental fractionation of the $^{206}Pb/^{238}U$ ratio and instrumental discrimination were based on the GJ-1 zircon standard (U-Pb mean age of 601 ± 3.5 Ma; Elhlou et al., 2006), which yielded an age of 600.7 ± 0.69 Ma in the analysis period. The raw data were processed on-line and reduced in an Excel worksheet adapted from SQUID 1.02 (Ludwig, 2001). The data were plotted on concordia diagrams using ISOPLOT/Ex®3.00 (Ludwig, 2003).

The samples dated using the U-Pb method were also analyzed to determine their Nd and Sr isotopic compositions to better understand the associated petrological processes. The Nd and Sr isotopic compositions were measured using the Triton-Thermo Scientific TIMS technique at the Center of Geochronology Research at the Institute of Geosciences, University of São Paulo. Sm and Nd were separated using HCl elution and RE and LN cationic exchange columns (EIChroM Industries Inc.), as described in Petronilho (2009). The isotopic ratios of $^{143}Nd/^{144}Nd$ were normalized to the value of $^{146}Nd/^{144}Nd = 0.7219$ (Wasserburg et al., 1981). The parameter $\varepsilon_{Nd(0)}$ was calculated according to the equation $= \{[(^{143}Nd/^{144}Nd)_{sample}/0.512638] - 1\}\times10^4$, where $^{143}Nd/^{144}Nd_{CHUR} = 0.512638$ (Hamilton et al., 1983). The parameter $\varepsilon_{Nd(t)}$ was obtained using the equation $= \varepsilon_{Nd(0)} - f_{Sm/Nd} - 25.13\times T$ where $f_{Sm/Nd} = [(^{147}Sm/^{144}Nd)_{sample}/0.1967] - 1$ (De Paolo, 1981). The Nd blank during the analysis was 22 pg, and the average value for the $^{143}Nd/^{144}Nd$ ratio of the standard JNdi-1 between April 2017 and March 2018 was 0.512109 ± 0.000004. The Sm-Nd depleted mantle model ages (T_{DM}) were obtained following the T_{DM} method of De Paolo (1981) according to the equation $= 1/\lambda\times Ln\times[(^{143}Nd/^{144}Nd)_{sample} - (^{143}Nd/^{144}Nd)_{DM}/(^{147}Sm/^{144}Nd)_{sample} - (^{147}Sm/^{144}Nd)_{DM}]$. The $\varepsilon_{Nd(t)}$ parameters and the T_{DM} were calculated based on the whole-rock geochemical results for Sm and Nd, such as the $^{147}Sm/^{144}Nd$ ratios, which were calculated according to the equation $= [Sm (ppm)/Nd (ppm)]\times(1/1.645)$.

The Sr isotopic analysis results were calculated with an absolute standard error of 2σ and involved an average of 100 measurements. The $^{87}Sr/^{86}Sr$ isotopic ratios were normalized to the value $^{86}Sr/^{88}Sr = 0.1194$. The Sr blank sample used during the analysis was 67 pg. The average value for the $^{87}Sr/^{86}Sr$ ratio for the standard NBS-987 between April 2017 and March 2018 was 0.710247 ± 0.000017. The final quoted errors were calculated based on replicate analyses of the $SrCO_3$ standard NBS-987, which yielded a mean ratio of 0.710251 ± 0.000043 during the period of the analyses. The decay constants used were those recommended by Steiger and Jäger (1977). The $^{87}Sr/^{86}Sr_i$ values were calculated according to the equation = $(^{87}Sr/^{86}Sr)_{sample} - (^{87}Rb/^{86}Sr)_{sample} \times [\exp(\lambda \times T) - 1]$, and the $^{87}Rb/^{86}Sr$ ratios were calculated based on the whole-rock geochemical results for Rb and Sr according to the equation $^{87}Rb/^{86}Sr = [Rb \ (ppm)/Sr \ (ppm)] \times (1/0.341)$.

4. Local geology

4.1. Gavião Block

The TTG orthogneiss and subordinate migmatites, metagranites and metarhyolites of the Gavião Block, which comprise the basement of the MNGB, occur mainly west of the greenstone. The Miguel Calmon and Fazenda Coqueiro metagranites (Fig. 2), which are important because of their occurrence near the MNGB, are deformed and metamorphosed plutons in which igneous textures and the mineralogical features of protoliths are still observable.

The metagranites are weakly deformed, whitish gray, and fine- to medium-grained. The Miguel Calmon metagranite has a gray color, is medium- to coarse-grained and has weak magnetism (Fig. 3A), and the Fazenda Coqueiro metagranite is pink and fine- to medium-grained, with incipient foliation and moderate magnetism (Fig. 3B).

The metarhyolites and subordinate metadacites in the basement mainly occur in the central portion of the MNGB and near the Fazenda Coqueiro deposit (Fig. 2). These units were tectonically emplaced between the mafic and metasedimentary rocks of the MNGB. One occurrence of metacomendite/metapantellerite was observed to the south of the MNGB. The metarhyolites have a gray color and are fine- to medium-grained, foliated, and, at some points, magnetic. Notably, some granitic bodies are spatially related to these metavolcanic rocks, and the mineralogical composition of these granites has a certain similarity to that of the metarhyolites.

To the south of the Fazenda Coqueiro deposit, metadacites occur in north-south-trending tectonic slices in contact to the west with gneisses and migmatites in the Gavião Block and to the east with siliciclastic metasedimentary rocks in the MNGB. The occurrence of metacomendite/metapantellerite appears to be restricted to the south of the MNGB, forming a north-south-trending lenticular feature inside the Gavião Block (Fig. 2).
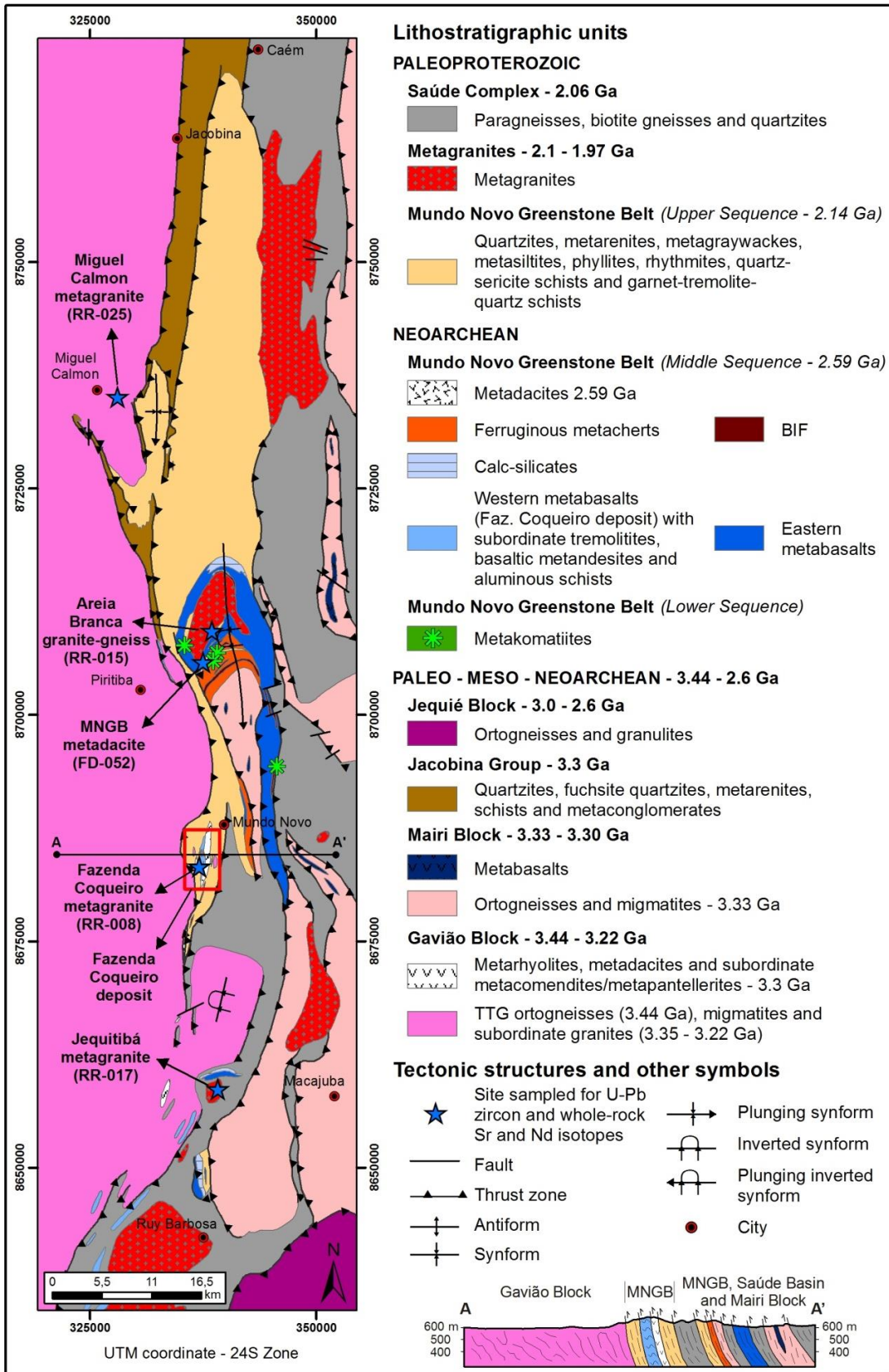
Fig. 2. Geological map of the MNGB and adjoining units, the new stratigraphy proposed and the location of the samples for U-Pb zircon geochronology and Nd and Sr isotopic analysis in the present study. Modified and updated from Loureiro (1991), Mascarenhas and Silva (1994) and Souza et al. (2002).

4.2. Mundo Novo greenstone belt

Many Paleo- to Neoarchean greenstone belts have been characterized as volcano-sedimentary sequences that have been deformed and metamorphosed at low to medium grades that show, from the base to the top, a progressive variation from volcanic to sedimentary rocks commonly associated with orthogneisses; this variation is intruded by syn- to posttectonic granites (Anhaeusser, 2014).

Based on these concepts, the MNGB is interpreted as part of a typical greenstone belt terrain divided into three stratigraphic sequences, considering that fractional crystallization processes controlled the order of formation of the ultramafic (first sequence), mafic and felsic (last sequences) volcanic rocks. Therefore, the **lower sequence** is composed of metakomatiites; the **middle sequence** is composed of metabasalts and, subordinately, tremolitites, calc-silicate rocks, aluminous schists, banded iron formations (BIFs), ferruginous metacherts, basaltic metandesites, metadacites and metarhyolites; and the **upper sequence** is composed of siliciclastic metasedimentary rocks, such as metarenites, quartzites, metagraywackes, metasiltites, phyllites, rhythmites, quartz-sericite schists and garnet-tremolite-quartz schists.

Lower Sequence

The lower sequence of the MNGB is composed of metakomatiites comprising ultramafic metavolcanics that have a light green color, a silky aspect and are not magnetic (Fig. 3C). The metakomatiites are in contact with the mafic metavolcanic rocks of the middle sequence; however, these rocks are separated into different sequences because of the mineral content, which allows the rocks to be classified as ultramafic or mafic, even if they are from the same source, by fractional crystallization, for example, and due to the textural particularities described below. There are four restricted occurrences of metakomatiites in the central portion of the MNGB (Fig. 2), northeast of Mundo Novo city and northeast of Piritiba city.

Middle Sequence

The middle sequence of the MNGB is composed of metabasalts and, subordinately, tremolitites, calc-silicate rocks, aluminous schists, BIFs, ferruginous metacherts, basaltic metandesites, metadacites and metarhyolites. This study focuses on the metabasalts and metadacites.

Metabasalt and metadacite are the terms used in this paper to define the metamorphosed mafic and felsic volcanic components, respectively, of the middle sequence of the MNGB. The metabasalts are distributed along a north-south trend (Fig. 2) and have been divided into two coeval groups based on petrographic and lithogeochemical data. The first group, defined as the eastern metabasalt, corresponds to the main outcrops of the sequence near Mundo Novo and Piritiba cities and extending to Ruy Barbosa city (Fig. 2). The second group, defined as the western metabasalt, mainly corresponds to the metabasalts that occur in the Fazenda Coqueiro deposit (Mundo Novo city) and in a restricted area with a north-south trend near Piritiba city (Fig. 2).

The eastern metabasalts contain pillow lava structures that occur in a large area to the south of the MNGB (Fig. 3D). Thus, these rocks show evidence of quickly chilled mafic volcanism in an underwater setting. The western metabasalts, with subordinate basaltic metandesites, are important because they host the Zn and Pb sulfides of the Fazenda Coqueiro

deposit, particularly in carbonate hydrothermal alteration zones, and are well-observed from drill hole samples (Fig. 3E).

Metadacites and metarhyolites have restricted occurrences and correspond to the top of the MNGB middle sequence based on field relationships and a felsic mineral content typical of the later stages of volcanism. These units occur to the northeast of Piritiba city and have been identified in drill hole samples obtained by CBPM and in outcrops (Fig. 3F). These rocks are distributed along a northeast-southwest trend and are in contact with eastern metabasalts and ferruginous metacherts (Fig. 2).

Upper Sequence

The upper sequence of the MNGB is composed of siliciclastic metasedimentary rocks, such as metarenites, quartzites, metagraywackes, metasiltites, and phyllites, which together account for approximately one-half of the rocks of the greenstone belt sequence (Fig. 2).

In the northern part of the MNGB, the area of metasedimentary rocks reaches a width of 12 km, and the rocks are in tectonic contact to the west and northwest with the metasedimentary rocks of the Jacobina Group and to the east with the paragneisses of the Saúde Complex (Fig. 2). These rocks are also extensively exposed between the cities of Mundo Novo and Piritiba and to the west of the Fazenda Coqueiro deposit, where they reach a thickness of 3 km (Fig. 2), and in the southern part of the MNGB, where they reach a thickness of less than 1 km. In the latter two areas, the siliciclastic metasedimentary rocks are in contact with, near or include fragments of the metabasalts of the middle sequence.

4.3. Paleoproterozoic metagranites

The syntectonic granites that intruded the MNGB are regionally distributed and aligned along a north-south trend. Three granitic bodies (Fig. 2) are defined herein and described and interpreted as typical of a greenstone belt terrain according to Anhaeusser (2014).

Three granites identified during geological mapping are as follows: (i) the Areia Branca granite-gneiss, which is gray in color and medium- to coarse-grained (Fig. 3G), is situated in the central portion of the MNGB; (ii) the Jequitibá metagranite, which is gray in color, fine- to medium-grained and foliated (Fig. 3H), is situated in the southern portion of the MNGB and retains igneous textures and the mineralogical features of the protolith, even after deformation and metamorphism; and (iii) the Cachoeira Grande granite, which is hypidiomorphic and medium-grained and has a pink color, is situated in the northeastern portion of the MNGB (Fig. 2).
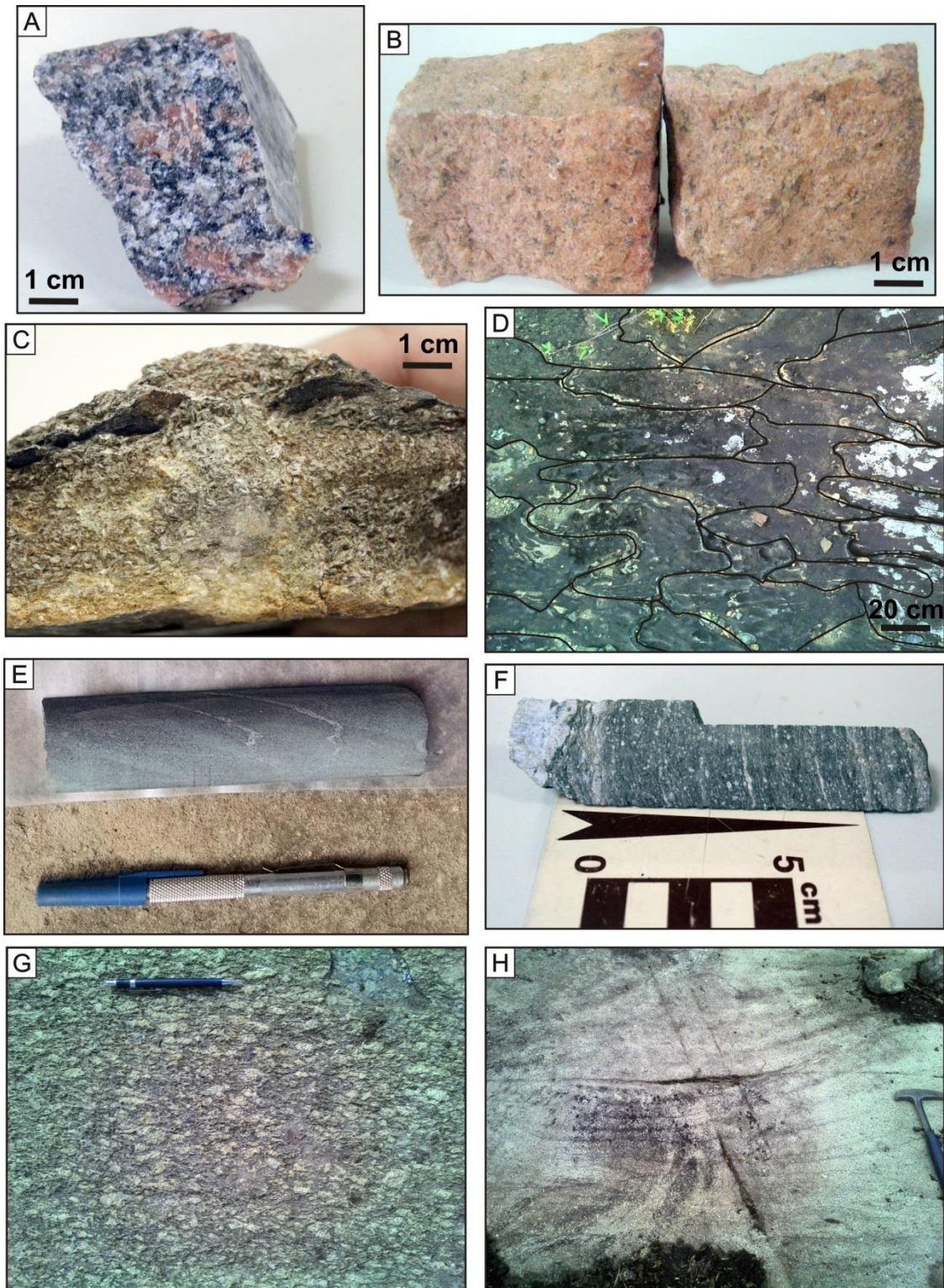
Fig. 3. A) Medium- to very coarse-grained Miguel Calmon metagranite. B) Fine- to medium-grained phaneritic texture of Fazenda Coqueiro metagranite. C) The fine-grained texture of the MNGB metakomatiites. D) Highlighted pillow lava structure of the eastern metabasalt from south of the MNGB. E) Drill hole sample of the very fine-grained western metabasalt in the MNGB. F) Drill hole sample of the porphyroclastic metadacite with porphyroclasts of plagioclase and quartz in the MNGB. G) Augen gneiss structure of the Areia Branca metagranite. H) Fine to medium-grained and foliated Jequitibá metagranite.

5. Petrography and mineral chemistry

5.1. Gavião Block

The Miguel Calmon metagranite preserves a porphyritic texture, and the phenocrysts are primarily microcline (50%) without perthitic exsolution (>16.0 mm) dispersed in a fine-grained groundmass composed of inequigranular and prismatic albite crystals (20%, 3.5 mm), quartz (20%) and fine biotite grains (10%) (Fig. 4A).

Based on petrographic analysis, the Fazenda Coqueiro metagranite comprises quartz (30%, minimum size of 0.2 mm), microcline (45%, a maximum size of 1.5 mm) without perthitic exsolution, albite (20%), biotite and stretched grains of muscovite (4%) forming incipient foliation (Fig. 4B). In this case, hydrothermal processes may explain the development of muscovite from the K-feldspar during deformation. The texture is mainly equigranular and finely to moderately phaneritic with subordinate mylonitic microstructures, along which some elements, such as K, Na, Al and Fe, were remobilized. A few euhedral titanite crystals that formed from the melt, magnetite grains, and rare zircon crystals are also present (1%, 0.25 mm in size).

The metarhyolites have a porphyroclastic microstructure and contain quartz, sanidine and albite porphyroclasts with a grain size of approximately 6.5 mm (35% of the rock). The larger minerals are dispersed in a fine-grained groundmass mainly composed of quartz, feldspar and fine biotite and muscovite grains that form up to 65% of the rock. In general, all grains are stretched and oriented, forming a foliation, which is in accordance with the ductile deformation that affected these rocks.

5.2. Mundo Novo greenstone belt

Lower Sequence

The olivine and pyroxene crystals in the metakomatiites are entirely replaced by acicular and prismatic pseudomorphic grains of anthophyllite and tremolite (80% of the rock) with a grain size of 0.5 mm (Fig. 4C). The fine-grained groundmass is composed of talc and clinochlore (20% of the rock) without a preferred orientation. Traces of pyrite and pyrrhotite are dispersed in the sample. Generally, the metakomatiites of the MNGB have a relict spinifex texture composed of skeletal grains with planar growths that intersect each other (Fig. 4C) and do not intercept the former structures, which Arndt (1994) described for igneous relict textures in komatiites. The fine-grained spinifex texture is identified only in hand samples or by using a hand lens or microscope, suggesting a relict spinifex texture preserved in the chilled margins of the komatiite flow.

Middle Sequence

5.2.1. Eastern metabasalts

The eastern metabasalts are composed mainly of hornblende (40%), bytownite (30%), small amounts of albite (5%) and low percentages (20% combined) of augite, tremolite, actinolite and quartz, as well as ilmenite as an accessory mineral and traces of pyrrhotite and chalcopyrite (5%) (Fig. 4D). The minerals show polyhedral contacts with nematoblastic and granonematoblastic textures, which may result from an amphibolitization process.

5.2.2. Western metabasalts

Based on petrography and mineral chemistry results, the western metabasalts are very fine-grained and are mainly composed of actinolite (20%) and oligoclase (65%), with a low percentage of augite, quartz and biotite (10%), as well as ilmenite and titanite as accessory minerals (Fig. 4E) and traces of pyrrhotite, pyrite, chalcopyrite, galena, sphalerite and arsenopyrite (5%). The grains of biotite and actinolite are oriented and define well-developed planes of foliation. The granonematoblastic textures of some samples show evidence of an amphibolitization process, and the occurrence of manganiferous ilmenite (Fig. 5A-B) indicates that these rocks formed via ocean-floor volcanism (Grachev et al., 2011).

5.2.3. Metadacites and metarhyolites

The metadacites contain submillimetric porphyroclasts of plagioclase with sericitized borders and quartz (40% of the rock), which are dispersed in a fine-grained groundmass composed of quartz, plagioclase, biotite, muscovite and sericite (60% of the rock) (Fig. 4F). The metarhyolites are fine-grained and foliated. They are composed of quartz (25%), K-feldspar (40%), plagioclase (20%), biotite (10%) and sericite (5%). These rocks contain granolepidoblastic grains that are submillimetric and well-oriented, tabular crystals of plagioclase (usually sericitized) and grains of quartz, fine biotite and opaque minerals.

5.3. Paleoproterozoic metagranites

The Areia Branca granite-gneiss is composed of quartz (30%), orthoclase (25%), microcline (15%), albite (20%) and biotite (10%) (Fig. 4G). This unit has an augen gneiss to protomylonitic microstructure with megacrystals of orthoclase (> 8.0 mm) and grains of microcline (2.0 mm) without perthitic exsolution, quartz (2.0 mm) and albite (2.0 mm) dispersed in a fine-grained groundmass composed of quartz, albite, biotite and muscovite. Coexisting orthoclase and microcline suggests that the metamorphic mineral assemblage formed in the transition temperature between them, which is 500° C and is compatible with greenschist to amphibolite metamorphic facies.

Based on petrography analysis, the Jequitibá metagranite is composed of quartz (25%), microcline (30%), orthoclase (10%), oligoclase (30%) and biotite (5%), which are the dominant minerals, and zircon and monazite are present as accessory minerals (Fig. 4H). This unit has a medium phaneritic texture composed of oligoclase (2.0 mm), microcline (3.0 mm), orthoclase (2.0 mm) without perthitic exsolution, quartz (2.5 mm), and biotite and a few muscovite grains that can form protomylonitic microstructures. Rare euhedral and submillimetric crystals of apatite occur within the microcline. Coexisting orthoclase and microcline, such as occur in Areia Branca granite-gneiss, may indicate the temperature of transition between them of 500° C (greenschist to amphibolite metamorphic facies).

The Cachoeira Grande granite is composed of plagioclase (40%), microcline with perthitic exsolution (35%), quartz (20%), biotite (2.5%) and muscovite (2.5%). Some grains of microcline and plagioclase are sericitized, and the muscovite is locally in contact with biotite.
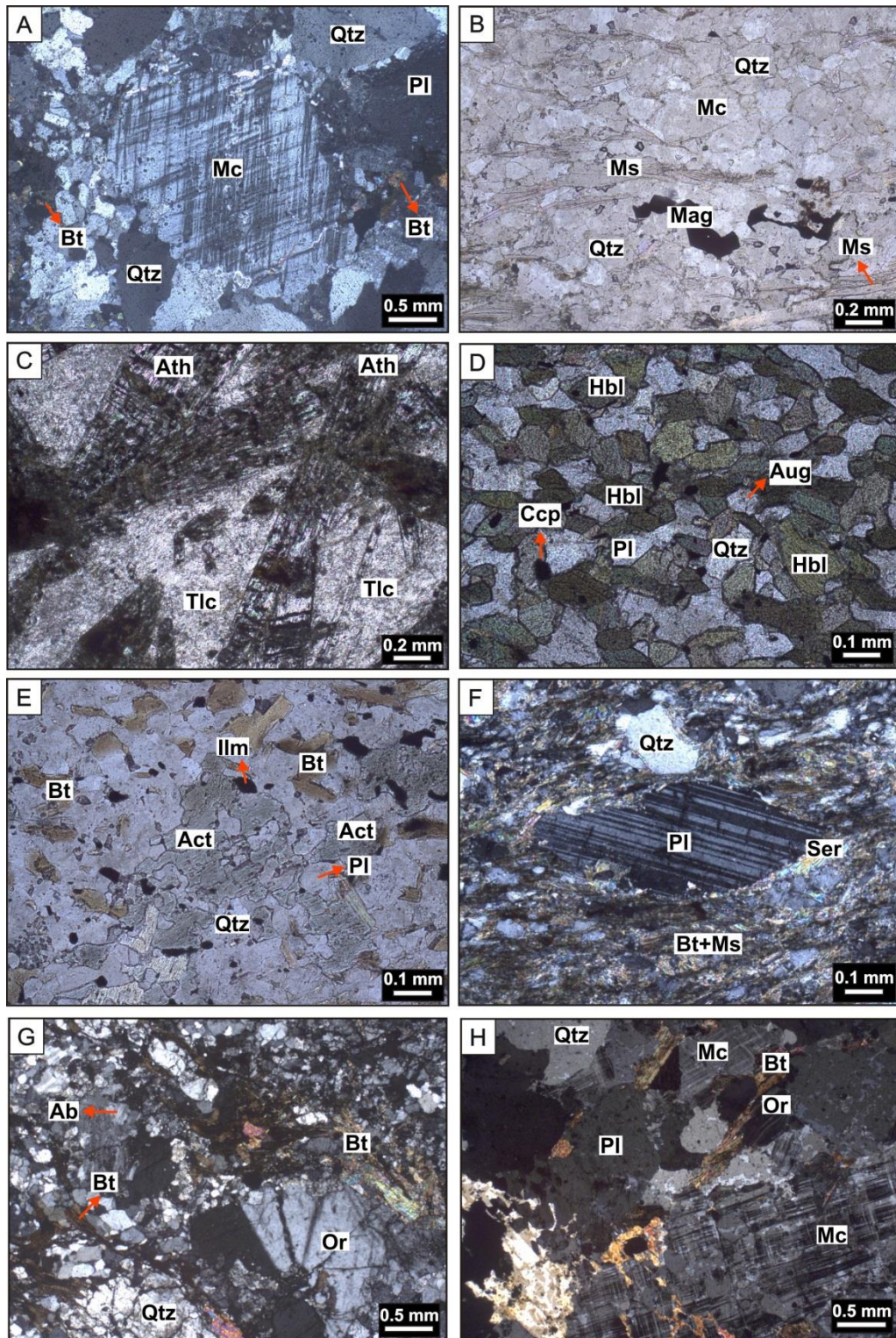
Fig. 4. Petrographic images of the MNGB and surrounding rocks. A) Porphyritic texture (relict of K-feldspar phenocryst) of the Miguel Calmon metagranite (XP; sample RR-025). B) Fine- to medium-grained texture and incipient foliation of the Fazenda Coqueiro metagranite (PPL; sample RR-008). C) Anthophyllite laths in a fine-grained groundmass of talc interpreted as pseudomorphs of spinifex texture of metakomatiites (PPL; sample FD-058A). D) Granonematoblastic texture of the amphibolitized eastern basalts. The main plagioclase is bytownite (PPL; sample RR-018A). E) Typical very fine-grained texture of the amphibolitized western basalts and subordinate basaltic metandesites. The plagioclase is oligoclase (PPL; sample RR-F6-001). F) Porphyroclast of plagioclase with sericitized border in a fine-grained groundmass of quartz, biotite and muscovite in the metadacite of the middle sequence of the MNGB (XP; sample FD-052). G) Protomylonitic augen gneiss of the Areia Branca granite-gneiss (XP; sample RR-015). H) Medium-grained Jequitibá metagranite with

protomylonitic microstructures produced by biotite and muscovite. The plagioclase is oligoclase (XP; sample RR-017). Mineral abbreviations (Kretz, 1983; Siivola and Schmid, 2007): Act: actinolite, Ab: albite, Ath: anthophyllite, Aug: augite, Bt: biotite, Ccp: chalcopyrite, Hbl: hornblende, Ilm: ilmenite, Mag: magnetite, Mc: microcline, Ms: muscovite, Or: orthoclase, Pl: plagioclase, Qtz: quartz, Ser: sericite, Tlc: talc. XP: crossed polarizers; PPL: uncrossed polarizers.

Fig. 5. A) Backscattered electron image with the analysis spot and B) the energy dispersive spectroscopy (EDS) spectrum of the manganiferous ilmenite present in the basaltic metandesite, which is part of the western metabasalts of the MNGB, as evidence of an ocean floor setting (sample RR-F16-027).

6. U-Pb geochronology in zircon

For U-Pb zircon age determination, four granites and one metadacite were selected (see sample sites in Fig. 2). The first samples corresponded to the Miguel Calmon (sample RR-025) and Fazenda Coqueiro (sample RR-008) metagranites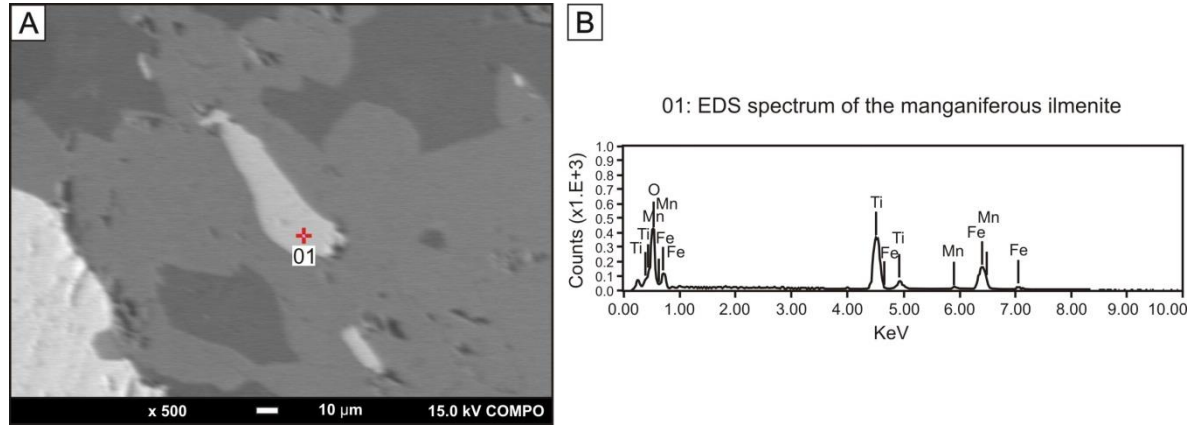 from the basement (Gavião Block) and the Areia Branca (sample RR-015) and Jequitibá (sample RR-017) metagranites from the MNGB. The metadacite sample FD-052 represents the middle sequence of the MNGB.

6.1 Gavião Block

The U-Pb age of sample **RR-025** (Miguel Calmon metagranite) was determined from transparent to translucent zircons that vary from pale yellow to brown. The zircons are euhedral and prismatic with rounded terminations, ranging in size from 118 to 250 μm in length and ranging in aspect ratio from 1.4 to 3.5. In the CL images, oscillatory and concentric zoning and unzoned grains are apparent. Grains with metamict structures, fracturing, igneous overgrowth and resorption in the center were not analyzed. Fifteen zircon analyses (Table 2) were conducted, mostly in cores of oscillatory zoned zircons, seven of which yielded an upper intercept of 3355 ± 16 Ma (MSWD = 0.56; Fig. 6A), which was assumed to represent the crystallization age of the Miguel Calmon metagranite. The age of 583 ± 36 Ma of the lower intercept indicates the loss of Pb, and this effect occurring as the result of a weak geologic event at this time is not totally discarded. The Th/U values vary from 0.10 to 2.50, which correspond to the values of igneous zircons (Th/U > 0.1) (Lopez-Sanchez et al., 2016). The negative Th and Th/U values can be explained by Th values near zero, which were not well measured by the detector. The nearly concordant $^{207}Pb/^{206}Pb$ ages, 3340 ± 29 Ma (97% concordance) and 3353 ± 27 Ma (96% concordance), are practically identical to the upper intercept age in the concordia diagram.

The zircon population of sample **RR-008** (Fazenda Coqueiro metagranite) consists of translucent to transparent crystals varying from pale brown to dark brown that are from 100 to

238.5 μm in length and from 1.6 to 2.0 in aspect ratio. Most grains are fractured, and some are subhedral, prismatic and show rounded terminations. The CL images show weak concentric oscillatory zoning, and some grains are unzoned or resorbed. Twenty-four spots (Table 3), measured mainly in oscillatory and zoned grains, were analyzed using LA-ICP-MS, and sixteen zircon data were used to calculate the age, in which a concordance of approximately 100% was observed. The Th/U values range from 0.19 to 0.82 and correspond to the values of igneous zircons. The negative U, Th and Th/U values correspond to low concentrations of U and Th, which were not well calculated by the detector. The discordance line intercepts the curve of the concordia in the upper intercept at 3227 ± 23 Ma, and the MSWD = 1.08 (Fig. 6B); thus, this age is considered to represent the crystallization age. The oscillatory and concentric zoning of the grains may suggest that the crystallization age obtained for Fazenda Coqueiro metagranite was not affected by inherited zircons from the protolith. However, in the grains with the possibility of the occurrence of inherited cores, the ages were obtained from the edges. The lower intercept at 632 ± 140 Ma indicates a loss of Pb, possibly due to the occurrence of a weak geologic event at this time.

6.2 Mundo Novo greenstone belt

Zircons in the **FD-052** sample (MNGB metadacite) are light to dark brown, translucent, subhedral and prismatic with subrounded terminations. The grain lengths range from 77 to 550 μm, and the aspect ratios range from 2.0 to 3.0. Some crystals show concentric oscillatory zoning, and some are unzoned. Generally, the zircons present thin metamorphic rims and resorbed portions. Twenty-four analyses (Table 4) were performed in the cores, and the results define the crystallization age. The data in the concordia diagram yield an upper intercept age of 2595 ± 21 Ma, and the MSWD = 2.3 (Fig. 6C); thus, this age is considered to represent the crystallization age. These data present concordances of between 55 and 91%, and the Th/U values range from 0.31 to 1.03 (values of igneous zircons). The lower intercept age of 616 ± 25 Ma also indicates a loss of Pb, possibly from low-intensity geological processes.

6.3 Paleoproterozoic metagranites

The U-Pb age of the **RR-015** sample (Areia Branca granite-gneiss) was determined from a population of translucent zircons that ranges in color from light to dark brown. The crystals form prisms, some with subrounded and rounded terminations, and range in length from 56.2 to 300 μm and in aspect ratio from 1.5 to 2.6. The grains show fracturing, resorption, thin metamorphic rims, concentric oscillatory zoning and a lack of zoning in the CL images. Twenty-four spot analyses (Table 5) were conducted in the zircon cores, and the concordances are between 38 and 120%. Six spot data (red circles; Fig. 6D) were selected for age determination. Eighteen analytical points in metamictized grains were not considered because of Pb loss in the zircon. Additionally, the Th/U values range from 0.15 to 0.99 (values of igneous zircons), and the upper intercept provided an age of 2106 ± 71 Ma and a MSWD = 3.1. This age is considered to represent the crystallization age. The lower intercept provided an age of 630 ± 103 Ma, which can suggest weak geological processes during this time.

The **RR-017** sample (Jequitibá metagranite) presents zircons that are light to dark brown in color, translucent to opaque, prismatic and subeuhedral. Most grains have rounded to subrounded terminations, lengths between 125 and 359.5 μm and aspect ratios between 3.4 and 4. The crystals show concentric oscillatory zoning and recrystallized rims, while others have unzoned portions and resorption textures. Thirty-six U-Pb zircon analyses (Table 6)

were performed, and seventeen provided an upper intercept of 1975 ± 36 Ma and a MSWD = 1.7 (Fig. 6E). This age is considered to represent the crystallization age. The lower intercept provided a younger age of 452 ± 42, which does not seem related to any geologic event reported in the São Francisco Craton. The Th/U values range from 0.15 to 4.72, with one value as high as 14.37 (these are values of igneous zircons). These high Th/U values suggest the crystallization of zircon in a high degree of disequilibrium with the melt (Xiang et al., 2011).

Table 2. U-Pb geochronological data, sample RR-025: Miguel Calmon metagranite (3355 ± 16 Ma)

Spot	U ppm	Th ppm	Th/U	Pb_{com}	$^{207}Pb/^{206}Pb$	1σ	$^{207}Pb/^{235}U$	1σ	$^{206}Pb/^{238}U$	1σ	$^{207}Pb/^{206}Pb$ age (Ma)	1σ	%Conc.	Error cor.
1.1	70.7	19.4	0.274	8.85	0.2244	0.0057	6.7197	0.1893	0.2172	0.0028	3.012	0.041	42	0.99
2.1	71.1	5.8	0.081	0.75	0.2369	0.0047	12.7163	0.2824	0.3893	0.0040	3.099	0.031	68	0.93
3.1	70.9	28.1	0.396	0.70	0.2511	0.0054	24.3970	0.5158	0.7046	0.0076	3.192	0.034	107	0.86
4.1	6.1	-15.4	-2.504	0	0.2514	0.0047	13.1981	0.2663	0.3808	0.0035	3.193	0.029	65	0.88
4.2	22.4	-0.1	-0.004	0.36	0.2224	0.0044	6.8924	0.1437	0.2247	0.0020	2.998	0.031	43	0.96
5.1	162.9	38.6	0.237	6.50	0.2680	0.0055	19.0844	0.3926	0.5164	0.0051	3.295	0.032	81	0.94
6.1	24.1	-0.5	-0.020	1.90	0.2411	0.0048	14.0696	0.3006	0.4233	0.0043	3.127	0.032	72	0.94
7.1	95	27.5	0.289	0.31	0.2448	0.0047	13.3775	0.2612	0.3963	0.0034	3.152	0.029	68	0.97
8.1	443.3	99.2	0.224	6.00	0.1696	0.0042	1.6813	0.0457	0.0719	0.0008	2.554	0.036	17	0.99
9.1	166	28.4	0.171	3.63	0.1789	0.0046	4.3265	0.2337	0.1754	0.0032	2.643	0.031	39	0.99
10.1	217.9	112.3	0.516	2.43	0.2126	0.0040	9.3068	0.1701	0.3175	0.0024	2.925	0.030	60	0.90
11.1	123.2	63.6	0.516	0.55	0.2760	0.0051	25.1706	0.4531	0.6615	0.0056	3.340	0.029	97	0.98
12.1	133.1	58	0.436	0.96	0.2782	0.0048	25.0211	0.4403	0.6523	0.0049	3.353	0.027	96	0.99
13.1	27.2	19.3	0.707	2.63	0.2766	0.0048	22.9411	0.4002	0.6015	0.0044	3.344	0.027	90	0.66
14.1	60	21	0.350	2.98	0.2320	0.0042	9.7089	0.1948	0.3036	0.0024	3.066	0.029	55	0.95

Table 3. U-Pb geochronological data, sample RR-008: Fazenda Coqueiro metagranite (3227 ± 23 Ma)

Spot	U ppm	Th ppm	Th/U	Pb_{com}	$^{207}Pb/^{206}Pb$	1σ	$^{207}Pb/^{235}U$	1σ	$^{206}Pb/^{238}U$	1σ	$^{207}Pb/^{206}Pb$ age (Ma)	1σ	%Conc.	Error cor.
1.1	96	75.6	0.788	0.90	0.2281	0.0053	9.2902	0.2726	0.2954	0.0040	3.039	0.036	54	0.89
2.1	4.9	1.3	0.263	12.39	0.2424	0.0143	19.7512	1.2632	0.5909	0.0196	3.136	0.100	95	0.01
3.1	24.4	15.3	0.627	2.71	0.2412	0.0104	22.6466	1.0109	0.6809	0.0157	3.128	0.075	107	0.23
4.1	10.5	-5.3	-0.510	7.31	0.2400	0.0066	16.1683	0.4650	0.4886	0.0067	3.120	0.044	82	0.67
5.1	27.2	17.7	0.651	4.88	0.2317	0.0066	13.1954	0.4626	0.4130	0.0069	3.064	0.043	72	0.93
6.1	14.9	7.5	0.505	2.86	0.2560	0.0105	23.9784	1.0431	0.6794	0.0159	3.222	0.068	103	0.49
7.1	9	5.7	0.630	5.89	0.2523	0.0067	21.1156	0.6286	0.6069	0.0091	3.199	0.042	95	0.39
8.1	34.6	23	0.664	2.21	0.2283	0.0074	19.4445	0.6781	0.6177	0.0104	3.040	0.052	101	0.94
9.1	-13.8	-11.1	0.806	-5.61	0.2333	0.0056	11.5548	0.3843	0.3592	0.0053	3.075	0.037	64	0.87
10.1	175.9	141.2	0.803	0.21	0.2699	0.0061	23.3634	0.5726	0.6277	0.0079	3.306	0.036	95	0.96
11.1	15.4	6.9	0.446	3.46	0.2720	0.0060	26.4286	0.6715	0.7048	0.0086	3.317	0.033	103	0.45
12.1	34.1	21.7	0.636	1.19	0.2329	0.0115	22.3139	1.1085	0.6949	0.0166	3.072	0.074	110	0.65
13.1	37.7	21.2	0.562	1.59	0.2359	0.0066	22.4587	0.7898	0.6906	0.0120	3.092	0.042	109	0.56
13.2	85.7	46	0.537	0.55	0.2647	0.0062	25.2886	0.7517	0.6929	0.0110	3.275	0.038	103	0.17
14.1	34.1	27.1	0.794	1.52	0.2523	0.0061	22.0668	0.6582	0.6343	0.0100	3.199	0.038	98	0.85
15.1	41.2	22.8	0.554	1.59	0.2638	0.0061	24.7763	0.7336	0.6813	0.0106	3.269	0.037	102	0.36
16.1	33.8	23.5	0.697	1.90	0.2651	0.0065	25.1389	0.7645	0.6877	0.0110	3.277	0.038	102	0.27
17.1	33.7	12.7	0.378	1.06	0.2611	0.0063	23.0693	0.6872	0.6408	0.0103	3.253	0.037	98	0.18
18.1	66.5	44.5	0.669	0.90	0.2476	0.0063	22.8091	0.7030	0.6680	0.0105	3.170	0.039	104	0.03
19.1	32.7	19.1	0.584	2.50	0.2465	0.0059	22.1553	0.7034	0.6520	0.0103	3.162	0.037	102	0.50
20.1	22.4	13	0.580	3.39	0.2541	0.0061	23.7592	0.6818	0.6782	0.0105	3.210	0.037	103	0.37
21.1	78.6	50.7	0.645	0.51	0.2435	0.0058	16.2424	0.4875	0.4839	0.0078	3.143	0.038	80	0.81
22.1	18	3.4	0.187	1.37	0.2624	0.0059	24.6943	0.6996	0.6825	0.0102	3.261	0.036	102	0.83
23.1	329.9	269.2	0.816	0.30	0.2646	0.0059	26.1063	0.7326	0.7156	0.0106	3.274	0.035	106	0.90

Table 4. U-Pb geochronological data, sample FD-052: metadacite from the middle sequence of the MNGB (2595 ± 21)

Spot	U ppm	Th ppm	Th/U	Pb$_{com}$	^{207}Pb/^{206}Pb	1σ	^{207}Pb/^{235}U	1σ	^{206}Pb/^{238}U	1σ	^{207}Pb/^{206}Pb age (Ma)	1σ	%Conc.	Error cor.
1.1	658.4	275.8	0.419	1.25	2.6011	0.1320	0.1667	0.0049	5.9986	0.1771	1.851	0.063	53	0.98
2.1	616.1	277.4	0.450	2.53	3.2253	0.1528	0.1887	0.0056	5.2998	0.1561	2.014	0.061	55	0.92
3.1	101.7	43.7	0.430	0.42	10.4939	0.4770	0.4391	0.0133	2.2776	0.0692	2.590	0.050	90	0.78
4.1	728.8	408	0.560	1.90	1.5881	0.0810	0.1275	0.0038	7.8457	0.2310	1.433	0.077	53	0.96
5.1	452.6	253.4	0.560	4.34	6.1109	0.2648	0.2899	0.0081	3.4494	0.0968	2.378	0.052	69	0.99
6.1	599	298	0.498	0.09	2.3350	0.1107	0.1497	0.0044	6.6794	0.1945	1.850	0.064	48	0.98
7.1	385.1	164.7	0.428	0.37	4.3756	0.1945	0.2258	0.0064	4.4288	0.1246	2.234	0.057	58	0.99
8.1	415.9	198.2	0.477	0.08	2.2921	0.1151	0.1508	0.0045	6.6297	0.1965	1.803	0.067	50	0.97
9.1	372.7	152.8	0.410	0.05	4.2641	0.1927	0.2212	0.0064	4.5215	0.1312	2.225	0.056	57	0.97
10.1	283.1	113.6	0.401	0.04	7.3544	0.3155	0.3365	0.0094	2.9720	0.0830	2.440	0.052	76	0.90
11.1	388	156.1	0.402	0.78	4.5986	0.2045	0.2332	0.0066	4.2885	0.1216	2.264	0.055	59	0.98
12.1	450.1	205.3	0.456	0.55	2.3444	0.1156	0.1531	0.0045	6.5328	0.1934	1.817	0.066	50	0.98
13.1	406.3	160.6	0.395	0.06	3.4443	0.1674	0.1995	0.0061	5.0133	0.1540	2.032	0.062	57	0.49
14.1	193.1	73.7	0.382	0.21	8.2819	0.3658	0.3638	0.0109	2.7491	0.0827	2.509	0.055	79	0.35
15.1	329.7	128.6	0.390	0.18	6.6123	0.3050	0.3032	0.0094	3.2986	0.1025	2.436	0.055	70	0.99
16.1	300.9	113.2	0.376	0.31	8.5090	0.3625	0.3804	0.0109	2.6287	0.0750	2.479	0.055	83	0.98
17.1	351.1	182.4	0.520	0.13	5.6869	0.2459	0.2766	0.0082	3.6159	0.1069	2.336	0.058	67	0.87
18.1	327.6	171.5	0.524	0.49	4.0965	0.1937	0.2147	0.0068	4.6585	0.1467	2.207	0.064	56	0.88
19.1	435.1	203.3	0.467	0.37	2.9071	0.1374	0.1726	0.0054	5.7929	0.1824	1.988	0.063	51	0.97
20.1	618.3	339.5	0.549	0.04	1.6806	0.0784	0.1288	0.0039	7.7629	0.2344	1.520	0.070	51	0.97
21.1	242.3	75	0.310	0.51	7.0616	0.3039	0.3297	0.0095	3.0326	0.0878	2.405	0.056	76	0.88
22.1	480.2	204.1	0.425	0.54	2.5025	0.1152	0.1625	0.0049	6.1542	0.1866	1.827	0.066	53	0.87
23.1	585.9	291.2	0.497	0.38	1.6196	0.0764	0.1275	0.0038	7.8418	0.2358	1.470	0.072	52	0.97
24.1	452.8	467	1.031	0.28	4.5256	0.2037	0.2310	0.0069	4.3296	0.1303	2.253	0.058	59	0.99

Table 5. U-Pb geochronological data, sample RR-015: Areia Branca granite-gneiss (2106 ± 71)

Spot	U ppm	Th ppm	Th/U	Pb$_{com}$	^{207}Pb/^{206}Pb	1σ	^{207}Pb/^{235}U	1σ	^{206}Pb/^{238}U	1σ	^{207}Pb/^{206}Pb age (Ma)	1σ	%Conc.	Error cor.
1.1	232	34.4	0.148	16.40	0.1428	0.0037	5.5026	0.1401	0.2795	0.0026	2.261	0.044	70	0.76
2.1	289.1	117.4	0.406	12.26	0.1565	0.0040	6.3817	0.1756	0.2957	0.0032	2.418	0.044	69	0.90
3.1	232	118	0.509	0.20	0.1360	0.0040	7.9259	0.2223	0.4228	0.0044	2.177	0.050	104	0.83
4.1	462.2	152.5	0.330	3.76	0.1477	0.0038	6.1203	0.1610	0.3005	0.0030	2.320	0.045	73	0.98
5.1	402.4	126	0.313	3.26	0.1350	0.0038	4.2998	0.1189	0.2311	0.0024	2.163	0.049	61	0.83
6.1	309.2	115.1	0.372	0.83	0.1590	0.0039	10.5756	0.2529	0.4824	0.0045	2.445	0.042	103	0.99
7.1	343.9	114.9	0.334	14.82	0.1427	0.0037	6.3221	0.1540	0.3213	0.0030	2.260	0.045	79	0.74
8.1	449.3	132.2	0.294	1.76	0.1486	0.0039	5.9285	0.1508	0.2894	0.0028	2.330	0.046	70	0.73
9.1	71.7	49.9	0.696	1.40	0.2007	0.0050	14.4996	0.3337	0.5240	0.0048	2.832	0.041	95	0.85
10.1	702.4	696.2	0.991	8.98	0.1642	0.0040	6.8281	0.1662	0.3016	0.0029	2.499	0.042	67	0.99
11.1	552.6	174.6	0.316	8.92	0.1322	0.0037	6.1432	0.1632	0.3369	0.0033	2.128	0.051	87	0.96
12.1	343.8	160.8	0.468	4.63	0.1495	0.0047	4.6104	0.1561	0.2236	0.0029	2.340	0.051	55	0.99
13.1	436.3	103.3	0.237	34.65	0.1093	0.0026	1.7083	0.0419	0.1134	0.0011	1.787	0.045	38	0.85
14.1	255.7	53.6	0.210	13.29	0.1258	0.0027	3.7471	0.0821	0.2161	0.0020	2.039	0.037	61	0.98
15.1	374.7	118.6	0.316	15.25	0.1028	0.0030	1.9433	0.0518	0.1371	0.0014	1.675	0.055	49	0.87
16.1	48.7	14.9	0.306	62.03	0.0949	0.0037	2.7994	0.1002	0.2141	0.0028	1.525	0.060	81	0.30
17.1	306.8	125.1	0.408	6.31	0.1275	0.0027	7.5484	0.1401	0.4292	0.0034	2.064	0.037	111	0.93
18.1	81.7	19	0.233	26.27	0.1387	0.0028	5.8849	0.1195	0.3078	0.0026	2.211	0.034	78	0.78
19.1	115	27.7	0.241	4.83	0.1508	0.0030	5.2514	0.1027	0.2526	0.0022	2.355	0.035	61	0.76
20.1	127.9	39.4	0.308	3.20	0.1555	0.0030	8.8652	0.1753	0.4135	0.0035	2.407	0.033	92	0.85
21.1	294.8	62.4	0.212	7.74	0.1314	0.0028	4.2364	0.0828	0.2339	0.0019	2.116	0.036	64	0.93
22.1	353.1	186.7	0.529	5.86	0.1558	0.0028	12.2618	0.2156	0.5709	0.0044	2.410	0.031	120	0.93
23.1	80.3	28.1	0.350	4.08	0.1472	0.0028	10.8090	0.2114	0.5327	0.0045	2.313	0.032	119	0.91
24.1	248.5	190.2	0.765	0.81	0.1259	0.0027	7.0833	0.1455	0.4079	0.0035	2.042	0.038	108	0.98

Table 6. U-Pb geochronological data, sample RR-017: Jequitibá metagranite (1975 ± 36)

| Spot	U ppm	Th ppm	Th/U	Pb_{com}	$^{207}Pb/^{206}Pb$	1σ	$^{207}Pb/^{235}U$	1σ	$^{206}Pb/^{238}U$	1σ	$^{207}Pb/^{206}Pb$ age (Ma)	1σ	%Conc.	Error cor.
1.1	343.4	102.2	0.298	4.49	0.1136	0.0024	3.7039	0.0765	0.2365	0.0018	1.857	0.039	73	0.9
2.1	332.6	132.1	0.397	8.31	0.1084	0.0026	3.0348	0.0664	0.2031	0.0017	1.772	0.045	67	0.93
3.1	861.2	216.8	0.252	7.35	0.1010	0.0021	1.7988	0.0366	0.1292	0.0009	1.642	0.038	47	0.98
4.1	650.1	125	0.192	8.54	0.0906	0.0021	1.5694	0.0344	0.1256	0.0010	1.438	0.044	53	0.99
5.1	875.4	278.9	0.319	8.29	0.0848	0.0020	1.1906	0.0264	0.1019	0.0008	1.310	0.046	47	0.87
6.1	473.1	152.9	0.323	8.88	0.0918	0.0022	1.8208	0.0387	0.1439	0.0011	1.462	0.044	59	0.95
7.1	755.5	314	0.416	10.32	0.0864	0.0020	1.2709	0.0291	0.1066	0.0008	1.348	0.042	48	0.95
8.1	345.3	92.8	0.269	11.17	0.1131	0.0024	3.0326	0.0615	0.1945	0.0015	1.850	0.039	61	0.87
9.1	469	73.3	0.156	6.16	0.0990	0.0023	2.1936	0.0469	0.1608	0.0013	1.604	0.043	59	0.76
10.1	603.6	139.5	0.231	8.71	0.1080	0.0023	2.1343	0.0420	0.1433	0.0010	1.767	0.038	48	0.98
11.1	1163.5	426.5	0.367	20.65	0.0922	0.0021	1.0873	0.0230	0.0855	0.0006	1.472	0.043	35	0.82
12.1	1038.4	281.8	0.271	8.86	0.0975	0.0020	1.8797	0.0364	0.1398	0.0010	1.577	0.038	53	0.89
13.1	466.5	144.4	0.310	11.24	0.0980	0.0032	2.1768	0.0717	0.1611	0.0018	1.587	0.061	60	0.97
13.2	959.6	303.9	0.317	13.41	0.0954	0.0029	1.7984	0.0546	0.1367	0.0013	1.536	0.057	53	0.97
14.1	514.9	2430.5	4.720	5.47	0.1050	0.0030	2.5800	0.0757	0.1782	0.0018	1.714	0.053	61	0.83
15.1	1258.1	512.3	0.407	5.24	0.0923	0.0024	1.3319	0.0370	0.1047	0.0010	1.473	0.049	43	0.98
16.1	431.5	131.7	0.305	5.08	0.1052	0.0024	2.7162	0.0691	0.1872	0.0017	1.718	0.041	64	0.64
17.1	882.2	324.5	0.368	10.24	0.0985	0.0025	1.8784	0.0502	0.1384	0.0013	1.595	0.047	52	0.86
18.1	149.9	95.7	0.639	1.09	0.1653	0.0041	11.8589	0.2906	0.5204	0.0050	2.510	0.041	107	0.71
18.2	260.5	183.9	0.706	1.66	0.1638	0.0045	11.0734	0.2919	0.4904	0.0044	2.495	0.046	103	0.74
19.1	1040.8	205.7	0.198	9.42	0.0910	0.0025	1.2156	0.0342	0.0969	0.0009	1.446	0.053	41	0.77
19.2	1277.2	198.7	0.156	18.70	0.0908	0.0030	1.0051	0.0336	0.0803	0.0008	1.442	0.064	34	0.90
20.1	438.5	93.7	0.214	3.14	0.1051	0.0028	2.9570	0.0841	0.2041	0.0020	1.716	0.049	69	0.99
21.1	849.5	157.1	0.185	7.33	0.0957	0.0024	2.1887	0.0580	0.1659	0.0015	1.542	0.047	64	0.83
22.1	515.1	116.3	0.226	7.31	0.1054	0.0026	2.8482	0.0728	0.1960	0.0017	1.721	0.045	67	0.89
22.2	1065.2	649.6	0.610	12.00	0.0957	0.0025	1.5753	0.0435	0.1194	0.0011	1.542	0.048	47	0.98
23.1	478.5	108.8	0.227	2.95	0.1160	0.0027	3.8318	0.0998	0.2395	0.0022	1.896	0.043	72	0.96
14.2	958.1	196.8	0.205	4.99	0.0958	0.0028	1.8690	0.0537	0.1415	0.0013	1.544	0.054	55	0.99
15.2	384.8	5531.4	14.376	1.64	0.0905	0.0026	1.1649	0.0391	0.0933	0.0010	1.437	0.055	40	0.96
16.2	1011	281.6	0.279	6.92	0.0959	0.0027	1.9501	0.0574	0.1474	0.0013	1.547	0.053	57	0.93
17.2	339.3	106.9	0.315	7.52	0.1057	0.0029	2.7251	0.0712	0.1871	0.0016	1.726	0.05	64	0.76
20.2	501.6	102.8	0.205	2.72	0.1061	0.0033	2.8664	0.0997	0.1958	0.0021	1.734	0.055	66	0.99
21.2	652.6	200.5	0.307	3.73	0.1029	0.0027	3.2459	0.0860	0.2287	0.0019	1.678	0.048	79	0.53
22.3	1289.9	294.5	0.228	9.30	0.1052	0.0028	2.4977	0.0639	0.1721	0.0014	1.718	0.05	59	0.91
22.4	659.8	145.8	0.221	7.25	0.0839	0.0029	1.5017	0.0490	0.1297	0.0013	1.291	0.068	60	0.87
23.2	483.5	102.7	0.212	2.79	0.1185	0.0033	4.9118	0.1349	0.3007	0.0027	1.933	0.049	87	0.93
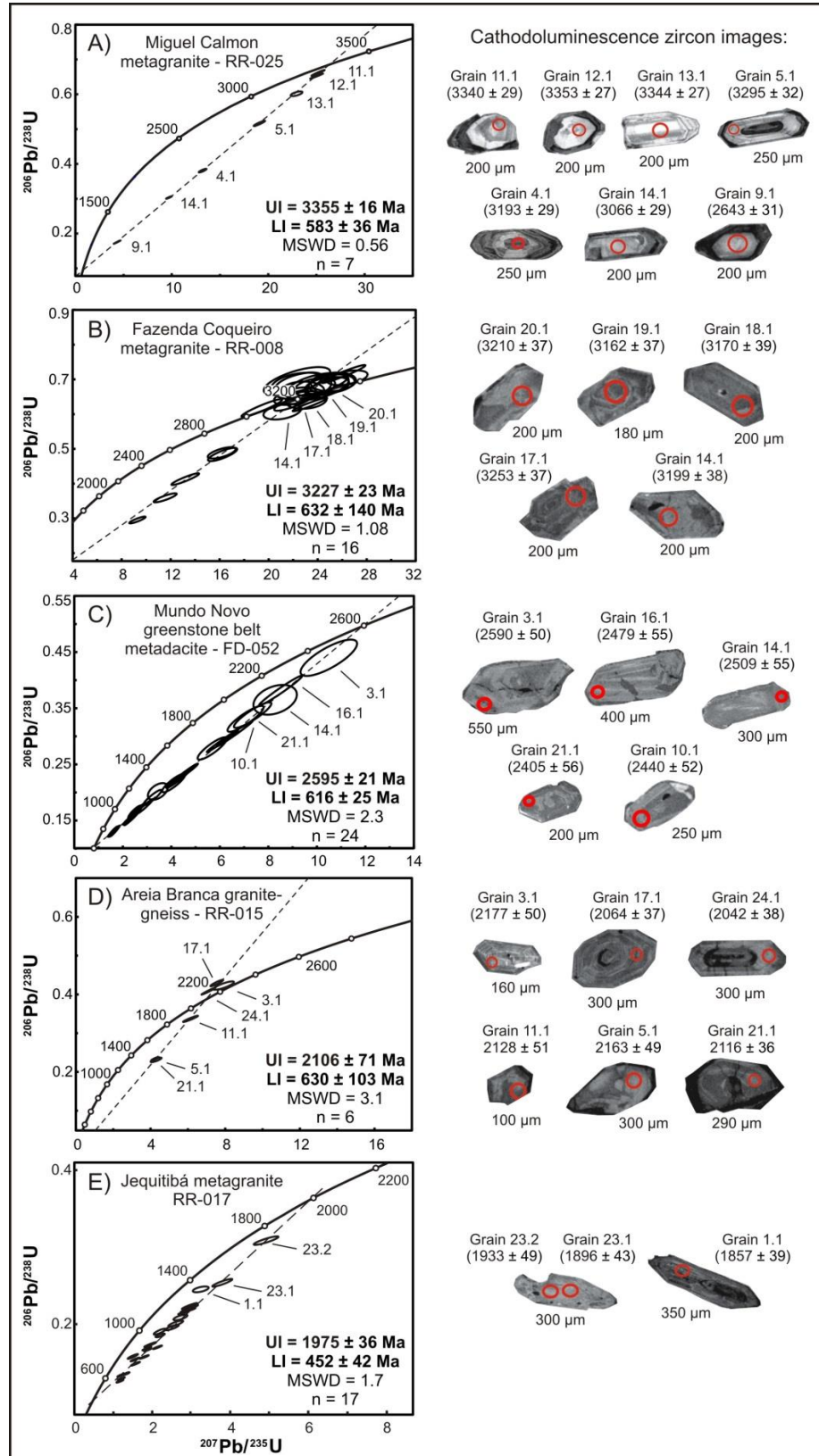
Fig. 6. U-Pb concordia diagram of the LA-ICP-MS data for the studied samples: a) Miguel Calmon metagranite (crystallization age of 3355 ± 16 Ma); b) Fazenda Coqueiro metagranite (crystallization age of 3227 ± 23 Ma); c) MNGB metadacite (crystallization age of 2595 ± 21 Ma); d) Areia Branca granite-gneiss (crystallization age of 2106 ± 71 Ma); e) Jequitibá metagranite (crystallization age of 1975 ± 36 Ma). Circles in the cathodoluminescence zircon images represent the spot size; the ages are reported in million years and the lengths are reported for each grain separately. UI: upper intercept, LI: lower intercept.

7. Nd and Sr isotopic analysis

The same samples analyzed by the U-Pb method were studied to investigate the petrogenetic processes, including the Miguel Calmon (sample RR-025) and Fazenda Coqueiro (sample RR-008) metagranites from the Gavião Block, the metadacite from the MNGB (sample FD-052) and the Paleoproterozoic Areia Branca (sample RR-015) and Jequitibá (sample RR-017) metagranites. The Nd and Sr isotopic data are shown in Table 7.

The dataset shows two groups of rocks: one associated with the Archean rocks and the other associated with the Paleoproterozoic rocks (Fig. 7). Samples RR-008 (Fazenda Coqueiro metagranite) and RR-025 (Miguel Calmon metagranite) of the Archean rocks show $\varepsilon_{Nd(t)}$ values of -3.6 and -3.7 calculated for the crystallization ages of 3.22 and 3.35 Ga, respectively. These values suggest crustal residence time. The T_{DM} ages are 3.7 Ga for sample RR-008 (Fazenda Coqueiro metagranite) and 3.6 Ga for sample RR-025 (Miguel Calmon metagranite). In contrast, the younger rocks, Areia Branca granite-gneiss (sample RR-015) and Jequitibá metagranite (sample RR-017), have crystallization ages of 2.1 and 1.97 Ga, $\varepsilon_{Nd(t)}$ values of -7.7 and -6.5 and Archean T_{DM} ages of 2.9 and 2.7 Ga, respectively. This set of data from the Areia Branca and Jequitibá granites indicates derivation from crustal protoliths comprised of TTG gneisses and other Archean rocks.

In the Rb-Sr system, samples RR-008 (Fazenda Coqueiro metagranite) and RR-025 (Miguel Calmon metagranite), with U-Pb zircon crystallization ages of 3.2 and 3.3, respectively, present low $^{87}Sr/^{86}Sr_i$ ratios of approximately 0.700 (Fig. 7). These data imply a genesis from partial melting of the lower continental crust (mafic or intermediate granulitic rocks and TTG plutons, for example) added to the negative $\varepsilon_{Nd(t)}$ values of -3.6 (Fazenda Coqueiro metagranite) and -3.7 (Miguel Calmon metagranite) (De Paolo, 1988). The fractionation of the $^{87}Rb/^{86}Sr$ ratio by processes occurring after the formation of the rock, as evidenced by the formation of igneous overgrowth zones in some zircons, may also have contributed to the low $^{87}Sr/^{86}Sr_i$ values of the Miguel Calmon (0.699) and Fazenda Coqueiro (0.705) metagranites.

The rocks with crystallization ages of 2.1 (Areia Branca granite-gneiss) and 1.97 Ga (Jequitibá metagranite) have $^{87}Sr/^{86}Sr_i$ ratio values that are extremely high, between 0.744 and 0.730, and $\varepsilon_{Nd(t)}$ values of -7.7 and -6.5, respectively, and plot strictly in the crustal source field (Fig. 7). Thus, these rocks are interpreted to be derived from continental crust with a longer time of crustal residence. The possibility of crustal contamination in the Areia Branca and Jequitibá granites may be contributed to the high $^{87}Sr/^{86}Sr_i$ ratio values.

The metadacite in the MNGB middle sequence (FD-052) was derived predominantly from a juvenile source and had a primitive evolution from the mantle based on the $\varepsilon_{Nd(t)}$ value of +1.5. However, this value also indicates the existence of a subordinate crustal component (De Paolo, 1988). Its $^{87}Sr/^{86}Sr_i$ ratio is lower than the basaltic achondrite best initial (BABI) value of 0.69899. This difference may be a result of sericitic alteration, which homogenized the initial $^{87}Sr/^{86}Sr$ after the formation of the rock (Alderton et al., 1998).

Table 7. Sm-Nd and Rb-Sr isotopic data for samples of the Gavião Block, MNGB and Paleoproterozoic granites

Unit/Sample ID	Sm (ppm)	Nd (ppm)	^{147}Sm/^{144}Nd	^{143}Nd/^{144}Nd	Error (2σ)	T_{DM} (Ma)	T (Ma)	$\varepsilon_{Nd(T)}$	Rb (ppm)	Sr (ppm)	^{87}Rb/^{86}Sr	^{87}Sr/^{86}Sr	Error (2σ)	^{87}Sr/^{86}Sr$_i$
Paleoproterozoic metagranites														
Jequitibá (RR-017)	9.6	53.2	0.1091	0.511171	0.000004	2752	1975	-6.5	312.2	59.0	15.5176699	1.170177	0.000024	0.7299
Areia Branca (RR-015)	3.5	20.6	0.1061	0.510997	0.000004	2931	2106	-7.7	118.6	43.0	10.1958525	1.052428	0.000025	0.7438
MNGB														
Metadacite (FD-052)	49.3	228.7	0.1304	0.511617	0.000004	2630	2595	+1.5	79.0	56.0	4.1369952	0.807358	0.000018	0.6821
Gavião Block metagranites														
Faz. Coqueiro (RR-008)	10.3	49.4	0.1261	0.510962	0.000004	3717	3227	-3.6	73.6	22.0	9.8107171	1.155501	0.000024	0.7059
M. Calmon (RR-025)	2.4	18.4	0.0789	0.510000	0.000004	3658	3355	-3.7	74.2	333.0	0.6534393	0.729151	0.000020	0.6992

Note: ^{147}Sm/^{144}Nd = [Sm (ppm) / Nd (ppm)] × (1/1.645); ^{87}Rb/^{86}Sr = [Rb (ppm) / Sr (ppm)] × (1/0.341); T (Ma) = U-Pb zircon age; (T_{DM}) Sm-Nd depleted mantle model age (De Paolo, 1981).
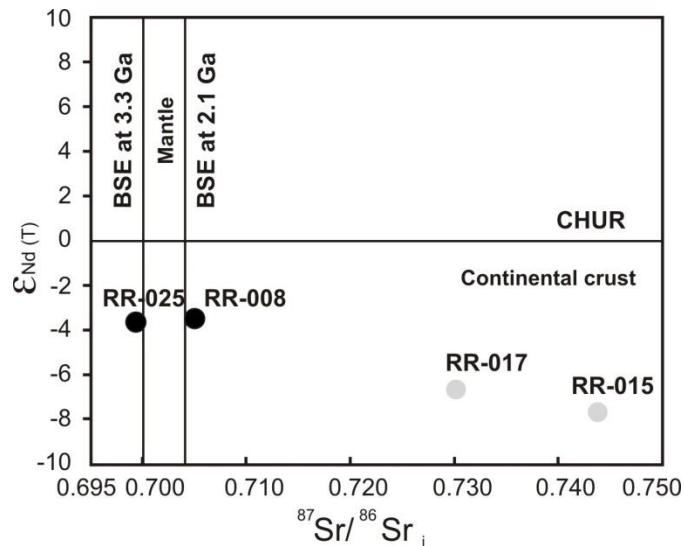
Fig. 7. ^{87}Sr/^{86}Sr$_i$ vs. $\varepsilon_{Nd(t)}$ diagram for studied rocks. RR-025: Miguel Calmon metagranite, RR-008: Fazenda Coqueiro metagranite, RR-017: Jequitibá metagranite, RR-015: Areia Branca granite-gneiss. BSE: bulk silicate earth and CHUR: chondritic uniform reservoir (Dickin, 2005).

8. Whole-rock geochemistry results

Whole-rock geochemical analysis of the major, minor, and trace elements, including REE, of 16 rock samples from the Gavião Block, 49 rock samples from the MNGB and 3 samples from the Paleoproterozoic metagranites was performed using the ICP-MS technique at the SGS-Geosol laboratory. This analysis was used to refine the classification of rocks previously classified on the basis of petrography and mineral chemistry and to characterize the petrological processes and tectonic settings. Therefore, this analysis included samples of metagranites and metarhyolites related to the TTG basement, samples of the metakomatiites, eastern metabasalts, western metabasalts and metadacites in the MNGB and samples of younger granites. The lithogeochemical data of all those rocks are listed in Tables 8, 9 and 10.

Table 8. Whole-rock major and minor oxide geochemical data (wt.%)

Unit and classification	Sample ID	W. Long.	S. Lat.	SiO₂	TiO₂	Al₂O₃	Fe₂O₃t	MnO	MgO	CaO	Na₂O	K₂O	P₂O₅	LOI	Sum
Gavião Block															
Faz. Coqueiro metagranite	RR-008	40°29'45.57"	11°54'25.27"	76.62	0.09	11.46	1.88	0.01	0.12	0.4	2.91	4.03	0.01	0.2	97.73
M. Calmon metagranite	RR-025	40°34'33.48"	11°26'15.07"	71.19	0.14	13.98	2.05	0.03	0.34	1.36	3.87	3.49	0.04	0.39	96.88
Metarhyolite/ metadacite	RR-007	40°29'12.58"	11°54'06.82"	75.07	0.14	10.25	3.16	0.03	0.71	0.15	3.18	2.27	0.005	0.49	95.46
Metarhyolite/ metadacite	RR-009	40°30'00.00"	11°54'10.84"	73.82	0.13	10.74	3.39	0.06	0.58	0.69	2.95	2.65	0.005	0.39	95.41
Metarhyolite/ metadacite	RR-374	40°31'51.99"	12°08'05.51"	79.93	0.25	8.5	3.65	0.05	0.42	0.91	2.81	1.27	0.005	0.36	98.16
Metarhyolite/ metadacite	RR-595	40°31'10.49"	11°58'43.29"	76.55	0.62	12.32	4.31	0.08	0.7	1.72	4.53	2.16	0.12	0.53	103.64
Metarhyolite/ metadacite	RR-598	40°31'05.66"	11°58'43.35"	76.44	0.43	12.63	3.69	0.04	0.47	1.36	3.68	4.04	0.06	0.29	103.13
Metarhyolite/ metadacite	RR-783B	40°30'43.04"	11°58'59.13"	76.39	0.39	12.41	3.47	0.03	1.18	0.44	3.8	4.02	0.04	0.34	102.51
Metarhyolite/ metadacite	RR-786	40°31'15.07"	11°59'10.90"	79.16	0.17	10.65	3.39	0.05	0.4	0.63	3.45	2.91	0.005	0.34	101.16
Metarhyolite/ metadacite	RR-896	40°30'01.87"	11°55'51.85"	72.39	0.23	12.26	3.7	0.05	1	0.4	4.05	3.94	0.005	0.48	98.51
Metarhyolite/ metadacite	RR-F16-001	40°29'27.40"	11°53'33.16"	79.52	0.18	11.63	4.11	0.03	0.64	0.26	3.62	2.98	0.005	0.2	103.18
Metarhyolite/ metadacite	RR-F16-004	40°29'27.40"	11°53'33.16"	80.14	0.18	11.21	4.85	0.04	1.28	0.15	3	2.17	0.005	0.72	103.75
Metarhyolite/ metadacite	RR-F16-005	40°29'27.40"	11°53'33.16"	81.07	0.17	10.94	4.45	0.03	0.95	0.13	3.1	1.87	0.005	0.7	103.42
Metarhyolite/ metadacite	RR-F16-007	40°29'27.40"	11°53'33.16"	81.27	0.18	10.94	3.92	0.03	1.13	0.23	4.19	1.08	0.005	0.38	103.36
Metarhyolite/ metadacite	RR-F16-008	40°29'27.40"	11°53'33.16"	80.59	0.17	10.68	4.64	0.05	1.85	0.2	2.27	1.73	0.005	1.08	103.27
Metarhyolite/ metadacite	RR-F16-009	40°29'27.40"	11°53'33.16"	78.36	0.15	10.07	3.92	0.04	1.18	0.25	2.95	1.42	0.005	0.55	98.90
Mundo Novo greenstone belt															
Metakomatiite	RR-011B	40°25'02.20"	11°48'39.22"	47.01	0.25	7.33	10.18	0.22	24.46	2.99	0.08	0.03	0.005	5.49	98.05
Metakomatiite	FD-37-017	40°30'22.03"	11°41'07.33"	54.39	0.23	7.12	6.68	0.65	17.57	10.15	0.65	0.3	0.19	3.73	101.66
Metakomatiite	FD-058A	40°28'45.53"	11°41'43.47"	57.22	0.07	2.19	6.12	0.11	24.38	2.42	0.05	0.03	0.005	4.52	97.12
Metakomatiite	FD-070	40°28'36.03"	11°41'39.19"	55.02	0.07	2.81	9.38	0.23	18.91	7.4	0.11	0.03	0.005	4.03	98.00
Eastern metabasalt	RR-006	40°25'40.85"	11°53'04.26"	49.78	0.83	14.05	11.97	0.21	8.1	12.53	0.96	0.25	0.04	0.55	99.27
Eastern metabasalt	RR-011C	40°25'02.20"	11°48'39.22"	49.08	1.19	13.39	14.03	0.24	6.98	10.67	0.8	0.32	0.05	0.8	97.55
Eastern metabasalt	RR-014B	40°30'21.91"	11°41'40.20"	50.49	1	13.71	13.42	0.22	6.33	10.69	2.2	0.26	0.06	1.22	99.60
Eastern metabasalt	RR-018A	40°30'07.88"	12°13'43.29"	48.93	1.04	14.18	14.11	0.23	7.16	11.39	2.1	0.26	0.07	0.52	99.99
Eastern metabasalt	RR-018B	40°30'07.94"	12°13'43.35"	51.33	1.07	13.74	14.04	0.24	7.26	10.41	2.55	0.26	0.08	0.53	101.51
Eastern metabasalt	RR-018C	40°30'08.01"	12°13'43.42"	52.48	1.1	14.19	13.39	0.21	5.68	11.57	1.95	0.18	0.1	0.43	101.28
Eastern metabasalt	RR-018D	40°30'08.08"	12°13'43.48"	51.83	1.06	14.16	13.4	0.21	5.47	13.27	1.39	0.15	0.09	0.48	101.51
Eastern metabasalt	RR-071	40°28'39.28"	11°36'42.51"	54.77	1.46	13.32	15.76	0.26	6.36	10.05	0.65	0.23	0.03	0.85	103.74
Eastern metabasalt	RR-072	40°29'25.44"	11°37'14.46"	54.68	1.52	13.45	15.19	0.22	6.72	9.73	0.41	0.13	0.05	0.67	102.77
Eastern metabasalt	RR-078	40°28'06.14"	11°39'32.83"	52.46	1.15	13.76	13.35	0.21	6.49	10.56	1.68	0.19	0.04	0.63	100.52
Eastern metabasalt	RR-080	40°26'38.53"	11°40'09.08"	51.14	0.97	15.65	13.38	0.2	6.47	10.27	2.88	0.31	0.09	0.6	101.96
Eastern metabasalt	FD-37-001	40°30'22.03"	11°41'07.33"	50.14	0.97	14.33	12.6	0.22	6.47	10.84	1.98	0.09	0.08	0.9	98.62
Eastern metabasalt	FD-37-002	40°30'22.03"	11°41'07.33"	52.47	0.98	14.47	12.95	0.21	6.63	10.72	2.14	0.12	0.07	0.57	101.33
Eastern metabasalt	FD-37-004	40°30'22.03"	11°41'07.33"	51.5	1.11	14.03	14.35	0.23	5.49	9.95	2.08	0.16	0.09	0.36	99.35
Eastern metabasalt	FD-37-005	40°30'22.03"	11°41'07.33"	50.92	1.21	13.21	15.04	0.23	4.97	9.92	2.13	0.15	0.1	0.68	98.56
Eastern metabasalt	FD-37-006	40°30'22.03"	11°41'07.33"	50.81	0.71	15.59	11.17	0.18	7.74	11.18	2.22	0.15	0.06	0.89	100.70
Eastern metabasalt	FD-37-007	40°30'22.03"	11°41'07.33"	51.08	0.99	14.56	13.92	0.21	6.58	9.96	2.57	0.25	0.09	0.92	101.13
Eastern metabasalt	FD-37-009	40°30'22.03"	11°41'07.33"	52.74	0.93	14.95	13.57	0.21	7.53	10.68	2.38	0.18	0.08	0.61	103.86
Eastern metabasalt	FD-37-011	40°30'22.03"	11°41'07.33"	52.94	1.02	13.62	13.86	0.21	6.88	10.32	2.06	0.24	0.04	0.89	102.08
Eastern metabasalt	FD-37-012	40°30'22.03"	11°41'07.33"	53.63	1.23	14.07	15.43	0.25	5.07	10.01	2.36	0.16	0.12	0.88	103.21
Eastern metabasalt	FD-37-013	40°30'22.03"	11°41'07.33"	52.66	0.99	14.75	13.09	0.22	6.23	10.62	2.16	0.18	0.09	0.82	101.81
Eastern metabasalt	FD-37-015	40°30'22.03"	11°41'07.33"	48.91	1.12	15.58	14.27	0.24	6.58	11.58	2.33	0.21	0.1	0.93	101.85

				SiO$_2$	TiO$_2$	Al$_2$O$_3$	Fe$_2$O$_3$t	MnO	MgO	CaO	Na$_2$O	K$_2$O	P$_2$O$_5$	LOI	Total
Eastern metabasalt	FD-37-016	40°30'22.03"	11°41'07.33"	48.7	1.28	17.47	13.65	0.18	7.7	9.23	2.04	0.93	0.17	2.46	103.81
Eastern metabasalt	FD-37-019	40°30'22.03"	11°41'07.33"	53.15	0.99	14.19	13.06	0.22	6.16	10.68	2.39	0.13	0.1	0.77	101.84
Eastern metabasalt	FD-016	40°29'24.00"	11°42'01.07"	53.15	1.02	12.62	12.62	0.26	5.85	8.6	2.1	0.34	0.06	0.94	97.56
Eastern metabasalt	FD-028	40°26'43.09"	11°48'24.59"	52.18	1.27	13.24	12.86	0.21	5.74	12.44	1.58	0.24	0.07	0.78	100.61
Western metabasalt	RR-022	40°36'07.38"	12°18'51.47"	49.47	0.95	14.28	12.39	0.23	5.88	10.75	2.3	0.61	0.07	0.76	97.69
Western basaltic metandesite	RR-F1-001	40°29'40.00"	11°53'22.35"	55.52	0.99	14.69	12.23	0.23	7.17	9.34	1.89	0.53	0.1	1.28	103.97
Western metabasalt	RR-F4-006	40°29'31.17"	11°54'14.89"	49.75	1.26	15.1	12.96	0.2	4.74	8.19	3.72	0.31	0.17	0.24	96.64
Western metabasalt	RR-F4-007	40°29'31.17"	11°54'14.89"	49.8	1.35	15.05	12.58	0.19	4.74	7.63	2.33	1.57	0.19	0.32	95.75
Western basaltic metandesite	RR-F6-001	40°29'35.54"	11°53'35.26"	57.06	1.34	16.4	7.24	0.11	2.37	5.92	4.71	1.18	0.2	0.8	97.33
Western metabasalt	RR-F6-002	40°29'35.54"	11°53'35.26"	48.04	1.56	17.37	11.27	0.19	4.64	7.21	4.03	0.99	0.17	0.64	96.11
Western metabasalt	RR-F6-003	40°29'35.54"	11°53'35.26"	46.4	1.45	15.54	12.8	0.24	5.95	8.21	2.93	0.98	0.17	0.68	95.35
Western metabasalt	RR-F6-004	40°29'35.54"	11°53'35.26"	48.72	1.3	14.51	11.68	0.2	5.15	9.4	2.04	0.83	0.19	1.04	95.06
Western metabasalt	RR-F6-005	40°29'35.54"	11°53'35.26"	50.26	1.28	15.5	13.09	0.2	4.94	8.52	3.14	0.96	0.17	0.35	98.41
Western metabasalt	RR-F6-006	40°29'35.54"	11°53'35.26"	50.5	1.34	15.71	12.96	0.2	4.44	8.48	3.53	0.83	0.19	0.26	98.44
Western metabasalt	RR-F6-007	40°29'35.54"	11°53'35.26"	52.73	1.4	15.78	10.57	0.17	4.16	8.13	3.74	0.18	0.2	0.25	97.31
Western metabasalt	RR-F6-008	40°29'35.54"	11°53'35.26"	48.98	1.29	15.2	12.44	0.2	5.18	8.36	3.3	0.91	0.16	0.35	96.37
Western metabasalt	RR-F6-009	40°29'35.54"	11°53'35.26"	48.1	1.33	15.23	13.02	0.22	6.3	8.15	2.59	0.22	0.16	0.14	95.46
Western metabasalt	RR-F6-010	40°29'35.54"	11°53'35.26"	50.64	1.4	15.08	12.75	0.22	5.37	7.19	2.54	0.63	0.18	0.05	96.05
Western metabasalt	RR-F6-016	40°29'35.54"	11°53'35.26"	54.48	0.71	16.43	11.03	0.23	6.07	3.52	4.04	1.19	0.07	2.47	100.24
Western metabasalt	RR-F6-018	40°29'35.54"	11°53'35.26"	53.79	0.63	15.71	9.44	0.2	6.19	9.82	2.35	0.24	0.09	0.77	99.23
Western basaltic metandesite	RR-F16-027	40°29'27.40"	11°53'33.16"	57.24	0.73	14.2	10.32	0.16	5.01	8.5	2.57	0.74	0.05	1.36	100.88
Metadacite	FD-052	40°29'26.72"	11°42'09.52"	70.98	0.34	14.22	5.08	0.07	2.09	1.24	2.02	2.46	0.04	1.55	100.09
Metarhyolite	RR-FST-002	40°29'33.55"	11°42'52.06"	73.2	0.41	11.49	6.58	0.08	1.63	1.81	1.41	2.69	0.08	0.74	100.12
Paleoproterozoic granites															
Jequitibá metagranite	RR-017	40°28'42.22"	12°07'46.24"	69.4	0.32	14.25	2.78	0.02	0.58	0.77	2.28	5.76	0.18	0.7	97.04
Areia Branca granite-gneiss	RR-015	40°28'53.96"	11°40'18.19"	77.35	0.19	14.58	2.18	0.03	0.35	0.63	3.11	5.56	0.06	0.5	104.54
Cachoeira Grande granite	RR-026	40°24'41.53"	11°25'44.37"	77.27	0.11	13.43	1.73	0.04	0.27	0.76	3.12	4.45	0.07	0.49	101.74

Note: Error interval for each element considering all samples analyzed and represented in terms of standard deviation (1σ) (Thompson, 1988): SiO$_2$ (1.55 - 2.71), TiO$_2$ (0.01 - 0.06), Al$_2$O$_3$ (0.08 - 0.59), Fe$_2$O$_3$t (0.06 - 0.53), MnO (0 - 0.03), MgO (0.01 - 0.82), CaO (0.01 - 0.45), Na$_2$O (0.01 - 0.17), K$_2$O (0 - 0.20), and P$_2$O$_5$ (0 - 0.01).

Table 9. Whole-rock REE geochemical data (ppm)

Unit and classification	Sample ID	La	Ce	Pr	Nd	Sm	Eu	Gd	Tb	Dy	Ho	Er	Tm	Yb	Lu
Gavião Block															
Fazenda Coqueiro metagranite	RR-008	54	119.8	13.13	49.4	10.3	0.89	10.42	1.83	11.5	2.46	7.35	1.1	7.4	1.08
Miguel Calmon metagranite	RR-025	32.5	54.2	5.62	18.4	2.4	0.63	1.34	0.15	0.7	0.12	0.38	0.025	0.3	0.025
Metarhyolite/metadacite	RR-007	51.1	0.49	11.96	46.6	9.3	1.65	9.49	1.54	9.67	1.98	6.16	0.93	6	0.92
Metarhyolite/metadacite	RR-009	52.1	0.39	12.13	47.3	9.5	1.76	9.64	1.61	10.29	2.18	6.58	0.95	6.2	0.92
Metarhyolite/metadacite	RR-374	96.9	0.36	19.56	72.9	14.4	1.29	11.79	1.58	8.56	1.46	3.42	0.46	2.9	0.43
Metarhyolite/metadacite	RR-595	54.4	0.53	12.16	44.7	8.1	1.3	6.97	1.21	7.91	1.74	4.91	0.75	5.2	0.69
Metarhyolite/metadacite	RR-598	36.9	0.29	7.09	27.2	5.2	0.97	5.41	0.87	5.73	1.2	3.57	0.58	3.7	0.58
Metarhyolite/metadacite	RR-783B	67.2	0.34	13.86	52.6	10.5	1.07	9.8	1.57	10.37	2.2	6.76	1.05	6.9	1.08
Metarhyolite/metadacite	RR-786	35.4	0.34	5.73	22.5	5	1.03	5.94	1.08	8.36	1.95	6.6	1.09	7.5	1.18
Metarhyolite/metadacite	RR-896	65.5	0.48	15.65	59.7	12.5	2.16	13.28	2.22	14.49	3.05	9.09	1.38	8.7	1.27
Metarhyolite/metadacite	RR-F16-001	72	0.2	15.75	61.7	11.8	2.02	11.26	1.8	11.81	2.56	7.64	1.13	7.7	1.11
Metarhyolite/metadacite	RR-F16-004	56.6	0.72	11.94	46.9	10	1.78	10.42	1.73	11.49	2.41	7.36	1.07	7.3	1.03
Metarhyolite/metadacite	RR-F16-005	53.5	0.7	11.81	45.8	9.5	1.64	9.71	1.62	10.53	2.17	6.41	0.98	6.6	0.99
Metarhyolite/metadacite	RR-F16-007	56.3	0.38	12.2	47.6	10.1	1.79	10.55	1.72	11.25	2.39	7.37	1.06	7.2	1.05
Metarhyolite/metadacite	RR-F16-008	50.3	1.08	10.87	42.7	9.1	1.69	9.37	1.64	10.8	2.28	7.03	1.04	7	1.05
Metarhyolite/metadacite	RR-F16-009	58.3	0.55	12.77	50.4	10.2	1.73	10.09	1.63	10.84	2.24	6.89	1	6.6	1
Mundo Novo greenstone belt															
Metakomatiite	RR-011B	9.5	13.2	1.18	3.8	0.6	0.2	0.68	0.12	0.74	0.16	0.49	0.07	0.5	0.07
Metakomatiite	FD-37-017	7.2	12.6	1.62	6.7	1.4	0.43	1.56	0.21	1.49	0.3	0.94	0.13	0.9	0.13
Metakomatiite	FD-058A	7.1	6.5	1.3	5.3	1.2	0.42	1.6	0.26	1.6	0.32	1	0.14	0.8	0.025
Metakomatiite	FD-070	4.9	3.7	1.17	4.7	1.3	0.51	1.74	0.29	1.81	0.41	1.11	0.19	1.1	0.11
Eastern metabasalt	RR-006	5	10.2	1.46	7	2.1	0.76	2.71	0.46	3.01	0.63	1.88	0.26	1.7	0.26
Eastern metabasalt	RR-011C	10.7	24.1	3.15	14.4	3.7	1.04	4.02	0.64	3.92	0.79	2.25	0.3	1.8	0.27
Eastern metabasalt	RR-014B	6.4	11.9	1.95	9.3	2.9	1	3.8	0.69	4.83	1.03	3.09	0.45	2.9	0.44
Eastern metabasalt	RR-018A	7	16.3	2.22	10.3	2.9	1	3.73	0.66	4.31	0.93	2.72	0.41	2.6	0.39
Eastern metabasalt	RR-018B	7.3	13.4	1.87	9.1	2.8	0.9	3.54	0.61	4.17	0.89	2.69	0.38	2.5	0.38
Eastern metabasalt	RR-018C	9.3	20.9	2.66	12.1	3.2	1.04	3.9	0.68	4.42	0.96	2.88	0.41	2.7	0.41
Eastern metabasalt	RR-018D	8	18	2.31	10.7	2.8	0.98	3.58	0.63	4.16	0.91	2.67	0.38	2.5	0.39
Eastern metabasalt	RR-071	11.6	19.1	2.9	13.1	3.4	1.06	4.63	0.69	4.52	0.87	2.54	0.33	2.1	0.32
Eastern metabasalt	RR-072	11	24.6	2.93	13.9	3.8	1.28	4.67	0.77	4.6	0.94	2.6	0.37	2.2	0.37
Eastern metabasalt	RR-078	10	12.8	2.19	10.3	3.1	1.17	4.41	0.75	5.28	1.09	3.39	0.5	3.3	0.51
Eastern metabasalt	RR-080	10.1	14.1	1.96	8.9	2.7	0.99	3.95	0.71	4.69	0.99	3.09	0.43	2.8	0.46
Eastern metabasalt	FD-37-001	6.1	12.6	1.83	8.9	2.5	0.99	3.62	0.64	4.28	0.88	2.76	0.38	2.6	0.4
Eastern metabasalt	FD-37-002	5	11.3	1.7	8.4	2.5	0.96	3.44	0.63	4.21	0.9	2.63	0.37	2.5	0.39
Eastern metabasalt	FD-37-004	5.7	13.7	2.08	9.9	3.4	1.22	4.39	0.79	5.28	1.15	3.22	0.5	3.3	0.49
Eastern metabasalt	FD-37-005	6.5	14.9	2.26	10.5	3.2	1.12	4.55	0.78	5.16	1.13	3.4	0.49	3.1	0.49
Eastern metabasalt	FD-37-006	4.9	8.4	1.2	6.2	1.9	0.7	2.73	0.49	3.09	0.68	1.96	0.3	1.9	0.28
Eastern metabasalt	FD-37-007	6.2	12	1.77	8.3	2.6	0.94	3.41	0.6	4.31	0.88	2.45	0.4	2.6	0.38
Eastern metabasalt	FD-37-009	5.7	11.7	1.61	7.9	2.4	0.86	3.31	0.59	4.05	0.83	2.54	0.38	2.4	0.37
Eastern metabasalt	FD-37-011	6.1	12.7	1.82	8.4	2.5	0.96	3.46	0.6	3.96	0.87	2.63	0.37	2.5	0.41
Eastern metabasalt	FD-37-012	6.3	14.1	2.02	10	3.3	1.16	4.49	0.77	5.42	1.11	3.33	0.49	3.3	0.48
Eastern metabasalt	FD-37-013	4.6	11.2	1.7	8.9	2.7	0.97	4	0.71	4.35	0.96	2.86	0.47	2.7	0.43
Eastern metabasalt	FD-37-015	6.9	12.9	1.91	9.2	3	1.07	4.21	0.73	4.82	1.06	3.12	0.46	3	0.5
Eastern metabasalt	FD-37-016	6.9	14.8	2.32	11.1	3.7	1.27	4.86	0.87	5.5	1.22	3.64	0.52	3.4	0.54
Eastern metabasalt	FD-37-019	7.1	14.1	1.95	9.3	2.8	1	3.62	0.67	4.45	0.96	2.81	0.42	2.8	0.46
Eastern metabasalt	FD-016	7.4	12	1.94	9	2.6	0.94	3.78	0.65	4.42	0.92	2.93	0.39	2.6	0.4
Eastern metabasalt	FD-028	5.7	13.1	1.99	10.2	3.2	1.12	4.34	0.72	4.82	1	2.92	0.44	2.9	0.42
Western metabasalt	RR-022	18.6	27.6	4.74	19.2	4.8	1.42	4.98	0.84	5.49	1.14	3.28	0.48	3.1	0.44
Western basaltic metandesite	RR-F1-001	21.1	39.1	5.18	20	4.7	1.41	5.23	0.84	5.07	0.98	2.72	0.38	2.6	0.41
Western metabasalt	RR-F4-006	23	44.3	5.6	23.4	5.5	1.54	6.15	1	6.56	1.33	4	0.57	3.8	0.56
Western metabasalt	RR-F4-007	25	45.8	5.79	23.4	5.6	1.59	6.4	1.04	6.79	1.31	3.94	0.56	3.7	0.58
Western basaltic metandesite	RR-F6-001	25.8	48.7	6.24	24.9	5.7	1.45	6.51	1.06	6.74	1.32	3.79	0.59	3.7	0.55
Western metabasalt	RR-F6-002	26.5	55.2	7.1	28.2	6.8	1.67	7.62	1.22	7.71	1.56	4.58	0.66	4.4	0.64
Western metabasalt	RR-F6-003	27.7	47.5	5.96	24.3	5.8	1.63	6.67	1.1	6.86	1.42	4.26	0.67	4	0.66

		La	Ce	Pr	Nd	Sm	Eu	Gd	Tb	Dy	Ho	Er	Tm	Yb	Lu
Western metabasalt	RR-F6-004	23.9	45.4	5.88	23.6	5.9	1.4	6.56	1.08	6.87	1.41	3.99	0.6	3.8	0.54
Western metabasalt	RR-F6-005	23.4	45.9	5.91	24.2	5.8	1.72	6.58	1.06	6.59	1.38	4.26	0.58	3.9	0.6
Western metabasalt	RR-F6-006	21.7	45.1	5.82	23	5.7	2.06	6.48	1	6.67	1.37	4.12	0.56	3.8	0.58
Western metabasalt	RR-F6-007	22.2	45.8	6.05	24.2	5.8	2.01	6.86	1.09	6.9	1.39	4.13	0.59	3.9	0.6
Western metabasalt	RR-F6-008	23.9	48	6.04	24.8	6	1.93	6.65	1.05	6.62	1.32	3.99	0.6	3.8	0.58
Western metabasalt	RR-F6-009	21.3	44.8	5.84	23.9	5.9	1.82	6.59	1.02	6.79	1.36	4.15	0.57	3.8	0.57
Western metabasalt	RR-F6-010	23	44.3	5.79	23.6	5.4	1.56	6.8	1.04	6.61	1.36	4	0.66	3.8	0.61
Western metabasalt	RR-F6-016	10.9	19.2	2.35	9.5	2	0.53	2.59	0.43	3.01	0.72	2.09	0.33	2.2	0.34
Western metabasalt	RR-F6-018	16.2	31.8	3.92	15.7	3.4	0.98	3.88	0.61	3.66	0.77	2.34	0.34	2.1	0.35
Western basaltic metandesite	RR-F16-027	24.1	30.9	3.65	14.2	3.1	0.83	3.61	0.56	3.64	0.75	2.17	0.35	2.1	0.33
Metadacite	FD-052	16.3	29.8	2.97	12.4	2.8	0.69	2.62	0.43	2.81	0.52	1.54	0.18	1.3	0.16
Metarhyolite	RR-FST-002	35.5	64.4	6.27	23.9	4.4	0.94	4.09	0.6	3.66	0.73	2.25	0.27	2.2	0.26
Paleoproterozoic granites															
Jequitibá metagranite	RR-017	61	131.7	14.83	53.2	9.6	0.73	5.14	0.55	2.06	0.29	0.68	0.08	0.4	0.05
Areia Branca granite-gneiss	RR-015	34.4	62.1	6.38	20.6	3.5	0.34	2.91	0.39	1.75	0.26	0.64	0.08	0.4	0.06
Cachoeira Grande granite	RR-026	22.5	42.9	4.55	15.5	3.5	0.45	3.15	0.5	2.8	0.49	1.36	0.19	1.2	0.17

Note: Error interval for each element considering all samples analyzed and represented in terms of standard deviation (1σ) (Thompson, 1988): La (0.23 - 3.31), Ce (0.09 - 4.47), Pr (0.08 - 0.69), Nd (0.21 - 2.51), Sm (0.10 - 0.56), Eu (0.05 - 0.11), Gd (0.06 - 0.48), Tb (0.04 - 0.11), Dy (0.06 - 0.52), Ho (0.04 - 0.14), Er (0.05 - 0.34), Tm (0.04 - 0.08), Yb (0.09 - 0.37), and Lu (0.04 - 0.08).

Table 10. Whole-rock trace and minor element geochemical data (ppm)

Unit and classification	Sample ID	Cs	Ba	Th	U	Ta	Nb	Zr	Hf	Ti	Y	Sr	Rb	Ni	V
Gavião Block															
Fazenda Coqueiro metagranite	RR-008	0.28	442	15.3	3.47	1.83	27.96	280	9.3	540	63.39	22	73.6	2.5	2.5
Miguel Calmon metagranite	RR-025	0.39	598	6	1.14	0.27	4.28	122	3.32	840	3.58	333	74.2	6	2.5
Metarhyolite/metadacite	RR-007	0.53	609	9.7	2.17	0.95	16.45	326	8.47	840	60.45	54	38	2.5	2.5
Metarhyolite/metadacite	RR-009	18.79	625	9.9	2.47	0.73	17.05	327	8.55	780	62.44	58	73.5	2.5	2.5
Metarhyolite/metadacite	RR-374	1.49	196	31.7	4.85	1.35	45.02	613	16.5	1500	35.25	60	93.1	32	104
Metarhyolite/metadacite	RR-595	0.78	631	10.6	1.7	1.19	18.86	417	10.57	3720	43.76	133	35.5	6	37
Metarhyolite/metadacite	RR-598	8.65	651	10.1	2.14	1.04	15.43	389	9.59	2580	30.78	123	87.2	8	73
Metarhyolite/metadacite	RR-783B	3.35	531	13.9	4.5	1.6	19.02	379	9.7	2340	61.91	75	79.5	30	145
Metarhyolite/metadacite	RR-786	1	579	11.8	3.58	2.24	20.71	436	11.85	1020	55.79	78	59.3	30	170
Metarhyolite/metadacite	RR-896	21.29	939	15	3.22	0.82	20.15	404	11.77	1380	79.99	73	112.1	6	2.5
Metarhyolite/metadacite	RR-F16-001	2.98	663	11.7	2.89	1.21	16.21	413	10.34	1080	69.77	45	39.9	16	69
Metarhyolite/metadacite	RR-F16-004	1.72	753	11.2	2.9	1.27	16.03	433	10.53	1080	65.51	42	42.8	16	121
Metarhyolite/metadacite	RR-F16-005	1.25	853	11	3.35	1.23	15.32	381	9.58	1020	60.09	36	36.3	6	27
Metarhyolite/metadacite	RR-F16-007	0.72	596	10.9	3.15	1.25	16.17	391	9.39	1080	64.62	67	22.8	23	91
Metarhyolite/metadacite	RR-F16-008	0.4	673	11.3	2.64	1.19	15.72	371	9.56	1020	62.32	33	37.8	15	69
Metarhyolite/metadacite	RR-F16-009	0.28	693	11.3	2.72	1.14	15.53	348	9.23	900	62.6	36	31.8	23	79
Mundo Novo greenstone belt															
Metakomatiite	RR-011B	0.37	5	1.2	0.35	0.025	2.45	13	0.53	1500	4.47	12	1.2	945	2.5
Metakomatiite	FD-37-017	0.51	176	2.8	1.38	0.3	1.69	43	1.31	1380	8.83	49	10.3	644	42
Metakomatiite	FD-058A	0.06	42	2.6	0.72	0.36	1.27	20	0.63	420	10.47	5	1.6	587	2.5
Metakomatiite	FD-070	0.11	50	0.8	0.39	0.025	0.58	15	0.2	420	12.02	5	1	493	2.5
Eastern metabasalt	RR-006	0.76	104	0.5	0.16	0.025	3.3	40	1.27	4980	18.07	90	8.1	115	207
Eastern metabasalt	RR-011C	1.52	134	2.3	0.66	0.17	7.32	93	2.48	7140	21.67	100	8.1	110	232
Eastern metabasalt	RR-014B	0.13	122	0.8	0.13	0.025	2.66	69	1.96	6000	28.43	108	6.1	112	283
Eastern metabasalt	RR-018A	0.3	110	1.8	0.31	0.025	5.3	77	2.15	6240	26.24	109	4	112	295
Eastern metabasalt	RR-018B	0.21	80	1	0.27	0.025	3.59	67	1.87	6420	24.46	120	5.8	110	306
Eastern metabasalt	RR-018C	0.17	132	1.8	0.42	0.025	9.69	75	1.99	6600	27.2	128	2.1	112	306
Eastern metabasalt	RR-018D	0.16	119	2.7	0.42	0.34	7.56	72	2.07	6360	25.88	162	1.8	109	292
Eastern metabasalt	RR-071	0.77	73	2.3	0.31	0.025	5.52	84	2.52	8760	22.27	66	5.2	92	306
Eastern metabasalt	RR-072	0.36	30	1.1	0.29	0.025	4.77	88	2.71	9120	22.77	185	4	97	315
Eastern metabasalt	RR-078	0.25	242	0.8	0.29	0.025	3.08	69	2.23	6900	28.29	94	7.6	125	315
Eastern metabasalt	RR-080	0.27	102	0.9	0.39	0.025	2.91	83	2	5820	24.88	133	11.7	124	386
Eastern metabasalt	FD-37-001	0.2	108	0.4	0.35	0.025	2.26	78	1.97	5820	22.32	109	2.6	90	366
Eastern metabasalt	FD-37-002	0.17	46	0.1	0.22	0.025	1.93	69	1.99	5880	22.86	110	2.8	108	371
Eastern metabasalt	FD-37-004	0.09	40	0.4	0.23	0.025	2.46	85	2.28	6660	27.81	107	2.3	72	423
Eastern metabasalt	FD-37-005	0.07	34	0.4	0.26	0.025	2.75	91	2.36	7260	29.87	127	1.6	62	425
Eastern metabasalt	FD-37-006	0.41	53	0.05	0.18	0.025	1	48	1.37	4260	16.4	107	4.9	152	298
Eastern metabasalt	FD-37-007	0.42	232	0.3	0.24	0.025	1.99	79	1.91	5940	23.31	122	6.6	142	362
Eastern metabasalt	FD-37-009	0.24	185	0.2	0.24	0.025	1.84	73	1.87	5580	22.88	117	3.3	164	374
Eastern metabasalt	FD-37-011	0.29	127	0.5	0.27	0.025	4.03	56	1.69	6120	22.3	111	4.7	148	299
Eastern metabasalt	FD-37-012	0.12	40	0.4	0.27	0.025	3.5	96	2.41	7380	28.27	109	2	49	490
Eastern metabasalt	FD-37-013	0.41	54	0.05	0.21	0.025	2.23	73	1.93	5940	22.35	113	4.6	106	379
Eastern metabasalt	FD-37-015	0.51	116	0.2	0.27	0.025	2.62	87	2.15	6720	26.05	120	5.5	116	415
Eastern metabasalt	FD-37-016	1.29	768	5	0.47	1.61	4.5	96	3.96	7680	28.83	107	32.9	110	451
Eastern metabasalt	FD-37-019	0.09	35	0.7	0.27	0.025	2.52	77	2.16	5940	23.28	112	1.5	77	409
Eastern metabasalt	FD-016	0.32	161	1.5	0.36	0.14	2.64	78	2.09	6120	24.9	111	8.2	104	323
Eastern metabasalt	FD-028	0.92	56	0.7	0.21	0.17	2.92	75	1.91	7620	25.05	132	8.9	111	322
Western metabasalt	RR-022	0.31	78	1.9	0.46	0.32	5.25	87	2.36	5700	28.44	574	13.7	83	192
Western basaltic metandesite	RR-F1-001	1.2	141	4.2	0.95	0.025	6.22	138	3.44	5940	25.4	127	16.3	148	257
Western metabasalt	RR-F4-006	0.12	72	3.4	1.06	0.15	7.06	169	4.5	7560	32.18	187	4.5	88	331
Western metabasalt	RR-F4-007	0.63	480	3.3	1.08	0.08	7.8	171	4.31	8100	35.3	180	46.2	89	338
Western basaltic metandesite	RR-F6-001	1.6	216	4.4	1.39	0.26	9.05	177	4.94	8040	32.77	131	43.7	106	358
Western metabasalt	RR-F6-002	1.9	188	4.3	1.3	0.24	8.7	192	5.27	9360	40.14	108	29.5	91	312
Western metabasalt	RR-F6-003	1.11	244	3.6	1.16	0.025	8.05	183	4.73	8700	36.53	127	19.8	97	366
Western metabasalt	RR-F6-004	1.31	184	3.3	1.09	0.025	7.05	161	4.52	7800	33.53	80	20.9	93	310
Western metabasalt	RR-F6-005	2.57	278	3.3	1.09	0.025	7.1	171	4.45	7680	34.07	205	19.2	92	316
Western metabasalt	RR-F6-006	0.46	228	3.3	1.11	0.025	7.49	167	4.41	8040	36.03	214	16.5	91	322

Western metabasalt	RR-F6-007	0.12	98	3.4	1.11	0.025	7.34	172	4.32	8400	35.58	148	2.7	86	322
Western metabasalt	RR-F6-008	1.01	157	3.2	1.01	0.025	6.82	163	4.46	7740	34.29	152	16.5	88	326
Western metabasalt	RR-F6-009	0.19	55	3.2	1.03	0.025	7.48	162	4.4	7980	37.08	204	3.3	93	319
Western metabasalt	RR-F6-010	0.55	184	3.1	1.08	0.025	7.51	170	4.36	8400	34.44	171	12.2	89	328
Western metabasalt	RR-F6-016	2	130	2.8	0.96	0.025	4.54	130	3.07	4260	17.1	54	27.2	51	241
Western metabasalt	RR-F6-018	0.33	59	2.7	0.93	0.025	4.04	118	2.86	3780	20.71	220	4.3	82	221
Western basaltic metandesite	RR-F16-027	0.55	136	3.1	1.08	0.31	2.85	121	2.82	4380	20.78	112	21.5	80	313
Metadacite	FD-052	3.29	553	7	5.24	1.01	9.57	83	2.72	2040	14.94	109	92.3	99	76
Metarhyolite	RR-FST-002	5.83	631	17.1	5.37	0.26	8.37	152	4.88	2460	19.91	144	95.3	49	67
Paleoproterozoic granites															
Jequitibá metagranite	RR-017	3.55	395	58.3	10.98	0.2	12.16	172	5.11	1920	9.35	59	312.2	12	2.5
Areia Branca granite-gneiss	RR-015	0.51	872	22.8	4.55	0.1	6.27	173	2.49	1140	13.71	43	118.6	2.5	2.5
Cachoeira Grande granite	RR-026	3.62	347	17.6	6.74	1.48	17.81	55	2.08	660	14.25	71	233.9	6	2.5

Note: Error interval for each element considering all samples analyzed and represented in terms of standard deviation (1σ) (Thompson, 1988): Cs (0.04 - 0.75), Ba (8.5 - 39.63), Th (0.08 - 2.02), U (0.04 - 0.40), Ta (0.04 - 0.11), Nb (0.06 - 1.54), Zr (8.77 - 28.77), Hf (0.05 - 0.59), Ti (see TiO_2 error in the Note of the Table 8), Y (0.16 - 2.71), Sr (8.50 - 27.46), Rb (0,2 - 10,57), Ni (4.25 - 35.67), and V (0.50 - 16.75).

8.1. Gavião Block

The granitic composition of the studied rocks of the Gavião Block was confirmed in the lithological classification diagram (Fig. 8A-B), and the data points slightly overlap the peraluminous field in the granite discrimination diagram based on the primary mineralogy (Maniar and Piccoli, 1989) (Fig. 8C). The chondrite-normalized REE patterns (Boynton, 1984) for the Miguel Calmon and Fazenda Coqueiro granitic bodies are distinct. The REE pattern of the Miguel Calmon metagranite is more fractionated than that of the Fazenda Coqueiro metagranite (Fig. 8D-E). The Miguel Calmon metagranite yields a Eu/Eu* ratio of 1.07, indicating a positive Eu anomaly (Eu/Eu* > 1: from Rollinson, 1993), unlike the Fazenda Coqueiro metagranite, which yields a Eu/Eu* value of 0.26 indicative of a negative Eu anomaly (Eu/Eu* < 1: from Rollinson, 1993) (Fig. 8D-E). This difference may be because of significant quantities of feldspar in the source of the latter unit or different temperature and oxidation conditions during magmatic crystallization of the two granitic bodies.

The felsic metavolcanic rocks of the Gavião Block were classified as metarhyolites and metadacites (Fig. 8A-B) and are slightly metaluminous to strongly peraluminous, probably because of the formation of muscovite and biotite during metamorphic and hydrothermal processes (Fig. 8C). However, the high SiO_2 contents in some of the metarhyolite and metadacite samples, some of which are approximately 80 wt.% (Table 8), suggest extraction from a protolith with a residual melt that was highly silicic.

The chondrite-normalized REE pattern of the felsic metavolcanic rocks (Boynton, 1984) (Fig. 8E) shows a flat pattern from Lu to Gd, with normalized values between 10 and 100, indicating that hornblende was not present in the liquid, and light REE fractionation from Sm to La, with La normalized values of approximately 200, which may mean that some crustal contamination occurred during magma ascent or during metamorphic processes. The average Eu/Eu* ratio of 0.51 is evidence of a negative Eu anomaly resulting from the retention of feldspar in the source during partial melting or early feldspar crystallization from the melt by fractional crystallization. Furthermore, the changing oxidation conditions during differentiation could also explain the negative Eu anomalies in the metarhyolites and metadacites.

Gavião Block

Classification diagrams:
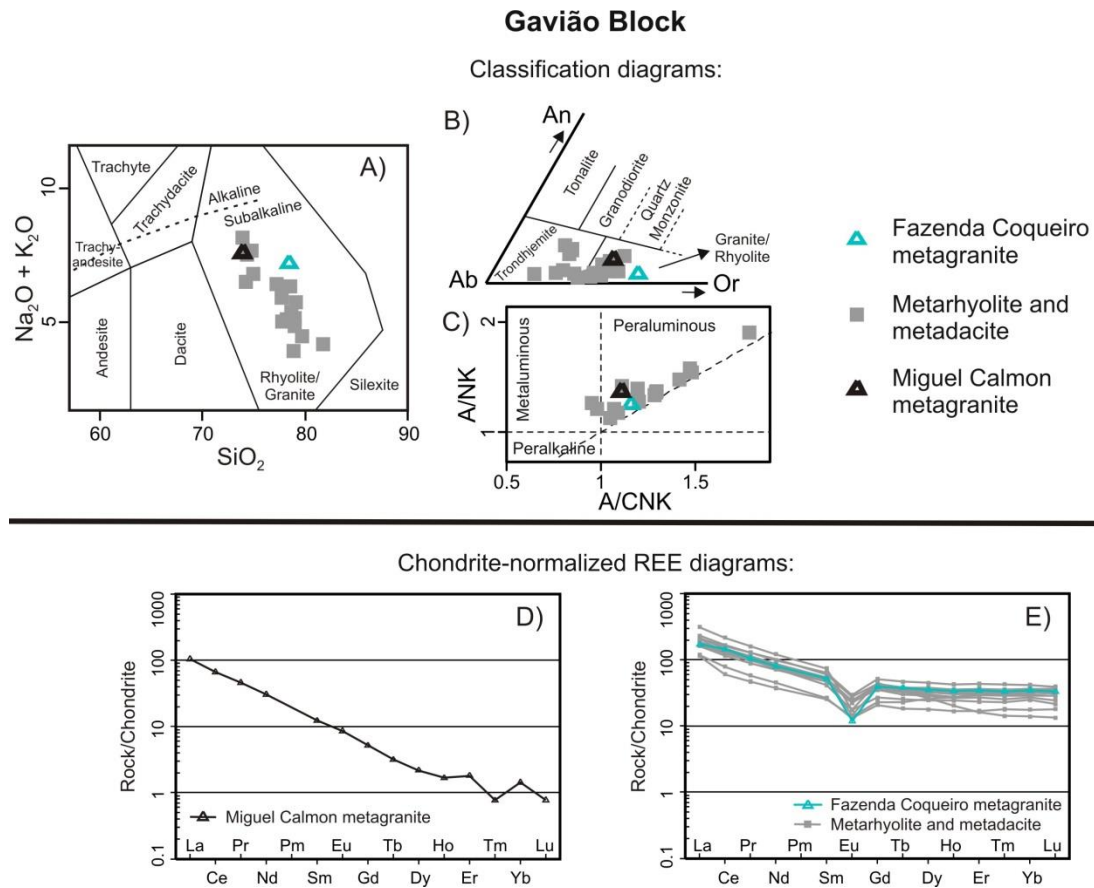
Fig. 8. Lithogeochemical diagrams for Gavião Block rocks. A) SiO_2 vs. $Na_2O + K_2O$ classification diagram (Middlemost, 1994). B) Ternary diagram of feldspar: Ab: albite, An: anorthite, Or: orthoclase (O'Connor, 1965). C) Molar concentration [Al_2O_3 / (CaO + Na_2O + K_2O)] vs. Molar concentration [Al_2O_3 / (Na_2O + K_2O)] diagram (Maniar and Piccoli, 1989). D-E) Chondrite-normalized REE diagram (Boynton, 1984).

8.2. Mundo Novo greenstone belt

The bivariate diagrams of TiO_2 and Al_2O_3 (the least mobile major elements), FeO_t and MgO (mobile major elements), Ni (conservative trace element), Y (immobile trace element), and La and Ce (light REE) versus Zr have been drawn for the metakomatiites from the lower sequence and the eastern and western metabasalts and metadacites from the middle sequence of the MNGB, as shown in Fig. 9, and show important correlations. Zr was used as a crystal fractionation index because of its immobility during alteration and metamorphism and its large range of concentration in igneous suites resulting from varying degrees of partial melting and fractional crystallization (Furnes et al., 2013). The Zr concentrations are 13-43 ppm in the metakomatiites, 40-192 ppm in the eastern and western metabasalts and 83–152 ppm in the metadacites.

TiO_2 defines a positive pattern versus Zr, and the eastern and western metabasalts form separate groups with the same slope. The Al_2O_3 diagram features a positive asymptotic pattern, in which the metakomatiite samples plot near the origin, the metabasalt samples form a trend where the western metabasalts exhibit relatively high values of Al_2O_3, and the metadacites are approximately aligned with this trend. Four distinct and dispersed groups are present in the FeO_t plot, possibly because of the mobility of Fe during alteration. The negative asymptotic patterns in the MgO and Ni diagrams form well-defined trends that can be explained by the fractional crystallization of olivine and pyroxene in the metakomatiites and metabasalts. Y, La and Ce, which are considered immobile elements, show well-defined positive correlations versus Zr. Therefore, they were used to demonstrate that the

metakomatiites, eastern and western metabasalts and metadacites from the MNGB could be related by fractional crystallization.

Mundo Novo greenstone belt
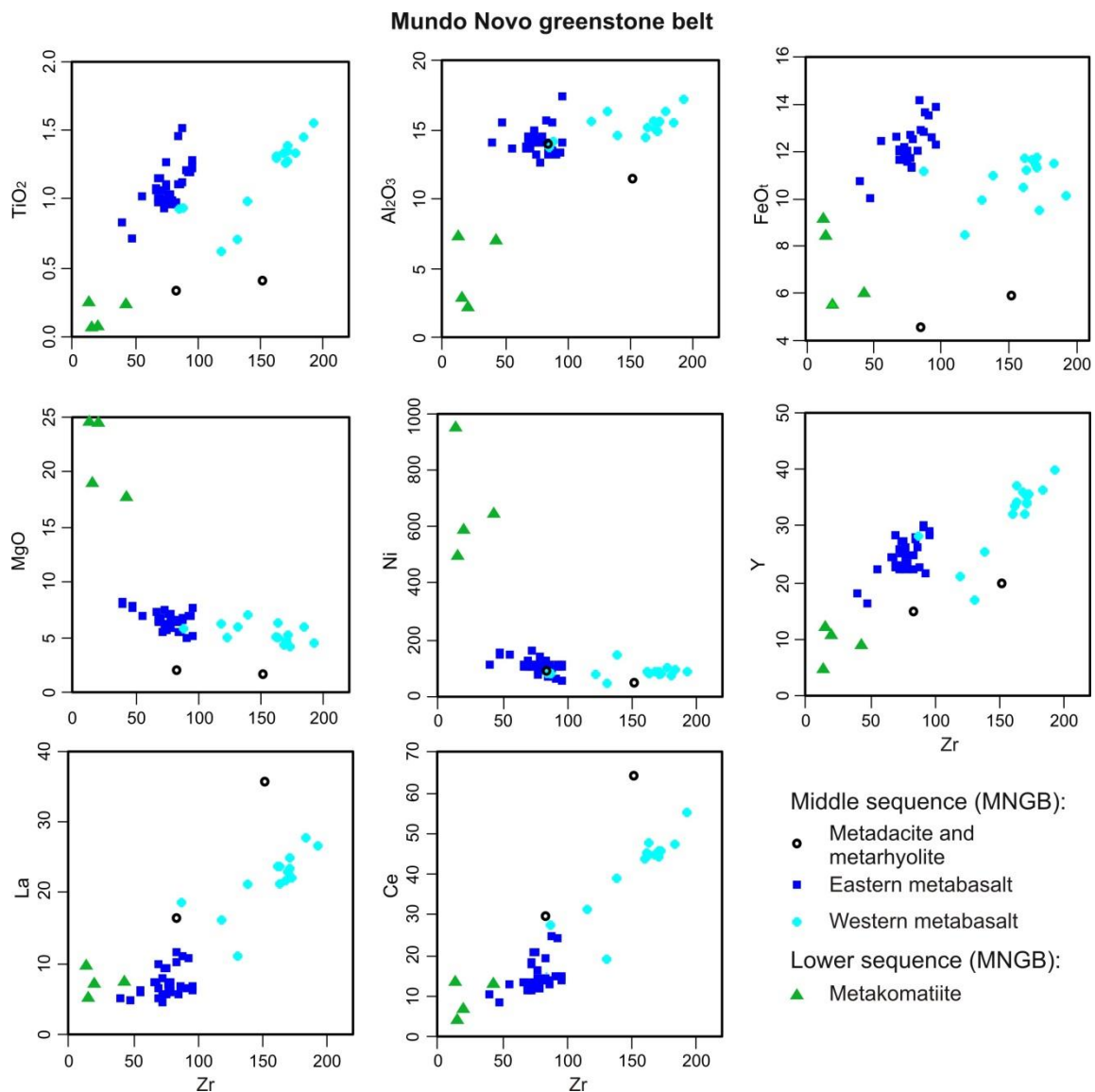
Fig. 9. Binary plots using Zr as a differentiation index for the metavolcanic rocks of the MNGB.

Lower Sequence

The metakomatiites of the MNGB are peridotitic, with MgO concentrations of 17-25 wt.% (Fig. 10A), and plot near the MgO vertex in the AFM diagram (Irvine and Baragar, 1971) (Fig. 10B). The high silica contents (greater than 50 wt.%) (Table 8) suggest the introduction of silica by ocean-floor hydrothermal activity. The chondrite-normalized REE geochemical pattern (Boynton, 1984) indicates enrichment in light REE in at least two samples of the metakomatiites in the MNGB, similar to the komatiite pattern from the Onverwacht Suite of the Barberton greenstone belt, South Africa (Jahn et al., 1982) (Fig. 10D). The other two samples did not show a representative pattern in the chondrite-normalized REE diagram. The $(La/Yb)_N$ ratios in the metakomatiites in the MNGB are low, with an average of approximately 5 and a minimum of 2.69. However, the low values of Nb (≤ 2.45 ppm) and Ti (≤ 0.150 ppm) and the Ti/Zr ratio (≤ 0.012), in addition to the enrichment in U and Th, may indicate possible crustal enrichment in the MNGB metakomatiites.

Middle Sequence

8.2.1. Eastern and western metabasalts

The division of MNGB metabasalts into the two eastern and western groups, as previously discussed based on petrography, was further confirmed by the REE patterns. The two groups have subtle geochemical differences. The eastern metabasalts have higher percentages of Fe and Ti than do the western metabasalts (Fig. 10A), with some western metabasalt samples showing a small andesitic trend. In the AFM diagram, it is also possible to see two distinct groups of samples, both in the tholeiitic series field, with just three samples of western metabasalts plotting in the calc-alkalic series field (Fig. 10B). These differences between the metabasalts may indicate different levels of crustal assimilation during the ascension of the magma or during metamorphic processes. The samples in the calc-alkalic series field correspond to basaltic metandesites related to the western metabasalts unit.

In the chondrite-normalized REE diagram (Boynton, 1984), the western metabasalts are more fractionated and enriched in light REE, with La normalized values near 100, than the eastern metabasalts, which show a flat REE pattern (Fig. 10E-F). The fractionation difference is also observed in the average $(La/Yb)_N$ ratio, in which the western metabasalts have a value of 5.11, and the eastern metabasalts have a value of 1.91. Moreover, the negative Ti anomaly is more accentuated in the western metabasalts than in the eastern metabasalts, and the western metabasalts are more enriched in Th, Cs, La, Ce and Nd than are the eastern metabasalt rocks.

However, both eastern and western metabasalts seem to be cogenetic and consistent with the nearby settings in the MNGB, but they experienced different levels of crustal assimilation during magma ascent, during volcanic processes in the ocean floor or through posterior tectonic processes.

8.2.2 Metadacites and metarhyolites

The felsic metavolcanic rocks of the middle sequence of the MNGB are classified as metadacites and metarhyolites (Fig. 10C). The chondrite-normalized REE diagram (Boynton, 1984) for these rocks subtly slopes from Lu to Gd, with a negative Eu anomaly (Fig. 10G), as indicated by the average Eu/Eu* ratio of 0.64. The Eu anomaly is likely due to the retention of feldspar in the source during partial melting or the removal of feldspar from the melt via crystal fractionation. Enrichment in light REE with strong fractionation from Sm through La is also observed.

The metadacites and metarhyolites in the MNGB have peculiar lithogeochemical characteristics that differ from those of the felsic metavolcanic rocks of the Gavião Block (metarhyolites and metadacites). The REE values of the MNGB rocks are lower, and the pattern implies slightly more fractionation than in the Gavião Block rock pattern. In addition, the values of Hf and Zr are lower and the depletion in Ti is more discrete in the MNGB metadacites than in the metarhyolites in the Gavião Block on the N-MORB-normalized multielement diagram of the trace elements, showing more crustal influence in the metarhyolites in the Gavião Block.

Mundo Novo greenstone belt

Classification diagrams:
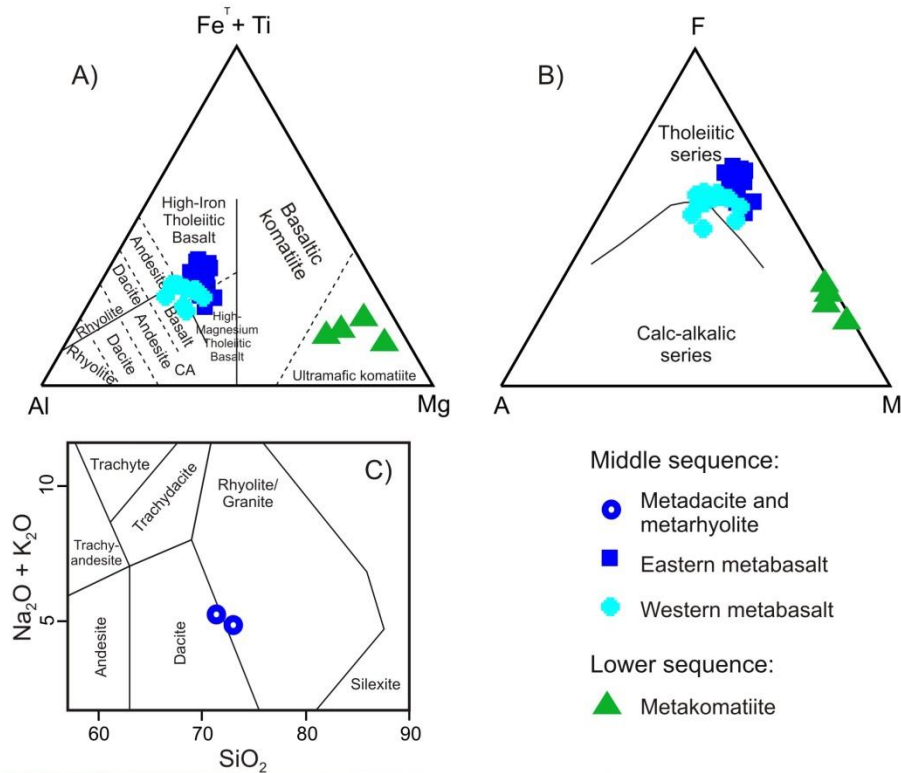
Chondrite-normalized REE diagrams:

Fig. 10. Lithogeochemical diagrams for MNGB rocks. A) Classification diagram of Jensen (1976): $Fe^T + Ti =$ $FeO + Fe_2O_3 + TiO_2$; $Al = Al_2O_3$; $Mg = MgO$. B) AFM diagram, tholeiitic and calc-alkalic series (Irvine and Baragar, 1971), $A = Na_2O + K_2O$; $F = 0.8998Fe_2O_3$; $M = MgO$. C) SiO_2 vs. $Na_2O + K_2O$ classification diagram (Middlemost, 1994). Chondrite-normalized REE diagram (Boynton, 1984): D) Metakomatiites in the MNGB lower sequence; E) Eastern metabasalts in the MNGB middle sequence; F) Western metabasalts in the MNGB middle sequence; G) Metadacite and metarhyolite in the MNGB middle sequence.

8.3. Paleoproterozoic metagranites

The Areia Branca, Cachoeira Grande and Jequitibá metagranites in the MNGB region were confirmed to be granitic in composition, as evidenced by the lithological classification diagram (Fig. 11A-B), and slightly peraluminous, as evidenced by the granite discrimination diagram based on the primary mineralogy (Maniar and Piccoli, 1989) (Fig. 11C).

The chondrite-normalized REE patterns (Boynton, 1984) for the three granites vary (Fig. 11D); however, all three generally have a high proportion of light REE relative to heavy REE, likely because of the crustal assimilation of felsic melt. The negative Eu anomalies (Fig. 11D) evidenced by the Eu/Eu* ratios of 0.32 (Areia Branca granite-gneiss), 0.40 (Cachoeira Grande granite) and 0.31 (Jequitibá metagranite) may imply significant quantities of feldspar in the source of the felsic melt.
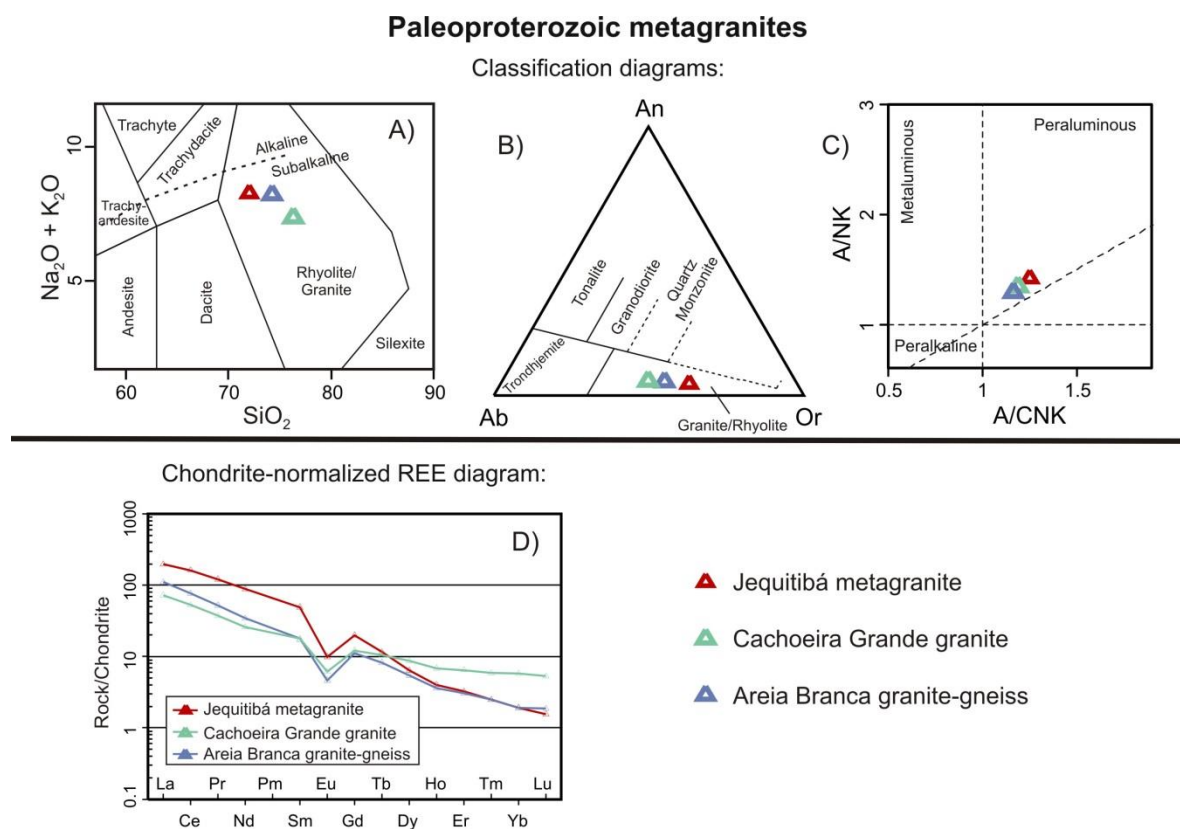
Fig. 11. Lithogeochemical diagrams for the Paleoproterozoic metagranites. A) SiO_2 vs. $Na_2O + K_2O$ diagram (Middlemost, 1994). B) Ternary diagram of feldspar: Ab: albite, An: anorthite, Or: orthoclase (O'Connor, 1965). C) Molar concentration [Al_2O_3 / ($CaO + Na_2O + K_2O$)] vs. Molar concentration [Al_2O_3 / ($Na_2O + K_2O$)] diagram (Maniar and Piccoli, 1989). D) Chondrite-normalized REE diagram (Boynton, 1984).

9. Discussion

9.1. Tectonic setting

Gavião Block

The multielement diagram normalized to N-MORB (Hofmann, 1988) indicates negative Ta and Nb anomalies in the Miguel Calmon metagranite, which may indicate association with a syn-collisional and subduction setting (Fig. 12A). These characteristics differ from those of the Fazenda Coqueiro metagranite, which showed higher values for these elements, suggesting a within-plate setting (Fig. 12B). Both granites probably experienced crustal contamination, given the high values of Cs, Ba, Th and U and the negative Ti anomaly.

In the tectonic discrimination diagram (Pearce et al., 1984), the Fazenda Coqueiro metagranite plots in the within-plate granite field, and the Miguel Calmon metagranite plots in the syn-collisional and volcanic arc granite fields (Fig. 12C-D), confirming the previous diagrams. The Miguel Calmon metagranite is characterized by a high $(La/Yb)_N$ ratio of 73.03, indicating intrusion in a continental setting (Condie and Kronër, 2013) and possibly the occurrence of hornblende in the felsic melt (Rollinson, 1993). The Fazenda Coqueiro metagranite exhibits a low $(La/Yb)_N$ ratio of 4.91, which is a transitional value for igneous rocks generated between continental and oceanic crust settings (Condie and Kronër, 2013). According to A (anorogenic)-type granitoid studies (Whalen et al., 1987), only the Fazenda Coqueiro metagranite overlaps the A-type granite field. Although these two granites feature distinct lithogeochemistry patterns and tectonic settings, the Miguel Calmon and Fazenda Coqueiro metagranites coexist in the same Paleoarchean basement related to the Gavião Block.

The multielement diagram normalized to N-MORB (Hofmann, 1988) (Fig. 12B) shows high Cs, Ba, Th and U values for metarhyolites and metadacites, indicating crustal contamination. The negative Ti anomaly could evidence fractionation of Ti-enriched phases, such as ilmenite and Ti-magnetite; however, the possibility of crustal contamination having contributed to these anomalies cannot be ruled out. The high normalized values for Ta and Nb, which are greater than 3 (Fig. 12B), may show that the felsic metavolcanic rocks are not related to a syn-collisional or subduction setting. The low average $(La/Yb)_N$ ratio of 6.67 may indicate felsic igneous components formed in the transitional setting between continental and oceanic crust (Condie and Kronër, 2013), possibly during a growth phase of oceanic crust related to a rifting process.

In general, the metarhyolites and metadacites should have originated in a within-plate tectonic setting (Fig. 12C-D) and may have contributed to the crustal contamination of the younger Fazenda Coqueiro metagranite, as indicated by the chemical similarities between them (Zincone et al., 2016; Spreafico et al., 2018). This relation would be possible through a plutonic-volcanic system that may have existed in the TTG basement of the Gavião Block (Zincone et al., 2016). It is important to emphasize that the metarhyolites and metadacites are part of the Paleoarchean basement of the MNGB sequence.

Gavião Block

Multielement diagrams:

Tectonic discrimination diagrams:
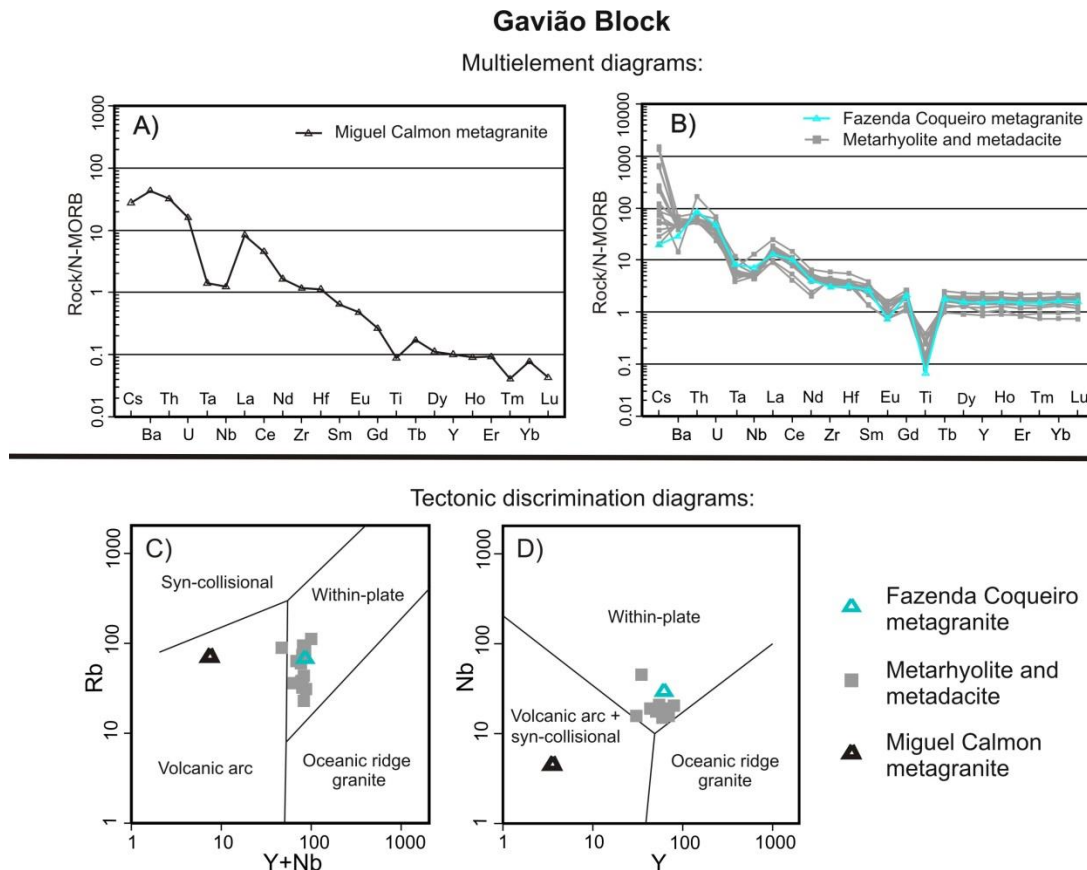
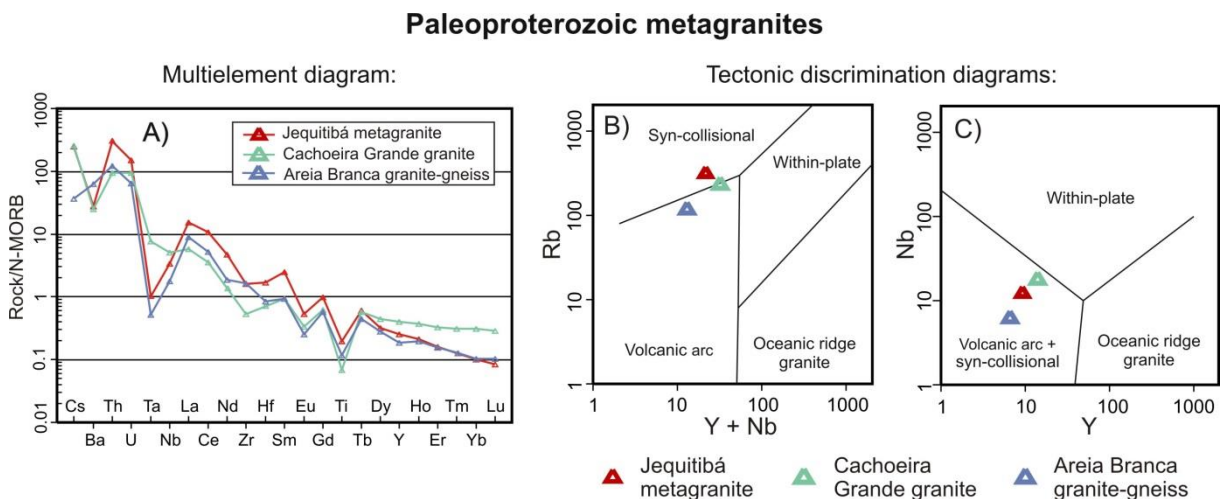**Fig. 12**. Lithogeochemical diagrams for Gavião Block rocks. A-B) Multielement diagram of trace elements normalized to N-MORB (Hofmann, 1988). C-D) Y + Nb vs. Rb and Y vs. Nb tectonic setting discrimination diagrams (Pearce et al., 1984).

Mundo Novo greenstone belt

The high CaO/Al_2O_3 ratios (Herzberg, 1995) in the metakomatiites in the MNGB, which are between 1.1 and 2.6, allow these rocks to be classified as Al-depleted. In addition, the high $(Gd/Yb)_N$ ratios (Herzberg, 1995), at between 1.09 and 1.60, indicate that the komatiitic magma was generated by partial melting at high pressures and that garnet remained in the residue during the melting process. Even so, the occurrence of garnet in the source implies the derivation of the komatiitic magma from deep levels corresponding to the upper mantle, possibly at an approximate depth of 350-400 km (Jayananda et al., 2008).

The high and anomalous concentrations of Cs, Ba, Th and U in the metakomatiites observed in the multielement diagram normalized to N-MORB (Hofmann, 1988) (Fig. 13A) may indicate that the komatiitic magma was related to a subduction zone (Furnes et al., 2013). The consistent enrichment of Cs, the flat pattern from Lu to Nd and the negative anomalies of Ta and Nb in the metakomatiites in the multielement diagram are equivalent to the geochemical pattern of lavas related to subduction in modern oceanic arcs (Furnes et al., 2013). Moreover, the tectonic setting discrimination diagram of immobile elements, Nb/Yb vs. Th/Yb (Pearce, 2008), indicates that the metakomatiites formed in a volcanic arc setting (Fig. 13E) that was active during the formation of the MNGB.

The geochemical patterns of the major and trace elements normalized to fertile mantle MORB (FMM) values as a tectonic setting marker (Pearce and Parkinson, 1993) are similar for both metabasalt types in the MNGB. The patterns in which normalized Nb (24.06) and Zr (11.48) > TiO_2 (6.47) and in which Y (6.98) and Yb (7.04) $\geq$ CaO (3.00), Al_2O_3 (3.91)

and V (4.20) in the metabasalts are similar to those in ocean floor basalts in a back-arc basin setting, as demonstrated in the Barberton greenstone belt (Furnes et al., 2013).

In the multielement diagram of trace elements normalized to N-MORB (Hofmann, 1988) (Fig. 13B-C), both metabasalt groups show a flat pattern from Lu to Zr and a negative Ta anomaly, indicating a relation to orogenic systems. Discrimination diagrams of immobile elements, Nb/Yb vs. Th/Yb (Pearce, 2008), in the eastern and western metabasalts of the MNGB indicate a volcanism process in an ocean floor setting, evidenced by the plots in the MORB-OIB array, such as a back-arc basin, with a subsequent Th enrichment produced by the subduction oceanic processes evidenced by the plots that tend toward a volcanic arc array (Fig. 13E). This plot distribution is similar to those of the South Abitibi (Xie and Kerrich, 1994) and Barberton (Chavagnac, 2004) Archean greenstone belts, which are interpreted as intraoceanic provenances, as discussed in Pearce (2008), and similar to the modern Mariana intraoceanic arc-basin system (Pearce et al., 2005).

The eastern metabasalts have an island arc tholeiitic (IAT)-type pattern, with some samples overlapping the MORB field, and the western metabasalts feature mainly a MORB pattern, with a few occurrences plotting in the within-plate basalts field (WPB) in the Zr vs. Zr/Y diagram. These patterns suggest proximity of the settings during volcanism, the transition from one setting to the other due subsequent tectonic event and crustal contamination, indicated mainly by the WPB pattern observed in some western metabasalt samples (Fig. 13F).

The fractionation of the light REE relative to the heavy REE in the metadacites of the MNGB suggests crustal contamination. The average $(La/Yb)_N$ ratio of 8.87 could be related to an oceanic crust setting (Condie and Kronër, 2013) with slight crustal assimilation of felsic magma. In the N-MORB-normalized multielement diagram (Hofmann, 1988) (Fig. 13D), the negative anomalies of Nb and Ta are potentially related to a syn-collisional or subduction setting. High Cs, Ba, Th and U values may indicate crustal contamination, similar to the negative Ti anomaly.

Therefore, the metadacites originated in a volcanic arc tectonic setting (Fig. 13G-H), interpreted as an island arc, similar to the setting suggested for the metakomatiites and metabasalts of the Neoarchean MNGB.

Mundo Novo greenstone belt
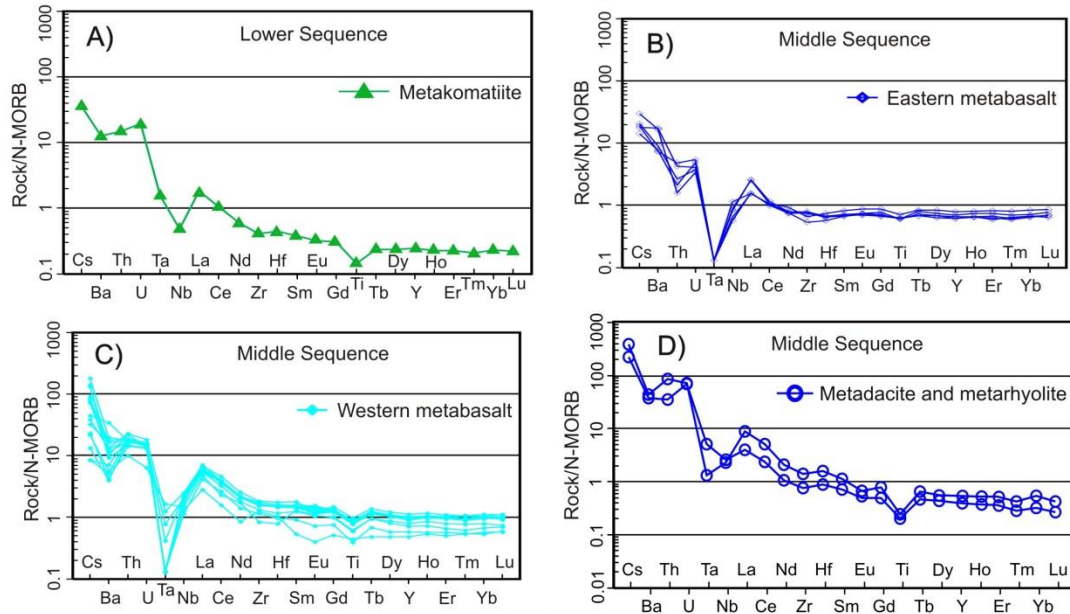
Multielement diagrams:
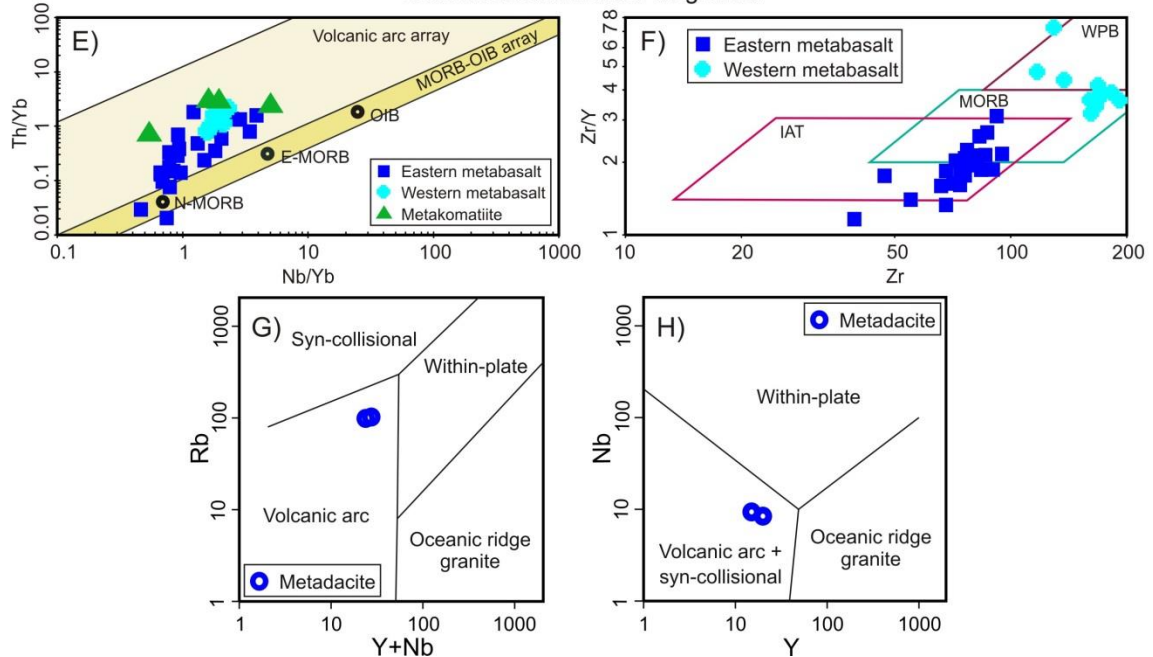
Fig. 13. Lithogeochemical diagrams for MNGB rocks. Multielement diagram of trace elements normalized to N-MORB (Hofmann, 1988): A) metakomatiites in the MNGB lower sequence; B) eastern metabasalts in the MNGB middle sequence; C) western metabasalts in the middle sequence and D) metadacite and metarhyolite in the MNGB middle sequence. Tectonic setting discrimination diagrams: E) metakomatiites and eastern and western metabasalts in the MNGB lower and middle sequence plotted in the Nb/Yb vs. Th/Yb diagram (N-MORB: normal mid-ocean ridge basalts, E-MORB: enriched mid-ocean ridge basalts, OIB: ocean island basalts) (Pearce, 2008); F) eastern and western metabasalts in the MNGB middle sequence plotted in the Zr vs. Zr/Y diagram (IAT: island arc tholeiitic, MORB: mid-ocean ridge basalts, WPB: within-plate basalts) and G-H) metadacites in the MNGB middle sequence plotted in the Y + Nb vs. Rb and Y vs. Nb diagrams (Pearce et al., 1984).

Paleoproterozoic metagranites

The three Paleoproterozoic granitic bodies in the MNGB, the Jequitibá, Areia Branca and Cachoeira Grande metagranites, show negative Ta anomalies in the multielement diagram normalized to N-MORB (Hofmann, 1988) (Fig. 14A), suggesting a subduction setting related to their origin. The high Th and U values may indicate crustal contamination, and the negative Ti anomaly demonstrates a crustal process related to the formation of these granites.

The Areia Branca, Cachoeira Grande and Jequitibá metagranites yield high $(La/Yb)_N$ ratios of 58.09, 12.64 and 102.81, respectively, which may indicate a continental collision setting (Condie and Kronër, 2013). In the discrimination tectonic diagrams (Pearce et al., 1984), the Jequitibá, Areia Branca and Cachoeira Grande metagranites overlap the syn-collisional and volcanic arc fields (Fig. 14B-C). As they are aligned along a north-south trend (Fig. 2) and possibly formed in a collisional tectonic setting, these three granitic bodies probably formed during the same tectonothermal Paleoproterozoic event.

Therefore, the Paleoproterozoic granites mark the last tectonic event registered in the MNGB, which was initially characterized by a continent-ocean compressional tectonic setting that gradationally changed to a west-vergent continent-continent collision. It is assumed that this collision amalgamated the MNGB along with the Gavião, Jequié and Serrinha blocks and generated the Itabuna-Salvador-Curaçá orogen (Barbosa et al., 2012a; Barbosa and Sabaté, 2002, 2003, 2004).

Paleoproterozoic metagranites

Fig. 14. Lithogeochemical diagrams for the Paleoproterozoic metagranites. A) Multielement diagram of trace elements normalized to N-MORB (Hofmann, 1988). B-C) Tectonic setting discrimination fields in the Y + Nb vs. Rb and Y vs. Nb diagrams (Pearce et al., 1984).

9.2. Tectonic evolution from the Paleoarchean to the Paleoproterozoic

The chronological history of the MNGB and adjoining rocks extends from the Paleoarchean, with the formation of the basement blocks, such as the Gavião Block, to subsequent tectonic events that led to the formation of rifts, the development of Neoarchean oceanic crust (in which the greenstone belt formed), and the final amalgamation of the cratonic blocks with the eastern part of the São Francisco Craton during the Orosirian period.

At least five stages can be identified in the tectonic evolution of the MNGB and surrounding region (Fig. 15):

1.   The first stage corresponds to the consolidation of the Gavião Block, culminating with the formation of the Miguel Calmon granite by 3355 ± 16 Ma. This stage also represents the rifting process that resulted in an extensional tectonic event at 3305 ± 9 Ma (Peucat et al.,

2002; Zincone et al., 2016), during which the rhyolites and dacites in the basement formed. Subsequently, the Fazenda Coqueiro granite formed in the lower continental crust at 3227 ± 23 Ma from TTG plutons and likely mafic or intermediate granulitic rocks, with contamination from the rhyolitic and dacitic rocks during its emplacement in the upper continental crust (Fig. 15A). These rocks provided detritus during the formation of the Jacobina Basin (Jacobina Group) at this stage.

2.   The second stage represents a tectonic inversion event during the Paleoarchean, resulting in an aborted rift and a collage of rhyolites and dacites inside the Gavião Block (Fig. 15B).

3.   The third stage represents the beginning of a complete orogenic cycle with the break-up of the eastern border of the Gavião Block and the separation of a fragment known as the Mairi Block. This event resulted in the formation of oceanic crust between the Gavião Block to the west and the Mairi Block to the east, and the volcanism of the MNGB occurred in back-arc and island arc settings at approximately 2595 ± 21 Ma (Fig. 15C).

4.   The fourth stage, which likely began at 2106 ± 71 Ma during the Rhyacian period, was characterized by the beginning of a collision of cratonic blocks, such as the Gavião Block, Mairi Block, Itabuna-Salvador-Curaçá Belt and Serrinha Block, and the consequent initiation of the amalgamation of the MNGB between the Gavião and Mairi blocks (Fig. 15D). This collisional tectonic process generated the first deformational phase (D_1) in the MNGB rocks, which is characterized by west-vergent recumbent folds with subhorizontal axial planes (S_1). During this stage, it is possible that the formation of Paleoproterozoic granitic bodies occurred, such as the syn-collisional Areia Branca granite, which was derived from crustal protoliths, including the TTG gneisses and other Archean rocks.

5.   The fifth and last stage represents the end of the orogenic cycle and likely extended to 1975 ± 36 Ma during the Orosirian period. This stage was characterized by the continuation of the amalgamation event, resulting in the progressive deformation that refolded the structures of the previous phase during a second deformational phase (D_2). This second deformation phase produced folds with subvertical axial planes (S_2) and west-vergent compressional to transpressional shear zones (Fig. 15E). During this stage, the last Paleoproterozoic granitic bodies likely formed, such as the syn-collisional Jequitibá granite, for example, which was derived from crustal protoliths, including the TTG gneisses and other Archean rocks, likely formed in a continent-continent collisional setting. By the end of the fifth stage, the current geologic configuration observed in the MNGB region had formed. However, a weak geologic event at approximately 600 Ma may have occurred, although there is no consistent evidence for any expressive geologic event in the study region in the eastern part of the São Francisco Craton at that time.

9.3 Late sedimentary events

The uplift generated during the Rhyacian-Orosirian convergent tectonic event could have exposed large portions of the MNGB and intrusive granites to erosion, and the resulting material may have been transported and deposited in nearby sedimentary basins (Fig. 15D). Such basins are represented by the siliciclastic rocks in the upper sequence of the MNGB, which lay discordantly on the metavolcanic rocks of the MNGB, and the Saúde Basin (Saúde Complex). The deposits in the Saúde Basin have experienced higher stress levels and higher metamorphic grades than have those in the MNGB. Later, the metasedimentary siliciclastic rocks in the upper sequence of the MNGB and the Saúde Complex were tectonically juxtaposed at the same crustal level, placing side-by-side metasedimentary rocks of different metamorphic grades separated by a tectonic contact (Fig. 15E).
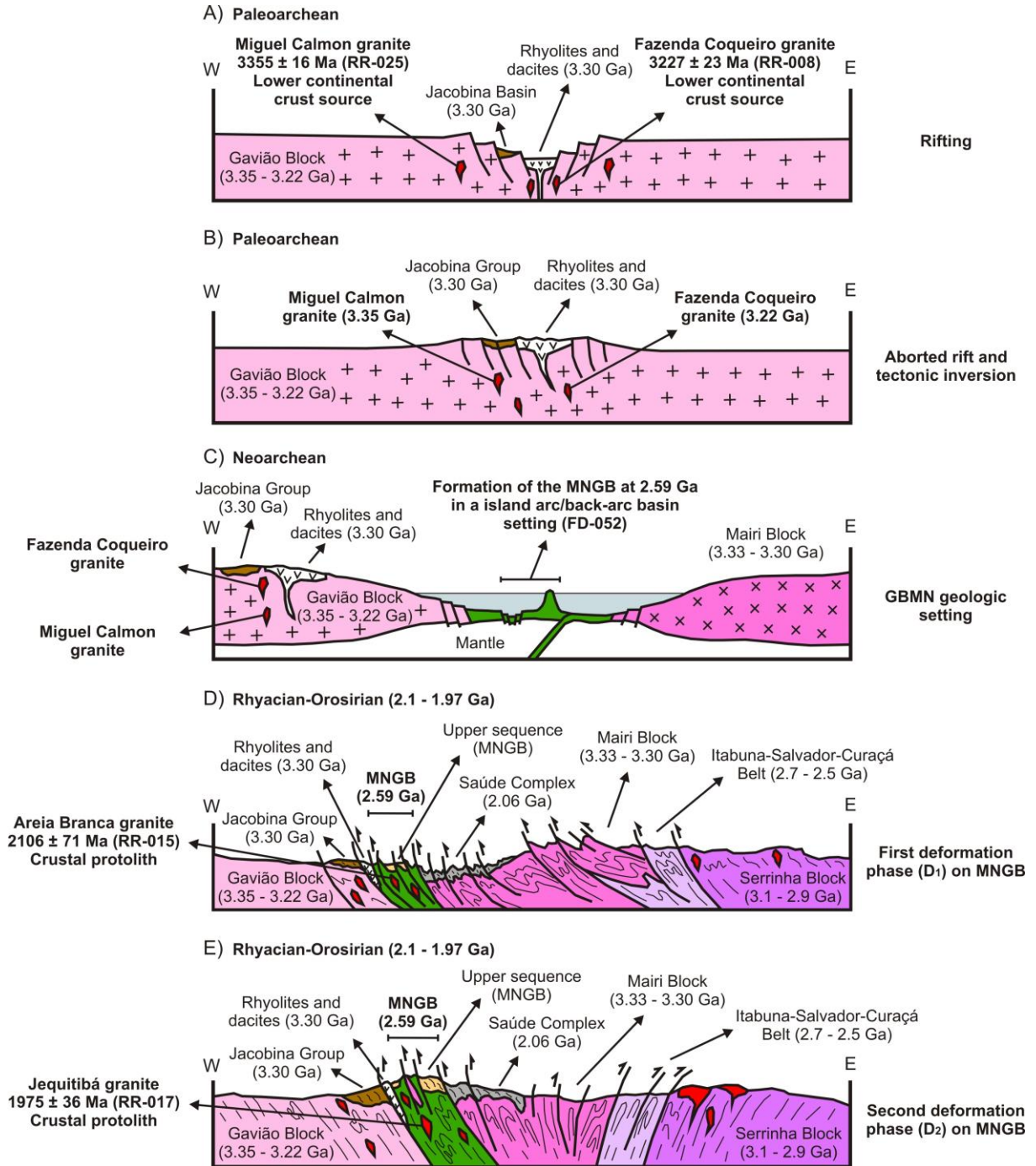
Fig. 15. Tectonic evolution proposed for the MNGB and adjoining units based on new ages presented in this study from samples RR-025 (Miguel Calmon metagranite), RR-008 (Fazenda Coqueiro metagranite), FD-052 (metadacite from MNGB), RR-015 (Areia Branca granite-gneiss) and RR-017 (Jequitibá metagranite) and compiled ages for rhyolites (Peucat et al., 2002; Zincone et al., 2016), the Mairi Block (Sousa et al., 2018), the Jacobina Group (Teles, 2013; Teles et al., 2015; Barbuena et al., 2016), Serrinha Block (Oliveira et al., 2002a; Oliveira et al., 2002b; Rios et al., 2009), Itabuna-Salvador-Curaçá Belt (Silva et al., 1997; Oliveira et al., 2010) and the Saúde Complex (Barbuena et al., 2016; Zincone et al., 2017). A) Rifting and the formation of the rhyolites and the Miguel Calmon and Fazenda Coqueiro granites in the Gavião Block. B) Aborted rifting and tectonic inversion of the Gavião Block. C) Formation of oceanic crust between the Gavião and Mairi blocks and formation of the MNGB at 2595 Ma. D-E) Rhyacian-Orosirian tectonic event that compressed the MNGB between the cratonic blocks.

The long gap of 455 Ma between the volcanism of the lower and middle sequences and the siliciclastic rocks of the upper sequence of the MNGB probably does not represent the time of existence of the oceanic crust. The siliciclastic rocks were likely deposited during the Rhyacian-Orosirian continent-continent collision, and they lay in the same site of the metavolcanic rocks in the MNGB. The basin would have also been filled by detrital grains from the MNGB, among other nearby sources. Therefore, despite being much younger, the siliciclastic rocks are interpreted as a stratigraphic sequence of the MNGB and are likely in geologic contact with the metavolcanic rocks by unconformity. A similar evolution was described for the Barberton greenstone belt by De Ronde and De Wit (1994), in which the rocks recorded a geological history of at least 490 Ma, beginning with mid-ocean ridge-like processes until sedimentary basin formation after amalgamation by accretion-like convergent processes.

10. Conclusions

Based on the new geological, petrographic, lithogeochemical, geochronological and isotopic data of the present study, combined with pre-existing regional data, we conclude the following:

- The Gavião Block, which had stabilized by 3.35 Ga (Miguel Calmon granite), was fractured by a rift process that generated rhyolites. Subsequently, granites such as the anorogenic Fazenda Coqueiro granite formed at 3.22 Ga and were derived from the lower continental crust from TTG plutons and mafic or intermediate granulitic rocks.
- The metakomatiites in the lower sequence and the eastern and western metabasalts and metadacites in the middle sequence of the MNGB seem to be related by fractional crystallization. Therefore, the 2.59 Ga metadacite, the metakomatiites and the metabasalts are evidence of Neoarchean island arc and back-arc volcanisms in the MNGB in an ocean floor setting.
- The Rhyacian-Orosirian closure of the oceanic crust was marked by granitogenesis that produced the slightly peraluminous Areia Branca and Jequitibá granites, which were derived from crustal protoliths, such as the TTG gneisses and other Archean rocks. This event was also marked by the formation of west-vergent thrusts and folds. During the closing process and resulting uplift, rocks in the MNGB and Rhyacian-Orosirian intrusive granites may have contributed material to the formation of sedimentary rocks in the upper sequence of the MNGB. Moreover, the Saúde Basin possibly formed at the same time as did the upper sequence; however, the former was subjected to a higher metamorphic grade. For a better understanding of the relationship between the rocks of the upper sequence and the Saúde Complex we consider that future contributions may bring new interpretations.
- We propose five stages in the tectonic evolution of the MNGB region: stages (i) and (ii) between 3.35 Ga and 3.22 Ga correspond to the rifting and closing tectonic processes in the Gavião Block; stage (iii) at 2.59 Ga corresponds to volcanism in the MNGB in the oceanic crust formed between the Gavião and Mairi blocks, and stages (iv) and (v) between 2.10 Ga and 1.97 Ga correspond to the two stages of progressive collision, in which the oceanic crust and the MNGB were compressed between cratonic blocks from the eastern part of the São Francisco Craton.

Acknowledgments

References

Alderton, D.H.M., Thirlwall M.F., Baker, J.A., 1998. Hydrothermal alteration associated with gold mineralization in the southern Apuseni Mountains, Romania: preliminary Sr isotopic data. Mineralium Deposita 33 (5), 520-523. https://doi.org/10.1007/s001260050167

Anhaeusser, C.R., 2014. Archaean greenstone belts and associated granitic rocks - A review. Journal of African Earth Sciences 100, 684-732. https://doi.org/10.1016/j.jafrearsci.2014.07.019

Arndt, N.T., 1994. Archean Komatiites. Developments in Pre Cambrian Geology 11, 11-44. https://doi.org/10.1016/S0166-2635(08)70219-6

Barbosa, J. S. F., 1997. Síntese do Conhecimento sobre a Evolução Geotectônica das Rochas Metamórficas Arqueanas e Paleoproterozóicas do Embasamento do Cráton do São Francisco na Bahia. Revista Brasileira de Geociências 27 (3), 241-256. DOI:10.25249/0375-7536.1997241256

Barbosa, J.S.F., Cruz, S.C.P., Souza, J.S., 2012a. Terrenos metamórficos do embasamento. In: Barbosa, J.S.F. (Ed.), Geologia da Bahia: Pesquisa e Atualização, CBPM, Salvador, p. 101-201. http://www.cbpm.ba.gov.br/modules/conteudo/conteudo.php?conteudo=24

Barbosa, J.S.F., Luciano, R.L., Moraes, A.M.V., Garrido, I.A.A., Menezes, R.C.L., Divino, J.S.A., Macedo, E.P., Sobrinho, V.R.S., 2018. Mapa Geotectônico-Geocronológico da Bahia. Implicações Metalogenéticas. In: 49° Congresso Brasileiro de Geologia. Rio de Janeiro, Anais, p. 1866. http://cbg2018anais.siteoficial.ws/resumos/7808.pdf

Barbosa, J.S.F., Martin, H., Peucat, J.J., 2004. Paleoproterozoic dome forming structures related to granulite facies metamorphism. Jequié Block, Bahia, Brazil: petrogenetic approaches. Precambrian Research 135 (1-2), 105-131. https://doi.org/10.1016/j.precamres.2004.08.002

Barbosa, J.S.F., Pinto, M.S., Cruz, S.C.P., Souza, J.S., 2012b. Granitoides. In: Barbosa, J.S.F. (Ed.), Geologia da Bahia: Pesquisa e Atualização, CBPM, Salvador, 327-396. http://www.cbpm.ba.gov.br/modules/conteudo/conteudo.php?conteudo=24

Barbosa, J.S.F., Sabaté, P., 2002. Geological features and the Paleoproterozoic collision of four Archean crustal segments of the São Francisco Craton, Bahia, Brazil. A synthesis. Anais da Academia Brasileira de Ciências, Rio de Janeiro 74 (2), 343-359. http://dx.doi.org/10.1590/S0001-37652002000200009

Barbosa, J.S.F., Sabaté, P., 2003. Colagem paleoproterozoica de placas arqueanas do Cráton do São Francisco na Bahia. Revista Brasileira de Geociências 33 (1-suplemento), 7-14. DOI: 10.25249/0375-7536.200333S10714

Barbosa, J.S.F., Sabaté, P., 2004. Archean and Paleoproterozoic crust of the São Francisco Craton, Bahia, Brazil: geodynamic features. Precambrian Research 133 (1-2), 1-27. https://doi.org/10.1016/j.precamres.2004.03.001

Barbuena, D., Oliveira, E.P., Zincone, S.A., 2016. Estudos de proveniência dos quartzitos do Greenstone Belt Mundo Novo (BA) e implicações tectono-estratigráficas. In: 48° Congresso Brasileiro de Geologia. Porto Alegre, Anais, p. 818. http://cbg2017anais.siteoficial.ws/anais48cbgcompleto.pdf

Boynton, W.V., 1984. Geochemistry of the rare earth elements: meteorite studies. In: Henderson, P. (Ed.), Rare Earth Element Geochemistry, Elsevier, 63-114. https://doi.org/10.1016/B978-0-444-42148-7.50008-3

Chavagnac, V., 2004. A geochemical and Nd isotopic study of Barberton komatiites (South Africa): implication for the Archean mantle. Lithos 75, 253-281. https://doi.org/10.1016/j.lithos.2004.03.001

Condie, K.C., Kronër, A., 2013. The building blocks of continental crust: Evidence for a major change in the tectonic setting of continental growth at the end of the Archean. Gondwana Research 23 (2), 394-402. https://doi.org/10.1016/j.gr.2011.09.011

Couto, P.A., Sampaio, A.R., Gil, C.A.A., Loureiro, H.C., Arcanjo, J.B., Fernandes Filho, J., Guimarães, J.T., Campelo, R., Mascarenhas, J.F., Bruni, D.C., Toledo, L.A.A., 1978. Projeto Serra de

Jacobina: Geologia e Prospecção Geoquímica. Convênio DNPM-CPRM, Relatório Final. Salvador, 1, 415 p. http://rigeo.cprm.gov.br/jspui/handle/doc/9602

De Paolo, D.J., 1981. A neodymium and strontium isotopic study of the Mesozoic calc-alkaline granitic batholiths of the Sierra Nevada and Peninsular Ranges, California. Journal of Geophysical Research, Solid Earth 86, 10470-10488. https://doi.org/10.1029/JB086iB11p10470

De Paolo, D.J., 1988. Neodymium Isotope Geochemistry - An Introduction, Springer-Verlag, 187 p. 10.1007/978-3-642-48916-7

De Ronde, C.E.J., De Wit, M., 1994. Tectonic history of the Barberton greenstone belt, South Africa: 490 million years of Archean crustal evolution. Tectonics 13 (4), 983-1005. https://doi.org/10.1029/94TC00353

De Wit, M.J., Hart, R.A., Hart, R.J., 1987. The Jamestown ophiolite complex, Barberton mountain belt: a section through 3.5 Ga oceanic crust. Journal of African Earth Sciences 5, 681-730. https://doi.org/10.1016/0899-5362(87)90007-8

Dickin, A.P., 2005. Radiogenic isotope geology. 2nd edition. Cambridge University, 492 p. https://doi.org/10.1017/CBO9781139165150

Dziggel, A., Stevens, G., Poujol, M., Anhaeusser, C.R., Armstrong, R.A., 2002. Metamorphism of the granite-greenstone terrane south of the Barberton greenstone belt, South Africa: an insight into the tectono-thermal evolution of the 'lower' portions of the Onverwacht Group. Precambrian Research 114, 221-247. https://doi.org/10.1016/S0301-9268(01)00225-X

Elhlou, S., Belousova, E., Griffin, W.L., Peasom, N.J., O'Reilly, S.Y., 2006. Trace element and isotopic composition of GJ red zircon standard by laser ablation. Geochimica et Cosmochimica Acta 70 (18), p. A158. https://doi.org/10.1016/j.gca.2006.06.1383

Furnes, H., de Wit, M., Robins, B., 2013. A review of new interpretations of the tectonostratigraphy, geochemistry and evolution of the Onverwacht Suite, Barberton Greenstone Belt, South Africa. Gondwana Research 23 (2), 403-428. https://doi.org/10.1016/j.gr.2012.05.007

Grachev, A.F., Pechersky, D.M., Tsel'movich, V.A. 2011. Titanomagnetites and ilmenites from the Early Cenozoic Basalts and Limburgites of the Northern Tien Shan. Physics of the Solid Earth 47 (6), 475-487. https://doi.org/10.1134/S106935131105003X

Hamilton, P.J., O'Nions, R.K., Bridgwater. D, Nutman, A. 1983. Sm-Nd studies of Archaean metasediments and metavolcanics from West Greenland and their implications for the Earth's early history. Earth and Planetary Science Letters 62, 263-272. https://doi.org/10.1016/0012-821X(83)90089-4

Herzberg, C., 1995. Generation of plume magmas through time: an experimental perspective. Chemical Geology 126 (1), 1-16. https://doi.org/10.1016/0009-2541(95)00099-4

Hofmann, A.W., 1988. Chemical differentiation of the Earth: the relationship between mantle, continental crust, and oceanic crust. Earth and Planetary Science Letters 90 (3), 297-314. https://doi.org/10.1016/0012-821X(88)90132-X

Irvine, T.N., Baragar, W.R.A., 1971. A guide to the Chemical Classification of the Common Volcanic Rocks. Canadian Journal of Earth Sciences 8, 523-548. https://doi.org/10.1139/e71-055

Jahn, B.M., Gruau, G., Glikson, A.Y., 1982. Komatiites of the Onverwacht Group, S. Africa: REE Geochemistry, Sm/Nd Age and Mantle Evolution. Contributions to Mineralogy and Petrology 80 (1), 25-40. https://link.springer.com/article/10.1007/BF00376732

Janousek, V., Farrow, C.M., Erban, V., 2006. Interpretation of whole-rock geochemical data in igneous geochemistry: introducing Geochemical Data Toolkit (GCDkit). Journal of Petrology 47 (6), 1255-1259. https://doi.org/10.1093/petrology/egl013

Jayananda, M., Kano, T., Peucat, J.J., Channabasappa, S., 2008. 3.35 Ga komatiite volcanism in the western Dharwar craton, southern India: Constraints from Nd isotopes and whole-rock geochemistry. Precambrian Research 162 (1-2), 160-179. https://doi.org/10.1016/j.precamres.2007.07.010

Jensen, L.S., 1976. A new cation plot for classifying subalkalic volcanic rocks. Ontario, Ontario Division of Mines, Miscellaneous Paper 66, 22 p. http://www.geologyontario.mndmf.gov.on.ca/mndmfiles/pub/data/imaging/MP066/MP066.pdf

Kretz, R., 1983. Symbols for rock-forming minerals. American Mineralogist 68 (1), 277-279. https://www.researchgate.net/publication/216831138_Symbols_for_rock-forming_minerals

Leal, L.R.B., 1998. Geocronologia U/Pb (SHRIMP), $^{207}Pb/^{206}Pb$, Rb/Sr, Sm/Nd e K/Ar dos Terrenos Granito-Greenstone do Bloco do Gavião: Implicações para a Evolução Arqueana e Paleoproterozoica do Cráton do São Francisco, Brasil. Ph. D. Thesis, Universidade de São Paulo, São Paulo, 178 p. http://www.teses.usp.br/teses/disponiveis/44/44134/tde-08012016-145912/pt-br.php

Leite, C.M.M., 2002. A Evolução Geodinâmica da Orogênese Paleoproterozóica nas Regiões de Capim Grosso, Jacobina e Pintadas - Mundo Novo (Bahia-Brasil): Metamorfismo, Anatexia Crustal e Tectônica. Ph. D. Thesis, Universidade Federal da Bahia, Salvador, 408 p.

Leite, C.M.M., Barbosa, J.S.F., Golçalves, P., Nicollet, C., Sabaté, P., 2009. Petrological evolution of sílica-undersaturated sapphirine-bearing granulite in the Paleoproterozoic Salvador-Curaçá Belt, Bahia, Brazil. Gondwana Research 15 (1), 49-70. https://doi.org/10.1016/j.gr.2008.06.005

Leite, C.M.M., Barbosa, J.S.F., Nicollet, C., Sabaté, P., 2007. Evolução metamórfica/metassomática paleoproterozóica do Complexo Saúde, da Bacia Jacobina e de leucogranitos peraluminosos na parte norte do Cráton do São Francisco. Revista Brasileira de Geociências 37 (4), 777-797. DOI: 10.25249/0375-7536.2007374777797

Leo, G.W., Cox, D.P., Carvalho, J.P.P., 1964. Geologia da parte sul da Serra de Jacobina, Bahia; Brasil. Rio de Janeiro: DNPM/DGM, Boletim 209, 84 p.

Lopez-Sanchez, M.A., Aleinikoff, L.N., Marcos, A., Martínez, F.J., Llana-Fúnez, S., 2016. An example of low-Th/U zircon overgrowths of magmatic origin in a late orogenic Variscan intrusion: the San Ciprián massif (NW Spain). Journal of the Geological Society 173, 282-291. doi:10.1144/jgs2015-071

Loureiro, H.S.C., 1991. Programa Levantamentos Geológicos Básicos do Brasil. Mundo Novo. Folha SC24-Y-D-IV. Estado da Bahia. Salvador, DNPM/CPRM, 177 p. http://rigeo.cprm.gov.br/jspui/handle/doc/8498

Ludwig, K.R., 2001. SQUID 1.03: A User's Manual. Berkeley Geochronology Center. Special Publication 2, 17 p.

Ludwig, K.R., 2003. User's manual for ISOPLOT 3.00. A geochronological toolkit for Microsoft Excel. Berkeley Geochronological Center Special Publication 4, 70 p.

Lynch, L., 1996. Provisional elemental values for four new geochemical soil and till reference materials, TILL-1, TILL-2, TILL-3 and TILL-4. Geostandards and Geoanalytical Research 20 (2), 277-287. https://doi.org/10.1111/j.1751-908X.1996.tb00189.x

Magee, C.W., Palin, J.M., Taylor, W.R., 2001. Laser ICP-MS U/Pb analyses of detrital zircons from Proterozoic sediments in Bahia state, Brazil; implications for the evolution of the São Francisco craton prior to 3,3 Ga. In: 11th V.M. Goldschmidt Conference, Hot Springs, abstract 3501. https://www.lpi.usra.edu/meetings/gold2001/pdf/3501.pdf

Maniar, P.D., Piccoli, P.M., 1989. Tectonic Discrimination of Granitoids. Geological Society of America Bulletin 101 (5), 635-643. https://doi.org/10.1130/0016-7606(1989)101<0635:TDOG>2.3.CO;2

Mascarenhas, J.F., Ledru, P., Souza, S.L., Filho, V.M.C., Melo, L.F.A., Lorenzo, C.L., Milesi, J.P., 1998. Geologia e recursos minerais do Grupo Jacobina e da parte sul do Greenstone Belt de Mundo

Novo. Série Arquivos Abertos, n. 13, 58 p. http://www.cbpm.ba.gov.br/modules/conteudo/conteudo.php?conteudo=23

Mascarenhas, J.F., Silva, E.F.A., 1994. Greenstone Belt de Mundo Novo: caracterização e implicações metalogenéticas e geotectônicas no Cráton do São Francisco. Série Arquivos Abertos, n. 5, 32 p. http://www.cbpm.ba.gov.br/modules/conteudo/conteudo.php?conteudo=23

Middlemost, E.A.K., 1994. Naming materials in the magma/igneous rock system. Earth Science Reviews 37 (3-4), 215-224. https://doi.org/10.1016/0012-8252(94)90029-9

Monteiro, M.D., Silva, R.W.S., Cunha, J.C., 2009. Projeto Fazenda Coqueiro. Salvador: CBPM, 57 p.

Mougeot, R., 1996. Étude de la limite Archéen-Protérozoïque et des minéralisations Au ± U associées. Exemples de la région de Jacobina (Etat de Bahia, Brésil) et de Carajas (Etat de Para, Brésil). 1996. 306 f. Thèse de l'Université de Montpellier II, Montpellier. http://www.theses.fr/1996MON20131

O'Connor, J.T. 1965. A classification for quartz-rich igneous rocks based on feldspar ratios. US Geologial Survey Professional Paper 525-B, 79-84.

Oliveira, E.P., Carvalho, M.J., McNaughton, N.J., 2004. Evolução do Segmento Norte do Orógeno Itabuna-Salvador-Curaçá: Cronologia da Acresção de Arcos, Colisão Continental e Escape de Terrenos. Geologia – USP, Série Científica 4 (1), 41-53. https://doi.org/10.5327/S1519-874x2004000100003

Oliveira, E.P., Mcnaughton, N.J., Armstrong, R., 2010. Mesoarchaean to Paleoproterozoic growth of the northern segment of the Itabuna-Salvador-Curaçá orogeny, São Francisco Cráton, Brazil. In: Kusky, T.M., Zhai, M.G., Xiao, W. (Eds.), The evolving continents: understanding processes of continental growth. London: Geological Society Special Publication 338, 263-286. https://doi.org/10.1144/SP338.1

Oliveira, E.P., Mello, E.F., Mcnaughton, N., 2002a. Reconnaissance U-Pb geochronology of Precambrian quartzites from the Caldeirão belt and their basement, NE São Francisco Craton, Bahia, Brazil: implications for the early evolution of the Paleoproterozoic Itabuna-Salvador-Curaçá orogeny. Journal of South American Earth Sciences 15 (3), 349-362. https://doi.org/10.1016/S0895-9811(02)00039-1

Oliveira, E.P., Mello, E.F., McNaughton, N.J., Choudhuri, A., 2002b. SHRIMP U-Pb age of the basement to the Rio Itapicuru Greenstone Belt, NE São Francisco craton. In: 41° Congresso Brasileiro de Geologia, João Pessoa, *Anais*, p. 522.

Parman, S.W., Grove, T.L., Dann, J.C., 2001. The production of Barberton komatiites in an Archean subduction zone. Geophysical Research Letters 28 (13), 2513-2516. https://doi.org/10.1029/2000GL012713

Pearce, J.A., 2008. Geochemical fingerprinting of oceanic basalts with applications to ophiolite classification and the search for Archean oceanic crust. Lithos 100, 14-48. https://doi.org/10.1016/j.lithos.2007.06.016

Pearce, J.A., Harris, N.B.W., Tindle, A.G., 1984. Trace element discrimination diagrams for the tectonic interpretation of granitic rocks. Journal of Petrology 25 (4), 956-983. https://doi.org/10.1093/petrology/25.4.956

Pearce, J.A., Parkinson, I.J., 1993. Trace element models for mantle melting: application to volcanic arc petrogenesis. In: Prichard, H.M., Alabaster, T., Harris, N.B.W., Neary, C.R. (Eds.), Magmatic Processes and Plate Tectonics. Geological Society of London, Special Publication 76, 373-403.

Pearce, J.A., Stern, R.J., Bloomer, S.H., Fryer, P., 2005. Geochemical mapping of the Mariana Arc-Basin System: implications for the nature and distribution of subduction components. Geochemistry, Geophysics, Geosystems 6 (7), 1-27. https://doi.org/10.1029/2004GC000895

Petronilho, L.A., 2009. O método Sm-Nd no CPGeo-IGc-USP: procedimentos analíticos atualmente em rotina. Simpósio 45 anos de Geocronologia no Brasil, Instituto de Geociências, USP. Boletim de Resumos Expandidos, p. 116–118.

Peucat, J.J., Barbosa, J.S.F, Pinho, I.C.A., Paquette, J.L., Martin, H., Fanning, C.M., Leal, A.B.M., Cruz, S.C.P., 2011. Geochronology of granulites from the south Itabuna-Salvador-Curaçá Block, São Francisco Craton (Brazil): Nd isotopes and U e Pb zircon ages. Journal of South American Earth Sciences 31 (4), 397-413. https://doi.org/10.1016/j.jsames.2011.03.009

Peucat, J.J., Mascarenhas, J.F., Barbosa, J.S.F., Souza, S.L., Marinho, M.M., Fanning, C.M., Leite, C.M.M., 2002. 3,3 Ga SHRIMP U-Pb zircon age of a felsic metavolcanic rock from the Mundo Novo Greenstone Belt in the São Francisco Craton, Bahia (NE Brazil). Journal of South American Earth Sciences 15 (3), 363-373. https://doi.org/10.1016/S0895-9811(02)00044-5

Reis, C., Menezes, R.C.L., Miranda, D.A., Santos, F.P., Loureiro, H.C., Neves, J.P., Viera, R., 2017. Mapa geológico-geofísico: Projeto ARIM Serra de Jacobina. Salvador: CPRM. http://rigeo.cprm.gov.br/jspui/handle/doc/18679

Reis, C., Oliveira, R.C.L., Miranda, D.A., Santos, F.P., Guimarães, J.T., Teles, G., 2018. Estratigrafia do Grupo Jacobina. In: 49° Congresso Brasileiro de Geologia, Rio de Janeiro, Anais, p. 1232. http://cbg2018anais.siteoficial.ws/resumos/7641.pdf

Rios, D.C., Davis, D.W., Conceição, H., Davis, W.J., Rosa, M.L.S., Dickin, A.P., 2009. Geologic evolution of the Serrinha nucleus granite-greenstone terrane (NE Bahia, Brazil) constrained by U-Pb single zircon geochronology. Precambrian Research 170 (3-4), 175-201. https://doi.org/10.1016/j.precamres.2008.10.001

Rollinson, H. R., 1993. Using Geochemical Data: Evaluation, Presentation, Interpretation. 1st edition. Longman Scientific and Technical, England, 352 p.

Sabaté, P., Marinho, M.M., Vidal, P., Caen Vachette, M., 1990. The 2-Ga peraluminous magmatism of the Jacobina–Contendas Mirante belts (Bahia, Brazil): geologic and isotopic constraints on the sources. Chemical Geology 83 (3-4), 325-338. https://doi.org/10.1016/0009-2541(90)90288-I

Siivola, J., Schmid, R. A systematic nomenclature for metamorphic rocks. 12. List of mineral abbreviations. Recommendations by the IUGS Subcommission on the Systematics of Metamorphic Rocks. Web version 01.02.07. IUGS Commission on the Systematics in Petrology. Available in: <https://www.bgs.ac.uk/downloads/start.cfm?id=3197>. Access in: 16 nov. 2017.

Silva, L.C., Armstrong, R., Delgado, I.M., Pimentel, M., Arcanjo, J.B., Melo, R.C., Teixeira, L.R., Jost, H., Cardoso Filho, J.M., Pereira, L.H.M., 2002. Reavaliação da evolução geológica em terrenos Pré-Cambrianos brasileiros com base em novos dados U-Pb SHRIMP, Parte I: Limite centro-oriental do Cráton São Francisco na Bahia. Revista Brasileira de Geociências 32 (4), 501-512. DOI: 10.25249/0375-7536.2002324501512

Silva, L.C., McNaughton, N.J., Melo, R.C., Fletcher, I.R., 1997. U-Pb SHRIMP ages in the Itabuna-Caraíba TTG high-grade complex: The first window beyond the Paleoproterozoic overprinting of the eastern Jequié Craton, NE Brazil. In: Isgam International Symposium on Granites and Associated Mineralization. Abstracts, Salvador, v. 1, p. 282-283. https://www.researchgate.net/publication/284106273

Sousa, D.F.M., Oliveira, E.P., Amaral, W.S., 2018. Geologia e geocronologia U-Pb em zircão de ortognaisses e K-granitoides relacionados ao Bloco Gavião (Complexo Mairi) e Cinturão Salvador-Curaçá - Região da Mina Caraíba - Bahia. In: 49° Congresso Brasileiro de Geologia, Rio de Janeiro, Anais, p. 980. http://cbg2018anais.siteoficial.ws/resumos/8534.pdf

Souza, S.L., Garrido, I.A.A., Oliveira, N.S., Fróes, R.J., 2002. Projeto Greenstone Belt de Mundo Novo: estudos geológicos regionais. Salvador: CBPM, 1, 62 p.

Spreafico, R.R., 2017. Projeto Mundo Novo: texto e mapas. Salvador: CBPM, 2017. 84 p.

Spreafico, R.R., Barbosa, J.S.F., Barbosa, N.S., Moraes, A.M.V., Souza Júnior, F.D., 2018. A idade Neoarqueana (2,59 Ga, U-Pb) do *greenstone belt* Mundo Novo, Bahia, Brasil. In: 49° Congresso Brasileiro de Geologia, Rio de Janeiro, Anais, p. 1930. http://cbg2018anais.siteoficial.ws/resumos/7518.pdf

Storey, M., Mahoney, J.J., Kroenke, L.W., Saunders, A.D., 1991. Are oceanic plateaus sites of komatiite formation? Geology 19, 376-379. https://doi.org/10.1130/0091-7613(1991)019<0376:AOPSOK>2.3.CO;2

Steiger, R.H., Jäger, E., 1977. Subcommision on geochronology convention on the use of decay constants in geo- and cosmochronology. Earth and Planetary Science Letters 36 (3), 359-362. https://doi.org/10.1016/0012-821X(77)90060-7

Teles, G.S., 2013. Proveniência e idades de deposição dos sedimentos auríferos da Bacia de Jacobina: Implicações sobre a evolução da bacia durante o Paleo-Arqueano e a gênese da mineralização. M.Sc. Thesis, Universidade de Brasília, Brasília, 122 p. http://repositorio.unb.br/handle/10482/14972

Teles, G.S., Chemale, F., Oliveira, C.G., 2015. Paleoarchean record of the detrital pyrite-bearing, Jacobina Au-U deposits, Bahia, Brazil. Precambrian Research 256, 289-313. https://doi.org/10.1016/j.precamres.2014.11.004

Thompson, M., 1988. Variation of precision with concentration in an analytical system. Analyst 113, 1579-1587. DOI: 10.1039/AN9881301579

Wasserburg, G.J., Jacobsen, S.B., De Paolo, D.J., McCulloch, M.T., Wen, T. 1981. Precise determination of Sm/Nd ratios, Sm and Nd isotopic abundances in standard solutions. Geochimica et Cosmochimica Acta 45 (12), 2311-2323. https://doi.org/10.1016/0016-7037(81)90085-5

Whalen, J.B., Currie, K.L., Chappell, B.W., 1987. A-type granites: geochemical characteristics, discrimination and petrogenesis. Contributions to Mineralogy and Petrology 95 (4), 407-419. https://link.springer.com/article/10.1007/BF00402202

Wilson, N., 1987. Combined Sm-Nd, Pb-Pb and Rb-Sr geochronology and isotope geochemistry in polymetamorphic Precambrian terrains: examples from Bahia, Brazil and Channel Island. M.Sc., U.K. Master, Oxford University, England, 150 p.

Xiang, W., Griffin, W.L., Jie, C., Pinyun, H., Xiang, L., 2011. U and Th Contents and Th/U Ratios of Zircon in Felsic and Mafic Magmatic Rocks: Improved Zircon-Melt Distribution Coefficients. Acta Geologica Sinica 85 (1), 164-174. https://onlinelibrary.wiley.com/doi/10.1111/j.1755-6724.2011.00387.x

Xie, Q., Kerrich, R., 1994. Silicate–perovskite and majorite signature komatiites from the Archean Abitibi greenstone belt; implications for early mantle differentiation and stratification. Journal of Geophysical Research 99 (B8), 15799-15812. https://doi.org/10.1029/94JB00544

Zincone, S.A., Barbuena, D., Oliveira, E.P., Baldim, M.R., 2017. Detrital zircon U-Pb ages as evidence for deposition of the Saúde Complex in a Paleoproterozoic foreland basin, northern São Francisco Craton, Brazil. Journal of South American Earth Sciences 79, 537-548. https://doi.org/10.1016/j.jsames.2017.09.009

Zincone, S.A., Oliveira, E.P., Laurent, O., Zhang, H., Zhai, M., 2016. 3.3 Ga High-Silica Intraplate Volcanic-Plutonic System of the Gavião Block, São Francisco Craton, Brazil: Implications of an intracontinental rift following the creation of insulating continental crust. Lithos 266-267, 414-434. https://doi.org/10.1016/j.lithos.2016.10.011

CAPÍTULO 4

ARTIGO 3 - TIMS Pb-Pb GEOCHRONOLOGY OF SULFIDES IN THE FAZENDA COQUEIRO VMS DEPOSIT, SÃO FRANCISCO CRATON, NE BRAZIL: TIMING AND GENESIS CONSTRAINTS ON THE MINERALIZATION

Abstract

TIMS Pb-Pb geochronologic data allow determination of the timing and genesis of the Fazenda Coqueiro volcanogenic massive sulfide (VMS) Zn-Pb deposit hosted in the Neoarchean Mundo Novo greenstone belt (MNGB), NE São Francisco Craton. The deposit is inserted in the Rhyacian-Orosirian Contendas-Jacobina lineament between Paleoarchean tectonic blocks. The basement of the deposit is composed of a Paleoarchean metagranite and metarhyolite nucleus tectonically emplaced in the supracrustal rocks. The volcanic-sedimentary rocks comprise the ocean floor western metabasalt, calc-silicate rock, aluminous schist, metachert, banded iron formation and tremolitite of the middle sequence and metasedimentary siliciclastic rocks of the upper sequence of the MNGB. The western metabasalt hosts two hydrothermal alteration zones: one carbonate (calc-silicate rock), proximal, hosting massive sulfides (eight meters thick) composed mainly of sphalerite and galena with minor chalcopyrite; and the other argillic and chloritic (aluminous schist), distal, hosting mainly disseminated chalcopyrite. Pb-Pb galena, chalcopyrite and sphalerite data from the massive and disseminated zones in the Fazenda Coqueiro deposit yield model ages of 2804 ± 11.15 Ma, 2794 ± 11.2 Ma and 2767 ± 11.1 Ma, respectively, sourced from the upper crust, based on the uranogenic and thorogenic diagrams. The Pb-Pb isochron crystallization age of 2747 ± 16 Ma obtained from chalcopyrite and sphalerite samples from the massive and disseminated zones suggests that the sulfides are coeval and were not strongly affected by later hydrothermal events. Therefore, the Fazenda Coqueiro deposit would have formed from Neoarchean ocean floor volcanic rocks interlayered with carbonate and pelitic sediments. The Rhyacian-Orosirian tectonic event compressed the deposit between Paleoarchean blocks along the Contendas-Jacobina lineament, preserving the sulfides from recrystallization processes.

Keywords: Fazenda Coqueiro Zn-Pb deposit; Pb-Pb geochronology; Neoarchean; VMS; Cogenetic sulfides; São Francisco Craton.

Resumo

Dados geocronológicos TIMS Pb-Pb permitiram determinar o tempo e a gênese do depósito de Zn-Pb do tipo *volcanogenic massive sulfide* (VMS) da Fazenda Coqueiro, hospedado no *greenstone belt* Mundo Novo (GBMN), NE do Cráton do São Francisco. O depósito está inserido no lineamento Riaciano-Orosiriano Contendas-Jacobina, entre blocos tectônicos Paleoarqueanos. O seu embasamento é composto de núcleos metagraníticos e metariolíticos Paleoarqueanos, tectonicamente colocados entre as rochas supracrustais. As rochas metavulcanossedimentares de fundo oceânico compreendem metabasalto oeste, calciossilicática, xisto aluminoso, metachert, formação ferrífera bandada e tremolitito da sequência média e rochas metassedimentares siliciclásticas da sequência superior do GBMN. O metabasalto oeste hospeda duas zonas de alteração hidrotermal: uma carbonática (calciossilicática), proximal, que hospeda o sulfeto maciço (oito metros de espessura), composta principalmente de esfalerita e galena, além de menores concentrações de calcopirita; e outra, argílica e clorítica (xisto aluminoso), distal, que hospeda principalmente calcopirita disseminada. Dados Pb-Pb em galena, calcopirita e esfalerita das zonas maciça e disseminada geraram idades modelo de 2804 ± 11,15 Ma, 2794 ± 11,2 Ma e 2767 ± 11,1 Ma, respectivamente, originadas na crosta superior com base nos diagramas uranogênico e torogênico. Uma idade de cristalização isocrônica de 2747 ± 16 Ma, obtida de amostras de calcopirita e esfalerita das zonas maciça e disseminada, sugere que os sulfetos sejam cogenéticos e que não tenham sido fortemente afetados por eventos hidrotermais posteriores. Portanto, o depósito da Fazenda Coqueiro teria se formado a partir de vulcanismos Neoarqueanos de fundo oceânico, intercalados por sedimentos carbonáticos e pelíticos. O evento tectônico Riaciano-Orosiriano comprimiu o depósito entre blocos Paleoarqueanos ao longo do lineamento Contendas-Jacobina, preservando os sulfetos de processos de recristalização.

Palavras-chave: Depósito de Zn-Pb Fazenda Coqueiro; Geocronologia Pb-Pb; Neoarqueano; VMS; Sulfetos cogenéticos; Cráton do São Francisco.

INTRODUCTION

Volcanogenic massive sulfide (VMS) deposits are stratabound sulfide accumulations at or near the ocean floor that are spatially, temporally and genetically associated with contemporaneous volcanism (Franklin et al., 2005). Thus, the Fazenda Coqueiro VMS Zn-Pb deposit, hosted in the Mundo Novo greenstone belt (MNGB), eastern São Francisco Craton and NE Brazil (Figures 1A, 1B and 1C), is important evidence of ocean floor hydrothermal activity with sulfide precipitation during the formation of the greenstone belt. Deformation during collisional tectonic events, the great depth of the deposit and the sulfide occurrences identified only in drill hole cores make it difficult to clearly define the typology features and the metallogenetic model of the deposit, as observed by Souza et al. (2002) and Monteiro et al. (2009).

The Fazenda Coqueiro deposit is hosted in the western metabasalt of the middle sequence of the MNGB, which is interlayered with two hydrothermal alteration zones that control the sulfide distribution. The carbonate hydrothermal alteration zone is the main portion of the deposit and hosts massive sphalerite and galena occurrences, and the argillic-chloritic hydrothermal alteration zone is peripheral and hosts disseminated chalcopyrite (Spreafico, 2017). A Rhyacian-Orosirian tectonic event (Leite, 2002) deformed the Fazenda Coqueiro deposit, obliterating the initial features, making it difficult to interpret the metallogenic model and leading to an interpretation of the possibility of post-hydrothermal processes in the study area. In addition, new geochronological data from metavolcanic felsic rock of the MNGB show Neoarchean ages for the MNGB (Spreafico et al., 2019), indicating that the Fazenda Coqueiro deposit should be coeval with those rocks.

Therefore, geological and thermal ionization mass spectrometry (TIMS) Pb-Pb geochronological studies of sulfides from the Fazenda Coqueiro deposit were conducted to more accurately understand and interpret the timing and genesis of the VMS deposit. An analogy with early VMS pipe components, the styles, controls and sources of mineralization, the Rhyacian-Orosirian deformation process and the relation to the Contendas-Jacobina lineament, in addition to the possibility of late sulfide remobilization processes, were also covered.
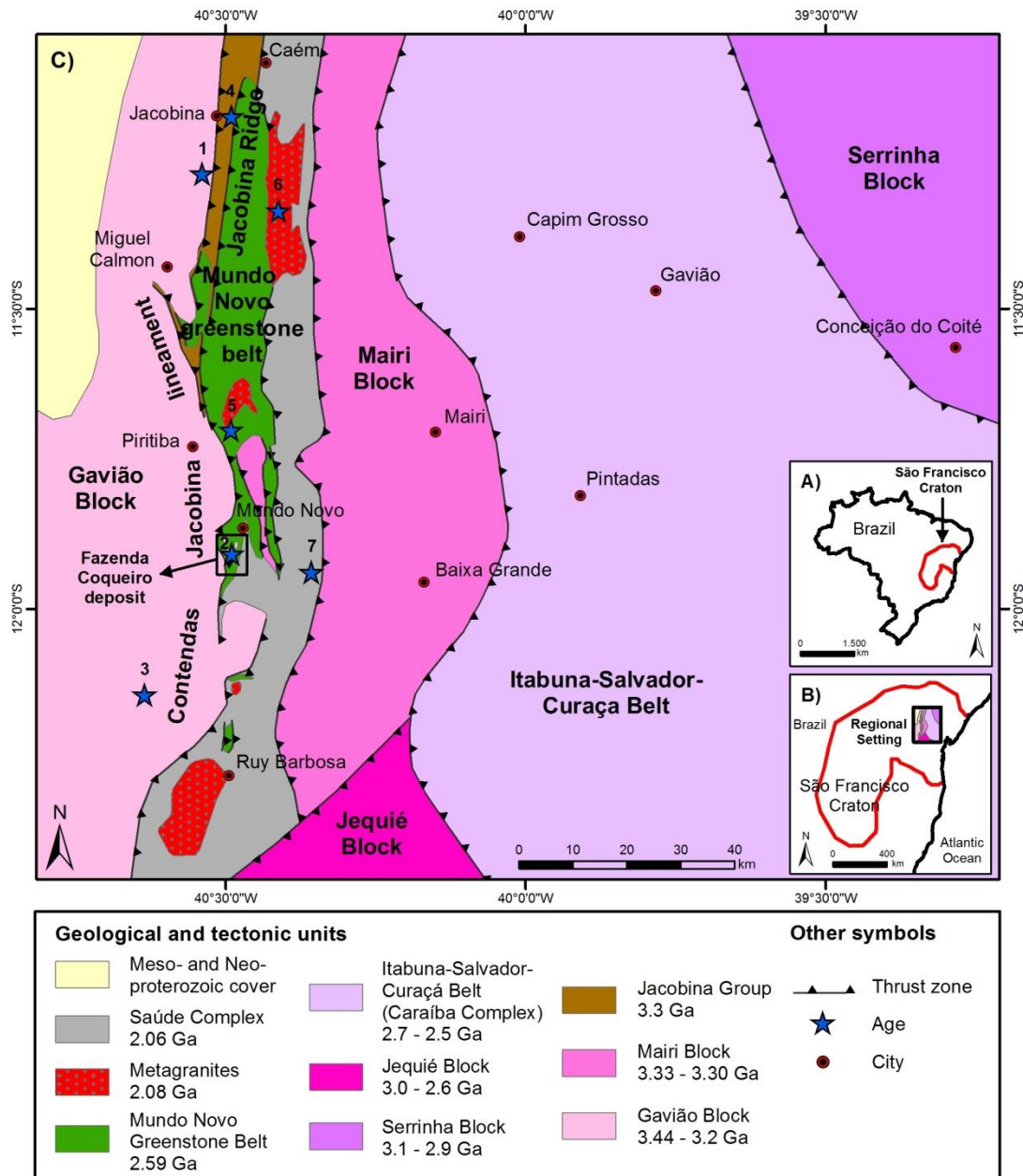
Figure 1. A) Location of the São Francisco Craton in NE Brazil. B) Regional setting in the eastern portion of the São Francisco Craton. C) Regional tectonic setting where the MNGB and the Fazenda Coqueiro deposit are inserted (modified from Barbosa and Sabaté, 2002, 2003, 2004). Ages at the points highlighted on the map: 1- 3442 ± 2 Ma (U-Pb zircon, TTG; Mougeot, 1996); 2- 3303 ± 11 Ma (U-Pb zircon, metarhyolite from the Gavião Block obtained by Zincone et al., 2016); 3- 3292 ± 3 Ma (U-Pb zircon, metagranite from the Gavião Block obtained by Zincone et al., 2016); 4- 3500 - 3220 Ma (U-Pb zircon, quartzite from the Jacobina Group obtained by Teles et al., 2015); 5- 2595 ± 21 Ma (U-Pb zircon, metadacite from the MNGB obtained by Spreafico et al., 2019); 6- 2080 ± 18 Ma (U-Pb monazite, Cachoeira Grande granite obtained by Leite, 2002); 7- 2068 ± 12 Ma (U-Pb zircon, biotite schist from the Saúde Complex obtained by Zincone et al., 2017).

GEOLOGICAL SETTING

The eastern portion of the São Francisco Craton, where the MNGB and the Fazenda Coqueiro deposit are situated (NE Bahia), was formed through the amalgamation of four Archean blocks during Paleoproterozoic continent-continent collisions (Barbosa and Sabaté, 2002, 2003, 2004): the Gavião, Serrinha and Jequié blocks and the Itabuna-Salvador-Curaçá Belt (Figure 1C). The Paleoproterozoic event captured the MNGB and surrounding crust between the cratonic blocks, resulting in the formation of the Contendas-Jacobina lineament.

The uplift caused by this event possibly resulted in erosion and the formation of Paleoproterozoic sedimentary basins, such as the uppermost sequence of the MNGB.

Briefly, the MNGB is in contact to the west with 3.4 Ga (Mougeot, 1996) tonalite-trondhjemite-granodiorite (TTG) basement rocks and subordinate metagranites in the Gavião Block and to the east and south with paragneisses in the Saúde Complex with maximum ages between 2.20 and 2.06 Ga (Zincone et al., 2017) (Figure 2). To the north and northwest, the MNGB is in contact with quartzites of the Jacobina Group that were deposited between 3.55 and 3.22 Ga (Teles et al., 2015) and Paleoproterozoic granitic intrusives.

Additionally, the geologic setting includes granulites (2.9 Ga) and multiple charnockite intrusions (2.7 and 2.6 Ga) in the Jequié Block (Wilson, 1987; Silva et al., 2002), tonalitic granulite (2.57 Ga) and enderbite (2.7 Ga) of the Itabuna-Salvador-Curaçá Belt (Silva et al., 1997; Oliveira et al., 2010), and the Mairi (3.33 - 3.30 Ga) and Serrinha (3.1 – 2.9 Ga) blocks (Oliveira et al., 2002a, 2002b; Rios et al., 2009; Sousa et al., 2018) (Figure 1C and Table 1). Although the Itabuna-Salvador-Curaçá Belt and Serrinha Block are far from the MNGB, they are important for understanding the tectonic evolution of the study area.

Table 1. Compilation of regional geochronological data from the MNGB and adjoining units.

Geological/tectonic unit	Lithotype	Age	Method	Mineral dated	Author
Saúde Complex	Biotite schist	2068 ± 12 Ma	U-Pb (LA-MC-ICP-MS)	Detrital zircon	Zincone et al. (2017)
Cachoeira Grande granite	Leucogranite	2080 ± 18 Ma	U-Pb (electron microprobe)	Monazite (crystallization age)	Leite (2002)
Upper sequence (MNGB)	Quartzite	2133 ± 14 Ma	U-Pb (LA-ICP-MS)	Detrital zircon	Barbuena et al. (2016)
MNGB (metavolcanic rocks)	Metadacite	2595 ± 21 Ma	U-Pb (LA-ICP-MS)	Zircon (crystallization age)	Spreafico et al. (2019)
Itabuna-Salvador-Curaçá Belt	Tonalitic granulite	2574 ± 6 Ma	U-Pb (SHRIMP)	Zircon (crystallization age)	Oliveira et al. (2010)
	Enderbite	2695 ± 12 Ma	U-Pb (SHRIMP)	Zircon (crystallization age)	Silva et al. (1997)
Jequié Block	Granulites	2715 ± 29 Ma	U-Pb (SHRIMP)	Zircon (crystallization age)	Silva et al. (2002)
	Charnockite	2900 ± 24 Ma	Rb-Sr	Whole-rock (crystallization age)	Wilson (1987)
Serrinha Block	Granitoid	2989 ± 11 Ma 3072 ± 2 Ma 3162 ± 26 Ma	U-Pb (SHRIMP)	Zircon (crystallization age)	Rios et al. (2009)
	Gneiss, migmatite	3152 ± 5 Ma	U-Pb (SHRIMP)	Zircon (crystallization age)	Oliveira et al. (2002a, 2002b)
Jacobina Group	Quartzite	3500 - 3220 Ma	U-Pb (LA-MC-ICP-MS)	Detrital zircon	Magee et al. (2001); Teles (2013); Teles et al. (2015); Barbuena et al. (2016)
Mairi Block	Orthogneiss	3.33 - 3.30 Ga	U-Pb (LA-SF-ICP-MS)	Zircon (crystallization age)	Sousa et al. (2018)
Gavião Block	Metagranite	3291 ± 2.5 Ma	U-Pb (LA-ICP-MS)	Zircon (crystallization age)	Zincone et al. (2016)
	Metarhyolite*	3303 ± 11 Ma	U-Pb (LA-ICP-MS and SHRIMP)	Zircon (crystallization age)	Peucat et al. (2002); Zincone et al. (2016)
	TTG	3442 ± 2 Ma	U-Pb (ID-TIMS)	Zircon (crystallization age)	Mougeot (1996)

* The metarhyolite with an age of 3303 ± 11 Ma is part of the basement (Gavião Block) of the Fazenda Coqueiro deposit.

The eastern margin of the Gavião Block is in tectonic contact with the MNGB along a north-south-trending thrust zone with a west vergence (Figure 1C) and is composed of TTG gneisses and migmatites that host mafic rock enclaves (Barbosa et al., 2012a), metagranites and metarhyolites (Zincone et al., 2016). This block corresponds to the basement of the MNGB. Three groups of TTG gneisses are described in the Gavião Block; two groups are trondhjemitic with U-Pb zircon ages (SHRIMP) of 3403 ± 5 Ma and 3158 ± 5 Ma (Barbosa, 1997; Leal, 1998), and the third group, with a granodioritic composition, includes the 3225 ± 10 Ma Aracatu granitoid (Barbosa et al., 2012a). The age of the Gavião Block is 3.4 Ga (Mougeot, 1996), but metarhyolites with ages of 3303 ± 11 Ma and metagranites, such as Boa Sorte at 3291 ± 2.5 Ma, occur as well (Zincone et al., 2016).

The Jacobina Group is in tectonic contact with the MNGB along thrust zones, all of which strike north-south and are vergent to the west (Figure 1C), with the Gavião Block in the footwall. The Jacobina Group comprises metaconglomerates, quartzites, metarenites, phyllites, chlorite schists and quartz-sericite schists (Mascarenhas et al., 1998) deposited in a passive margin setting (Reis et al., 2018). This group has a depositional age, based on detrital zircons, between 3500 Ma and 3220 Ma (Magee et al., 2001; Teles, 2013; Teles et al., 2015; Barbuena et al., 2016). Jacobina Ridge represents an Archean supracrustal sequence with a maximum depositional age of 3.22 Ga, and its sources are likely rocks from both the plutonic-volcanic system and the TTG suite in the Gavião Block (Zincone et al., 2016).

The MNGB is divided into three stratigraphic sequences (Spreafico et al., 2019): a lower sequence (ultramafic rocks), a middle sequence (mafic and felsic igneous rocks and clastic and chemical metasedimentary rocks) and an upper sequence composed of siliciclastic metasedimentary rocks with an inherited age of 2133 ± 14 Ma (Barbuena et al., 2016) (Figure 2). Two ductile and progressive Paleoproterozoic deformational phases are described in the MNGB. The D_1 deformational phase is characterized by isoclinal and recumbent folds vergent to the west that generated greenschist-facies metamorphic rocks. The D_2 deformational phase is characterized by refolding that generated vertical and subvertical axial planes and eventually resulted in the formation of coaxial interference patterns or compressive and transpressive shear zones, which bounded the MNGB lithologies and generated rocks of greenschist- to amphibolite-facies metamorphism. The most prominent brittle structures are east-trending faults and fractures. The Neoarchean volcanism in the MNGB (Spreafico et al., 2019) with Paleoproterozoic sedimentation at the top of the sequence (Barbuena et al., 2016) and the coeval Paleoproterozoic tectonic event (Leite, 2002) have been considered the main geological and tectonic events in the study area. Drill hole programs previously realized by Companhia Baiana de Pesquisa Mineral (CBPM) in the Fazenda Coqueiro deposit quantified resources of 4,200,000 t in the massive sulfide body at 6.12% Zn and 0.41% Pb and one intersection with a length of one meter that reached 28 g/t Ag content (Monteiro et al., 2009). Gold occurrences related to the massive sulfides reached 2.75 g/t in an intersection with a length of two meters, and one Cu-rich disseminated zone in an intersection with a length of four meters reached 0.75% average Cu content (Monteiro et al., 2009).

The Saúde Complex occurs to the east of the MNGB (Figure 1C), where the two units are in tectonic contact along west-vergent thrust zones, and it is distributed along the Contendas-Jacobina lineament. The Saúde Complex comprises aluminous paragneisses, biotite gneisses and subordinate quartzites widely distributed in a north-south trend with significant occurrences in the Mundo Novo region and in the eastern portion of Jacobina Ridge (Couto et al., 1978; Mascarenhas et al., 1998; Leite et al., 2007; Reis et al., 2017) (Figure 1C). The maximal depositional age of 2.06 Ga (Zincone et al., 2017) for the Saúde Complex again indicates the presence of a basin near the MNGB in the Paleoproterozoic that was later subjected to a high-grade metamorphic process.

Finally, Paleoproterozoic granites are present along the Contendas-Jacobina lineament (Figure 1C) (Leite, 2002); however, occurrences near the Fazenda Coqueiro deposit have not been found (Spreafico et al., 2019). In general, these granites are undeformed leucogranites, comprising quartz, feldspar, biotite and muscovite, with some occurrences of garnet and sillimanite (Barbosa et al., 2012b). The Cachoeira Grande granite, for example, is a peraluminous leucogranite situated to the northeast of the MNGB that has an average age of 2080 ± 18 Ma (Leite, 2002), coeval with the Rhyacian-Orosirian granitic intrusions in the MNGB.

ANALYTICAL METHODOLOGY

The geological and TIMS Pb-Pb geochronological studies on the Fazenda Coqueiro deposit involved the description of five drill hole cores acquired by CBPM (Figure 3) in the 1990s and the collection of sulfides and hydrothermal alteration samples from three of these drill holes for timing and genesis constraints on the mineralization.

The description of drill hole cores was represented in a geological and structural section and in a diagram block, where the hydrothermal alteration zones were represented and the locations of collected samples for geochronological study were indicated. To better illustrate the mineral paragenesis of the host rocks, we used backscattered electron images of polished thin sections from a Kevex energy dispersive spectroscope (EDS) in a CAMECA SX50 electron microprobe at the University of Brasília. The standards used were synthetics with defined compositions, such as AsGa (for the element As), ZnS (for the element Zn), PbS (for the element Pb), pyrite (for the element Fe), $CuFeS_2$ (for the element Cu) and Ni. The mineral abbreviations used in the figures mainly follow those of Kretz (1983) and Siivola & Schmid (2007).

With regard to the geochronology, twelve samples of sulfides from the Fazenda Coqueiro deposit were selected to determine their model and crystallization ages using the Pb-Pb method on sulfides. The Pb-Pb geochronology was carried out at the Isotope Geology Laboratory of the Institute of Geosciences, Federal University of Pará. The sulfide grains from each sample were separated using binocular microscopy. To determine the Pb isotope compositions from galena, sphalerite and chalcopyrite, three different techniques were applied: whole digestion, leached fractions and galena analysis. Before acid digestion, 100 μg samples were cleaned, alternating among deionized H_2O (three times), 1 ml HCl 6N (50°C, five minutes) and five minutes in ultrasound (twice). For whole digestion, 2 ml of a 6N HCl $+HNO_3$ cc (1:1) solution plus 1 drop of 8N HBr were introduced twice in the sample, left for twenty-four and six hours, separated by five minutes of ultrasound and finally evaporated. For leaching fractions, 4 ml of 4N HBr + 2N HCl (12:1) solution was introduced into the sample and left for fifteen minutes at 110°C. In sequence, the supernatant was collected and evaporated. The residue was evaporated, and 4 ml of 2N HBr was introduced and left for four hours at 110°C. The procedure was repeated, but the acid solution was changed to 4 ml of 4N HCl for twelve hours at 110°C; 4 ml of 6N HCl for six hours at 110°C; and 4 ml of 50% aqua regia for twenty-four hours at 110°C until the whole sample was consumed, which generated a maximum of five leaching fractions. For galena digestion, three drops of 8N HBr were introduced into the sample and evaporated, followed by 2 ml of 13N HNO_3 and evaporation; another 2 ml of 13N HNO_3 plus 4 ml of deionized H_2O was added, and finally, 20 μl of H_3PO_4 (0.125M) was introduced, and the solution was evaporated. Except for galena solution, the others were processed in a chromatographic separation column filled with Dowex AG 1×8 resin in the following sequence: cleaning of the resin (6N HCl, deionized H_2O, 0.5N HBr twice), introduction of the sample solution into the column, and elution four times with 0.5N HBr; finally, the Pb was recovered with 6N HCl. Before evaporation, 10 μL of 0.125N H_3PO_4

was introduced for analysis in a Finnigan Mat 262 TIMS. The final results were plotted in the Pb-Pb diagrams for model and isochron age determination, as well as plumbotectonic models, using the Isoplot Excel program.
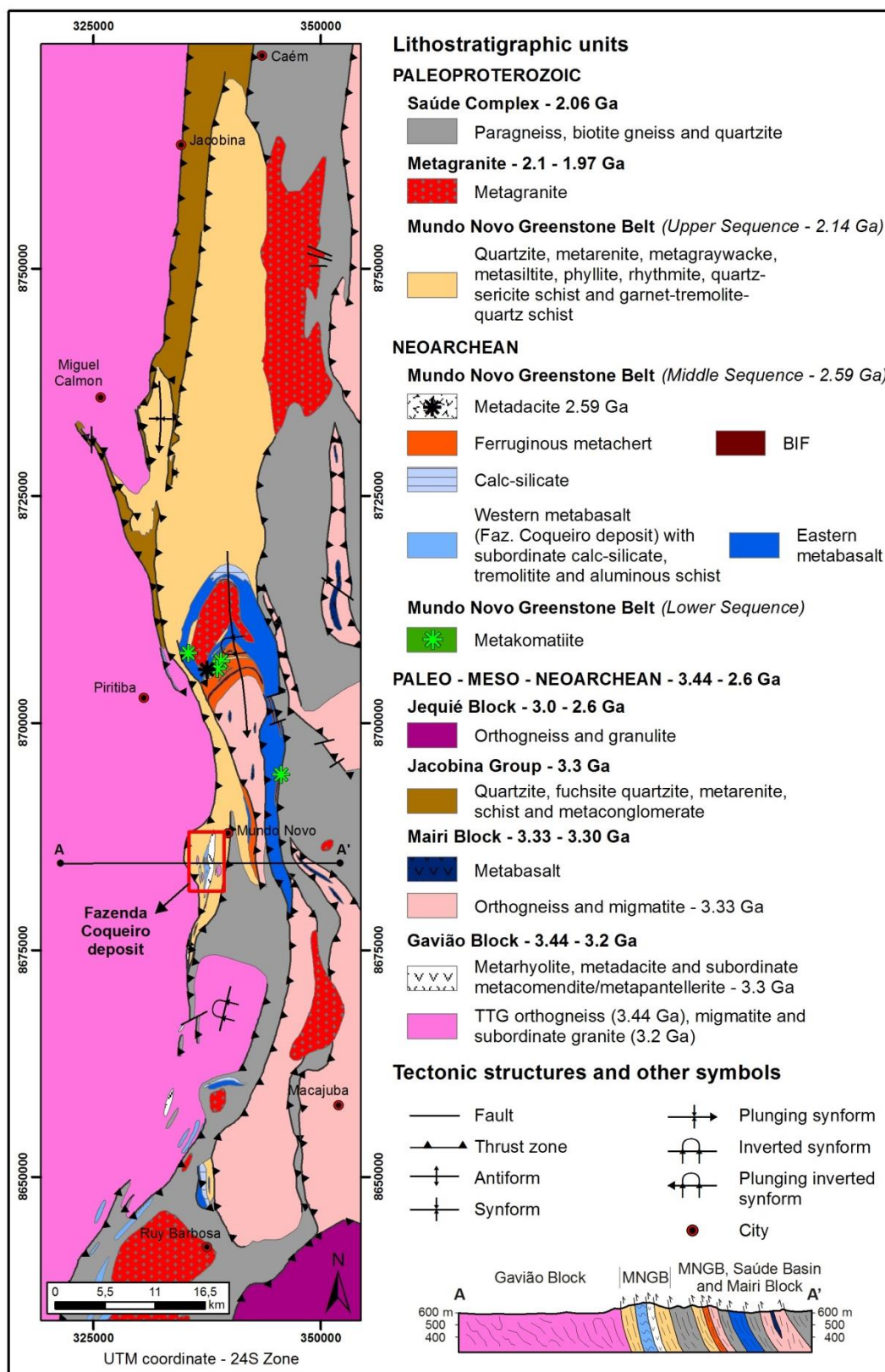
Figure 2. Geologic map of the MNGB and adjoining units. From Spreafico et al. (2019).

RESULTS

Geology of the Fazenda Coqueiro VMS deposit

The MNGB is divided into three stratigraphic sequences according to Spreafico et al. (2019): the lowermost sequence, composed of metakomatiite; the middle sequence, composed of eastern and western metabasalts and, subordinate tremolitite, calc-silicate rock, aluminous schist, banded iron formation, ferruginous metachert, basaltic metandesite, metadacite and metarhyolite; and the uppermost sequence, composed of siliciclastic metasedimentary rocks, such as metarenites, quartzites, metagraywackes, metasiltites, phyllites, rhythmites, quartz-sericite schists and garnet-tremolite-quartz schists.

In the Fazenda Coqueiro deposit, two supracrustal lithological sequences of the MNGB are present and tectonically related to basement rocks (Figure 3). The Paleoarchean metagranite and metarhyolite of the Gavião Block occur as tectonic slices emplaced in the rocks of the middle and uppermost sequence of the MNGB. The lithotypes of the middle sequence in the Fazenda Coqueiro deposit consist of the western metabasalt with aluminous schist and calc-silicate interlayered, in addition to tremolitite, ferruginous metachert and banded iron formation occurrences. The metasedimentary rocks of the upper sequence in the Fazenda Coqueiro deposit comprise mainly metarenites, quartzites, metagraywackes, metasiltites, phyllites and rhythmites in the eastern and western contacts of the deposit where these rocks can reach three kilometers in thickness.

The geological and geochronological studies of the Fazenda Coqueiro VMS deposit focused on galena, chalcopyrite and sphalerite grains from the western metabasalt (host rock), aluminous schist (metamorphosed argillic-chloritic hydrothermal alteration zone) and calc-silicates (metamorphosed carbonate hydrothermal alteration zone) of the middle sequence of the MNGB.

Host hock

The western metabasalt hosts two distinct metamorphosed hydrothermal alteration zones and is distributed along a north-south trend in the Fazenda Coqueiro deposit (Figure 3). The western metabasalt differs from the eastern metabasalt by enrichment in light rare earth elements and higher crustal contamination; however, the two metabasalts are inserted in the same ocean floor geological context as described in Spreafico et al. (2019).

These rocks are very fine-grained, mainly composed of actinolite and oligoclase, with low percentages of augite, quartz and biotite, as well as ilmenite and titanite as accessory minerals and traces of pyrrhotite, pyrite, chalcopyrite, galena, sphalerite and arsenopyrite (Figures 4A and 5A). The grains of biotite and actinolite are oriented and define well-developed planes of foliation.

The western metabasalts are five hundred meters thick and five to six kilometers long in the deposit and constitute the central and main portion of the mineralization (Figure 6). They make tectonic contact along thrust zones with metarhyolites of the basement to the east and with siliciclastic metasedimentary rocks to the west (Figure 3).

Two metamorphosed hydrothermal alteration zones occur interlayered within the western metabasalt: one is a proximal carbonate zone that hosts massive sulfides in the Fazenda Coqueiro deposit composed mainly of sphalerite and galena; and the other is a distal argillic-chloritic zone that hosts disseminated sulfides composed mainly of chalcopyrite.
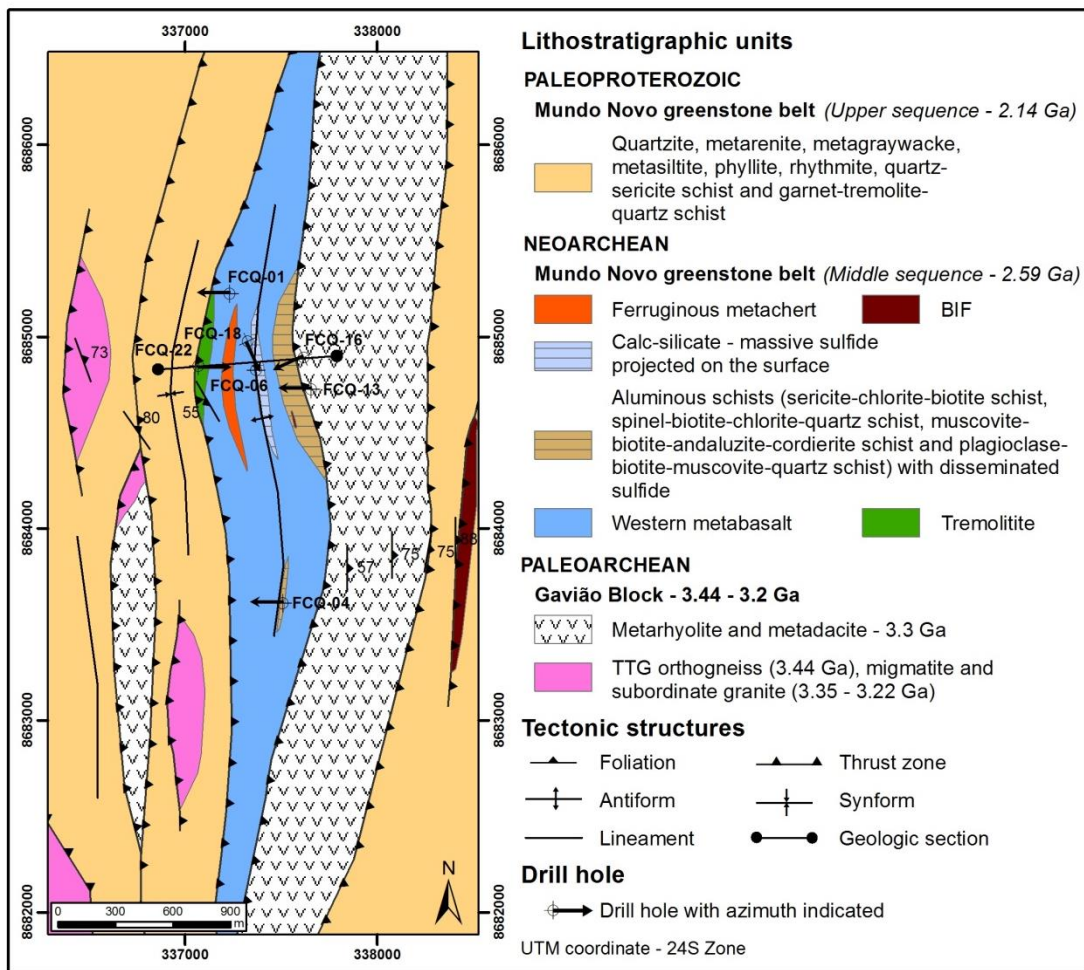
Figure 3. Geologic map of the Fazenda Coqueiro VMS deposit and the sites of drill holes where the sulfide samples were collected for Pb-Pb analyses.

Argillic-chloritic hydrothermal alteration zone (aluminous schist)

The argillic-chloritic alteration zone corresponds to aluminous schist (metapelitic) occurrences (Figure 4B), is pervasive and distal in relation to volcanic sources and is observable mainly in drill cores. This alteration zone hosts disseminated and lower content sulfide with a predominance of chalcopyrite that normally precedes the main mineralization formed by ocean floor hydrothermal processes. The metamorphic products of the argillic-chloritic alteration zone are aluminous schists, such as sericite-chlorite-biotite schist (Figures 5B and 5D), spinel-biotite-chlorite-quartz schist, muscovite-biotite-andalusite-cordierite schist and plagioclase-biotite-muscovite-quartz schist. A thin silicate level can occur between the argillic-chloritic and the carbonate zone, hosting mainly galena and chalcopyrite disseminated grains (Figure 5C).

The aluminous schist is interlayered with the western metabasalt at different levels and comprises the footwall of the massive sulfide level (Figures 6 and 7). Beyond chalcopyrite occurrences, paragenesis also involves galena and pyrrhotite (Figure 5C), in addition to pyrite, pentlandite and rutile (Figure 5D).
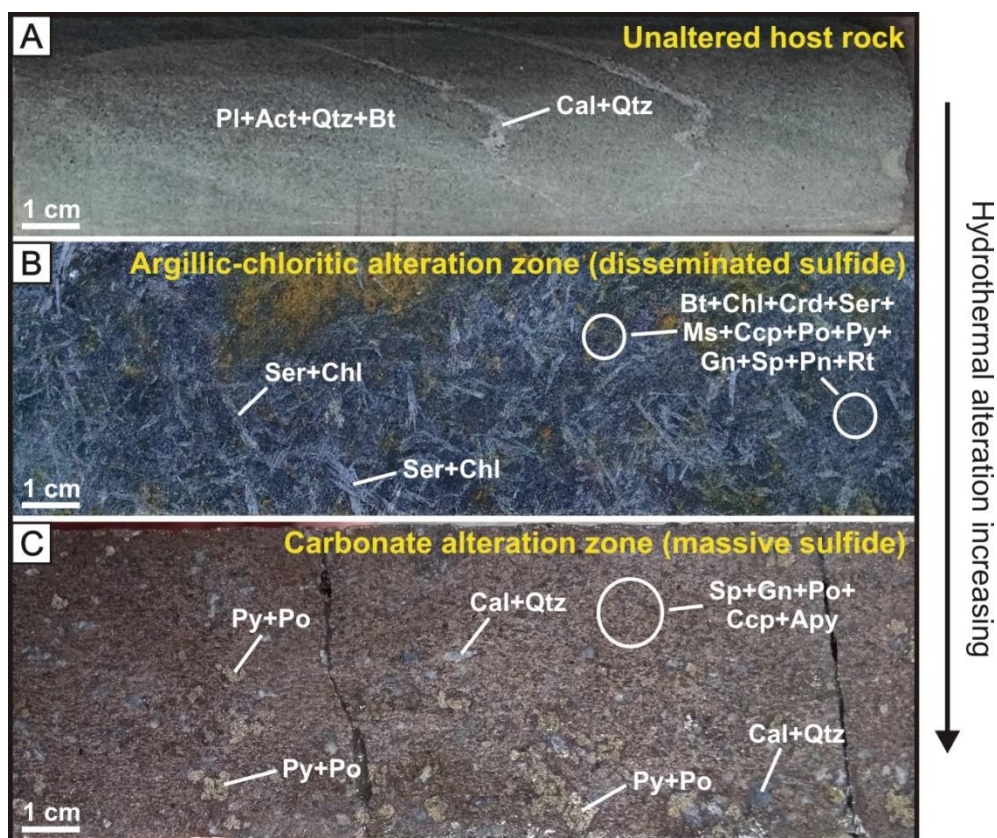
Figure 4. Core samples of the host rock and hydrothermal alteration zones in the Fazenda Coqueiro VMS deposit with the hydrothermal alteration increasing from the unaltered western metabasalt to the carbonate hydrothermal alteration zone. A) Unaltered western metabasalt host rock composed of plagioclase, actinolite, quartz and biotite intersected by calcic-quartz veins. B) Argillic-chloritic hydrothermal alteration zone (aluminous schist) composed of sericite, chlorite, biotite, cordierite and muscovite with disseminated chalcopyrite and traces of pyrrhotite, pyrite, galena, sphalerite, pentlandite and rutile. C) Carbonate hydrothermal alteration zone (calc-silicate rock) composed of calcite and quartz with paragenesis composed of massive sphalerite and traces of galena, pyrrhotite, pyrite and arsenopyrite. Mineral abbreviations: Act: actinolite, Apy: arsenopyrite, Bt: biotite, Cal: calcite, Ccp: chalcopyrite, Chl: chlorite, Crd: cordierite, Gn: galena, Ms: muscovite, Pl: plagioclase, Pn: pentlandite, Po: pyrrhotite, Py: pyrite, Qtz: quartz, Rt: rutile, Ser: sericite and Sp: sphalerite.

Carbonate hydrothermal alteration zone (calc-silicate)

The carbonate alteration zone, observable only in the drill cores, hosts massive and higher content sulfides and is proximal to volcanic sources. This massive sulfide is stratabound and composed mainly of sphalerite with minor amounts of galena, chalcopyrite, pyrrhotite and pyrite resulting from the final process of mineralization on the ocean floor. The metamorphic product of the carbonate alteration zone is a calc-silicate rock composed of calcite, quartz and diopside (Figures 4C and 5E). The ore paragenesis comprises sphalerite, often with inclusions of galena (Figure 5F) and pyrrhotite, with minor occurrences of chalcopyrite and pyrite and restricted occurrences of silver and gold.

The carbonate alteration zone forms a subvertical lens in the eastern limb of a tight antiform with a north-south and subhorizontal hinge line plunging southward (Figure 6). The hanging wall is composed of the western metabasalt, and the footwall consists of one level of aluminous schist, where thin silicate levels can occur with low contents of galena, chalcopyrite, pyrrhotite and arsenopyrite. The carbonate lens is eight meters thick and at least one hundred meters long along the north-south direction, based on available drill hole data, with the top at a depth of approximately three hundred seventy meters (Figure 7). However, the extent of the massive sulfide lens at greater depths is yet unknown.
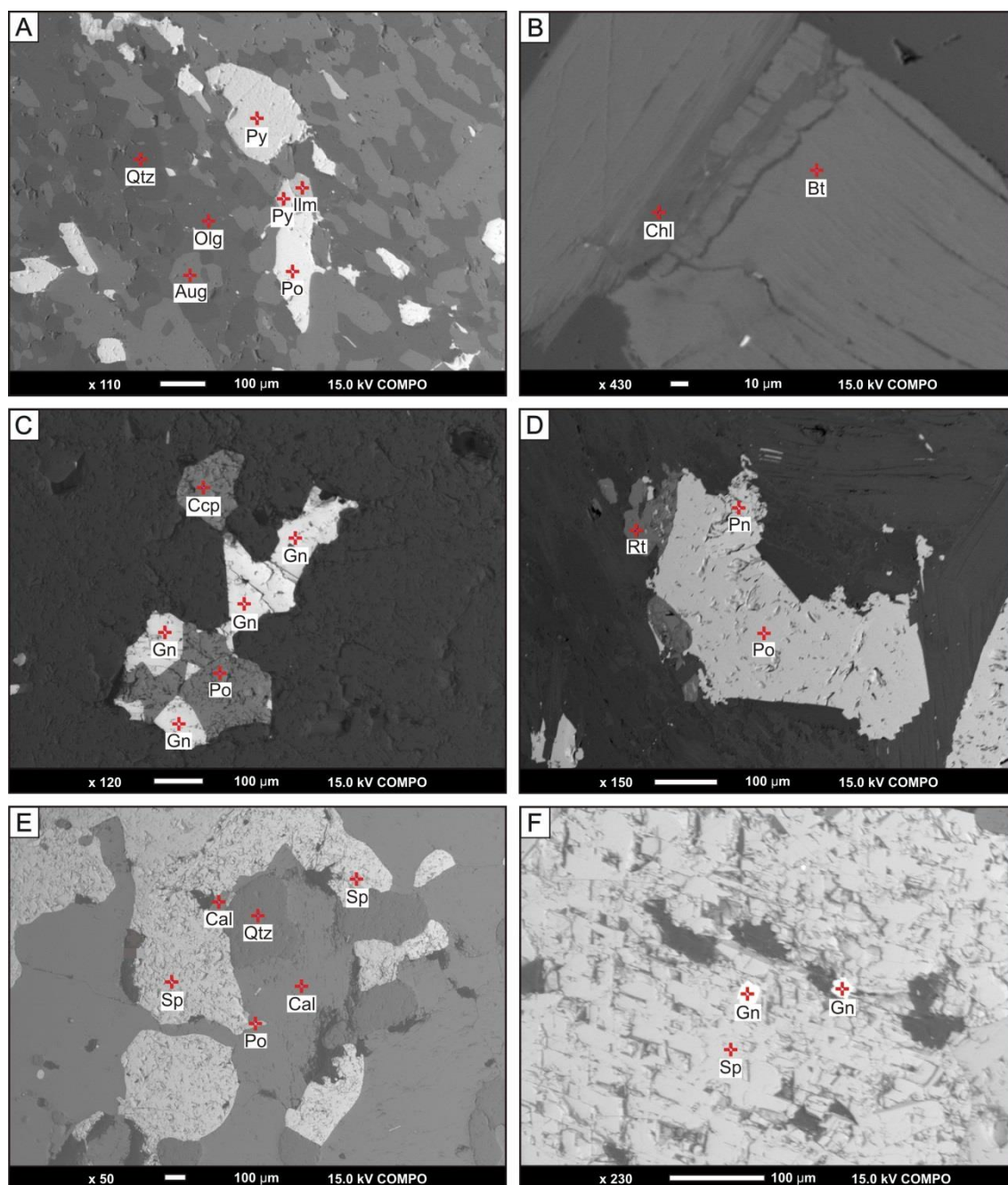
Figure 5. Backscattered electron images with the analytical spots in the core samples of the Fazenda Coqueiro VMS deposit. A) Mineral paragenesis in the western metabasalt: B) Chlorite and biotite relation in the aluminous schist. C) Mineral paragenesis of the silica-rich level in the aluminous schist composed of chalcopyrite, galena and pyrrhotite. D) Mineral paragenesis of the aluminous schist composed of pyrrhotite, pentlandite and rutile. E) Interstitial sphalerite and pyrrhotite in calcite and quartz grains of the calc-silicate rock. F) Inclusions of galena grains in sphalerite hosted in the calc-silicate rock. Mineral abbreviations: Aug: augite, Bt: biotite, Cal: calcite, Ccp: chalcopyrite, Chl: chlorite, Gn: galena, Ilm: ilmenite, Olg: oligoclase, Pn: pentlandite, Po: pyrrhotite, Py: pyrite, Qtz: quartz, Rt: rutile and Sp: sphalerite.

Structural geology

The rocks of the Fazenda Coqueiro deposit were affected by two progressive and west vergent deformational phases related to the Rhyacian-Orosirian tectonic event described for the MNGB (Leite, 2002; Spreafico et al., 2019). The result was a tectonic tightening of the rocks with slices of the basement metarhyolites emplaced in the supracrustal rocks along thrust zones. Therefore, the metarhyolites overlapped on the western metabasalts of the

middle sequence in the eastern part of the deposit, and the western metabasalts overlapped on the metasedimentary siliciclastic rocks of the upper sequence in the western part of the deposit (Figure 6).
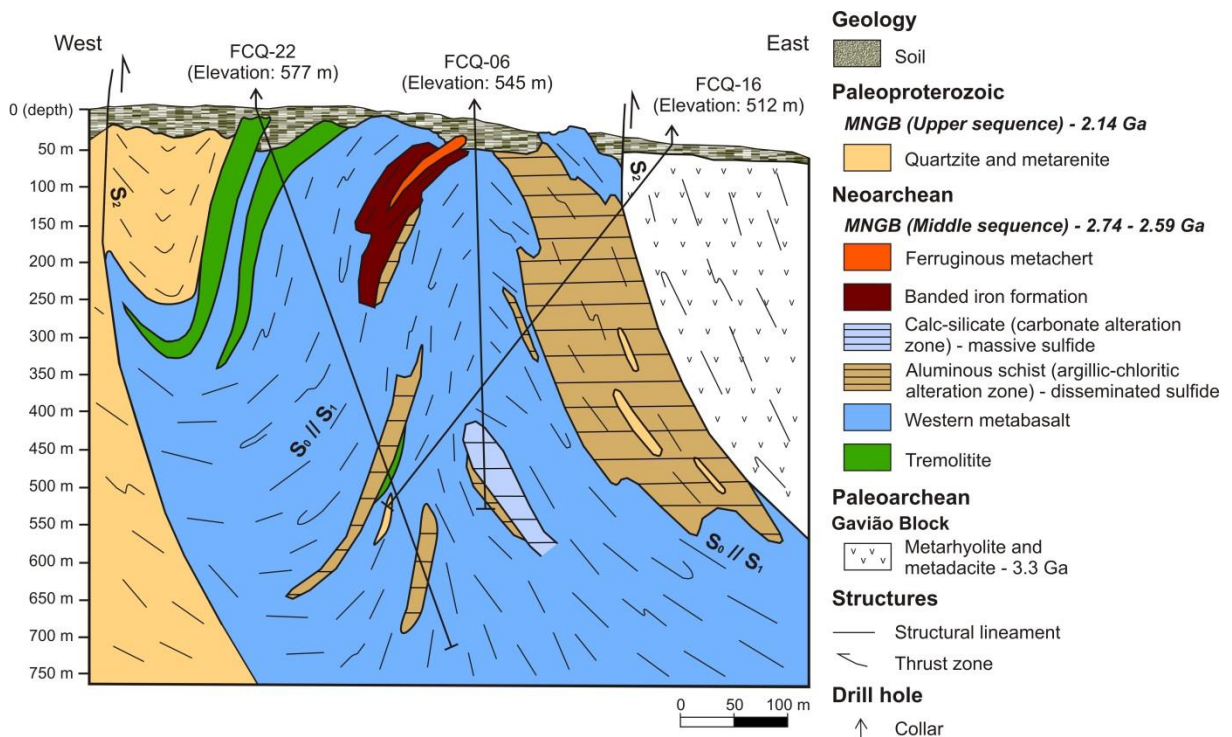
Figure 6. Geologic cross section of the Fazenda Coqueiro VMS deposit showing the antiform, the distribution of the western metabasalt and the hydrothermal alteration zones (calc-silicate rock and aluminous schist) based on outcrops and drill core descriptions. The site of the geologic cross section is represented in the geologic map of Figure 3.

The antiform outlined by the carbonate and argillic-chloritic hydrothermal alteration zones (Figure 7) encloses the Fazenda Coqueiro deposit and continues to a synform to the west. Like the antiform, the synform also has a north-south hinge line plunging to the south and limbs with high-angle dips.

The S_0 and S_1 structures were parallelized during the first west vergent deformational phase constituting the limbs of the antiform and synform that developed during the second west vergent deformational phase. This second deformational phase produced subvertical axial planes and thrust zones, both interpreted as S_2 structures. The concordance of the massive sulfide lens with the S_0 and S_1 structures and its subvertical position suggest that the massive sulfide zone may also be parallel to the subvertical S_2 structures.
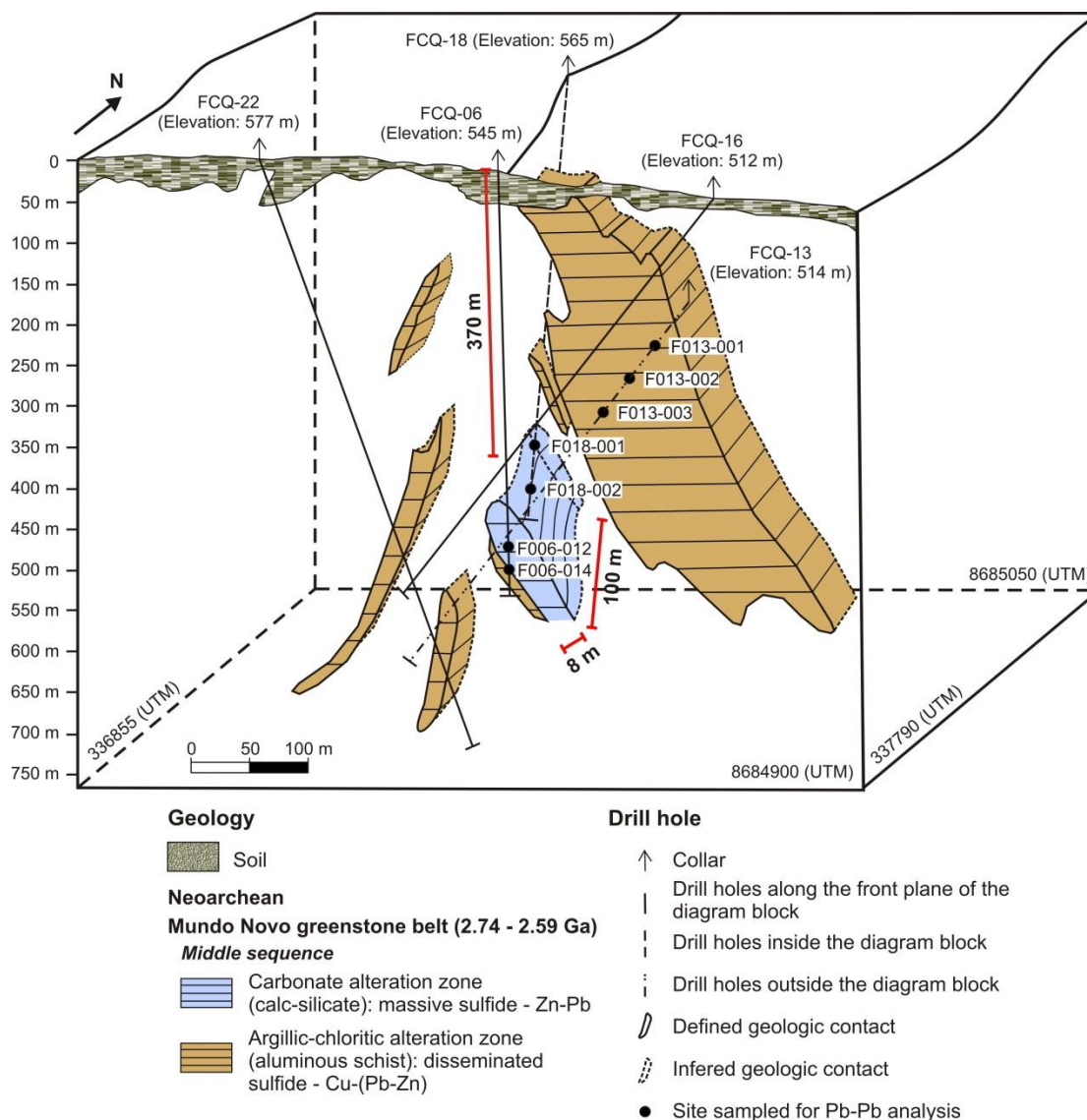
Figure 7. Block diagram of the Fazenda Coqueiro VMS deposit showing the distribution and geometry interpreted for hydrothermal alteration halos, the associated mineralization and the sites sampled for Pb-Pb analysis. Collar coordinates of the drill holes sampled: FCQ-06: W. Long.: 40° 29' 35.54"/ S. Lat.: 11° 53' 35.25"; FCQ-013: W. Long.: 40° 29' 24.71"/ S. Lat.: 11° 53' 37.09"; FCQ-018: W. Long.: 40° 29' 37.04"/ S. Lat.: 11° 53' 30.44".

Pb-Pb geochronology of sulfides

The twelve sulfide samples for Pb-Pb geochronology analysis were collected from cores of three drill holes in the Fazenda Coqueiro deposit: FCQ-06, FCQ-12 and FCQ-18 (Figures 3 and 7). The five samples collected from drill hole FCQ-06 are F006-012a, F006-012b, F006-012c, F006-012d and F006-014; the three samples collected from drill hole FCQ-13 are F013-001, F013-002 and F013-003; and the four samples collected from drill hole FCQ-18 are F018-001a, F018-001b, F018-002 and F018-002L (Figure 8). The F018-002L sample generated three more samples through the leached preparation technique, which were used in the tectonic source diagrams. All isotopic results obtained and used for diagram plots are presented in Table 2.

Table 2. Isotopic data for sulfide samples from the Fazenda Coqueiro VMS deposit used for geochronological study.

Sample	Mineral* analyzed	Host rock	Preparation technique	$^{206}Pb/^{204}Pb$	2σ	$^{207}Pb/^{204}Pb$	2σ	$^{208}Pb/^{204}Pb$	2σ
F006-12a	Sp	Carbonate zone	Whole digestion	13.884	0.002	14.855	0.002	33.662	0.006
F006-12b	Sp	Carbonate zone	Whole digestion	13.783	0.001	14.825	0.001	33.547	0.003
F006-12c	Sp	Carbonate zone	Whole digestion	13.849	0.002	14.837	0.002	33.616	0.005
F006-12d	Sp	Carbonate zone	Whole digestion	13.766	0.002	14.824	0.002	33.528	0.005
F006-014	Gn	Rich-silica level	Galena analysis	13.742	0.002	14.816	0.002	33.495	0.010
F013-001	Ccp	Argillic-chloritic zone	Whole digestion	24.836	0.043	16.952	0.028	43.039	0.073
F013-002	Ccp	Argillic-chloritic zone	Whole digestion	17.143	0.044	15.355	0.040	36.853	0.100
F013-003	Ccp	Argillic-chloritic zone	Whole digestion	16.460	0.022	15.369	0.022	36.148	0.053
F018-001a	Sp	Carbonate zone	Whole digestion	36.809	0.028	17.220	0.013	36.941	0.027
F018-001b	Sp	Carbonate zone	Whole digestion	13.759	0.001	14.832	0.002	33.556	0.006
F018-002	Ccp	Carbonate zone	Whole digestion	13.819	0.001	14.856	0.001	33.614	0.004
F018-002-L1	Ccp	Carbonate zone	Leached fraction	13.814	0.001	14.905	0.002	33.749	0.004
F018-002-L2	Ccp	Carbonate zone	Leached fraction	13.798	0.003	14.883	0.003	33.684	0.008
F018-002-L3	Ccp	Carbonate zone	Leached fraction	13.842	0.004	14.951	0.004	33.885	0.009

*Mineral abbreviations: Ccp: chalcopyrite, Gn: galena and Sp: sphalerite.

A galena grain sampled from a silica-rich level of the argillic-chloritic alteration zone in the FCQ-06 drill hole and sphalerite and chalcopyrite grains sampled from the carbonate alteration zone (massive sulfide) in the FCQ-18 drill hole core were used to determine the model ages. These ages have naturally high errors because they take into consideration Pb evolution in the Earth according the Stacey and Kramers (1975) model, which is certainly not obeyed in all geological cases. However, the similarity (we can say that the ages are the same) of the results obtained for the three samples show that the model was obeyed, in addition to indicating a unique and isotopically homogeneous source for the three analyzed sulfides. Thus, the galena yields a model age of 2804 ± 11.15 Ma (Figure 9A), the chalcopyrite yields a model age of 2794 ± 11.2 Ma (Figure 9B), and the sphalerite yields a model age of 2767 ± 11.1 Ma (Figure 9C), indicating the moment that Pb was separated from the terrestrial reservoir to form the analyzed minerals.
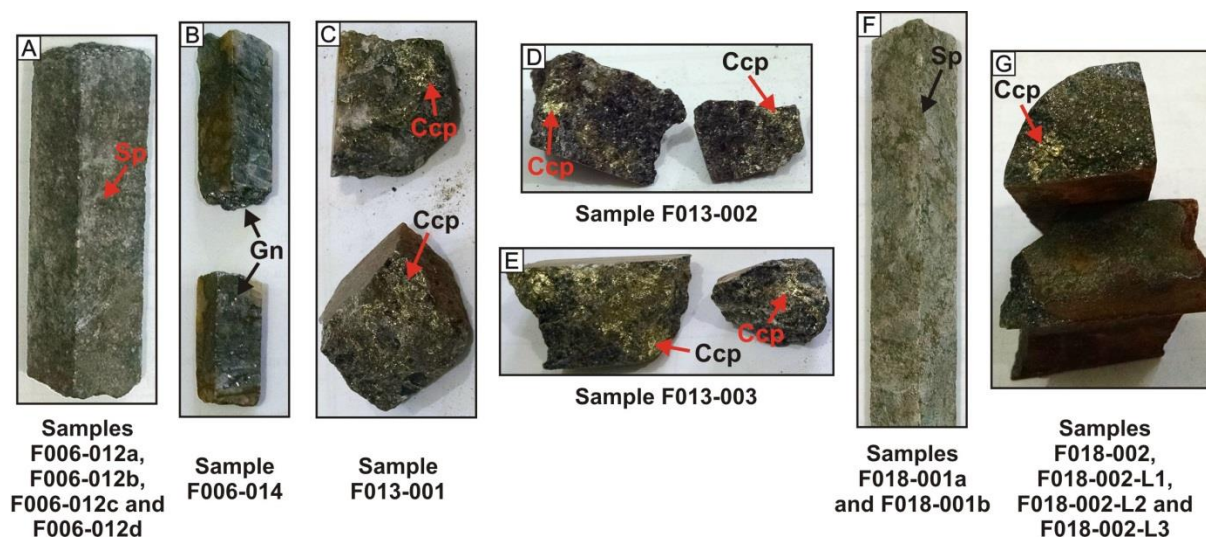
Figure 8. Drill cores used for Pb-Pb geochronological study of sulfides from the Fazenda Coqueiro VMS deposit. A) Carbonate hydrothermal alteration core with massive sphalerite from which four samples were obtained for the source study. B) Silica-rich core level in the argillic-chloritic alteration zone with galena sampled for model age study. C), D) and E) Argillic-chloritic hydrothermal alteration cores with disseminated chalcopyrite sampled for crystallization age and source study. F) Carbonate hydrothermal alteration core with massive sphalerite from which two samples were obtained for model and crystallization ages and source study. G) Carbonate hydrothermal alteration core with chalcopyrite from which four samples (whole digestion and leached fractions) were obtained for model and crystallization ages and source study. Mineral abbreviations: Ccp: chalcopyrite, Gn: galena and Sp: sphalerite.

Samples F013-001 (chalcopyrite), F013-002 (chalcopyrite) and F013-003 (chalcopyrite) collected from the argillic-chloritic alteration zone in drill hole FCQ-013 and samples F018-001b (sphalerite) and F018-002 (chalcopyrite) collected from the carbonate alteration zone (massive sulfide) in drill hole FCQ-18 were used for isochron determination according to the Ludwig (2008) algorithm. The first isochron yielded a crystallization age of 2753 Ma with a deviation of 210 Ma and a very high MSWD of 68 (Figure 10A). However, using three points, samples F013-001 (chalcopyrite) and F013-003 (chalcopyrite) from the argillic-chloritic alteration zone and sample F018-002 (chalcopyrite) from the carbonate alteration zone, the isochron yielded a crystallization age of 2747 ± 16 Ma with a deviation satisfactorily low and an ideal MSWD near one (Figure 10B). The age obtained using a greater diversity of samples, including sphalerite, is practically the same as the age obtained using three chalcopyrite samples. However, the last age obtained is more accurate. Therefore, 2747 ± 16 Ma is interpreted as the crystallization age of the sulfides analyzed.
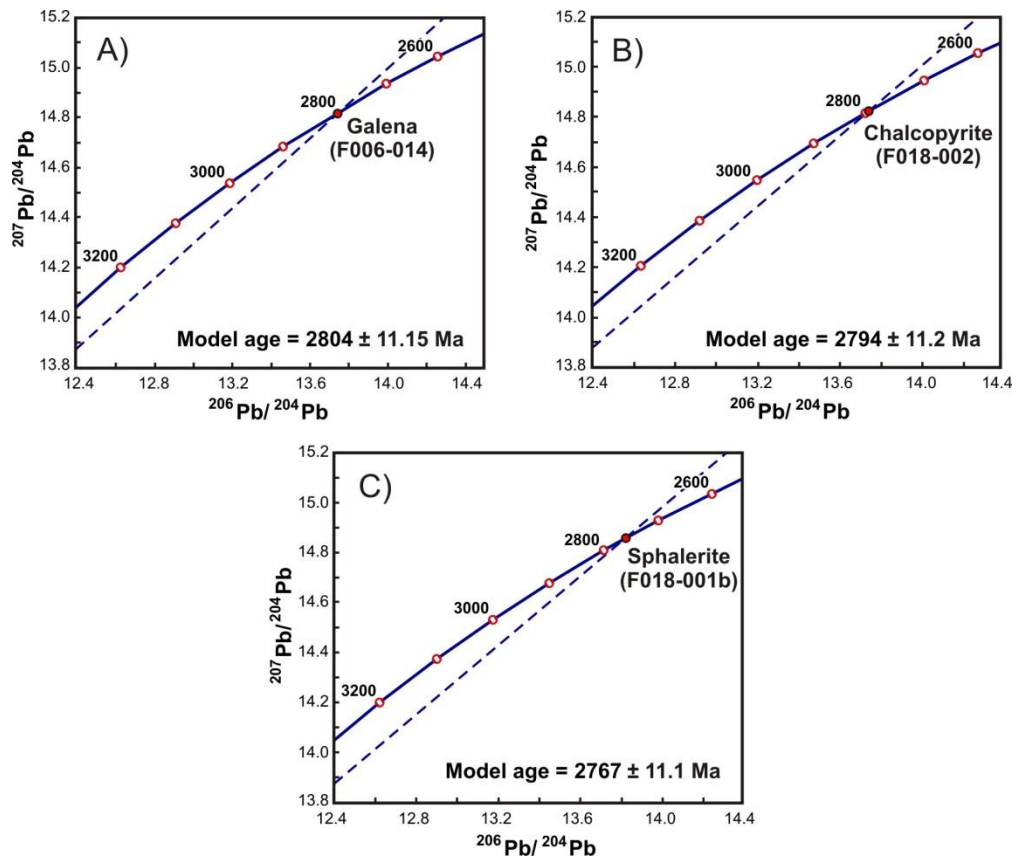
Figure 9. ^{206}Pb/^{204}Pb vs. ^{207}Pb/^{204}Pb diagram for model age determination for three sulfide samples from the Fazenda Coqueiro VMS deposit: A) Galena sample from the silica-rich level in the argillic-chloritic alteration zone. B) Chalcopyrite sample from the carbonate and massive sulfide zone. C). Sphalerite sample from the carbonate and massive sulfide zone.
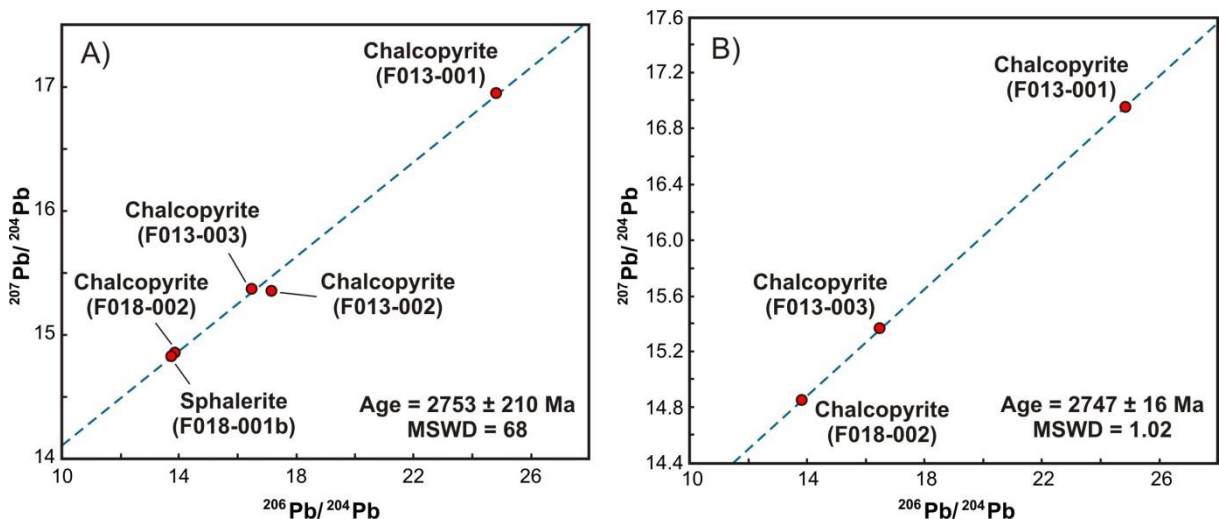
Figure 10. Detail of the isochron on the ^{206}Pb/^{204}Pb vs. ^{207}Pb/^{204}Pb diagram to determine the crystallization age of sulfides from the Fazenda Coqueiro VMS deposit. A) Detailed isochron using five sulfide samples yields an age of 2753 ± 210 Ma with, however, a high MSWD of 68. B) Detailed isochron using one sample of chalcopyrite from the massive sulfide zone (F018-002) and two samples of chalcopyrite from the disseminated sulfide zone in the argillic-chloritic alteration halo (F013-001 and F013-003) that yield an age of 2747 ± 16 Ma and MSWD of 1.02.

The thorogenic (^{208}Pb-^{206}Pb) and uranogenic (^{207}Pb-^{206}Pb) diagrams follow the Zartman and Doe (1981) model, where the curves represent the tectonic settings of mantle, lower crust, upper crust and orogen/mixture. On the thorogenic diagram (Figure 11A), the samples plot near the upper crust curve, but they are nearer the mantle and orogen curves,

which are close together in this diagram. On the uranogenic diagram (Figure 11B), the samples are near the upper crust and orogen, but they move away from the mantle curve. Only two points are far from the set and are near the mantle and lower crust curves. Therefore, in terms of tectonic setting, according these models, we suggest that the Pb that composes the sulfides would be more coherent with an origin from the upper crust.
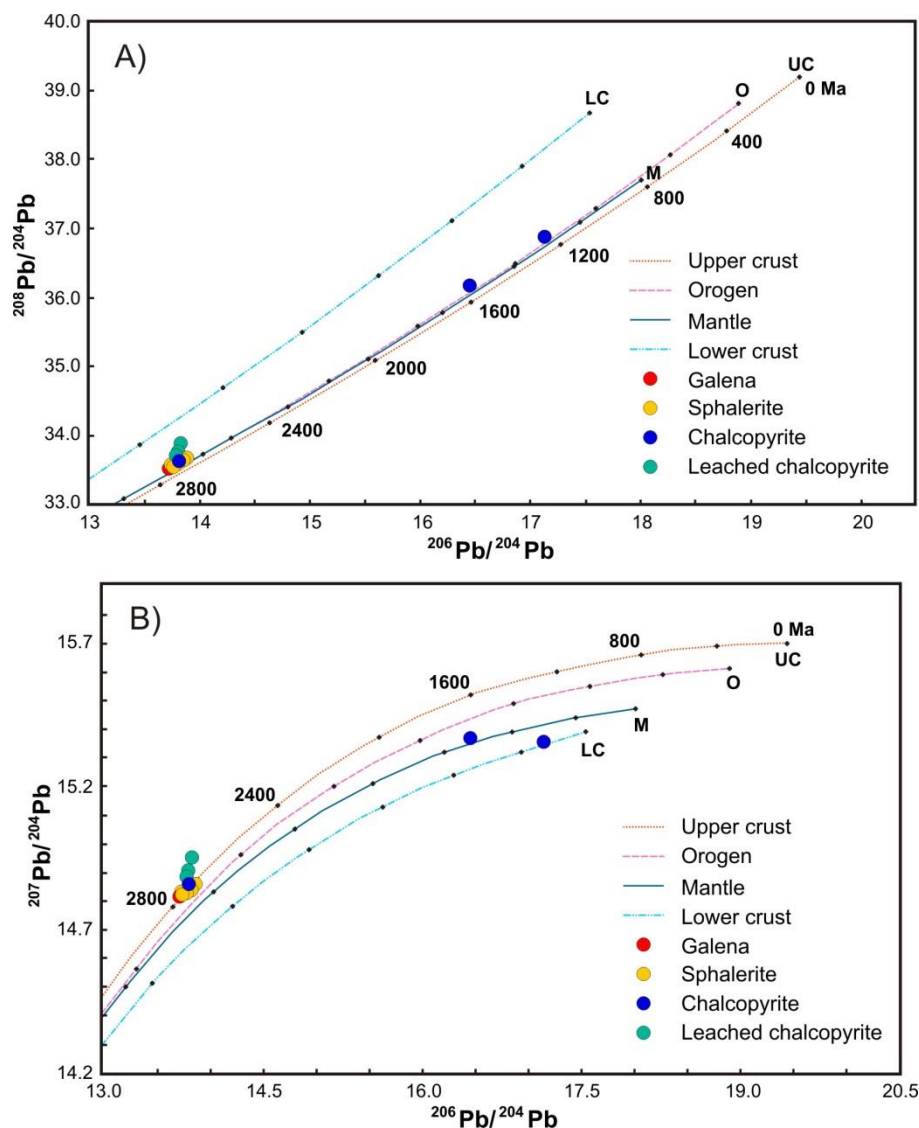
Figure 11. A) Thorogenic and B) uranogenic diagrams (Zartman and Doe, 1981) used for source study of the sphalerite, galena and chalcopyrite samples from the Fazenda Coqueiro VMS deposit.

DISCUSSION

The sphalerite analyses from samples F006-12a, F006-12b, F006-12c and F006-12d, each with different mass, yield isotopic results that are close but not exactly the same, such as the different isotopic values for sphalerite from samples F018-001a and F018-001b. This result indicates that the sphalerite grains analyzed from the massive sulfide zone are distinct, suggesting that they are not perfectly homogeneous or show inclusions or blends with other minerals.

The similarity among the model ages of galena, chalcopyrite and sphalerite, 2804 ± 11.15 Ma, 2794 ± 11.2 Ma and 2767 ± 11.1 Ma, respectively, and the isochron age of 2747 ± 16 Ma suggest coherence in the data set, indicating an initial isotopic homogeneity and a

common evolutionary history until the formation of the sulfides. The crystallization age of sulfides obtained by the isochron is approximately 2595 Ma (Spreafico et al., 2019) from a metadacite occurrence in the central-north portion of the MNGB. Further, the isochron age of 2747 Ma can be interpreted as synchronous to ocean floor basaltic volcanism, and the interval of 152 Ma can be estimated as the period of existence of oceanic crust during the Neoarchean when the Fazenda Coqueiro VMS deposit formed.

The geochronological data suggest a coeval paragenesis for sulfides in both the massive and disseminated mineralized zones. The genesis of the western metabasalt and the argillic-chloritic and carbonate alteration zones seems to be related to the same ocean floor volcanic event. Moreover, a possible sulfide remobilization during the Rhyacian-Orosirian tectonic event is not confirmed based on Pb-Pb sulfide geochronological data. The broad distribution and variety of sulfide samples collected in different parageneses and rocks among the deposit and the absence of substitution and interdigitated textures observed in the backscattered images reinforce the hypothesis of low or no Paleoproterozoic activity able to considerably remobilize and recrystallize the sulfides previously formed during the Neoarchean.

Although the actinolite and plagioclase contents of the western metabasalt indicate low- to medium-temperature metamorphic facies between greenschist and amphibolite, showing that there was heat in the system, the absence of recrystallization in the sulfides suggests that the tensional structures developed were restricted and that the Rhyacian-Orosirian tectonic event was probably heterogeneous at the mineralization site. Therefore, the non-recrystallized sulfides show that a nucleus of less intense deformation along the limbs of folds in the Fazenda Coqueiro deposit may have been preserved.

The VMS model

Based on metabasalt and ocean floor hydrothermal halo occurrences, the syngenetic origin, and the back-arc and island arc patterns of the western metabasalt described in Spreafico et al. (2019), we propose the initial morphology of the Fazenda Coqueiro deposit according the classical VMS model of Hannington et al. (1998) and Galley et al. (2007) (Figure 12).

The central upflow zone, also described as silicified and pyritic stockworks or stringers in the VMS model, may yet be observed in the footwall of the deposit where the high-silica level, with mainly galena occurrences, occurs inserted in the argillic-chloritic alteration zone. However, this silicified level could also be interpreted as secondary conduits of the main deposit.

The argillic-chloritic alteration halo seems to be related to the chloritized halo of the VMS model of Hannington et al. (1998) and Galley et al. (2007). However, deposition of pelitic sediments on the ocean floor must also have contributed to the development of the aluminous halos distal to volcanic sources in the debris flow and metalliferous sediment zone of the VMS model (Figure 12). The formation of the massive sulfide comprising mainly sphalerite corresponds to compact ore and Zn-rich marginal facies of the model of Hannington et al. (1998) and Galley et al. (2007) (Figure 12). Carbonate precipitation on the ocean floor concomitant with volcanism seems to be a determinate for the massive concentration of sphalerite, showing the importance of carbonate as a chemical metallotect.

According to the VMS classification of Barrie and Hannington (1999), the Fazenda Coqueiro deposit is closer to the mafic-siliciclastic type, which contains significant amounts of carbonate within the siliciclastic rocks. In relation to the VMS deposit classification of Franklin et al. (2005), the pelitic-mafic mature oceanic back-arc seems more appropriate to classify the Fazenda Coqueiro deposit, where the predominant basaltic and subordinate pelitic

rocks of back-arc successions occur in juvenile and accreted arc assemblages. In both cases, the absence of felsic rocks (flows or volcaniclastic) coeval to the stratigraphic package of the Fazenda Coqueiro deposit also conforms with these classifications. Moreover, the pelitic contents in the Fazenda Coqueiro would be smaller than the mafic contents together with the absence of coarser siliciclastic rocks.
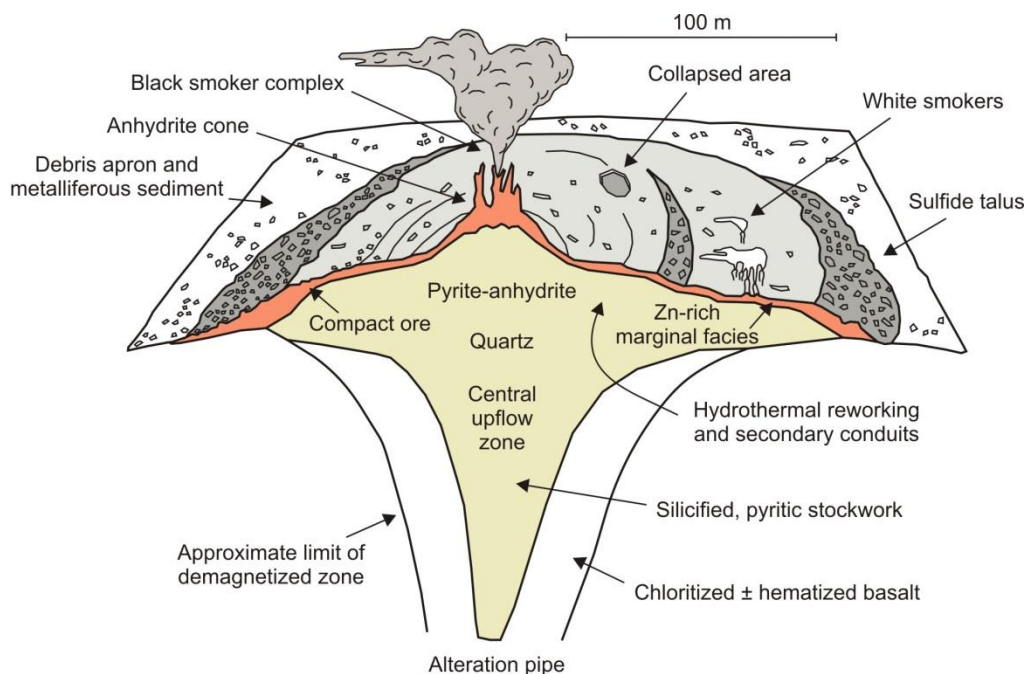
Figure 12. Classic cross section of a volcanogenic massive sulfide deposit. The concordant massive sulfide deposit is underlain by a discordant stockwork vein system (Central upflow zone) and associated alteration halo (alteration pipe). From Hannington et al. (1998) and Galley et al. (2007).

Regarding the source of the metals in the Fazenda Coqueiro deposit, contributions from the upper crust may have played an important role according the thorogenic and uranogenic diagrams for the Pb element. Therefore, the metals were probably transported during volcanism from the upper crust until their distribution and precipitation in the ocean floor setting, as proposed for the formation of the Fazenda Coqueiro VMS deposit. This proposal agrees with the most widely accepted source for metals and sulfur, where these elements are derived through high-temperature interactions between modified seawater and rock within the footwall strata of the VMS deposit (Franklin et al., 2005). The Cu precipitation correlated with temperature and the Zn content related primarily to pH, as discussed in Franklin et al. (2005), may explain the zoning of Cu occurrence in the alteration halos of the stringer zone and the Zn concentration in the strata on the ocean floor in the case of the Fazenda Coqueiro deposit.

The chemical trap on the ocean floor observed in the Fazenda Coqueiro deposit can be satisfactorily compared to the Garpenberg, Dammsjö and Garpenberg Norra VMS deposits in the Garpenberg District, Sweden. These deposits are interpreted as limestone-skarn Zn-Pb-Ag-Cu-Au deposits and as syn-volcanic stratabound subseafloor replacements (Allen et al., 1996). The relatively shallow water and limestone-associated variations in volcanic-associated massive sulfide ores and the ore deposition occurred by reaction of the ascending hydrothermal solutions with limestones below the ocean floor (Allen et al., 1996). This interpretation would be applicable to the genesis of the Zn-Pb massive sulfide deposit, with Ag and Au occurrences hosted in the carbonate alteration zone of the Fazenda Coqueiro deposit.

Regarding a more regional interpretation, the Fazenda Coqueiro deposit would have formed in a Neoarchean oceanic crust, most likely in a back-arc and/or island arc setting, developed between the Gavião and Mairi blocks (Figure 13A). Finally, the oceanic crust was compressed by the Rhyacian-Orosirian tectonic event imbricating the basement and the middle and upper sequences in the Fazenda Coqueiro deposit (Figure 13B). This event was coeval to the formation of the Contendas-Jacobina lineament when the area reached tectonic stability.
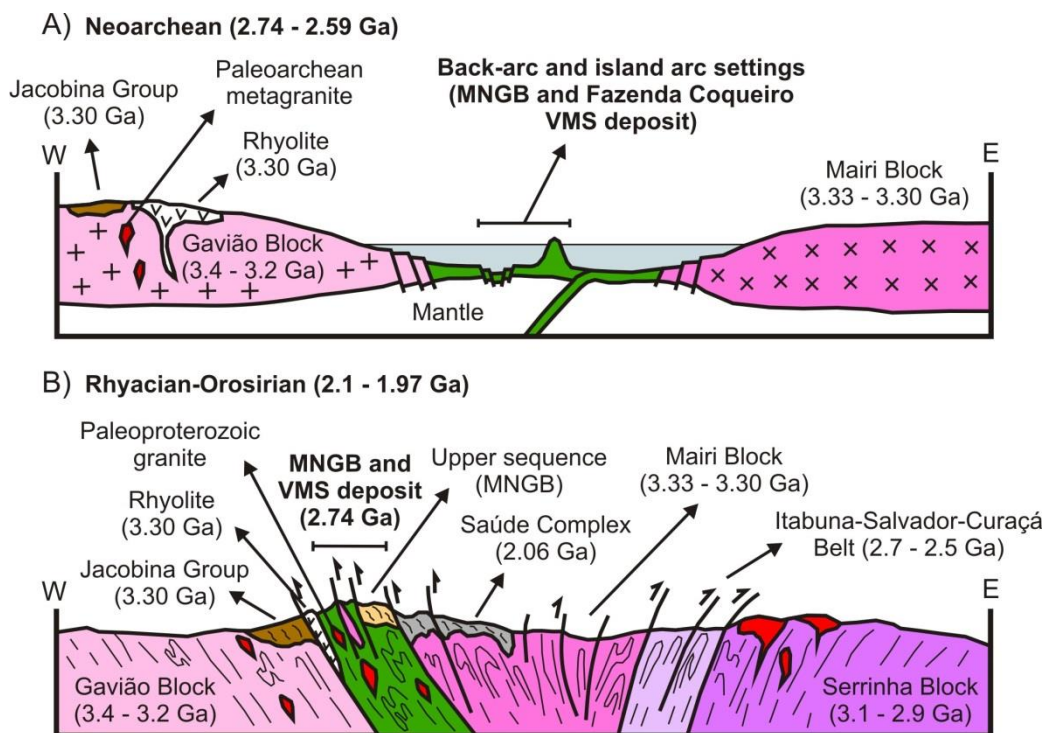
Figure 13. Intraoceanic setting of the MNGB and Fazenda Coqueiro deposit based on this study and compiled ages for the Gavião Block, MNGB and Rhyacian-Orosirian granites (Mougeot, 1996; Leite, 2002; Peucat et al., 2002; Zincone et al., 2016; Spreafico et al., 2019), Mairi Block (Sousa et al., 2018), Jacobina Group (Teles, 2013; Teles et al., 2015; Barbuena et al., 2016), Serrinha Block (Oliveira et al., 2002a, 2002b; Rios et al., 2009), Itabuna-Salvador-Curaçá Belt (Silva et al., 1997; Oliveira et al., 2010) and Saúde Complex (Barbuena et al., 2016; Zincone et al., 2017). A) Oceanic crust between the Gavião and Mairi blocks and formation of the Fazenda Coqueiro deposit at 2747 Ma. B) Rhyacian-Orosirian tectonic event that compressed the MNGB and the Fazenda Coqueiro deposit between the cratonic blocks of the eastern São Francisco Craton.

CONCLUSIONS

The Zn-Pb-rich massive sulfide lens of the Fazenda Coqueiro deposit is stratabound and hosted in the metamorphosed carbonate hydrothermal alteration zone that consists of previous carbonate-rich strata on the ocean floor. The Cu-rich disseminated sulfide levels are hosted in the metamorphosed argillic-chloritic hydrothermal alteration zone that is composed of previous pelitic strata on the ocean floor. Both alteration zones are interlayered in the western metabasalt.

According to the classic VMS model, the massive body of the Fazenda Coqueiro deposit corresponds to the Zn-rich marginal facies of the mount with lower occurrences of Pb, Cu, Ag and Au, and the Cu disseminated levels are associated with the distal halos of the main volcanic conduit in the alteration pipe or the debris apron with metalliferous sediments.

The Pb in galena, chalcopyrite and sphalerite was sourced from the upper crust between 2804 Ma and 2767 Ma, and the sulfides crystallized at 2747 Ma during volcanic processes in an ocean floor setting such as a back-arc basin or an island arc. Therefore, we

suggest that a main carbonate chemical trap reacted with hydrothermal solutions in a volcanic setting, changing the pH of the system and contributing to the formation of conditions for the precipitation of the Zn-Pb-rich massive sulfide. However, the temperature contrast between the proximal and distal zones relative to the volcanic source controlled the precipitation of disseminated chalcopyrite in pelitic zones.

Paleoproterozoic remobilization of the sulfides is not supported by the data presented in this study, suggesting that the Rhyacian-Orosirian tectonic event was heterogeneous at the mineralization site of the Fazenda Coqueiro deposit, preserving portions from deformation.

Based on the present model, remnant fragments of oceanic crust along the Contendas-Jacobina lineament with evidence of ocean floor hydrothermal activity are good guides to prospecting for VMS-type deposits similar to the Fazenda Coqueiro deposit.

ACKNOWLEDGEMENTS

REFERENCES

Allen, R.L., Lundström, I., Ripa, M., Simeonov, A., Christofferson, H. (1996). Facies analysis of a 1.9 Ga, Continental Margin, Back-Arc, Felsic Caldera Province with Diverse Zn-Pb-Ag-(Cu-Au) sulfide and Fe Oxide Deposits, Bergslagen Region, Sweden. *Economic Geology*, 91, 979-1008. https://doi.org/10.2113/gsecongeo.91.6.979

Barbosa, J. S. F., 1997. Síntese do Conhecimento sobre a Evolução Geotectônica das Rochas Metamórficas Arqueanas e Paleoproterozóicas do Embasamento do Cráton do São Francisco na Bahia. *Revista Brasileira de Geociências*, 27(3), 241-256. DOI:10.25249/0375-7536.1997241256

Barbosa, J.S.F., Cruz, S.C.P., Souza, J.S. (2012a). Terrenos metamórficos do embasamento. In: Barbosa, J.S.F. (Ed.), *Geologia da Bahia: Pesquisa e Atualização*, 1, 101-201. Salvador: CBPM. http://www.cbpm.ba.gov.br/modules/conteudo/conteudo.php?conteudo=24

Barbosa, J.S.F., Pinto, M.S., Cruz, S.C.P., Souza, J.S. (2012b). Granitoides. In: Barbosa, J.S.F. (Ed.), *Geologia da Bahia: Pesquisa e Atualização*, 1, 327-396. Salvador: CBPM. http://www.cbpm.ba.gov.br/modules/conteudo/conteudo.php?conteudo=24

Barbosa, J.S.F., Sabaté, P. (2002). Geological features and the Paleoproterozoic collision of four Archean crustal segments of the São Francisco Craton, Bahia, Brazil. A synthesis. *Anais da Academia Brasileira de Ciências*, Rio de Janeiro, 74(2), 343-359. http://dx.doi.org/10.1590/S0001-37652002000200009

Barbosa, J.S.F., Sabaté, P. (2003). Colagem paleoproterozoica de placas arqueanas do Cráton do São Francisco na Bahia. *Revista Brasileira de Geociências*, 33(1-suplemento), 7-14. DOI: 10.25249/0375-7536.200333S10714

Barbosa, J.S.F., Sabaté, P. (2004). Archean and Paleoproterozoic crust of the São Francisco Craton, Bahia, Brazil: geodynamic features. *Precambrian Research*, 133(1-2), 1-27. https://doi.org/10.1016/j.precamres.2004.03.001

Barbuena, D., Oliveira, E.P., Zincone, S.A. (2016). Estudos de proveniência dos quartzitos do Greenstone Belt Mundo Novo (BA) e implicações tectono-estratigráficas. *XLVIII Congresso Brasileiro de Geologia*, 818. Porto Alegre: SBG. http://cbg2017anais.siteoficial.ws/anais48cbgcompleto.pdf

Barrie, C.T., Hannington, M.D. (1999). Classification of Volcanic-Associated Massive Sulfide Deposits Based on Host-Rock Composition. In: C.T. Barrie, M.D. Hannington (Eds.), *Volcanic-Associated Massive Sulfide Deposits: Processes and Examples in Modern and Ancient Settings: Reviews in Economic Geology*, 8, 2-10. Canada: Geological Survey of Canada. https://doi.org/10.5382/Rev.08.01

Couto, P.A., Sampaio, A.R., Gil, C.A.A., Loureiro, H.C., Arcanjo, J.B., Fernandes Filho, J., Guimarães, J.T., Campelo, R., Mascarenhas, J.F., Bruni, D.C., Toledo, L.A.A. (1978). *Projeto Serra de Jacobina: Geologia e Prospecção Geoquímica*. Salvador: DNPM-CPRM. http://rigeo.cprm.gov.br/jspui/handle/doc/9602

Franklyn, J.M., Gibson, H.L., Jonasson, I.R., Galley, A.G. (2005). Volcanogenic Massive Sulfide Deposits. *Economic Geology*, 100th anniversary volume, 523-560. https://doi.org/10.5382/AV100.17

Galley, A.G., Hannington, M.D., Jonasson, I.R. (2007). Volcanogenic massive sulfide deposits. In: W.D. Goodfellow (Ed.), *Mineral deposits of Canada: A Synthesis of Major Deposit-Types, District Metallogeny, the Evolution of Geological Provinces, and Exploration Methods*, 5, 141-161. Ottawa: Geological Association of Canada. https://doi.org/10.2113/gsecongeo.102.7.1355

Hannington, M.D., Galley, A.G., Herzig, P.M., Petersen, S. (1998). Comparison of the Tag Mound and Stockwork Complex with Cyprus-type massive sulfide deposits. In: P.M. Herzig, S.E. Humphris, D.J. Miller, R.A. Zierenberg (Eds.), *Proceedings of the Ocean Drilling Program, Scientific Results*, 158, 389-415. College Station: Texas A&M University Digital Library. doi: 10.2973/odp.proc.sr.158.217.1998

Kretz, R. (1983). Symbols for rock–forming minerals. *American Mineralogist*, 68, 277-279. https://www.researchgate.net/publication/216831138_Symbols_for_rock-forming_minerals

Leal, L.R.B., 1998. *Geocronologia U/Pb (SHRIMP), 207Pb/206Pb, Rb/Sr, Sm/Nd e K/Ar dos Terrenos Granito-Greenstone do Bloco do Gavião: Implicações para a Evolução Arqueana e Paleoproterozoica do Cráton do São Francisco, Brasil*. Tese (Doutorado). São Paulo: Universidade de São Paulo - USP. http://www.teses.usp.br/teses/disponiveis/44/44134/tde-08012016-145912/pt-br.php

Leite, C.M.M., 2002. A Evolução Geodinâmica da Orogênese Paleoproterozóica nas Regiões de Capim Grosso, Jacobina e Pintadas - Mundo Novo (Bahia-Brasil): Metamorfismo, Anatexia Crustal e Tectônica. Ph. D. Thesis, Universidade Federal da Bahia, Salvador, 408 p.

Leite, C.M.M., Barbosa, J.S.F., Nicollet, C., Sabaté, P. (2007). Evolução metamórfica/metassomática paleoproterozóica do Complexo Saúde, da Bacia Jacobina e de leucogranitos peraluminosos na parte norte do Cráton do São Francisco. *Revista Brasileira de Geociências*, 37(4), 777-797. DOI: 10.25249/0375-7536.2007374777797

Ludwig, K.R. (2008). User's manual for ISOPLOT/EX: a geochronological toolkit for Microsoft Excel (version 3.68). *Special Publication (Berkeley Geochronology Center)*, 4, 171.

Magee, C.W., Palin, J.M., Taylor, W.R. (2001). Laser ICP-MS U/Pb analyses of detrital zircons from Proterozoic sediments in Bahia state, Brazil; implications for the evolution of the São Francisco craton prior to 3.3 Ga. *XI V.M. Goldschmidt Conference*, 3501. Hot Springs - Geochemical Society. https://www.lpi.usra.edu/meetings/gold2001/pdf/3501.pdf

Mascarenhas, J.F., Ledru, P., Souza, S.L., Filho, V.M.C., Melo, L.F.A., Lorenzo, C.L., Milesi, J.P. (1998). Geologia e recursos minerais do Grupo Jacobina e da parte sul do Greenstone Belt de Mundo Novo. *Série Arquivos Abertos (CBPM)*, 13, 1-58. http://www.cbpm.ba.gov.br/modules/conteudo/conteudo.php?conteudo=23

Monteiro, M.D., Silva, R.W.S., Cunha, J.C. (2009). *Projeto Fazenda Coqueiro.* Salvador: CBPM.

Mougeot, R. (1996). *Étude de la limite Archéen-Protérozoïque et des minéralisations Au ± U associées. Exemples de la région de Jacobina (Etat de Bahia, Brésil) et de Carajas (Etat de Para, Brésil).* Thèse (Doctorat). Montpellier: Université de Montpellier II. http://www.theses.fr/1996MON20131

Oliveira, E.P., Mcnaughton, N.J., Armstrong, R. (2010). Mesoarchaean to Paleoproterozoic growth of the northern segment of the Itabuna-Salvador-Curaçá orogeny, São Francisco Cráton, Brazil. In: Kusky, T.M., Zhai, M.G., Xiao, W. (Eds.), The evolving continents: understanding processes of continental growth. London: Geological Society Special Publication, 338, 263-286. https://doi.org/10.1144/SP338.1

Oliveira, E.P., Mello, E.F., Mcnaughton, N. (2002a). Reconnaissance U–Pb geochronology of Precambrian quartzites from the Caldeirão belt and their basement, NE São Francisco Craton, Bahia, Brazil: implications for the early evolution of the Paleoproterozoic Itabuna-Salvador-Curaçá orogeny. *Journal of South American Earth Sciences*, 15(3), 349-362. https://doi.org/10.1016/S0895-9811(02)00039-1

Oliveira, E.P., Mello, E.F., McNaughton, N.J., Choudhuri, A. (2002b). SHRIMP U-Pb age of the basement to the Rio Itapicuru Greenstone Belt, NE São Francisco craton. *XLI Congresso Brasileiro de Geologia*, 522. João Pessoa: SBG.

Peucat, J.J., Mascarenhas, J.F., Barbosa, J.S.F., Souza, S.L., Marinho, M.M., Fanning, C.M., Leite, C.M.M. (2002). 3,3 Ga SHRIMP U-Pb zircon age of a felsic metavolcanic rock from the Mundo Novo Greenstone Belt in the São Francisco Craton, Bahia (NE Brazil). *Journal of South American Earth Sciences*, 15, 363-373. https://doi.org/10.1016/S0895-9811(02)00044-5

Reis, C., Menezes, R.C.L., Miranda, D.A., Santos, F.P., Loureiro, H.C., Neves, J.P., Viera, R. (2017). *Mapa geológico-geofísico: Projeto ARIM Serra de Jacobina*. Salvador: CPRM. http://rigeo.cprm.gov.br/jspui/handle/doc/18679

Reis, C., Oliveira, R.C.L., Miranda, D.A., Santos, F.P., Guimarães, J.T., Teles, G. (2018). Estratigrafia do grupo Jacobina. *XLIX Congresso Brasileiro de Geologia*, 1232. Rio de Janeiro: SBG. http://cbg2018anais.siteoficial.ws/resumos/7641.pdf

Rios, D.C., Davis, D.W., Conceição, H., Davis, W.J., Rosa, M.L.S., Dickin, A.P. (2009). Geologic evolution of the Serrinha nucleus granite-greenstone terrane (NE Bahia, Brazil) constrained by U-Pb single zircon geochronology. *Precambrian Research*, 170(3-4), 175-201. https://doi.org/10.1016/j.precamres.2008.10.001

Siivola, J., Schmid, R. (2007). *A systematic nomenclature for metamorphic rocks. List of mineral abbreviations. Recommendations by the IUGS Subcommission on the Systematics of Metamorphic Rocks*. USA - IUGS, <https://www.bgs.ac.uk/downloads/start.cfm?id=3197>.

Silva, L.C., Armstrong, R., Delgado, I.M., Pimentel, M., Arcanjo, J.B., Melo, R.C., Teixeira, L.R., Jost, H., Cardoso Filho, J.M., Pereira, L.H.M. (2002). Reavaliação da evolução geológica em terrenos Pré-Cambrianos brasileiros com base em novos dados U-Pb SHRIMP, Parte I: Limite centro-oriental do Cráton São Francisco na Bahia. *Revista Brasileira de Geociências*, 32(4), 501-512. DOI: 10.25249/0375-7536.2002324501512

Silva, L.C., McNaughton, N.J., Melo, R.C., Fletcher, I.R. (1997). U-Pb SHRIMP ages in the Itabuna-Caraíba TTG high-grade complex: the first window beyond the Paleoproterozoic overprinting of the eastern Jequié Craton, NE Brazil. *International Symposium on Granites and Associated Mineralization*, 1, 282-283. Salvador. https://www.researchgate.net/publication/284106273

Sousa, D.F.M., Oliveira, E.P., Amaral, W.S. (2018). Geologia e geocronologia U-Pb em zircão de ortognaisses e K-granitoides relacionados ao Bloco Gavião (Complexo Mairi) e Cinturão Salvador-Curaçá – Região da Mina Caraíba – Bahia. *XLIX Congresso Brasileiro de Geologia*, 980. Rio de Janeiro: SBG. http://cbg2018anais.siteoficial.ws/resumos/8534.pdf

Souza, S.L., Garrido, I.A.A., Oliveira, N.S., Fróes, R.J. (2002). Projeto Greenstone Belt de Mundo Novo: estudos geológicos regionais. Salvador: CBPM, 1, 62 p.

Spreafico, R.R. (2017). *Projeto Mundo Novo: texto e mapas*. Salvador: CBPM.

Spreafico, R.R., Barbosa, J.S.F., Barbosa, N.S., Moraes, A.M.V. (2019). Tectonic evolution of the Neoarchean Mundo Novo greenstone belt, eastern São Francisco Craton, NE Brazil: petrology, U-Pb geochronology, and Nd and Sr isotopic constraints. *Journal of South American Earth Sciences*, 95. https://doi.org/10.1016/j.jsames.2019.102296

Stacey, J.S., Kramers, J.D. (1975). Approximation of terrestrial lead isotope evolution by a two stage model. *Earth and Planetary Science Letters*, 26(2), 207-221. https://doi.org/10.1016/0012-821X(75)90088-6

Teles, G.S. (2013). *Proveniência e idades de deposição dos sedimentos auríferos da Bacia de Jacobina: Implicações sobre a evolução da bacia durante o Paleo-Arqueano e a gênese da mineralização*. Dissertação (Mestrado). Brasília: Instituto de Geociências - UnB. http://repositorio.unb.br/handle/10482/14972

Teles, G.S., Chemale, F., Oliveira, C.G. (2015). Paleoarchean record of the detrital pyrite-bearing, Jacobina Au-U deposits, Bahia, Brazil. *Precambrian Research*, 256, 289-313. https://doi.org/10.1016/j.precamres.2014.11.004

Wilson, N. (1987). *Combined Sm-Nd, Pb-Pb and Rb-Sr geochronology and isotope geochemistry in polymetamorphic precambrian terrains: examples from Bahia, Brazil and Channel Island*. Dissertation (Master). Oxford: Oxford University.

Zartman, R.E., Doe, B.R. (1981). Plumbotectonics - the model. *Tectonophysics*, 75(1-2), 135-162. https://doi.org/10.1016/0040-1951(81)90213-4

Zincone, S.A., Barbuena, D., Oliveira, E.P., Baldim, M.R. (2017). Detrital zircon U-Pb ages as evidence for deposition of the Saúde Complex in a Paleoproterozoic foreland basin, northern São

Francisco Craton, Brazil. *Journal of South American Earth Sciences*, 79, 537-548. https://doi.org/10.1016/j.jsames.2017.09.009

Zincone, S.A., Oliveira, E.P., Laurent, O., Zhang, H., Zhai, M. (2016). 3,3 Ga High-Silica Intraplate Volcanic-Plutonic System of the Gavião Block, São Francisco Craton, Brazil: Implications of an intracontinental rift following the creation of insulating continental crust. *Lithos*, 266, 414-434. https://doi.org/10.1016/j.lithos.2016.10.011

CAPÍTULO 5
CONCLUSÕES

Com base em novos dados geológicos, petrográficos, litogeoquímicos, geocronológicos e isotópicos obtidos no GBMN e no depósito de Zn e Pb da Fazenda Coqueiro, apresentados nesta Tese, conclui-se que:

• O GBMN mostra padrões litológicos e geoquímicos de proveniência intraoceânica, semelhante a outras sequências metavulcanossedimentares inseridas no Lineamento Contendas-Jacobina, incluindo a sequência metavulcanossedimentar Contendas-Mirante. O GBMN também possui similaridades geológicas, como estruturas *pillow lavas* e associações com sedimentos químicos e rochas vulcânicas, e similaridades tectônicas, como origem em ambientes de fundo oceânico, com relação a outros *greenstone belts* de outras regiões do Cráton do São Francisco, como por exemplo, o *greenstone belt* Rio das Velhas, no estado de Minas Gerais.

• O metakomatiito e os metabasaltos leste e oeste se formaram em ambientes próximos, como bacia de *back-arc* e arco de ilha, com padrões geoquímicos do tipo MORB, principalmente para o metabasalto oeste, mas também para algumas amostras do metabasalto leste, e IAT, somente para o metabasalto leste. Possíveis assimilações crustais das rochas vulcânicas no sistema arco-bacia levaram ao enriquecimento destas rochas em Cs, Ba, Th e ETR leves. Entretanto, o evento tectonotermal compressional Riaciano-Orosiriano deve ter contribuído para um maior enriquecimento destes elementos no metabasalto oeste, que foi sobreposto às rochas do Bloco Gavião durante o tectonismo compressional e também formou lascas tectônicas no embasamento oeste do GBMN. Por sua vez, tanto o metakomatiito quanto o metabasalto leste, diferentemente do anterior, devem ter sido afetados principalmente pelas assimilações intraoceânicas. O tectonismo Riaciano-Orosiriano, no entanto, deve ter sido heterogêneo nestas rochas, pois as texturas primárias como a *spinifex* no metakomatiito, e as estruturas primárias no metabasalto leste, como as *pillow lavas*, foram preservadas.

• As particularidades mineralógicas entre os metabasaltos leste e oeste do GBMN são produtos de assimilações crustais durante processos metamórficos do Riaciano-Orosiriano. Entretanto, diferenças mineralógicas primárias podem ter permanecido, visto que os processos vulcânicos ocorreram em ambientes distintos, porém, próximos (*back-arc* e arco de ilha).

• O Bloco Gavião, estabilizado desde 3,35 Ga (representado pelo granito Miguel Calmon), foi fraturado pelo processo de rifteamento que gerou riolitos. Posteriormente, granitos, como o anorogênico Fazenda Coqueiro, se formaram em 3,22 Ga, provavelmente derivados da crosta inferior tendo como fonte plútons TTG e granulitos máficos ou intermediários.

• O metakomatiito da sequência inferior do GBMN e os metabasaltos leste e oeste e o metadacito da sequência média do GBMN parecem estar relacionados pelo processo de cristalização fracionada. Portanto, o metadacito formado em 2,59 Ga, o metakomatiito e os metabasaltos são evidências de vulcanismos Neoarqueanos formados no sistema arco-bacia em ambiente de fundo oceânico.

• A colisão dos blocos Gavião e Mairi, no Riaciano-Orosiriano, incluindo a crosta oceânica do GBMN, foi marcada por uma granitogênese tardia que produziu granitos levemente peraluminosos como o Areia Branca e o Jequitibá, derivados de protólitos crustais

Arqueanos. Este evento foi marcado também pela existência de cavalgamentos e dobras vergentes para oeste. Durante o processo de fechamento e do *uplift* resultante, rochas do GBMN e os granitos Riacianos-Orosirianos devem ter contribuído com material detrítico para a formação das rochas sedimentares da sequência superior do GBMN. Além disso, o Complexo Saúde se formou possivelmente no mesmo tempo da sequência superior do GBMN, embora o primeiro tenha sido submetido a um grau metamórfico mais alto.

• Cinco estágios são propostos para a evolução tectônica do GBMN: estágios (i) e (ii), entre 3,35 Ga e 3,22 Ga, que correspondem aos processos de riftamento e fechamento tectônico no Bloco Gavião; estágio (iii) em 2,59 Ga, que corresponde ao vulcanismo komatiítico, basáltico e dacítico entre os blocos Gavião e Mairi, e estágios (iv) e (v), entre 2,10 Ga e 1,97 Ga, que correspondem aos dois estágios de colisão progressiva no qual o GBMN foi amalgamado entre os blocos cratônicos da porção leste do Cráton do São Francisco.

• A lente de sulfeto maciço rica em Zn e Pb do depósito da Fazenda Coqueiro é *stratabound* e está hospedada na zona de alteração hidrotermal carbonática, metamorfisada na fácies anfibolito, que consiste de estratos ricos em carbonato superpostos ao assoalho oceânico. Os níveis de sulfeto de Cu disseminado estão hospedados em zona de alteração hidrotermal argílica-clorítica, representante de estratos pelíticos de fundo oceânico. Ambas as zonas de alteração estão intercaladas no metabasalto oeste.

• De acordo com o modelo clássico de depósitos do tipo VMS, o corpo maciço do depósito da Fazenda Coqueiro corresponde à fácies marginal do *mount*, rica em Zn, com menores ocorrências de Pb, Cu, Ag e Au. Deve-se ressaltar que os níveis de sulfeto de Cu disseminado estão associados aos halos distais do conduto vulcânico principal do pipe de alteração ou aos desníveis distais onde se acumularam sedimentos metalíferos.

• O Pb que ocorre na galena, na calcopirita e na esfalerita se originou na crosta vulcânica entre 2804 Ma e 2767 Ma, embora os sulfetos tenham se cristalizado em 2747 Ma durante processos vulcânicos em ambientes de fundo oceânico, tais como arco de ilha e bacia de *back-arc*. Portanto, sugere-se que um metalotecto químico e carbonático principal reagiu com soluções hidrotermais no ambiente vulcânico, alterando o pH do sistema e contribuindo para a formação de condições redutoras que levaram à precipitação de esfalerita no nível de sulfeto maciço. Entretanto, o contraste de temperatura entre as zonas proximais and distais, em relação à fonte vulcânica, deve ter controlado a precipitação da calcopirita nas porções pelíticas.

• Processos de remobilização de sulfetos durante o Paleoproterozoico não são significativos diante dos dados apresentados neste trabalho, sugerindo que o evento tectônico Riaciano-Orosiriano tenha sido heterogêneo no local da mineralização da Fazenda Coqueiro. Dessa forma, porções da mineralização teriam sido preservadas durante o processo de deformação.

• Por fim, com base no modelo apresentado para a gênese do depósito da Fazenda Coqueiro, sugere-se que fragmentos remanescentes de crosta oceânica, ao longo do Lineamento Contendas-Jacobina, com evidências de atividade hidrotermal de fundo oceânico, sejam bons guias para a prospecção de depósitos do tipo VMS, similares ao depósito da Fazenda Coqueiro.

APÊNDICE A - JUSTIFICATIVA DA PARTICIPAÇÃO DOS COAUTORES

Antônio Marcos Vitória de Moraes (Artigos 1 e 2) - Geólogo da Companhia Baiana de Pesquisa Mineral, deu contribuições na área de petrografia.

Francisco Dias de Souza Júnior (Artigo 1) - Geólogo da Companhia Baiana de Pesquisa Mineral, participou de trabalhos de campo e contribuiu com discussões sobre a área de estudo.

Marco Antônio Galarza (Artigo 3) - Professor do Instituto de Geociências da Universidade Federal do Pará, auxiliou na análise isotópica Pb-Pb de sulfetos, realizada no Laboratório de Geologia Isotópica/UFPA, e no tratamento de dados.

Moacir José Buenano Macambira (Artigo 3) - Professor do Instituto de Geociências da Universidade Federal do Pará, orientou sobre os procedimentos de preparação de amostras e análises geocronológicas Pb-Pb de sulfetos realizadas no Laboratório de Geologia Isotópica/UFPA. Também auxiliou na interpretação dos dados obtidos.

Natali Silva Barbosa (Artigo 2) - Professora do Núcleo de Geologia Básica/Universidade Federal da Bahia, deu apoio laboratorial para as análises de geocronologia U-Pb e de isótopos de Nd e Sr de metagranitos e metadacitos realizadas no Centro de Pesquisas Geocronológicas do Instituto de Geociências da Universidade de São Paulo. A Profa. Natali também auxiliou na interpretação dos dados obtidos.

ANEXO A - REGRAS DE FORMATAÇÃO DA REVISTA "BRAZILIAN JOURNAL OF GEOLOGY" (ARTIGO 1)

SCOPE AND POLICY

Aims and scope

The Brazilian Journal of Geology (BJG) is a quarterly journal published by the Brazilian Geological Society with an electronic open access version that provides an internacional medium for the publication of original scientific work of broad interest concerned with all aspects of the earth sciences in Brazil, South America, and Antarctica, in-cluding oceanic regions adjacent to these regions. The BJG publishes papers with a regional appeal and more than local significance in the fields of mineralogy, petrology, geochemistry, paleontology, sedimentology, stratigraphy, structural geology, tectonics, neotectonics, geophysics applied to geology, volcanology, metallogeny and mineral deposits, marine geology, glaciology, paleoclimatology, geochronology, biostratigraphy, engineering geology, hydrogeology, geological hazards and remote sensing, providing a niche for interdisciplinary work on regional geology and Earth history.

The BJG publishes articles (including review articles), rapid communications, articles with accelerated review processes, editorials, and discussions (brief, objective and concise comments on recent papers published in BJG with replies by authors).

Manuscripts must be written in English. Companion papers will not be accepted.

Ethics in publishing

The BJG follows the Code of Good Scientific Practice published by the São Paulo State Research Foundation – FAPESP, see http://www.fapesp.br/boaspraticas/FAPESP-Code_of_Good_Scientific_Practice_2014.pdf.

Funding sources

Authors should identify the sources of financial support for the research and/or preparation of the article and briefly describe the role of sponsor(s), if any, in study design; in the collection, analysis and interpretation of data; in the writing of the report; and in the decision to submit the article for publication.

Copyright and open access

Upon acceptance of an article, authors will be asked to complete a "BJG publishing agreement" transferring the copyright to the Brazilian Geological Society.

The BJG is an open access journal which means that all articles will be freely available to the wider public and that reuse will be permitted.

Conflicts of interests

All authors are requested to disclose any actual or potential conflict of interest including any financial, personal or other relationships with other people or organizations that could inappropriately influence, or be perceived to influence, their work.

Submission declaration and verification

Submission of an article implies that the work described has not been published previously (except in the form of an abstract or as part of a published lecture or academic thesis), that it is not under consideration for publication elsewhere, that its publication is approved by all authors as well as tacitly or explicitly by the responsible authorities where the work was carried out, and that, if accepted, it will not be published elsewhere in the same form, in English or in any other language, including electronically, without the written consent of the copyright-holder. Authors should verify the originality of the article by checking for plagiarism with any available software.

In addition, the corresponding author must state that:

- The article has not been partitioned and that its con- tents are fully and independently understandable;
- The article, edited in Microsoft Word, A4 format, does not exceed 12,000 words;
- Each illustration or table is being sent in a separate file (.tif for figures);
- No text or illustration file exceeds 10 Mb;
- The authors are aware that submissions that do not comply with the "Instructions to authors" for BJG will be returned to the corresponding author;
- The authors are aware that if reviewers indicate the need for major or minor revision, they will have 30 days to make the corrections suggested by the editors;
- The authors are aware that they should carefully check and correct print proofs and return them to publishers within 48 hours to ensure the publication of the article without errors;
- The authors are aware that, should the article be accepted for publication, copyright will be transferred to the Brazilian Geological Society by sending a letter signed by all authors ("BJG publishing agreement").

Submission

Our online submission system (ScholarOne – SciELO) will guide you stepwise through the process of entering details on your article and uploading your files. The system will convert your article files to a single PDF file for use in the peer-review process. Editable files (e.g., Word, LaTeX) are required to typeset your article for final publication. All correspondence, including notification of the Editor's decision and requests for revision, will be sent by e-mail.

Evaluation

Peer review: Articles will be submitted to critical analysis by least two reviewers.
Type of evaluation: Authors will be identified in the manuscripts received by the reviewers.

FORM AND PREPARATION OF MANUSCRIPTS

Use of word processing software

Regardless of the file format of the original submission, at revision you must provide us with an editable file of the entire article. Keep the layout of the text as simple as possible.

Most formatting codes will be removed and replaced on processing the article. The electronic text should be prepared in a way very similar to that of conventional manuscripts.

To avoid errors you are strongly advised to use the 'spell-check' and 'grammar-check' functions of your word processor.

Article structure

There are no strict formatting requirements, but all manuscripts must contain the essential elements needed to convey your manuscript, for example, Abstract, Keywords, Introduction, Materials and Methods, Results, Conclusions, References, Artwork and Tables with Captions.

Divide the article into clearly defined and numbered sections. Subsections should be numbered 1.1 (then 1.1.1, 1.1.2 ...), 1.2, etc. (the abstract is not included in section numbering). Use this numbering also for internal cross-referencing: do not just refer to 'the text'. Any subsection may be given a brief heading. Each heading should appear on its own separate line.

Introduction

State the objectives of the work and provide an adequate background, avoiding a detailed literature survey or a summary of the results.

Material and methods

Provide sufficient detail to allow the work to be re- produced. Methods already published should be indicated by a reference. Only relevant modifications should be described.

Theory/calculation

A Theory section should extend, not repeat, the back- ground to the article already dealt with in the Introduction and lay the foundation for further work. In contrast, a Calculation section represents a practical development from a theoretical basis.

Results

Results should be clear and concise.

Discussion

This should explore the significance of the results of the work, not repeat them. A combined Results and Discussion section is often appropriate. Avoid extensive citations and discussion of published literature.

Conclusions

The main conclusions of the study may be presented in a short Conclusions section, which may stand alone or form a subsection of a Discussion or Results and Discussion section.

Appendices

If there is more than one appendix, they should be identified as A, B, etc. Formulae and equations in appendices should be given separate numbering: Eq. (A.1), Eq. (A.2), etc.; in a subsequent appendix, Eq. (B.1) and so on. This also applies to tables and figures: Table A.1; Fig. A.1, etc.

Essential title page information:

Title

Concise, informative, and interesting. Titles are often used in information-retrieval systems. Avoid abbreviations and formulae where possible.

Author names and affiliations

Please clearly indicate the given name(s) and family name(s) of each author and check that all names are accurately spelled. Present the authors' affiliation addresses (where the actual work was done) below the names. Indicate all affiliations with a lower-case superscript number immediately after the author's name and in front of the appropriate address. Provide the full postal address of each affiliation, including the country name and, if available, the e-mail address of each author.

Corresponding author

Clearly indicate who will handle correspondence at all stages of refereeing, publication, and post-publication. Ensure that the e-mail address is given and that contact details are kept up to date by the corresponding author.

Present/permanent address

If an author has moved since the work described in the article was done, or was visiting at the time, a 'Present address' (or 'Permanent address') may be indicated as a footnote to that author's name. The address at which the author actually did the work must be retained as the main, affiliation address. Superscript Arabic numerals are used for such footnotes.

Abstract

A concise and factual abstract is required. The abstract should state briefly the purpose of the research, the principal results and major conclusions. An abstract is often presented separately from the article, so it must be able to stand alone. For this reason, References should be avoided, but if essential, then cite the author(s) and year(s). Also, non-standard or uncommon abbreviations should be avoided, but if essential they must be defined at their first mention in the abstract itself.

Keywords

Immediately after the abstract, provide a maximum of 6 keywords, using American spelling and avoiding general and plural terms and multiple concepts (avoid, for example,

'and', 'of '). Be sparing with abbreviations: only abbreviations firmly established in the field may be eligible. These keywords will be used for indexing purposes.

Abbreviations

Define abbreviations that are not standard in this field in a footnote to be placed on the first page of the article. Such abbreviations that are unavoidable in the abstract must be defined at their first mention there, as well as in the footnote. Ensure consistency of abbreviations throughout the article.

Acknowledgements

Collate acknowledgements in a separate section at the end of the article before the references and do not, there- fore, include them on the title page, as a footnote to the title or otherwise. List here those individuals who provided help during the research (e.g., providing language help, writing assistance or proof reading the article, etc.), as well as institutions and funding agencies.

Units

Follow internationally accepted rules and conventions: use the international system of units (SI). If other units are mentioned, please give their equivalent in SI.

Math formulae

Please submit math equations as editable text and not as images. Present simple formulae in line with normal text where possible and use the solidus (/) instead of a horizontal line for small fractional terms, e.g., X/Y. In principle, variables are to be presented in italics. Powers of e are often more conveniently denoted by exp. Number consecutively any equations that have to be displayed separately from the text (if referred to explicitly in the text).

Electronic artwork:

General points

- Make sure you use uniform lettering and sizing of your original artwork.
- Preferred fonts: Arial (or Helvetica), Times New Roman (or Times), Symbol, Courier.
- Number the illustrations according to their sequence in the text.
- Use a logical naming convention for your artwork files.
- For Word submissions only, you may provide figures, their captions, and tables within a single file at the revision stage.

Formats

Regardless of the application used, when your electronic artwork is finalized, please 'save as' or convert the images to one of the following formats (note the resolution requirements for line drawings, halftones, and line/halftone combinations given below):

- EPS (or PDF): Vector drawings. Embed the font or save the text as 'graphics'.

- TIFF (or JPG): Color or grayscale photographs (half- tones): always use a minimum of 300 dpi.
- TIFF (or JPG): Bitmapped line drawings: use a mini- mum of 1000 dpi.
- TIFF (or JPG): Combined bitmapped line/half-tone (color or grayscale) images: a minimum of 500 dpi is required. **Please do not:**
- Supply files that are optimized for screen use (e.g., GIF, BMP, PICT, WPG); the resolution is too low.
- Supply files that are too low in resolution.
- Submit graphics that are disproportionately large for the content.

Color artwork

Please make sure that artwork files are in an acceptable format - TIFF (or JPEG), EPS (or PDF), or MS Office files - and with the correct resolution. If, together with your accepted article, you submit usable color figures, the- se will appear in color online.

Figure captions

Ensure that each illustration has a caption. A caption should comprise a brief title (not on the figure itself) and a description of the illustration. Keep text in the illustrations to a minimum, but be sure to explain all symbols and abbreviations used.

Tables

Please submit tables as editable text and not as images. Tables can be placed either next to the relevant text in the article, or on separate page(s) at the end. Number tables consecutively in accordance with their appearance in the text and place any table notes below the table body. Be spa- ring in the use of tables and ensure that the data presented in them do not duplicate results described elsewhere in the article. Please avoid using vertical rules.

Citation in text

Please ensure that every reference cited in the text is also present in the reference list (and vice versa). Any references cited in the abstract must be given in full. Unpublished results and personal communications are not recommended in the reference list, but may be mentioned in the text. If these references are included in the reference list they should follow the standard reference style of the journal and should include a substitution of the publication date with either 'Unpublished results' or 'Personal communication'. Citation of a reference as 'in press' implies that the item has been accepted for publication.

Web references

As a minimum, the full URL should be given and the date when the reference was last accessed. Any further in- formation, if known (DOI, author names, dates, reference to a source publication, etc.), should also be given. Web references can be listed separately (e.g., after the reference list) under a different heading if desired, or can be included in the reference list.

Reference formatting

There are no strict requirements on reference format- ting at submission. References can be in any style or format as long as the style is consistent. Where applicable, name(s) of author(s), journal title/book title, chapter title/article title, year of publication, volume number/book chapter and the pagination must be present. Use of DOI is highly encouraged. The reference style used by the journal will be applied to the accepted article by SCIELO at the proof stage. Note that missing data will be highlighted at proof stage for the author to correct.

Reference style

All publications cited in the text should be presented in a list of references following the text of the manuscript. In the text refer to the author's name (without initials) and year of publication (e.g. "Since Almeida (1986) has shown that..." or "This is in agreement with results obtained later (Trompette 1994; Heilbron and Machado 2003)."

For three or more authors use the first author followed by "et al.", in the text. The list of references should be arranged alphabetically by authors' names. The manuscript should be carefully checked to ensure that the spelling of authors' names and dates are exactly the same in the text as in the reference list.

References should be given in the following form:

Papers in scientific journals

Almeida F.F.M. 1986. Distribuição regional e relações tectônicas do magmatismo pós-paleozóico no Brasil. *Revista Brasileira de Geociências*, **16:**325-349.

Costa I.P., Bueno G.V., Milhomem P.S., Silva H.S.R.L., Kosin M.D. 2007. Sub-bacia de Tucano Norte e Bacia de Jatobá. *Boletim de Geociências da Petrobras*, **15:**445-453.

Escayola M.P., Pimentel M.M., Armstrong R. 2007. Neoproterozoic backarc basin: sensitive high-resolution ion microprobe U-Pb and Sm-Nd isotopic evidence from the eastern Pampean Ranges, Argentina. *Geology*, **35:**495-498.

Heilbron, M. and Machado, N. 2003, Timing of terrane accretion in the Neoproterozoic-Eopaleozoic Ribeira orogen (SE Brazil). *Precambrian Research*, **125:**87-112.

Books and book chapters

Bedell R., Crósta A.P., Grunsky E. (eds.). 2009. *Remote Sensing and Spectral Geology*. Littleton, Society of Economic Geologists, 270 p.

Kaufman A.J., Sial A.N., Frimmel H.E., Misi A. 2009. Neoproterozoic to Cambrian paleoclimatic events in southwestern Gondwana In: Gaucher C., Sial A.N., Frimmel H.E., Helverson G.P. (eds.). Neoproterozoic- Cambrian tectonics, global change and evolution: a focus on southwestern Gondwana. *Developments in Precambrian Geology*, 16, Amsterdam, Elsevier, p. 369-388.

Pankhurst R.J. & Rapela C.W. (eds.). 1998. The P*roto- Andean margin of Gondwana*. London, Geological Society of London Special Publication, **142**, 382 p.
Trompette R. 1994. *Geology of western Gondwana (2000–500 Ma)*. Rotterdam, Balkema, 350 p.

Papers in scientific meetings

Astini R., Ramos V.A., Benedetto J.L., Vaccari N.E., Cañas F.L. 1996. La Precordillera: un terreno exótico a Gondwana. In: 13°Congreso Geológico Argentino y 3° Congreso Exploración de Hidrocarburos. Buenos Aires, *Actas*, v. 5, p. 293-324.

Leite-Junior W.B, Bettencourt J.S., Payolla B.L. 2003. Evidence for multiple sources inferred from Sr and Nd isotopic data from felsic rocks in the Santa Clara Intrusive Suite, Rondonia, Brazil. In: SSAGI, South American Symposium on Isotope Geology. Salvador, *Short Papers*, p. 583-585.

Milani E.J. & Thomaz-Filho A. 2000. Sedimentary basins of South América. In: Cordani U.G., Milani E.J., Thomaz- Filho A., Campos D.A. (eds.). Tectonic evolution of South America. *31st International Geological Congress*. Rio de Janeiro, p. 389-452.

Thesis and dissertations

Paes V.J.C. 1999. *Geologia da quadrícula Alvarenga, MG, e a geoquímica:* implicações geotectônicas e metalogenéticas. MS Dissertation, Instituto de Geociências, Universidade Federal de Minas Gerais, Belo Horizonte, 144 p.

Ávila C.A. 2000. *Geologia, petrografia e geocronologia de corpos plutônicos paleoproterozóicos da borda meridional do Cráton São Francisco, região de São João Del Rei, Minas Gerais*. PhD Thesis, Universidade Federal do Rio de Janeiro, Rio de Janeiro, 401 p.

Printed maps

Inda H.A.V. & Barbosa J.F. 1978. *Mapa geológico do Estado da Bahia, escala 1:1.000.000*. Salvador, Secretaria das Minas e Energia, Coordenação da Produção Mineral. Mascarenhas J.F. & Garcia T.M. 1989. *Mapa geocronológico do Estado da Bahia, escala 1:1.000.000*. Texto explicativo. Salvador, Secretaria das Minas e Energia, Coordenação da Produção Mineral, 186 p.

Schobbenhaus C. (coord.). 1975. *Carta Geológica do Brasil ao Milionésimo – Folha Goiás (SD 22)*. Texto explicativo. Brasília, Departamento Nacional da Produção Mineral, 114 p.

Internal reports

Internal reports will not be accepted, unless of open access for the scientific community and authorized by ad hoc consultants.

Submission checklist

The following list will be useful during the final checking of an article prior to sending it to the journal for review. Please consult this Guide for Authors for further details of any item.

Ensure that the following items are present:

One author has been designated as the corresponding author with contact details:

- E-mail address
- Full postal address

All necessary files have been uploaded, and contain:

- Keywords
- All figure captions
- All tables (including title, description, footnotes)

Further considerations:

- Manuscript has been 'spell-checked' and 'grammar-checked'.
- All references mentioned in the Reference list are cited in the text, and vice versa.
- Permission has been obtained for use of copyrighted material from other sources (including the Internet).

Rapid communications

Rapid communications are limited to 2000 words, including references. Summary and abstract are limited to 100 words. At the discretion of the editors, these communications may be scheduled for the first available edition.

Articles with accelerated review process

An accelerated review process may be requested for complete original studies, for which urgency of publication is adequately justified. At the discretion of the editors, these can be programmed for the first available edition. They must follow the same format described for original articles.

Editorials

Editorials should cover some aspect of the broad spectrum of the Geological Sciences. They will be authored by the editors of BJG, by people linked to the Brazilian Geological Society or by industry personalities. These documents will not be submitted to peer review and will be published at the discretion of the editors.

Review articles

Review articles should cover relevant topics of Geology. These articles may be requested by the editors, but recognized experts may spontaneously submit review articles in their field of expertise. In this case, potential authors should contact the editors to ascertain their interest prior to submitting the article.

ANEXO B - REGRAS DE FORMATAÇÃO DA REVISTA "JOURNAL OF SOUTH AMERICAN EARTH SCIENCES" (ARTIGO 2)

DESCRIPTION

The *Journal of South American Earth Sciences* provides an international medium for the publication of scientific work concerned with all aspects of the **earth sciences** in the **South American continent** and the surrounding **oceans**. Work is also accepted from the adjacent regions of the **Caribbean**, **Central America**, **Mexico**, and **Antarctic Peninsula**.

Papers must have a regional appeal and should present work of more than local significance. Research papers dealing with the **regional geology** of South American cratons and mobile belts; **economic geology** particularly metallogenesis and hydrocarbon genesis; stratigraphy, structure and **basin evolution**; **geophysics** and **geochemistry**; **volcanology**; **tectonics** and **Quaternary geology** are featured.

New developments in already established regional projects and new initiatives dealing with the geology of the continent will be summarized and presented on a regular basis. Short notes, discussions, book reviews and conference and workshop reports will also be included when relevant. See http://www.elsevier.com/locate/sames-edit for the editorial.

The *Journal of South American Earth Sciences* is also available as part of the Geoscience Package which comprises *Journal of African Earth Sciences*, *Journal of Asian Earth Sciences* and *Journal of South American Earth Sciences*. See Geoscience Package for details.

GUIDE FOR AUTHORS

Your Paper Your Way
We now differentiate between the requirements for new and revised submissions. You may choose to submit your manuscript as a single Word or PDF file to be used in the refereeing process. Only when your paper is at the revision stage, will you be requested to put your paper in to a 'correct format' for acceptance and provide the items required for the publication of your article. **To find out more, please visit the Preparation section below**.

Submission checklist
You can use this list to carry out a final check of your submission before you send it to the journal for review. Please check the relevant section in this Guide for Authors for more details.

Ensure that the following items are present:

One author has been designated as the corresponding author with contact details:
• E-mail address
• Full postal address
All necessary files have been uploaded:
Manuscript:

• Include keywords
• All figures (include relevant captions)
• All tables (including titles, description, footnotes)
• Ensure all figure and table citations in the text match the files provided
• Indicate clearly if color should be used for any figures in print
Graphical Abstracts / Highlights files (where applicable)
Supplemental files (where applicable)

Further considerations
• Manuscript has been 'spell checked' and 'grammar checked'
• All references mentioned in the Reference List are cited in the text, and vice versa
• Permission has been obtained for use of copyrighted material from other sources (including the Internet)
• A competing interests statement is provided, even if the authors have no competing interests to declare
• Journal policies detailed in this guide have been reviewed
• Referee suggestions and contact details provided, based on journal requirements

PREPARATION

Paper length
The maximum number of words per article is 19,000.

NEW SUBMISSIONS
Submission to this journal proceeds totally online and you will be guided stepwise through the creation and uploading of your files. The system automatically converts your files to a single PDF file, which is used in the peer-review process.
As part of the Your Paper Your Way service, you may choose to submit your manuscript as a single file to be used in the refereeing process. This can be a PDF file or a Word document, in any format or layout that can be used by referees to evaluate your manuscript. It should contain high enough quality figures for refereeing. If you prefer to do so, you may still provide all or some of the source files at the initial submission. Please note that individual figure files larger than 10 MB must be uploaded separately.

References
There are no strict requirements on reference formatting at submission. References can be in any style or format as long as the style is consistent. Where applicable, author(s) name(s), journal title/book title, chapter title/article title, year of publication, volume number/book chapter and the pagination must be present. Use of DOI is highly encouraged. The reference style used by the journal will be applied to the accepted article by Elsevier at the proof stage. Note that missing data will be highlighted at proof stage for the author to correct.

Formatting requirements
There are no strict formatting requirements but all manuscripts must contain the essential elements needed to convey your manuscript, for example Abstract, Keywords, Introduction, Materials and Methods, Results, Conclusions, Artwork and Tables with Captions.
If your article includes any Videos and/or other Supplementary material, this should be included in your initial submission for peer review purposes.
Divide the article into clearly defined sections.

Figures and tables embedded in text
Please ensure the figures and the tables included in the single file are placed next to the relevant text in the manuscript, rather than at the bottom or the top of the file. The corresponding caption should be placed directly below the figure or table.

Peer review
This journal operates a single blind review process. All contributions will be initially assessed by the editor for suitability for the journal. Papers deemed suitable are then typically sent to a minimum of two independent expert reviewers to assess the scientific quality of the paper. The Editor is responsible for the final decision regarding acceptance or rejection of articles. The Editor's decision is final.

Article structure
Subdivision - numbered sections
Divide your article into clearly defined and numbered sections. Subsections should be numbered 1.1 (then 1.1.1, 1.1.2, ...), 1.2, etc. (the abstract is not included in section numbering). Use this numbering also for internal cross-referencing: do not just refer to 'the text'. Any subsection may be given a brief heading. Each heading should appear on its own separate line.

Introduction
State the objectives of the work and provide an adequate background, avoiding a detailed literature survey or a summary of the results.

Material and methods
Provide sufficient details to allow the work to be reproduced by an independent researcher. Methods that are already published should be summarized, and indicated by a reference. If quoting directly from a previously published method, use quotation marks and also cite the source. Any modifications to existing methods should also be described.

Theory/calculation
A Theory section should extend, not repeat, the background to the article already dealt with in the Introduction and lay the foundation for further work. In contrast, a Calculation section represents a practical development from a theoretical basis.

Results
Results should be clear and concise.

Discussion
This should explore the significance of the results of the work, not repeat them. A combined Results and Discussion section is often appropriate. Avoid extensive citations and discussion of published literature.

Conclusions
The main conclusions of the study may be presented in a short Conclusions section, which may stand alone or form a subsection of a Discussion or Results and Discussion section.

Appendices
If there is more than one appendix, they should be identified as A, B, etc. Formulae and equations in appendices should be given separate numbering: Eq. (A.1), Eq. (A.2), etc.; in a

subsequent appendix, Eq. (B.1) and so on. Similarly for tables and figures: Table A.1; Fig. A.1, etc.

Essential title page information

• *Title.* Concise and informative. Titles are often used in information-retrieval systems. Avoid abbreviations and formulae where possible.

• *Author names and affiliations.* Please clearly indicate the given name(s) and family name(s) of each author and check that all names are accurately spelled. You can add your name between parentheses in your own script behind the English transliteration. Present the authors' affiliation addresses (where the actual work was done) below the names. Indicate all affiliations with a lowercase superscript letter immediately after the author's name and in front of the appropriate address. Provide the full postal address of each affiliation, including the country name and, if available, the e-mail address of each author.

• *Corresponding author.* Clearly indicate who will handle correspondence at all stages of refereeing and publication, also post-publication. This responsibility includes answering any future queries about Methodology and Materials. Ensure that the e-mail address is given and that contact details are kept up to date by the corresponding author.

• *Present/permanent address.* If an author has moved since the work described in the article was done, or was visiting at the time, a 'Present address' (or 'Permanent address') may be indicated as a footnote to that author's name. The address at which the author actually did the work must be retained as the main, affiliation address. Superscript Arabic numerals are used for such footnotes.

Abstract

A concise and factual abstract is required. The abstract should state briefly the purpose of the research, the principal results and major conclusions. An abstract is often presented separately from the article, so it must be able to stand alone. For this reason, References should be avoided, but if essential, then cite the author(s) and year(s). Also, non-standard or uncommon abbreviations should be avoided, but if essential they must be defined at their first mention in the abstract itself.

Highlights

Highlights are mandatory for this journal. They consist of a short collection of bullet points that convey the core findings of the article and should be submitted in a separate editable file in the online submission system. Please use 'Highlights' in the file name and include 3 to 5 bullet points (maximum 85 characters, including spaces, per bullet point). You can view example Highlights on our information site.

Keywords

Immediately after the abstract, provide a maximum of 6 keywords, using American spelling and avoiding general and plural terms and multiple concepts (avoid, for example, 'and', 'of'). Be sparing with abbreviations: only abbreviations firmly established in the field may be eligible. These keywords will be used for indexing purposes.

Abbreviations

Define abbreviations that are not standard in this field in a footnote to be placed on the first page of the article. Such abbreviations that are unavoidable in the abstract must be defined at their first mention there, as well as in the footnote. Ensure consistency of abbreviations throughout the article.

Acknowledgements

Collate acknowledgements in a separate section at the end of the article before the references and do not, therefore, include them on the title page, as a footnote to the title or otherwise. List here those individuals who provided help during the research (e.g., providing language help, writing assistance or proof reading the article, etc.).

Formatting of funding sources

List funding sources in this standard way to facilitate compliance to funder's requirements:

Funding: This work was supported by the National Institutes of Health [grant numbers xxxx, yyyy]; the Bill & Melinda Gates Foundation, Seattle, WA [grant number zzzz]; and the United States Institutes of Peace [grant number aaaa].

It is not necessary to include detailed descriptions on the program or type of grants and awards. When funding is from a block grant or other resources available to a university, college, or other research institution, submit the name of the institute or organization that provided the funding.

If no funding has been provided for the research, please include the following sentence:

This research did not receive any specific grant from funding agencies in the public, commercial, or not-for-profit sectors.

Units

Follow internationally accepted rules and conventions: use the international system of units (SI). If other units are mentioned, please give their equivalent in SI.

Math formulae

Please submit math equations as editable text and not as images. Present simple formulae in line with normal text where possible and use the solidus (/) instead of a horizontal line for small fractional terms, e.g., X/Y. In principle, variables are to be presented in italics. Powers of e are often more conveniently denoted by exp. Number consecutively any equations that have to be displayed separately from the text (if referred to explicitly in the text).

Footnotes

Footnotes should be used sparingly. Number them consecutively throughout the article. Many word processors build footnotes into the text, and this feature may be used. Should this not be the case, indicate the position of footnotes in the text and present the footnotes themselves separately at the end of the article.

Electronic artwork

General points

• Make sure you use uniform lettering and sizing of your original artwork.
• Preferred fonts: Arial (or Helvetica), Times New Roman (or Times), Symbol, Courier.

• Number the illustrations according to their sequence in the text.
• Use a logical naming convention for your artwork files.
• Indicate per figure if it is a single, 1.5 or 2-column fitting image.
• For Word submissions only, you may still provide figures and their captions, and tables within a single file at the revision stage.
• Please note that individual figure files larger than 10 MB must be provided in separate source files.

Formats

Regardless of the application used, when your electronic artwork is finalized, please 'save as' or convert the images to one of the following formats (note the resolution requirements for line drawings, halftones, and line/halftone combinations given below):
EPS (or PDF): Vector drawings. Embed the font or save the text as 'graphics'.
TIFF (or JPG): Color or grayscale photographs (halftones): always use a minimum of 300 dpi.
TIFF (or JPG): Bitmapped line drawings: use a minimum of 1000 dpi.
TIFF (or JPG): Combinations bitmapped line/half-tone (color or grayscale): a minimum of 500 dpi is required.

Please do not:
• Supply files that are optimized for screen use (e.g., GIF, BMP, PICT, WPG); the resolution is too low.
• Supply files that are too low in resolution.
• Submit graphics that are disproportionately large for the content.

Color artwork

Please make sure that artwork files are in an acceptable format (TIFF (or JPEG), EPS (or PDF), or MS Office files) and with the correct resolution. If, together with your accepted article, you submit usable color figures then Elsevier will ensure, at no additional charge, that these figures will appear in color online (e.g., ScienceDirect and other sites) regardless of whether or not these illustrations are reproduced in color in the printed version. For color reproduction in print, you will receive information regarding the costs from Elsevier after receipt of your accepted article. Please indicate your preference for color: in print or online only. Further information on the preparation of electronic artwork.

Figure captions

Ensure that each illustration has a caption. A caption should comprise a brief title (**not** on the figure itself) and a description of the illustration. Keep text in the illustrations themselves to a minimum but explain all symbols and abbreviations used.

Tables

Please submit tables as editable text and not as images. Tables can be placed either next to the relevant text in the article, or on separate page(s) at the end. Number tables consecutively in accordance with their appearance in the text and place any table notes below the table body. Be sparing in the use of tables and ensure that the data presented in them do not duplicate results described elsewhere in the article. Please avoid using vertical rules and shading in table cells.

References
Citation in text
Please ensure that every reference cited in the text is also present in the reference list (and vice versa). Any references cited in the abstract must be given in full. Unpublished results and personal communications are not recommended in the reference list, but may be mentioned in the text. If these references are included in the reference list they should follow the standard reference style of the journal and should include a substitution of the publication date with either 'Unpublished results' or 'Personal communication'. Citation of a reference as 'in press' implies that the item has been accepted for publication.

Web references
As a minimum, the full URL should be given and the date when the reference was last accessed. Any further information, if known (DOI, author names, dates, reference to a source publication, etc.), should also be given. Web references can be listed separately (e.g., after the reference list) under a different heading if desired, or can be included in the reference list.

Data references
This journal encourages you to cite underlying or relevant datasets in your manuscript by citing them in your text and including a data reference in your Reference List. Data references should include the following elements: author name(s), dataset title, data repository, version (where available), year, and global persistent identifier. Add [dataset] immediately before the reference so we can properly identify it as a data reference. The [dataset] identifier will not appear in your published article.

References in a special issue
Please ensure that the words 'this issue' are added to any references in the list (and any citations in the text) to other articles in the same Special Issue.

Reference management software
Most Elsevier journals have their reference template available in many of the most popular reference management software products. These include all products that support Citation Style Language styles, such as Mendeley and Zotero, as well as EndNote. Using the word processor plug-ins from these products, authors only need to select the appropriate journal template when preparing their article, after which citations and bibliographies will be automatically formatted in the journal's style. If no template is yet available for this journal, please follow the format of the sample references and citations as shown in this Guide.
Users of Mendeley Desktop can easily install the reference style for this journal by clicking the following link:
http://open.mendeley.com/use-citation-style/journal-of-south-american-earth-sciences
When preparing your manuscript, you will then be able to select this style using the Mendeley plugins for Microsoft Word or LibreOffice.

Reference Formatting
There are no strict requirements on reference formatting at submission. References can be in any style or format as long as the style is consistent. Where applicable, author(s) name(s), journal title/book title, chapter title/article title, year of publication, volume number/book chapter and the pagination must be present. Use of DOI is highly encouraged. The reference style used by the journal will be applied to the accepted article by Elsevier at the proof stage. Note that missing data will be highlighted at proof stage for the author to correct. If you do

wish to format the references yourself they should be arranged according to the following examples:

[dataset] Oguro, M., Imahiro, S., Saito, S., Nakashizuka, T., 2015. Mortality data for Japanese oak wilt disease and surrounding forest compositions. Mendeley Data, v1. http://dx.doi.org/10.17632/xwj98nb39r.1.

Reference style
All publications cited in the text should be presented in a list of references following the text of the manuscript. In the text refer to the author's name (without initials) and year of publication (e.g. "Since Condie (2001) has shown that..." or "This is in agreement with results obtained later (Meert, 2003; Burrett and Berry, 2000)."
For three or more authors use the first author followed by "et al.", in the text. The list of references should be arranged alphabetically by authors' names. The manuscript should be carefully checked to ensure that the spelling of authors' names and dates are exactly the same in the text as in the reference list.

References should be given in the following form:

Kusky, T.M., Stern, R.J., Tucker, R.D., 2003. Evolution of East African and related orogens, and the assembly of Gondwana. Precambrian Research, 123, 81–85.

Pili, E., Sheppard, S.M.F., Lardeaux, J.M.,1999. Fluid–rock interaction in the granulites of Madagascar and lithospheric transfer of fluids. Gondwana Research, 2, 341–350.

Suzuki, K., Adachi, M., 1992. Middle Precambrian detrital monazite and zircon from Hida gneiss in Oki-Dogo island, Japan: their origin and implications for the correlation of basement gneiss of Southwest Japan and Korea. Tectonophysics, 235, 277–292.

Touret, J.L.R., 1985. Fluid regime in southern Norway, the record of fluid inclusions. In: Tobi, A.C., Touret, J.L.R. (Eds.), The Deep Proterozoic Crust in the North Atlantic Provinces. Reidel, Dordrecht, 517–549.

Kinny, P. D., Collins, A. S., Razakamanana, T., 2004. Provenance hints and age constraints of metasedimentary gneisses of Southern Madagascar from SHRIMP U–Pb zircon data. In: Chetty, T.R.K. and Bhaskar Rao, Y.J. (Eds.), International Field Workshop on the Southern Granulite Terrane. National Geophysical Research Institute, Hyderabad, India, 97–98.

Rogers, J.J.W. and Santosh, M., 2004. Continents and Supercontinents. Oxford University Press, New York. Li, Z.X., Metcalfe, I., Powell, C.M. (Eds.), 1996. Breakup of Rodinia and Gondwanaland and Assembly of Asia. Australian Journal of Earth Sciences 43.

Albee, H.F., Cullins, H.L., 1975. Geologic map of the Alpine Quadrangle, Bonneville County, Idaho, and Lincoln County Wyoming. United States Geological Survey Geologic Quadrangle Map GQ–1259, scale 1:24,000.

Sajeev, K., 2003. Evolution and metamorphic zoning of Highland Complex, Sri Lanka: a comparison with Madurai Block, southern India. Ph.D. thesis, Okayama University.

ANEXO C - REGRAS DE FORMATAÇÃO DA REVISTA "GEOLOGIA USP, SÉRIE CIENTÍFICA" (ARTIGO 3)

Diretrizes para Autores

1. PÁGINA DE ROSTO – deverá conter: três títulos, em português, em inglês e título curto no idioma principal do manuscrito com no máximo 50 caracteres, contando os espaços; nome completo e instituição de origem dos autores; endereço completo **somente do autor principal** (logradouro, CEP, cidade, estado, país, caixa postal e **telefone para contato** - *pode ser o endereço da Universidade*), **e-mail de todos os autores**; número de palavras; total de figuras e de tabelas.

2. RESUMO E ABSTRACT – em um único parágrafo, **devem ser concisos, com no máximo 270 palavras**. Textos mais longos devem vir acompanhados de justificativa circunstanciada.

3. PALAVRAS-CHAVE E KEYWORDS – **máximo seis**, separadas por ponto e vírgula, com a primeira letra em maiúscula. Ex.: Bacia do Araripe; Quaternário; Fácies; Depósitos magmáticos.

Os descritores em inglês devem acompanhar os termos em português.

4. TEXTO PRINCIPAL – poderá ser redigido em português ou inglês. Elaborar em Word, fonte Times New Roman, tamanho 12, espaço simples. **O tamanho máximo aceito para publicação é de 25 páginas, incluindo: texto, resumo, abstract, tabelas, figuras e referências bibliográficas.** (Trabalhos mais longos podem ser aceitos desde que argumentos científicos que os justifiquem sejam apresentados e aceitos).

a) Na fase de submissão, inserir numeração de páginas, bem como as figuras, tabelas, legendas e referências.

b) Quando o artigo estiver devidamente aprovado para publicação, as figuras, tabelas e legendas devem ser retiradas do texto. Enviá-las separadamente e numeradas, cada uma num arquivo. As legendas devem vir em um único arquivo, separadas das figuras e tabelas.

5. TÍTULOS

a) Título do artigo:
Título principal – **Negrito, caixa alta na primeira letra da primeira palavra e caixa baixa nas demais.**
Título em inglês – Itálico, caixa alta na primeira letra da primeira palavra e caixa baixa nas demais (sem negrito).
Título curto - Caixa alta na primeira letra da primeira palavra e caixa baixa nas demais (sem negrito /sem itálico).

b) Títulos e subtítulos no interior do artigo:
NÍVEL 1 – **NEGRITO, CAIXA ALTA.**
Nível 2 – **Negrito, caixa alta na primeira letra da primeira palavra e caixa baixa nas demais.**

Nível 3 – Itálico, caixa alta na primeira letra da primeira palavra e caixa baixa nas demais (sem negrito).

Nível 4 – Caixa alta na primeira letra da primeira palavra e caixa baixa nas demais (sem negrito).

6. TABELAS E QUADROS – considerar quadro como tabela. Elaborar em Word, no modo "tabela", com formato aberto, fonte Arial, tamanho 8. Obedecer as medidas: 8,2 cm (uma coluna) ou 17 cm (duas colunas), comprimento máximo de 22 cm, incluindo a legenda. Tabelas muito extensas deverão ser divididas.

a) Na fase de submissão, inserir as tabelas no texto, juntamente com a legenda, com a devida numeração sequencial.

b) Quando o artigo estiver devidamente aprovado para publicação, as tabelas devem ser retiradas do texto. Enviá-las separadamente e numeradas, cada uma num arquivo. As legendas devem vir em um único arquivo, separadas das tabelas.

c) Legendas: fonte Times New Roman, tamanho 12. (sem itálico)

7. ILUSTRAÇÕES – mapas, fotos, figuras, gráficos, pranchas, fotomicrografias etc., considerar como figuras. Utilizar fonte Arial, tamanho 9. Obedecer as medidas: 8,2 cm (uma coluna) ou 17 cm (duas colunas), comprimento máximo de 22 cm, incluindo a legenda.

a) Na fase de submissão, inserir as figuras no texto, juntamente com a legenda, com a devida numeração sequencial.

b) Quando o artigo estiver devidamente aprovado para publicação, as figuras devem ser retiradas do texto. Enviá-las separadamente e numeradas, cada uma num arquivo. **Deverão estar em formato JPEG, TIFF ou EPS, com resolução mínima de 300 dpi.** As legendas devem vir em um único arquivo, separadas das figuras.

c) Legendas: fonte Times New Roman, tamanho 12. (sem itálico)

8. CITAÇÕES NO TEXTO – exemplos de citação direta / citação indireta:

a) Um autor

Santos (1980) / (Santos, 1980)

b) Dois autores

Norton e Long (1995) / (Norton e Long, 1980)

c) Mais de dois autores

Moorbath et al. (1992) / (Moorbath et al., 1992)

d) Congressos, conferências, seminários etc.

... no Congresso Brasileiro de Geologia (1984) / (Congresso Brasileiro de Geologia, 1984)

e) Vários trabalhos de diferentes autores

Smith (1985), Rose e Turner (1986) e Johnson et al. (1990) / (Smith, 1985; Rose e Turner, 1986; Johnson et al., 1990)

f) Citação de vários trabalhos de um mesmo autor

Smith (1979a, 1979b, 1981) / (Smith, 1979a, 1979b, 1981)

9. REFERÊNCIAS – listar no final do texto, em ordem alfabética de autores e, dentro dessa sequência, em ordem cronológica.

EXEMPLOS DE REFERÊNCIAS:

a) Livro com um autor

Middlemost, E. A. K. (1997). *Magmas, rocks and planetary development: A Survey of Magma/Igneous Rock Systems.* Harlow: Longman.

b) Livro com dois autores

Anderson, M. P., Woessnr, W. W. (1992). *Applied groundwater modeling. Simulation of low and advecti transport.* San Diego: Academic Press.

c) Livro com três ou mais autores

Harland, W. B., Armstrong, R. L., Cox, A. L. V., Craig, L. E., Smith, A., Smith, D. (1989). *A geologic time scale* (2nd ed.). Cambridge: Cambridge University Press.

d) Capítulo de livro

Almeida, F. F. M., Amaral, G., Cordani, U. G., Kawashita, K. (1973). The Precambrian evolution of the South American cratonic margin south of Amazonas River. In: A. E. Nairn, F. G. Stille (Eds.), *The ocean basin and margins,* 1, 411-446. New York: Plenum.

(Exemplo de Publicação seriada)

L. Harris, N., Pearce, J., Tindle, A. (1986). Geochemical collision-zone magmatism. In: Coward M. P., Ries A. C. (ed.) *Collision tectonics*. 67-81. London: Geological Society. (Geological Society Special Publication, 19).

e) Artigo de periódico

Caffe, P. J., Soler, M. M., Coira, B. L., Cordani, U. G., Onoe, A. T. (2008). The granada ignimbrite: a compound pyroclastic unit and its relationship with upper miocene caldera volcanism in the northern Puna. *Journal of South American Earth Science*, 25(4), 464-484.

f) Trabalho apresentado em evento

Danni, J. C. M., Ribeiro, C. C. (1978). Caracterização estratigráfica da sequência vulcano-sedimentar de Pilar de Goiás e de Guarinos, Goiás. *XXX Congresso Brasileiro de Geologia*, 2, 582-596. Recife: SBG.

g) Mapa

Inda, H. A. W., Barbosa, J. F. (1978). *Mapa Geológico do Estado da Bahia*. Escala 1:1.000.000. Salvador: Secretaria de Minas e Energia do Estado da Bahia/ CBPM.
h) Teses e Dissertações

Petta, A. R. (1995). *Estudo geoquímico e relações petrogenéticas do batólito múltiplo composto São Vicente/ Caicó (RN-Brasil)*. Tese (Doutorado). Rio Claro: Instituto de Geociências e Ciências Exatas – UNESP.

Pressi, L. F. (2012). *Evolução magmática do Plúton Piracaia (SP): parâmetros físico-químicos e evidências de mistura entre magmas monzodioríticos e sieníticos*. Dissertaçao (Mestrado). São Paulo: Instituto de Geociências – USP.

i) Documentos em meio eletrônico

Livro

Sharkov, E. (2012). *Tectonics: Recent Advances*. Croatia: InTech, <http://www.intechopen.com/books/ tectonics-recent-advances>

Artigo de periódico

Soares, E. A., Tatumi, S. H. (2010). OSL age determinations of pleistocene fluvial deposits in Central Amazonia. *Anais da Academia Brasileira de Ciências*, 82(3), 691-699. Acesso em 14 de fevereiro de 2011, <http://www.scielo.br/pdf/aabc/ v82n3/17.pdf>

Trabalho apresentado em evento

Souza-Lima, W., Farias, R. M. (2007). A flora quaternária dos travertinos de Itabaiana, Sergipe. *PALEO 2007* (p. 7). Itabaiana: SBP. Acesso em 18 de dezembro de 2008, <http://www.phoenix.org.br/ Paleo2007_Boletim.pdf>.

j) Com numeração DOI

Livro

Zavattini, J. A. (2009). *As chuvas e as massas de ar no estado de Mato Grosso do Sul: estudo geográfico com vista à regionalização climática.*

https://doi.org/10.7476/9788579830020.

Artigo de periódico

Evandro, L., Kleina, E. L., Rodrigues, J. B., Lopesa, E. C. S., Gilvana, L. Soledade, G. L. (2012). Diversity of Rhyacian granitoids in the basement of the Neoproterozoic-Early Cambrian Gurupi Belt, northern Brazil: Geochemistry, U–Pb zircon geochronology, and Nd isotope constraints on the Paleoproterozoic magmatic and crustal evolution. *Precambian Research*, 220-221, 192-216.

https://doi.org/10.1016/j.precamres.2012.08.007.

ANEXO D - COMPROVANTE DE SUBMISSÃO DOS ARTIGOS